Cell cycle regulation of structure-selective endonucleases during homologous recombination

Kumulative Dissertation
zur Erlangung des Doktorgrades
der Fakultät für Biologie
der Ludwigs-Maximilians-Universität München

vorgelegt von

Julia Bittmann

aus Nürnberg, Bayern

August 2020

Eidesstattliche Erklärung

Hiermit erkläre ich an Eides statt, dass ich die vorliegende Dissertation selbstständig und ohne unerlaubte Hilfe angefertig habe. Ich habe weder anderweitig versucht, eine Dissertation einzureichen oder eine Doktorprüfung durchzuführen, noch habe ich diese Dissertation oder Teile derselben einer anderen Prüfungskommision vorgelegt.

_____

Julia Bittmann
München, den 06.08.2020

Promotionsgesuch eingereicht:	06.08.2020
Tag der mündlichen Prüfung:	29.01.2021
Erstgutachter:	Prof. Dr. Heinrich Leonhardt
Zweitgutachter:	Prof. Dr. Peter Becker

Table of Contents

LIST OF ORIGINAL PUBLICATIONS 1

PUBLICATION 1 | BITTMANN ET AL., (2020) ELIFE 1
PUBLICATION 2 | PRINCZ ET AL., (2017) EMBO J 1

CONTRIBUTION STATEMENT 2

ABBREVIATIONS 3

SUMMARY 4

INTRODUCTION 6

1 FORMATION OF DNA BREAKS 6
1.1 EXOGENOUS AND ENDOGENOUS SOURCES 6
1.2 PROGRAMMED DSBS 7
1.3 REPAIR CHOICE 8
2 REPAIR OF DNA BREAKS BY HOMOLOGOUS RECOMBINATION 11
2.1 MECHANISMS OF HOMOLOGOUS RECOMBINATION AT A DOUBLE-ENDED DSB 11
2.2 HOMOLOGOUS RECOMBINATION DURING REPLICATION 14
3 RESOLUTION OF RECOMBINATION INTERMEDIATES 17
3.1 DISSOLUTION AND RESOLUTION 17
3.2 CELL CYCLE REGULATION OF RESOLUTION 19
3.3 SSE ACTIVITY DURING REPLICATION 21

AIMS OF THE STUDIES 23

PUBLICATION 1 | BITTMANN ET AL., (2020) ELIFE 23
PUBLICATION 2 | PRINCZ ET AL., (2017) EMBO J 24

CUMULATIVE THESIS: PUBLICATIONS 25

PUBLICATION 1 | BITTMANN ET AL., (2020) ELIFE 25
PUBLICATION 2 | PRINCZ ET AL., (2017) EMBO J 81

DISCUSSION 129

1 CELL CYCLE TAGS AS VALUABLE TOOL TO STUDY CELL CYCLE REGULATION 129
1.1 THE LIMITATIONS OF PREVIOUS CELL CYCLE TAG SYSTEMS 129
1.2 AN ADVANCED CELL CYCLE TAG TOOLBOX 131
2 THE FUNCTION OF MUS81-MMS4 IS RESTRICTED TO M-PHASE 133
2.1 REPLICATION PERTURBATION REQUIRES LATE RESPONSE BY MUS81-MMS4 133
2.2 A SWITCH-LIKE UPREGULATION OF MUS81-MMS4 ACTIVITY AT THE ONSET OF M-PHASE 137
2.3 CONSEQUENCES OF PREMATURE SSE ACTIVATION 138
3 HIERARCHY DURING THE PROCESSING OF JM STRUCTURES 139

REFERENCES 142

ACKNOWLEDGEMENTS 157

CURRICULUM VITAE 159

List of original publications

Publication 1 | Bittmann et al., (2020) eLife

Bittmann, J., Grigaitis, R., Galanti, L., Amarell, S., Wilfling, F., Matos, J., Pfander, B. An advanced cell cycle tag toolbox reveals principles underlying temporal control of structure-selective nucleases. eLife (2020) 9:e52459 DOI: 10.7554/eLife.52459

Publication 2 | Princz et al., (2017) EMBO J

Princz, L.N., Wild, P., **Bittmann, J.**, Aguado, F.J., Blanco, M.G., Matos, J., Pfander, B. Dbf4-dependent kinase and the Rtt107 scaffold promote Mus81-Mms4 resolvase activation during mitosis. EMBO J (2017) 36: 664-678 DOI: 10.15252/embj.201694831

Contribution statement

The data presented in this doctoral thesis were acquired from June 2015 until May 2020 in the laboratory of Dr. Boris Pfander (MPI Biochemistry, Martinsried, Munich) and are published in the listed publications.

Publication 1 | Bittmann et al. (2020) eLife

In this publication we established an advanced toolbox of cell cycle tags and applied the tags to the question of cell cycle regulation of the structure-selective endonucleases Mus81-Mms4 and Yen1. This paper constitutes the main part of my doctoral studies. I conceived the study together with Boris Pfander and designed/performed all experiments except for 2D, 2 - supplement 3, 5 B-D, which were performed by collaborators of our lab (Lorenzo Galanti, Silas Amarell) and the lab of Joao Matos (Rokas Grigaitis). I prepared all the figures and edited the manuscript.

Publication 2 | Princz et al., (2017) EMBO J

In this paper we established an additional layer of Mus81-Mms4 cell cycle control by the cell cycle kinase Dbf4-Cdc7 and the Rtt107 scaffold protein. I established the *in vivo* assay for the analysis of recombination outcomes and performed experiments in 4F and 7B. I further helped with experiments during the revision period and commented on the manuscript.

Abbreviations

BIR	break induced replication
BLM	Bloom helicase
CDK	cyclin dependent kinase
CFS	common fragile site
CO	crossover
CPT	camptothecin
DDK	Dbf4-dependent kinase (Dbf4-Cdc7)
DDT	DNA damage tolerance
DSB	double-strand break
DSBR	double-strand break repair
(d)HJ	(double) Holliday junction
gRNA	guide RNA
HR	homologous recombination
HU	hydroxy urea
IR	ionizing radiation
JM	joint molecule
MMS	methyl methanosulfonate
MRX	Mre11-Rad50-Xrs2
NHEJ	non-homologous end joining
NCO	non-crossover
nt	nucleotide
PAM	protospacer adjacent motif
ROS	reactive oxygen species
SCJ	sister chromatid junction
SDSA	synthesis-dependent strand annealing
SSB	single-strand break
ssDNA	single-strand DNA
SSE	structure-selective endonuclease
STR	Sgs1-Top3-Rmi1
TALEN	TAL effector nuclease
TS	template switch
TLS	translesion synthesis
ZFN	zink-finger nuclease

Summary

The eukaryotic cell cycle is a complex process that coordinates protein function with the changing requirements of the different cell cycle phases. Many proteins are therefore regulated in a cell cycle-specific manner to make them available/active at a specific cell cycle phase, or prevent their action at other phases. Two proteins regulated in such a cell cycle-specific manner are the structure-selective endonucleases (SSEs) Mus81-Mms4 and Yen1 – repair factors required for the removal of DNA structures arising during homologous recombination (HR). Research in the last years thereby identified a variety of regulatory pathways leading to cell cycle-specific upregulation of the Mus81-Mms4 and Yen1 catalytic activity during M-phase. Despite accumulating evidence that the catalytic activity of the two SSEs is cell cycle-regulated, it remained elusive at which cell cycle phase they would exhibit their key function and how the different regulatory mechanisms upregulating Mus81-Mms4 and Yen1 during M-phase are working together.

To address these questions, we developed an advanced toolbox of cell cycle tags which allowed us to restrict the expression of *Saccharomyces cerevisiae* Mus81-Mms4 and Yen1 to different cell cycle phases and thus analyze at which cell cycle phase these SSEs exhibit their key function. The advanced toolbox of cell cycle tags generally refines the methodology of cell cycle tags and overcomes critical limitations observed for previous cell cycle tag systems, such as the limited number of cell cycle tag constructs that did not allow adaption of expression levels. We circumvented this problem using genetic approaches like chimeric protein fusions, 5´UTR truncations and out-of-frame ATGs which resulted in a toolbox of 46 cell cycle tag constructs with a broad range of expression levels. In general, these advancements will help to answer the question of cell cycle regulation for many proteins and, more specifically, allowed us to address this question for the SSEs Mus81-Mms4 and Yen1.

Applying the advanced cell cycle tag toolbox to Mus81-Mms4 and Yen1, we were able to restrict their expression to different cell cycle phases and attribute their key function to M-phase. Furthermore, we used the approach to reinstall cell cycle restriction to deregulated SSE versions, which highlights the importance of restricting SSE function to M-phase as their premature function during S-phase interferes with replication progression. As such, the observed function in M-phase matches the temporal regulation of the catalytic activity of Mus81-Mms4 and Yen1 which has been shown to be high in M-phase. For Mus81-Mms4, this upregulation of the catalytic activity is known to depend on phosphorylation by the cell cycle kinases CDK (cyclin-dependent kinase) and Cdc5 as well as on the formation of a scaffold protein complex. Here, we add a new kinase – the cell cycle kinase DDK (Dbf4-dependent kinase) – to this cell cycle regulatory network and gain insights into the interplay between the regulatory mechanisms involved. We establish that the

two regulatory pathways, phosphorylation and scaffold protein complex formation, are highly interdependent and imply a switch-like activation mechanism.

Taken together, our studies contribute to the understanding of the cell cycle regulation of Mus81-Mms4 and Yen1 and introduce an advanced toolbox of cell cycle tags which provides a technical source for studying cell cycle-regulated processes in general.

Introduction

1 Formation of DNA breaks

1.1 Exogenous and endogenous sources

Together with other types of DNA lesions, single- and double-strand breaks (SSBs and DSBs, respectively) build a constant threat for genome integrity. At first glance, the estimated number of 10-50 DSBs one cell encounters per day might feel marginal compared to the overall number of 10^5 lesions every cell potentially faces on a daily basis (Vilenchik and Knudson, 2003, Ciccia and Elledge, 2010). Nonetheless, due to the potential of evoking genome rearrangements and chromosomal aberrations, DSBs are considered as extremely toxic lesions. Consequently, even a single DSB is sufficient to block replication and arrest the cell cycle resulting in a window of time for break repair (Bennett et al., 1993, Sandell and Zakian, 1993, Huang et al., 1996). The occurrence of a DSB can have various origins which are typically grouped into exogenous and endogenous sources. In addition, DSBs are also deliberately introduced during programmed cell developmental events and genome editing (**Figure 1**).

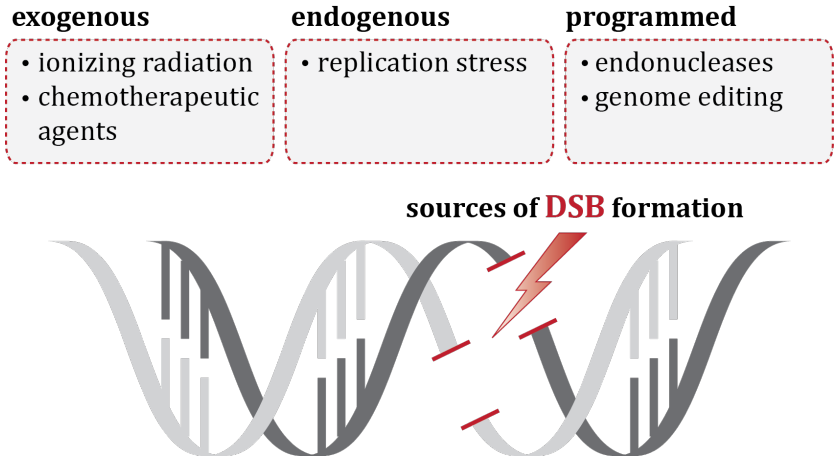

Figure 1: Sources of DSB formation. DSBs are produced by exogenous or endogenous factors and can also be deliberately introduced. Common exogenous factors are ionizing radiation and chemotherapeutic agents, while replication stress constitutes the main endogenous source for the production of DSBs. In addition, programmed DSB formation involves the activity of endonucleases during programmed cell developmental events and genome editing.

Common exogenous sources that are known to lead to DSB formation and are therefore exploited during cancer therapy are chemotherapeutic drugs (like DNA alkylating agents, topoisomerase inhibitors, crosslinking agents or radiomimetic compounds) and ionizing radiation (IR) (Helleday et al., 2008). Besides the usage during radiotherapy, cosmic rays and the decay of radioactive isotopes present natural sources of IR. High-energy particles and photons present in ionizing rays lead to the formation of DNA breaks (both SSBs and DSBs) either directly during their interaction with the DNA molecule or indirectly upon radiolysis of water molecules and generation of reactive oxygen species (ROS) (Ward, 1988). ROS are highly energetic

molecules which can react with DNA to form oxidized bases or SSBs. In contrast to ROS produced during normal cell metabolism where the formation happens randomly distributed across the entire cell, the production of ROS in response to IR is highly localized to specific regions. The consequence is an enrichment, also referred to as clustering, of DNA lesions and SSBs at specific genomic loci which bears a high risk of DSB formation if two SSBs are positioned on complementary DNA strands in close proximity (Mehta and Haber, 2014, Cannan and Pederson, 2016).

In contrast, DSBs can also arise endogenously and are in that case often associated with replication. Due to the yet unfinished genome duplication, replication associated DSBs are typically single-ended which are different from the classical double-ended DSBs arising in the context of a fully replicated genome and will influence the repair decision later on (note that the difference lies in the availability of the second DSB end; see chapter 2.2 for the repair of single-ended DSBs). Single-ended DSB formation during replication is either derived from replication forks encountering single-stranded DNA (ssDNA) gaps (induced for example by IR or the topoisomerase inhibitor camptothecin (CPT)) or replication fork collapse of stalled forks whereby fork stalling can result from a variety of natural impediments: aberrant DNA structures, sites of chromatin compaction, DNA protein barriers or the transcription machinery (Aguilera and Gaillard, 2014, Hamperl and Cimprich, 2016, Berti and Vindigni, 2016). In addition, replication fork stalling can be induced by extrinsic factors like the alkylating agent methyl methanesulfonate (MMS) or the ribonuclease reductase inhibitor hydroxyurea (HU) (Mehta and Haber, 2014). Together, these factors interrupt DNA replication so frequently that even leading strand synthesis is considered discontinuous as the stalling process might require repriming of DNA synthesis distal to the lesion (Lehmann and Fuchs, 2006, Branzei and Foiani, 2010).

1.2 Programmed DSBs

While DNA breaks can be pathological on the one hand and proper repair is critical to ensure cell survival, controlled induction of DSBs during several biological processes on the other hand is important to enable genetic diversity. Such programmed DSBs occur for example in ciliates during programmed genomic rearrangements, in mammals during lymphocyte development, in yeast during mating type switching and mitochondrial intron mobility as well as in eukaryotes during meiotic recombination. These DSBs are induced by the PiggyMac transposase, the Rag1/2 recombinase, the HO and I-Sce1 endonuclease as well as the Spo11 recombinase, respectively (Betermier et al., 2019).

Interestingly, the site-specific cleavage potential of these endonucleases – especially of HO and I-Sce1 – contributed tremendously to our knowledge concerning DSB repair. The introduction of galactose-inducible versions of HO and I-Sce1 allowed to synchronously induce DSBs in budding yeast and monitor the subsequent repair events (Jensen et al., 1983, Connolly et al., 1988,

Plessis et al., 1992, Jasin and Haber, 2016). These studies gave insights into various processes happening after DSB induction, including the disentanglement of Holliday junction (HJ) structures that can arise during homologous recombination (HR)-dependent repair of a DSB which is a central process in this thesis (Schwartz and Heyer, 2011, Wu and Hickson, 2003, Ira et al., 2003).

Furthermore, induced expression of a site-specific DSB by I-Sce1 led to the observation that DSB formation increases gene targeting rates (Rouet et al., 1994, Choulika et al., 1995, Smih et al., 1995, Jasin, 1996, Donoho et al., 1998) and laid the foundation for the development of advanced genome editing techniques. Given the limited number of genes that could be targeted by the use of site-specific endonucleases, further efforts during the development of genome editing techniques focused on increasing the flexibility of the DNA recognition process. Today, two principles are commonly used to specifically and flexibly target endonucleases to the genomic region of choice: first, fusion of the endonuclease to the modular DNA binding domains of zinc fingers or TAL effector proteins which can be varied to bind specific DNA sequences; second, targeting of the endonuclease via specific RNA sequences which find their target sequence by Watson-Crick base pairing during CRISPR/Cas9. DNA binding domains of zinc fingers and TAL effector proteins possess a modular structure and can therefore be adapted to recognize different base sequences (Miller et al., 1985, Nardelli et al., 1991, Pavletich and Pabo, 1991, Boch et al., 2009, Moscou and Bogdanove, 2009, Deng et al., 2012). Fused to an endonuclease, the resulting zinc finger nuclease (ZFN) or TAL effector nuclease (TALEN) is efficiently targeted to a specific genomic locus (Kim et al., 1996, Urnov et al., 2005, Christian et al., 2010, Urnov et al., 2010). While adaption of the DNA binding modules of ZFN´s or TALEN´s involves time consuming cloning procedures, the simplicity of targeting by Watson-Crick base pairing in form of CRISPR/Cas9 has revolutionized our genome editing possibilities (Jinek et al., 2012, Gasiunas et al., 2012, Cong et al., 2013, Mali et al., 2013). Expression of a sequence-specific guide RNA (gRNA) efficiently targets the Cas9 endonuclease to the genomic locus of choice by annealing to the target sequence. Binding of Cas9 to the DNA further requires the presence of a protospacer adjacent motif (PAM), a short nucleotide (nt) sequence (usually comprising 2-6 nt) specific to the utilised Cas9 protein, directly adjacent to the gRNA target sequence. Binding of Cas9 to the PAM coordinates its nuclease domains on the DNA sequence and initiates the gene editing process by introduction of a DSB (Deveau et al., 2008).

Overall, DSBs are not only a consequence of coincidental DNA damaging processes but are also deliberately introduced during various biological processes and by genome editing techniques (**Figure 1**).

1.3 Repair choice

Independent from the source of DSB formation, subsequent repair of the break is important to avoid chromosomal aberrations, ensure cell survival and provides the basis for altering the DNA

during genome editing. Generally, DSBs can be repaired by two main pathways and the choice between them is influenced by the cellular context of the cell. The two pathways competing for the repair procedure at a DSB are homologous recombination (HR) and non-homologous end-joining (NHEJ) (note that this applies to DSBs where both ends of the DSB can engage in the repair process; see chapter 2.2 for the repair of single-ended DSBs and ssDNA gaps). Since the two mechanisms are overall well conserved, I will focus on the *Saccharomyces cerevisiae* proteins during this thesis and only mention differences to the mammalian system where considered necessary.

Mechanistically, NHEJ involves the direct re-ligation of the two DSB ends and does not rely on a repair template (**Figure 2**). Direct re-ligation requires binding by the end-protection factors Yku70 and Yku80 (Yku complex) which inhibits extensive degradation of the DSB ends and leads to recruitment of further NHEJ factors including DNA ligase IV (Dnl4) (Wilson et al., 1997, Daley et al., 2005). Processing of the DSB ends and ligation by Dnl4 frequently involves small insertions or deletions and NHEJ is therefore considered intrinsically error-prone.

In contrast, HR uses a homologous template sequence to copy the missing information which results in high repair fidelity. As the homologous template usually presents the sister chromatid (Kadyk and Hartwell, 1992, Liang et al., 1998, Johnson and Jasin, 2000), HR is restricted to the S- and G2/M-phases of the cell cycle where such a second copy of the chromatid is present while the template independent NHEJ pathway can act throughout the cell cycle (**Figure 2**). Interestingly, in mammalian cells, this cell cycle-specific initiation of HR is locally coupled to the presence of the sister chromatid by recruitment of HR factors specifically to post-replicative chromatin marks (Duro et al., 2010, O'Donnell et al., 2010, Saredi et al., 2016, Nakamura et al., 2019). Throughout eukaryotes, repair pathway choice is adapted to the cell cycle phase by the cell cycle kinase CDK (cyclin-dependent kinase) (Mathiasen and Lisby, 2014, Hustedt and Durocher, 2016). CDK activity rises once cells enter a new round of cell division and start replicating their genome. Consequently, CDK-mediated phosphorylation and activation of HR factors is restricted to S- and G2/M-phase thus limiting HR function to these cell cycle phases. The critical step that determines pathway choice between NHEJ and HR is the initiation of resection – the nucleolytic digestion of the 5´strands of DSB ends (Symington, 2016) (**Figure 2**). While resection is a critical intermediate for HR, it prevents re-ligation of the DNA ends and inevitably excludes repair by NHEJ. Not surprisingly, CDK-dependent regulation of repair pathway choice therefore targets (and activates) resection factors and thus preferentially channels the repair towards HR during S- and G2/M-phase (Huertas and Jackson, 2009, Chen et al., 2011, Falck et al., 2012, Wohlbold et al., 2012, Ferretti et al., 2013, Cannavo and Cejka, 2014, Tomimatsu et al., 2014, Chen et al., 2016, Hustedt and Durocher, 2016, Symington, 2016, Bantele et al., 2017).

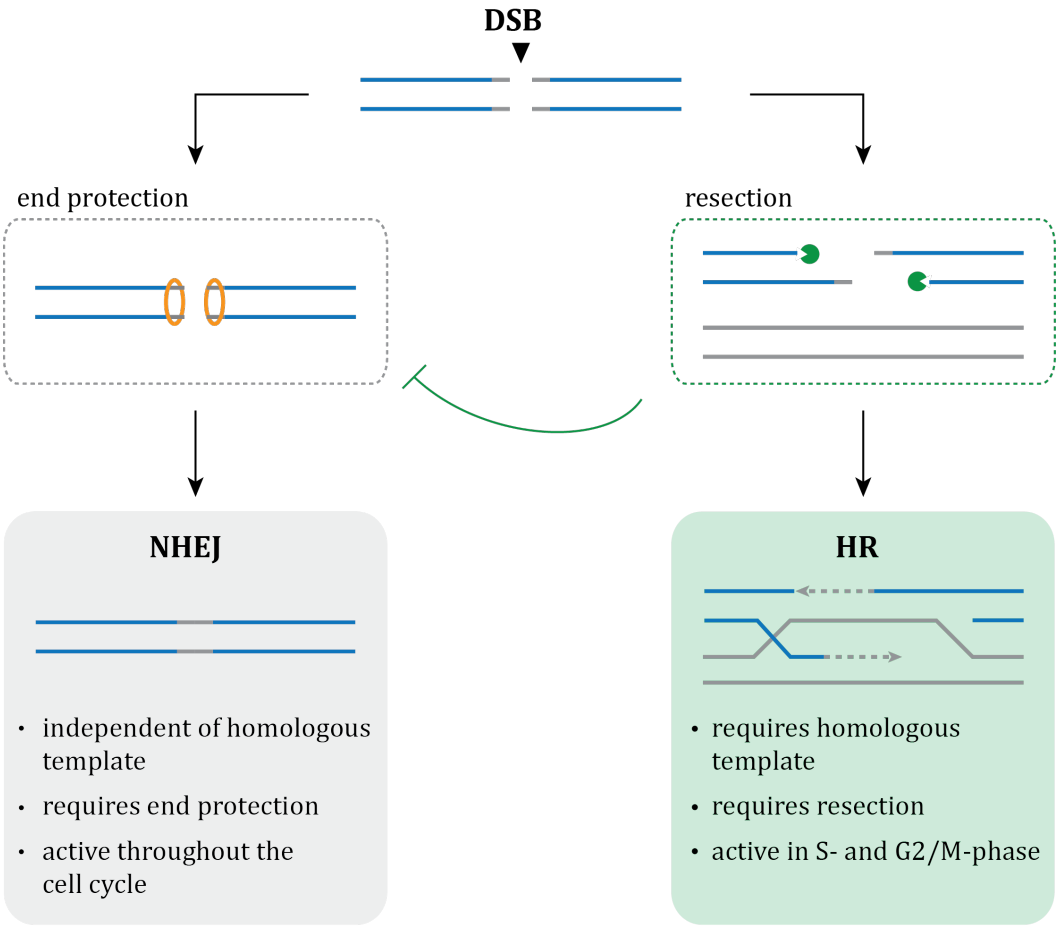

Figure 2: DSB repair pathway choice. At a DSB, HR and NHEJ are competing for the repair procedure. NHEJ, due to the re-ligation process involved, is independent of a homologous template and requires protection of the DSB ends by the KU complex to avoid extensive processing by resection nucleases. HR, in contrast, requires a homologous chromatid as template sequence and is initiated by resection of the 5´strands of both DSB ends. Resection excludes re-ligation of the DSB ends by NHEJ and thus constitutes the pathway committing step. While HR is active during S- and G2/M-phase where a homologous template in form of the sister chromatid is present, NHEJ can in principal act throughout the cell cycle.

In addition to the competition with NHEJ and the repair of double-ended DSBs, HR-dependent processes are also involved in the repair of single-ended DSBs or ssDNA gaps arising during the bypass of stalled replication forks. The different nature of the lesions thereby demands adaption of the HR process which leads to the co-existence of several HR sub-pathways sharing similar core mechanisms. In the following chapter I will therefore describe the individual steps involved in a typical HR process as well as highlight the variety of HR sub-pathways acting at different DNA lesions.

2 Repair of DNA breaks by homologous recombination

2.1 Mechanisms of homologous recombination at a double-ended DSB

All HR-dependent mechanisms share four core biochemical features: (1) resection of the DSB ends, (2) homology search and invasion of the resected DNA end(s) into the template sequence, (3) DNA synthesis and (4) disentanglement of HR intermediates. As HR is best described during the repair of DSBs where both DSB ends are available for the repair procedure, the individual steps required for HR will be explained in detail on the example of such a double-ended DSB (**Figure 3**).

The first step – resection of DSB ends – is initiated by an endonucleolytic incision close to the break site (Cannavo and Cejka, 2014, Anand et al., 2016, Deshpande et al., 2016, Reginato et al., 2017). The Mre11 endonuclease together with Rad50, Xrs2 (MRX complex) and the cofactor Sae2 is among the first proteins observed at DSB sites (Nelms et al., 1998, Lisby et al., 2004) and responsible for the endonucleolytic incision that initiates the resection process (Cannavo and Cejka, 2014, Anand et al., 2016, Deshpande et al., 2016, Reginato et al., 2017). Starting from the endonucleolytic cut, resection proceeds in two directions: first, the additional exonuclease function of the MRX complex proceeds back to the DSB site (3´-5´) which is termed short-range resection and results in a short patch of ssDNA close to the break site (Trujillo et al., 1998, Mimitou and Symington, 2008, Zhu et al., 2008, Deshpande et al., 2016, Symington, 2016); second, long-range resection originating at the Mre11 incision side removes the DNA in 5´-3´direction and thus creates a long 3´ssDNA tail which can be used for homology search (**Figure 3**, step (1) - resection). The long-range resection machinery involves two independent enzymatic activities which are the exonuclease Exo1 and the helicase/nuclease activities of the Sgs1-Top3-Rmi1 (STR) complex in conjunction with Dna2 (Gravel et al., 2008, Mimitou and Symington, 2008, Zhu et al., 2008, Cejka et al., 2010a, Niu et al., 2010, Symington, 2016). While Dna2 in principle harbours both 3´-5´and 5´-3´ nuclease activity (Masuda-Sasa et al., 2006), the concomitant coverage of the 3´ssDNA overhang with RPA inhibits the 3´-5´nuclease function of Dna2 and thus drives the long-range resection process away from the break (Cejka et al., 2010a, Niu et al., 2010). Coating of the 3´ssDNA overhang by RPA furthermore prevents the formation of DNA secondary structures and signals the repair process to the checkpoint machinery (Brush et al., 1996, Zou and Elledge, 2003, Nguyen et al., 2014, Deshpande et al., 2017).

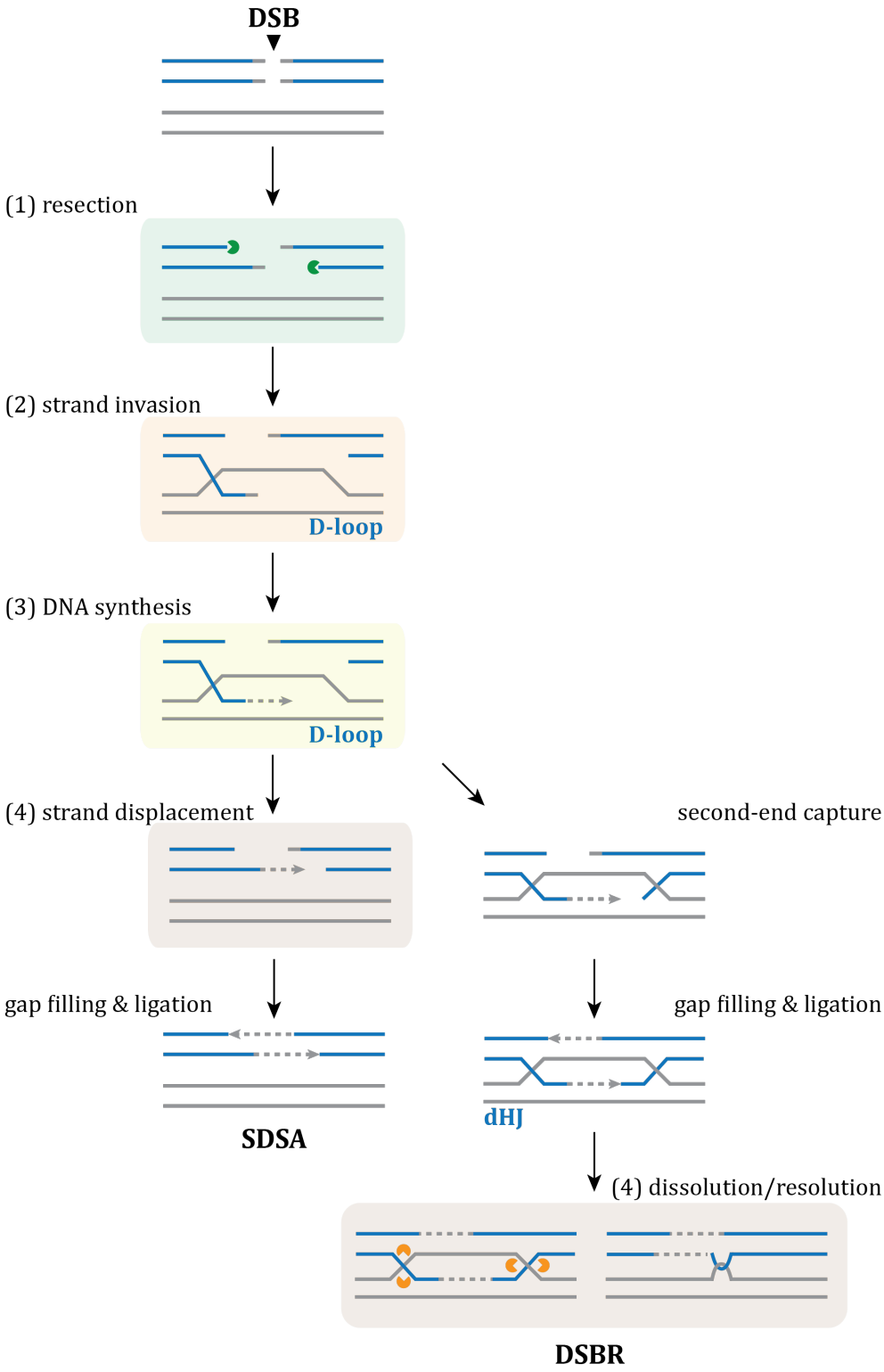

Figure 3: HR-dependent repair of a double-ended DSB. The repair of a double-ended DSB by HR can be channeled into two different pathways, SDSA or DSBR. The first steps are common to both pathways and involve the resection of the 5´ DNA strands (step (1), resection – green box) to result in 3´ssDNA overhangs which can undergo homology search and invade into the homologous template (step (2), strand invasion – orange box). The resulting D-loop structure facilitates DNA synthesis (step (3), DNA synthesis – yellow box) to restore the information hampered by the DSB and constitutes the point of divergence for the SDSA and DSBR sub-pathways. SDSA and DSBR differ in the last steps of the HR procedure, the disentanglement of JM structures (steps (4) – brown boxes). During SDSA the invaded strand gets displaced from the D-loop structure after DNA synthesis and reanneals with the second DSB end (step (4), strand displacement). DSBR, on the contrary, involves capture and invasion of the second DSB end leading to the formation of a dHJ, a JM which links both DNA molecules and needs to be removed by dissolution or resolution activities (step (4), dissolution/resolution). Recombination intermediates in form of JMs (D-loop, dHJ) are marked with blue writing.

Subsequent exchange of RPA with Rad51 then builds the substrate for the second step of the HR process – homology search and invasion of the resected DNA end. Thereby, the exchange of RPA with Rad51 depends on the function of several mediator proteins with core functions of Rad52 in yeast and BRCA2 in human cells (Sung, 1997, Shinohara and Ogawa, 1998, New et al., 1998, Sugiyama and Kowalczykowski, 2002, Jensen et al., 2010, Liu et al., 2010, Thorslund et al., 2010, Zelensky et al., 2014). The so-called presynaptic filament (ssDNA coated with Rad51) exhibits an extended DNA structure (Ogawa et al., 1993, Sung and Robberson, 1995, Yu et al., 2001), which allows the Rad51 recombinase to efficiently scan the template DNA and facilitate base pairing at a site of homology (Wright et al., 2018) (**Figure 3**, step (2) – strand invasion). Base pairing at a homologous locus leads to the formation of a three stranded DNA structure where the invading strand hybridizes with one strand of the template duplex while the second strand is displaced in a D-loop structure (San Filippo et al., 2008). This D-loop tethers the two DNA molecules together and forms a joint-molecule (JM) structure – a typical recombination intermediate linking the two DNA molecules involved in the HR process.

Starting from the invaded 3´end, DNA synthesis initiates and extends the D-loop in the third step of the HR process (**Figure 3**, step (3) – DNA synthesis). During DNA synthesis the missing information is copied from the template sequence by the polymerases Polδ and Polε with the help of the replication factors PCNA and Dpb11. Notably, other core replication proteins like ORC, Dbf4-Cdc7, the MCM complex, Cdc45 or DNA Polα are dispensable for HR-associated DNA synthesis (Wang et al., 2004, Li et al., 2009, Germann et al., 2011, Hicks et al., 2011, Sebesta et al., 2011).

After DNA synthesis has initiated, HR can differentiate into two pathways in case both ends of the DSB are available (see chapter 2.2 for description of HR at single-ended DSBs): (1) synthesis-dependent strand annealing (SDSA) or (2) double-strand break repair (DSBR). The two pathways hereby mainly differ in the nature of the involved JM structures and the enzymatic activities required for the last step of HR – disentanglement of these JMs.

During SDSA (**Figure 3**, SDSA), the JM in form of the D-loop is counteracted by helicases like Srs2, Mph1 or Sgs1 (van Brabant et al., 2000, Ira et al., 2003, Bachrati et al., 2006, Prakash et al., 2009). The invaded DSB end thereby gets displaced from the template (**Figure 3**, SDSA, step (4) – strand displacement) and can reanneal with the second DSB end in case DNA synthesis has restored sufficient homologous information. Prior to reannealing with the second DSB end the processes of D-loop invasion and disruption can alternate several times. This allows reannealing of the displaced strand to the second DSB end as soon as a sufficient amount of the homologous sequence has been copied and thus might provide a mechanism to limit DNA synthesis (Wright et al., 2018). After reannealing, the remaining gaps are filled by further DNA synthesis prior to ligation of the DSB ends (**Figure 3**, SDSA, gap filling and ligation).

Absent displacement of the D-loop and continuing DNA synthesis, in contrast, channels the repair towards the second HR mechanism acting on double-ended DSBs – DSBR (**Figure 3**, DSBR). During DSBR, invasion of the second DSB end into the D-loop (**Figure 3**, DSBR, second end capture) and subsequent ligation of the DSB end leads to the formation of a dHJ (**Figure 3**, DSBR, gap filling and ligation), a JM that covalently links the two DNA strands (Holliday, 1964, Bzymek et al., 2010, Heyer et al., 2010). Due to the structurally different nature of a dHJ compared to the D-loop that gets displaced by helicases during SDSA, their disentanglement requires additional enzymatic activities which can be grouped into (1) dissolution and (2) resolution activities (**Figure 3**, DSBR, step (4) dissolution/resolution). Together, the pathways of dissolution and resolution allow the timely removal of dHJs and will be explained in more detail in chapter 3.

2.2 Homologous recombination during replication

Besides the classical HR pathways discussed in the previous chapter which are involved in the repair of double-ended DSBs, HR-dependent mechanisms also play an important role in the repair of replication-associated lesions. Although the core principals are comparable to HR acting at double-ended DSBs, the structural difference of HR substrates arising during replication demand adaption of the particular HR process. Therefore, several sub-pathways of HR can be classified in response to replication-associated lesions.

As a consequence of a replication fork encountering a ssDNA break or being stalled by an impediment on the DNA (see chapter 1.1 for sources of replication fork stalling) (**Figure 4**, first column), three replication-dependent structures can be distinguished that require repair by HR-dependent mechanisms: (a) single-ended DSBs, (b) ssDNA gaps and (c) reversed forks (**Figure 4**, second column). Individually, these structures constitute the starting point for the strand invasion process that initiates the corresponding HR sub-pathway (**Figure 4**, third column).

Single-ended DSBs (**Figure 4**, (a) single-ended DSB) arise during the replication of an SSB containing DNA template or after the collapse of a stalled replication fork and initiate an HR process termed break-induced replication (BIR) (**Figure 4**). In contrast to the repair of double-ended DSBs by SDSA or DSBR where only a short patch of DNA gets synthesized, during BIR, robust replication is established which copies a large fraction of the template chromosome in a conservative manner (Donnianni and Symington, 2013, Saini et al., 2013). Due to the missing second DSB end which could anneal to the synthesized DNA or join into the D-loop, DNA synthesis during BIR proceeds until the end of the chromosome or until it encounters another replication fork (Mayle et al., 2015). This bears the risk of loss of heterozygosity (LOH) of large proportions of the chromosome. In addition, the conservative replication mechanism together with exposure of long ssDNA tracts during the replication process leads to an increased rate of mutagenesis and genome rearrangements (Smith et al., 2007, Deem et al., 2008, Jain et al., 2009, Deem et al., 2011, Pardo and Aguilera, 2012, Sakofsky et al., 2014, Vasan et al., 2014, Sakofsky et al., 2015). Initiation

of BIR is therefore suppressed for several hours (5-6h) which usually results in out-competition of BIR by SDSA or DSBR in case a second DSB end is present (Sugawara et al., 2003, Malkova et al., 2005, Lydeard et al., 2007, Jain et al., 2009, Mehta et al., 2017). As single-ended DSBs are typically associated with replication (in principal, single-ended DSBs can also arise in case the second DSB end does not share homology to the template sequence), BIR commonly initiates in S-phase but can also occur in M-phase, for example, when replication is delayed at difficult to replicate regions like common fragile sites (CFS) (Minocherhomji et al., 2015, Bhowmick et al., 2016).

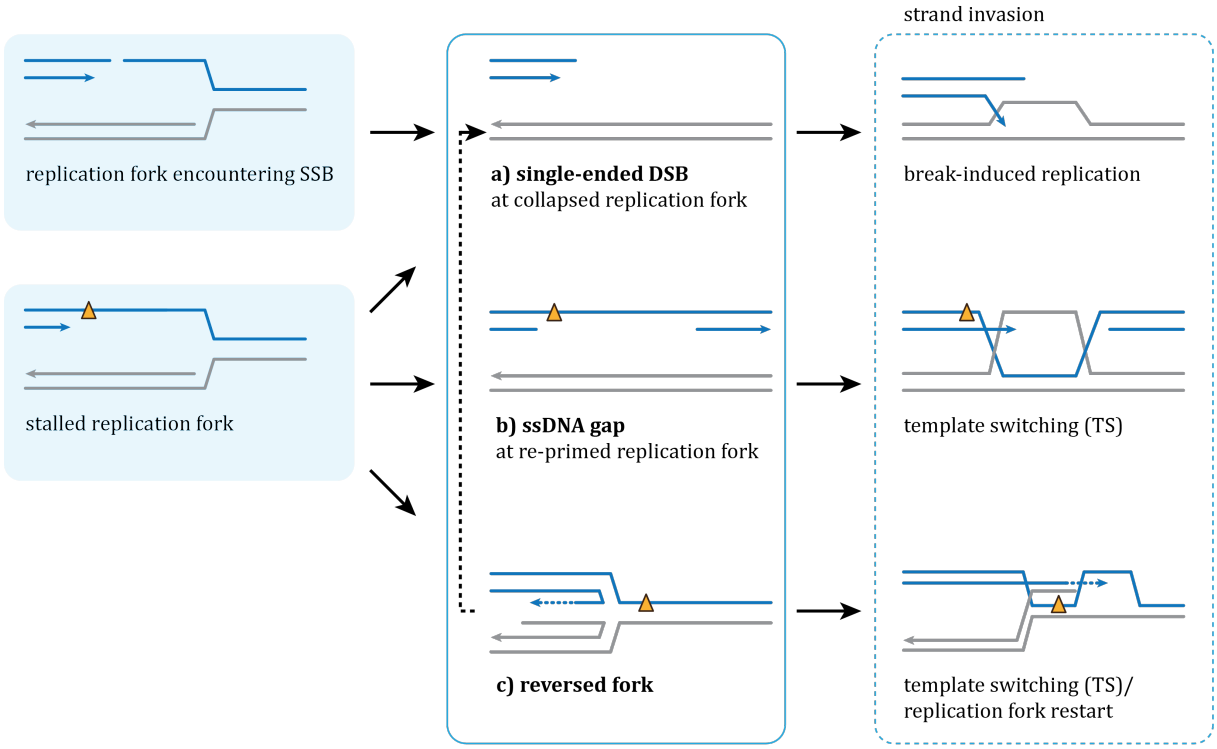

Figure 4: Sub-pathways of HR-dependent repair in response to replication associated DNA lesions. Three typical DNA structures arise as a consequence of a replication fork encountering an SSB or replication fork stalling (first column): a) single-ended DSBs, b) ssDNA gaps and c) reversed forks (second column). Strand invasion by the different structures initiates the HR sub-pathways of break-induced replication, template switching and replication fork restart, respectively (third column).

ssDNA gaps (**Figure 4**, (b) ssDNA gap) are formed during the tolerance of replication blocking lesions (DNA damage tolerance, DDT) and can initiate template switching (TS). During TS, the strand invasion process is started by annealing of the ssDNA gap with the parental strand of the sister chromatid as suggested by recent electron microscopic studies (Giannattasio et al., 2014). Similar to the repair of DSBs, the resulting D-loop can either be disrupted during SDSA or mature into a dHJ. Disruption of the D-loop and dissolution/resolution of the dHJ structure thereby rely on similar enzymatic activities as during DSB repair (Liberi et al., 2005, Ashton et al., 2011, Mankouri et al., 2011, Szakal and Branzei, 2013, Giannattasio et al., 2014) (see chapter 3). Alternative to TS, ssDNA gaps can be filled by specialized polymerases in a process termed translesion synthesis (TLS). Due to the use of low fidelity polymerases TLS is considered error-

prone, while the HR-based TS mechanism constitutes the error-free pathway during DDT. The decision between the two pathways is thereby regulated locally at the corresponding replication fork and involves modification of the replication factor PCNA by the ubiquitylation activities of Rad6-Rad18, Rad5 and Ubc13-Mms2 (Hoege et al., 2002, Stelter and Ulrich, 2003, Branzei et al., 2004, Haracska et al., 2004, Kannouche et al., 2004, Papouli et al., 2005, Pfander et al., 2005, Zhang and Lawrence, 2005). Interestingly, although the process of repairing ssDNA gaps by TS or TLS preferentially takes places directly during S-phase, both pathways can also act timely uncoupled from the replication fork and repair ssDNA gaps efficiently later in M-phase (Daigaku et al., 2010, Karras and Jentsch, 2010).

Additionally, the bypass of a replication stalling lesion by HR-dependent mechanisms can be initiated from a reversed replication fork (**Figure 4**, (c) reversed fork). Fork reversal can initiate upon stalling of the replication fork and involves the coordinated displacement and reannealing of the nascent DNA strands to form a HJ-like structure, often also referred to as chicken-foot structure (Sogo et al., 2002, Ray Chaudhuri et al., 2012). The reversed fork can be restarted by HR either directly by invasion of the regressed arm into a template sequence and initiation of a template switch event or by nuclease-dependent fork breakage which would result in a single-ended DSB (**Figure 4**, (a) single-ended DSB) in turn initiating a BIR-like procedure (Branzei and Foiani, 2010, Saugar et al., 2014). Notably, the evidence for fork reversal in eukaryotes was sparse for a long time and detection of reversed forks exclusively in checkpoint deficient yeast cells led to the proposal that fork reversal is a pathological process resulting from replisome inactivation and fork collapse (Lopes et al., 2001, Sogo et al., 2002). By now, the existence of reversed forks has been validated in checkpoint-proficient cells as a general response to enhanced replication stress (Zellweger et al., 2015, Ray Chaudhuri et al., 2012). Although these data revealed reversed forks in both yeast and human cells, fork reversal generally seems to be a more prominent mechanism in human cells and the overall usage of replication fork reversal during replication restart is still a matter of ongoing investigation (Ray Chaudhuri et al., 2012, Neelsen and Lopes, 2015, Zellweger et al., 2015, Branzei and Szakal, 2016).

Together, HR-dependent processes build a valuable source for the recovery of replication-dependent lesions arising due to the collapse or stalling of replication forks (**Figure 4**). Despite the adaption of the individual pathways to the nature of the lesion and the cellular context, an involvement of similar recombination structures can be observed independently of the HR sub-pathway implicating an overall similar mechanism for the repair of different lesions from a homologous template.

3 Resolution of recombination intermediates

3.1 Dissolution and resolution

All HR-based processes during DSB repair or at the replication fork result in the formation of JMs in form of D-loops or HJs. Although JMs constitute an important intermediate during HR, their subsequent removal is crucial for avoiding interference with the separation of sister-chromatids during mitosis. In fact, persistent JM structures are known to entail anaphase bridges – DNA fibres connecting the dividing chromatin masses – (Chan et al., 2007, Mankouri et al., 2013, Germann et al., 2014, Gritenaite et al., 2014) and thus underline the importance of a timely removal of JM structures.

JMs are removed by different enzymatic activities depending on the nature of the JM structure. D-loops are usually counteracted early on by helicase activities during SDSA (van Brabant et al., 2000, Ira et al., 2003, Bachrati et al., 2006, Prakash et al., 2009). However, some D-loops escape this disengagement process and mature into dHJs when the second end of the DSB or post-replicative ssDNA gap invades into the D-loop (Holliday, 1964, Szostak et al., 1983, Bzymek et al., 2010, Giannattasio et al., 2014) (see chapter 2.1 for a more detailed description of the maturation of dHJs). The removal of dHJs relies on two alternative pathways: (1) dissolution and (2) resolution (**Figure 5**). These two pathways not only differ in the enzymatic activities involved but also in their ability to result in crossing-overs. While dissolution produces exclusively non-crossover (NCO) outcomes, resolution can additionally create cross-overs (CO).

Mechanistically, dissolution produces NCO outcomes by implying a two-step process; the dHJ is first converted into a hemicatenane by convergent branch migration, which is subsequently cleaved and resealed by decatenation processes (Cejka et al., 2010b, Chen et al., 2014, Bizard and Hickson, 2014) (**Figure 5**, (1) dissolution). In this context, dissolution uses the combined activity of the helicase Sgs1 and the topoisomerase Top3 that act together in a single protein complex called the "dissolvasome" or STR (Sgs1-Top3-Rmi1) complex (Bizard and Hickson, 2014). Interestingly, deletion of any of the STR components leads to an increased CO rate (Ira et al., 2003, Wu and Hickson, 2003) indicating that dissolution acts in parallel with the CO producing resolution pathway and limits the number of JMs that are processed into crossing-overs. The importance of counteracting crossing-over events with dissolution activities also becomes emphasized by the phenotypes associated with a rare genetic disorder called Bloom syndrome. Bloom (BLM) is the human homolog of the Sgs1 helicase and is mutated in Bloom syndrome patients. These mutations lead to elevated levels of sister chromatid exchanges (SCEs) derived from enhanced levels of crossing-over events (German et al., 1974, Chaganti et al., 1974).

The enhanced crossing-over rates in *BLM* mutant cells can thereby be accounted to the second pathway required for the removal of JM structures, the resolution pathway, as depletion of resolution factors in *BLM* mutant cells leads to a concomitant decrease of SCEs (Wyatt et al.,

2013). In addition, the co-depletion or -deletion of resolution factors in dissolution defective cells (for example *BLM* negative human cells or *sgs1Δ* yeast cells) is accompanied by high mortality rates in yeast and human cells placing resolution as alternative pathway to dissolution (Kaliraman et al., 2001, Mullen et al., 2001, Wechsler et al., 2011, Wyatt et al., 2013). The enzymatic activities involved in resolution are structure-selective endonucleases (SSEs) also referred to as resolvases. SSEs process specific DNA secondary structures and in budding yeast, the two main SSEs involved in the resolution of branched HR intermediates are Mus81-Mms4 and Yen1 (Matos and West, 2014, Blanco and Matos, 2015). In mammalian cells a third SSE, SLX1-SLX4, acts in conjunction with the human homolog of Mus81-Mms4, MUS81-EME1 (Guervilly and Gaillard, 2018). All three resolvases display distinct substrate specificities and together are capable of processing a variety of branched structures including dHJs (Boddy et al., 2001, Kaliraman et al., 2001, Doe et al., 2002, Bastin-Shanower et al., 2003, Ciccia et al., 2003, Fricke and Brill, 2003, Gaillard et al., 2003, Ehmsen and Heyer, 2008, Ip et al., 2008, Jessop and Lichten, 2008, Oh et al., 2008, Munoz et al., 2009, Rass et al., 2010, Wechsler et al., 2011, Saugar et al., 2013, Wyatt et al., 2013, Saugar et al., 2017). Depending on the symmetry of the cutting procedure resolution of a dHJ by SSEs thereby results in a mixture of NCO and CO outcomes (**Figure 5**, (2) resolution).

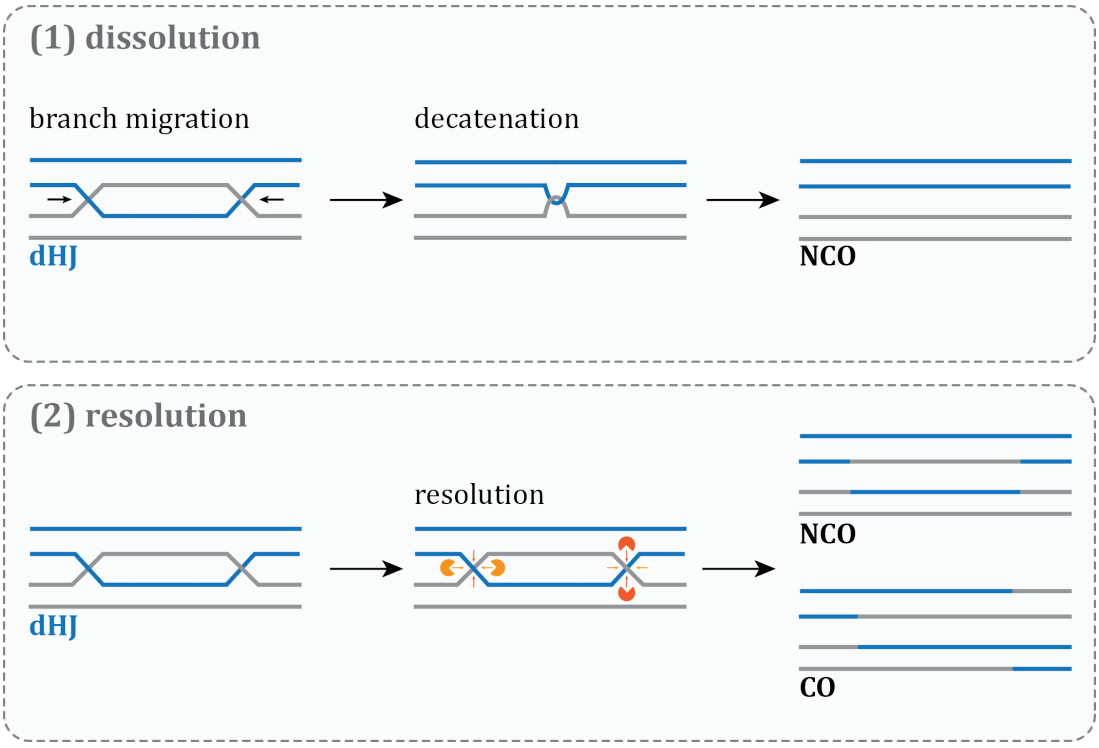

Figure 5: Dissolution and resolution of dHJs. During (1) dissolution, the dHJ is dissolved by the action of the STR complex which catalyzes a consecutive process of branch migration and decatenation resulting exclusively in NCO outcomes. (2) Resolution, in contrast, involves the enzymatic activity of SSEs which can cut the dHJ to result in both NCO and CO outcomes.

3.2 Cell cycle regulation of resolution

Given the significance of limiting the number of CO products, dissolution is currently seen as the default mechanism for removing dHJ structures in mitotically dividing cells while resolution is thought to provide a backup pathway. This hierarchical view is supported by the temporal separation of NCO and CO producing pathways, hence dissolution and resolution activities. While STR dissolves most dHJs in form of NCOs early in the cell cycle (Ira et al., 2003, Dayani et al., 2011), endonucleolytic digestion of remaining JM structures happens at later cell cycle stages (Matos et al., 2011, Gallo-Fernandez et al., 2012, Matos et al., 2013, Szakal and Branzei, 2013) and thus restricts the formation of COs to a short timeframe. How cells are tailoring the involved enzymatic activities to achieve such a hierarchical setup has been a longstanding question in the field and has been addressed extensively in the last years.

The picture emerging from these studies reveals that resolution and thereby CO production is restricted to M-phase and depends on cell cycle-specific phosphorylation/dephosphorylation events of the key resolvases Mus81-Mms4 and Yen1 (Matos et al., 2011, Gallo-Fernandez et al., 2012, Matos et al., 2013, Szakal and Branzei, 2013, Kosugi et al., 2009, Blanco et al., 2014, Eissler et al., 2014, Garcia-Luis et al., 2014) (**Figure 6**).

In the context of Mus81-Mms4, mitotic phosphorylation affects the protein function by two different means: (1) direct upregulation of the enzymatic activity (Matos et al., 2011, Matos et al., 2013, Gallo-Fernandez et al., 2012, Schwartz et al., 2012) and (2) incorporation into a higher order complex comprising several scaffold proteins that might play a role in targeting the endonuclease to its cellular substrates (Gritenaite et al., 2014, Princz et al., 2015) (**Figure 6**, upper left). The first evidence indicating that Mus81-Mms4 activity is regulated in a cell cycle-specific manner was deduced from data derived in meiotic cells where Mus81-Mms4 was found to undergo cell cycle-specific phosphorylation (Matos et al., 2011). Subsequently, it became clear that also in mitosis Mus81-Mms4 undergoes cell cycle-specific phosphorylation on the Mms4 subunit which takes place at the G2/M transition and depends on the two kinases polo-like kinase Cdc5 and cyclin-dependent kinase (CDK) Cdc28 (Matos et al., 2011, Gallo-Fernandez et al., 2012, Matos et al., 2013, Szakal and Branzei, 2013). Notably, mitotic phosphorylation correlates with an upregulation of the catalytic activity towards different model substrates like HJs and replication fork structures. Dephosphorylation, phospho-deficient mutants and the use of immunopurified protein from cell cycle phases where Mms4 is unmodified, on the other hand, abolished the stimulatory effect observed for the catalytic activity (Matos et al., 2011, Gallo-Fernandez et al., 2012, Schwartz et al., 2012, Matos et al., 2013). Collectively, these studies established that phosphorylation of Mus81-Mms4 is directly linked with its catalytic activity whereas the exact molecular mechanism of this upregulation is still a matter of ongoing investigation.

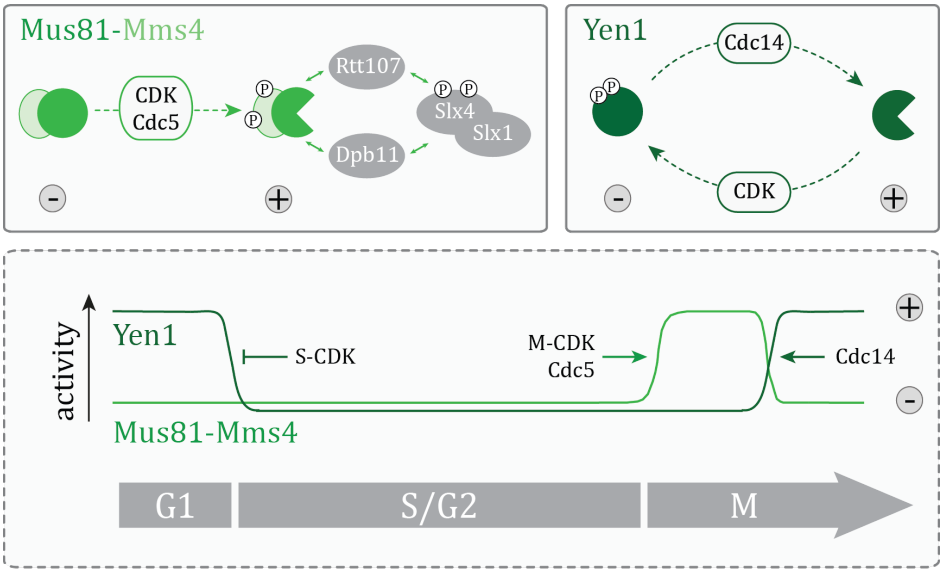

Figure 6: Cell cycle regulation of Mus81-Mms4 and Yen1. Both Mus81-Mms4 and Yen1 are regulated by cell cycle-dependent phosphorylation/dephosphorylation events. Mus81-Mms4 gets activated by CDK- and Cdc5-dependent phosphorylation of the Mms4 subunit at the onset of M-phase (upper left). Simultaneously, M-phase-specific phosphorylation events lead to the formation of a higher order complex comprising the scaffold proteins Dpb11, Rtt107 and Slx1-Slx4 in addition to Mus81-Mms4. Yen1 (upper right) is kept inactive by CDK phosphorylation during S- and early M-phase and becomes active at the transition to anaphase when Cdc14-dependent dephosphorylation removes the inhibitory phosphorylation on Yen1. Together, Mus81-Mms4 and Yen1 become sequentially activated during M-phase (lower).

In addition to the direct influence on the catalytic activity, mitotic phosphorylation of Mms4 leads to the formation of a cell cycle-specific complex comprising several scaffold proteins together with Mus81-Mms4: Dpb11, Slx4 and Rtt107. While Dpb11 and Slx4 associate upon CDK-dependent phosphorylation of Slx4 already during S-phase, Mus81-Mms4 joins the complex after Cdc5-dependent phosphorylation of Mms4 in M-phase (Gritenaite et al., 2014, Princz et al., 2015). In human cells, the association of a similar complex has been observed in M-phase where MUS81-EME1 (the human homolog of Mus81-Mms4) interacts directly with SLX1-SLX4 in a phosphorylation (CDK1 and PLK1)-dependent manner (Wyatt et al., 2013). In contrast to the human SLX1-SLX4-MUS81-MMS4 complex in which the interaction of the two endonucleases leads to coordinated and enhanced activity (Wyatt et al., 2013), the Slx1 nuclease activity does not seem to contribute to Mus81-dependent resolution in budding yeast (Gritenaite et al., 2014). Instead, the exact mechanism by which mitotic complex formation enhances the resolution activity of Mus81-Mms4 still needs to be fully elucidated but it has been speculated that the scaffold complex plays a role in targeting Mus81-Mms4 to its substrates (Gritenaite et al., 2014, Princz et al., 2015).

Yen1, the second endonuclease involved in JM resolution, is similarly regulated during the cell cycle and shows fluctuating activity during different cell cycle stages (Matos et al., 2011). In contrast to Mus81-Mms4, phosphorylation of Yen1 has an inhibitory function and needs to be removed to allow full endonuclease activity (Kosugi et al., 2009, Matos et al., 2011, Matos et al.,

2013, Blanco et al., 2014, Eissler et al., 2014, Garcia-Luis et al., 2014) (**Figure 6**, upper right). CDK-dependent phosphorylation of 9 serines clustered in the Yen1 N- and C-terminal regions (Eissler et al., 2014, Blanco et al., 2014) controls its function by two different means and thus keeps the protein inactive during S- and early M-phase: (i) export of Yen1 from the nucleus and (ii) downregulation of the enzymatic activity (Matos et al., 2011, Blanco et al., 2014, Eissler et al., 2014, Garcia-Luis et al., 2014). These mechanisms are further reinforced by active degradation of Yen1 at the G1/S transition (Talhaoui et al., 2018). Subsequent removal of the inhibitory phosphorylation by Cdc14 at the onset of anaphase leads to a window of Yen1 activity during late M-phase (Kosugi et al., 2009, Matos et al., 2011, Matos et al., 2013, Blanco et al., 2014, Eissler et al., 2014, Garcia-Luis et al., 2014).

Taken together, coordinated phosphorylation and dephosphorylation events lead to the successive upregulation of resolvase activities during M-phase and thus allow completion of HR as well as efficient removal of JMs. The windows of Mus81-Mms4 and Yen1 activity thereby appear to be separated from each other and imply a hierarchy in the usage of resolution mechanisms (**Figure 6**, lower).

3.3 SSE activity during replication

As a consequence of the establishment of such a clear cell cycle regulation of the resolvases Mus81-Mms4 and Yen1 and their specific upregulation during M-phase, the necessity of the observed regulation has become a matter of ongoing investigations.

In this context, the development of genetic tools that allow prolonged activation of the SSEs provided an entry point to address this question. The bypass of the Mus81-Mms4 regulation and prolonged activation of the SSEs was thereby independently achieved by the use of a phosphomimetic Mms4 variant as well as premature over-expression of the Cdc5 kinase involved in Mms4 phosphorylation (Szakal and Branzei, 2013, Matos et al., 2013). Along the same line, a constitutively active Yen1 version has been established by mutating CDK sites required for the inactivation of Yen1 (Yen1-ON) (Blanco et al., 2014). Together, the use of these prematurely active SSEs resulted in decreased viability in response to replication perturbation and enhanced CO rates (Matos et al., 2013, Blanco et al., 2014, Szakal and Branzei, 2013). Given the broad substrate specificity of Mus81-Mms4 and Yen1, which in principal are able to cleave replication forks or related structures (Boddy et al., 2001, Kaliraman et al., 2001, Doe et al., 2002, Bastin-Shanower et al., 2003, Ciccia et al., 2003, Gaillard et al., 2003, Ehmsen and Heyer, 2008, Ip et al., 2008, Rass et al., 2010), the observed upregulation of the catalytic activity during M-phase has been considered a safeguard mechanism that protects cells from unwanted cleavage of replication intermediates (Matos et al., 2013, Blanco et al., 2014, Szakal and Branzei, 2013). This hypothesis is further supported by the fact that the *S. pombe* homolog of Mus81-Mms4, Mus81-Eme1, is regulated by the S-phase checkpoint in response to acute HU treatment. Phosphorylation of Mus81 by the

checkpoint kinase Cds1 thereby leads to the dissociation of Mus81-Eme1 from chromatin implying a direct mechanism to protect cells from Mus81 activity during replication (Kai et al., 2005, Froget et al., 2008).

However, genetic data clearly implicating Mus81-Mms4 in the response to replication fork stalling are seemingly contradictory to the restriction of Mus81-Mms4 function to M-phase and the potential toxicity during replication. Using replication fork stalling agents like MMS, HU or CPT, *MUS81-MMS4* has been found essential for cell survival and thereby directly connected with the response to replication fork stalling (Xiao et al., 1998, Interthal and Heyer, 2000, Boddy et al., 2001, Mullen et al., 2001, Doe et al., 2002, Bastin-Shanower et al., 2003, Kai et al., 2005, Saugar et al., 2013). These findings are complemented by genetic interaction studies where Mus81-Mms4, as well as the *S.pombe* homolog Mus81-Eme1, show strong genetic interactions with factors involved in replication fork protection (Noguchi et al., 2003, Noguchi et al., 2004, Bellaoui et al., 2003, Pebernard et al., 2004, Boddy et al., 2003, Irmisch et al., 2009, Torres-Rosell et al., 2005). In addition, studies performed in mammalian cells have established that loss of MUS81 function leads to replication perturbation and checkpoint activation (Hanada et al., 2007, Shimura et al., 2008, Regairaz et al., 2011, Buisson et al., 2015, Fu et al., 2015, Xing et al., 2015). The observation that stalled forks undergo MUS81-dependent cleavage after long treatment with HU or CPT to facilitate replication fork restart (Hanada et al., 2007, Shimura et al., 2008, Regairaz et al., 2011, Pepe and West, 2014a, Fu et al., 2015) further strengthens the argument that SSEs might be required directly during replication despite their potential toxicity and non-matching temporal profile.

Taken together, the observed discrepancy between the temporal regulation of SSEs, specifically Mus81-Mms4, and their implication during replication is still a matter of ongoing discussions.

Aims of the studies

Publication 1 | Bittmann et al., (2020) eLife

The catalytic activity of SSEs is tightly regulated within the cell cycle and a consecutive upregulation of Mus81-Mms4 and Yen1 activity can be detected during M-phase (Matos et al., 2011, Gallo-Fernandez et al., 2012, Matos et al., 2013, Szakal and Branzei, 2013, Blanco et al., 2014, Eissler et al., 2014, Garcia-Luis et al., 2014, Blanco and Matos, 2015). Conversely, the phenotypes associated with *MUS81-MMS4* mutants would connect the endonuclease with a function during replication perturbation and thus seemingly with S-phase (Xiao et al., 1998, Interthal and Heyer, 2000, Boddy et al., 2001, Mullen et al., 2001, Doe et al., 2002, Bastin-Shanower et al., 2003, Kai et al., 2005, Saugar et al., 2013). Starting from this observed discrepancy we set out to understand at which cell cycle phase Mus81-Mms4 would fulfill its *in vivo* function: in S-phase, where the DNA lesions connected with replication perturbation arise or in M-phase, where the catalytic activity of Mus81-Mms4 is high.

The first aim of the study was therefore to separate the possible functions of Mus81-Mms4 during S- and M-phase and analyze the influence of such a separation-of-function. To do so we aimed to apply the genetic tool of cell cycle tags to the Mus81-Mms4 endonuclease (Karras and Jentsch, 2010, Hombauer et al., 2011, Johnson et al., 2016) in order to restrict its expression to either S- or M-phase. Generally, cell cycle tags use the regulatory elements (the 5´UTR + the N-terminal degrons) of cyclins and allow to restrict the protein of interest (in our case Mus81-Mms4) to different cell cycle phases (S-, M- or G1-phase) by simple fusion to the protein. Using the cell cycle tags for our purpose we quickly realized that the low number of cell cycle tags available to the scientific community (one tag each for S-, M- or G1-phase) (Karras and Jentsch, 2010, Hombauer et al., 2011, Johnson et al., 2016) did not allow us to sufficiently vary expression levels. We were neither able to adapt protein levels to the endogenous levels of Mus81-Mms4 nor to achieve comparable expression levels for the different cell cycle phases.

The second major aim of the study therefore became to extend the variability of cell cycle tags in order to allow for an adaption of expression levels and thus the use of cell cycle-restricted proteins under physiological and comparable conditions. We thereby aimed at creating a universal toolbox of cell cycle tags that could be used to generally restrict any protein of interest with variable expression levels to the different cell cycle phases. The cell cycle tag toolbox should then be applied to the initial aim of restricting Mus81-Mms4 function to different cell cycle phases and address the question whether Mus81-Mms4 responds to replication fork stalling lesions in S- or M-phase.

Additionally, in a third aim we tried to complement the study by using the cell cycle tag system on a constitutively active version of the SSE Yen1 (Yen1-ON) to address which

consequences the presence of an active SSE would have in cell cycle phases where the catalytic activity of that SSE would normally be low.

Publication 2 | Princz et al., (2017) EMBO J

The upregulation of the Mus81-Mms4 catalytic activity during M-phase depends on both phosphorylation of the Mms4 subunit by the CDK and Cdc5 kinase (Matos et al., 2011, Gallo-Fernandez et al., 2012, Matos et al., 2013, Szakal and Branzei, 2013) as well as the engagement of Mus81-Mms4 into a higher order complex comprising the scaffold proteins Dpb11, Rtt107 and Slx1-Slx4 (Gritenaite et al., 2014, Princz et al., 2015). Interestingly, initial mass spectrometric analysis of this complex forming around Mus81-Mms4 during M-phase (Gritenaite et al., 2014) revealed the presence of a third cell cycle kinase – Dbf4-Cdc7 (DDK).

The major aim of this study was therefore to address the role of the DDK kinase in the phosphorylation and activation of Mus81-Mms4. During this analysis it turned out that Cdc5 and DDK cooperatively target Mms4 and that the phosphorylation of Mms4 by the two kinases additionally depends on the Rtt107 scaffold.

Consequently, the second aim of the study became to analyse this interdependency between the kinases and scaffold proteins during the activation of Mus81-Mms4. Generally, one readout of Mus81-Mms4 activity during the resolution of recombination intermediates is the relative number of COs produced.

My specific aim was to establish an experimental setup (Ho et al., 2010) that would allow us to quantify the relative number of COs and NCOs occurring during the disentanglement of recombination intermediates. Using this setup, we aimed to complement the study by unravelling the contribution of the DDK kinase and the Rtt107 scaffold on the activation of Mus81-Mms4 and thus the number of produced COs.

Cumulative Thesis: Publications

Publication 1 | Bittmann et al., (2020) eLife

Bittmann, J., Grigaitis, R., Galanti, L., Amarell, S., Wilfling, F., Matos, J., Pfander, B. An advanced cell cycle tag toolbox reveals principles underlying temporal control of structure-selective nucleases. eLife (2020) 9:e52459 DOI: 10.7554/eLife.52459

RESEARCH ARTICLE

An advanced cell cycle tag toolbox reveals principles underlying temporal control of structure-selective nucleases

Julia Bittmann[1], Rokas Grigaitis[2], Lorenzo Galanti[1], Silas Amarell[1], Florian Wilfling[3], Joao Matos[2], Boris Pfander[1]*

[1]Max Planck Institute of Biochemistry, DNA Replication and Genome Integrity, Martinsried, Germany; [2]Institute of Biochemistry, Eidgenössische Technische Hochschule, Zürich, Zürich, Switzerland; [3]Max Planck Institute of Biochemistry, Molecular Cell Biology, Martinsried, Germany

Abstract Cell cycle tags allow to restrict target protein expression to specific cell cycle phases. Here, we present an advanced toolbox of cell cycle tag constructs in budding yeast with defined and compatible peak expression that allow comparison of protein functionality at different cell cycle phases. We apply this technology to the question of how and when Mus81-Mms4 and Yen1 nucleases act on DNA replication or recombination structures. Restriction of Mus81-Mms4 to M phase but not S phase allows a *wildtype* response to various forms of replication perturbation and DNA damage in S phase, suggesting it acts as a post-replicative resolvase. Moreover, we use cell cycle tags to reinstall cell cycle control to a deregulated version of Yen1, showing that its premature activation interferes with the response to perturbed replication. Curbing resolvase activity and establishing a hierarchy of resolution mechanisms are therefore the principal reasons underlying resolvase cell cycle regulation.

***For correspondence:** bpfander@biochem.mpg.de

Competing interests: The authors declare that no competing interests exist.

Funding: See page 23

Received: 04 October 2019
Accepted: 29 April 2020
Published: 01 May 2020

Reviewing editor: Bernard de Massy, CNRS UM, France

Introduction

Eukaryotic chromosomes undergo dramatic structural changes during the cell cycle often referred to as the chromosome cycle (***Blow and Tanaka, 2005***). In order to maintain the integrity of genetic information cells need to adjust their DNA repair and genome integrity pathways to the different requirements within this chromosome cycle. Accordingly, many DNA repair enzymes are regulated by transcriptional and post-translational mechanisms or otherwise adjusted to act at specific stages of the cell cycle (***Hustedt and Durocher, 2017***). While our knowledge of regulatory mechanisms has grown over the past years, a question that often arises is whether a certain enzyme or protein has a function, or not, at a specific cell cycle stage.

Answering this question usually involves cell cycle synchronization and sophisticated tools to induce/deplete protein expression at specific time points. Moreover, not all phenotypes can be investigated in single cell cycle experiments. A simple system that promises to overcome these limitations utilizes so called 'cell cycle tags'. The cell cycle tag methodology was initially developed for budding yeast by the Jentsch group (***Karras and Jentsch, 2010***) and expanded by Kolodner and colleagues (***Hombauer et al., 2011***) and Kubota and colleagues (***Johnson et al., 2016***). Cell cycle tagging involves both the replacement of the endogenous promoter of a gene of interest by a cell cycle-regulated promoter as well as the addition of a protein-coding sequence containing a cell cycle-regulated degradation signal (degron), restricting the expression of the fusion protein to a specific phase of the cell cycle. So far, three cell cycle tags have been developed based on the S phase cyclin Clb6, the M phase cyclin Clb2 and the G1 regulator Sic1 (***Karras and Jentsch, 2010***; ***Hombauer et al., 2011***; ***Johnson et al., 2016***). These tags constrain protein expression to S phase,

early M phase and late M to G1 phase, respectively. Single constructs, and also combinations have been used in several studies (**Karras and Jentsch, 2010**; **Hombauer et al., 2011**; **Karras et al., 2013**; **González-Prieto et al., 2013**; **Gonzalez-Huici et al., 2014**; **Menolfi et al., 2015**; **Renaud-Young et al., 2015**; **Johnson et al., 2016**; **Siler et al., 2017**; **Hung et al., 2017**; **Lafuente-Barquero et al., 2017**; **Kahli et al., 2019**; **Lockhart et al., 2019**). Notwithstanding, the current three-construct-system has major limitations: (i) peak expression levels from the three constructs are vastly different (Sic1 > Clb2 > Clb6, compare **Figure 1C**) and (ii) expression levels cannot be adjusted, which can lead to under- or overexpression of the protein of interest. Collectively, these limitations may confound the interpretation of cell cycle tag experiments.

To overcome these limitations, we have set out to generate an advanced toolbox of 46 cell cycle tag constructs with varied expression levels. To achieve these variations in expression, we have used additional promoters/degrons from cyclins Clb5 and Clb1 and introduced chimeric constructs with new promoter/degron combinations (**Figure 1A**). Furthermore, in order to cripple expression from specific promoters, we introduced 5'UTR truncations (**Merrick and Pavitt, 2018**) and upstream out of frame ATGs (**Araujo et al., 2012**; **Yun et al., 2012**; **Dvir et al., 2013**; **Figure 1A**). This construct toolbox will allow comparable and, within a certain range, titratable expression of the protein of interest.

As a proof of principle, we applied the advanced cell cycle tag toolbox to study the regulation of two structure-selective endonucleases (SSEs), Mus81-Mms4 and Yen1. SSEs are involved in many DNA repair pathways and defined by their ability to recognize and cleave branched DNA structures (**Ciccia et al., 2008**; **Schwartz and Heyer, 2011**; **Dehé and Gaillard, 2017**). While required for the corresponding repair mechanisms, it is obvious that cells must also tightly control SSEs, as unscheduled activation of nucleolytic activities might lead to genome instability (**Dehé and Gaillard, 2017**; **Pfander and Matos, 2017**). A number of SSEs have the ability to cleave Holliday junction (HJ) structures and are therefore involved in processing DNA intermediates arising during homologous recombination (HR) and/or as consequence of replication stalling (**Boddy et al., 2001**; **Kaliraman et al., 2001**; **Doe et al., 2002**; **Bastin-Shanower et al., 2003**; **Ciccia et al., 2003**; **Fricke and Brill, 2003**; **Gaillard et al., 2003**; **Ehmsen and Heyer, 2008**; **Ip et al., 2008**; **Jessop and Lichten, 2008**; **Oh et al., 2008**; **Muñoz et al., 2009**; **Rass et al., 2010**; **Wechsler et al., 2011**; **Saugar et al., 2013**; **Wyatt et al., 2013**; **Saugar et al., 2017**). In mitotically dividing budding yeast three HJ-processing SSEs are active – Mus81-Mms4, Yen1 and Slx1 (**Matos and West, 2014**; **Blanco and Matos, 2015**; **Guervilly and Gaillard, 2018**).

The heterodimeric Mus81-Mms4 nuclease is known to undergo cell cycle regulation with the Mms4 subunit becoming phosphorylated in M phase (**Matos et al., 2011**; **Gallo-Fernández et al., 2012**; **Matos et al., 2013**; **Szakal and Branzei, 2013**; **Princz et al., 2017**). This phosphorylation is mediated by the budding yeast cyclin dependent kinase (CDK) Cdk1/Cdc28 and by a complex consisting of two kinases – polo-like kinase Cdc5 and Dbf4-dependent kinase DDK (Cdc7+Dbf4) (**Gallo-Fernández et al., 2012**; **Matos et al., 2013**; **Szakal and Branzei, 2013**; **Princz et al., 2017**), whereby the timing of Cdc5 expression determines the M phase restriction of Mms4 phosphorylation (**Matos et al., 2013**; **Princz et al., 2017**). Cell cycle regulation impinges on Mus81-Mms4 by two mechanisms. While phosphorylation of Mus81-Mms4 directly stimulates its catalytic activity (**Matos et al., 2011**; **Gallo-Fernández et al., 2012**; **Schwartz et al., 2012**; **Matos et al., 2013**), a second layer of cell cycle regulation requires the engagement of Mus81-Mms4 in a phosphorylation-dependent multi-protein complex comprising several scaffold proteins such as Slx4, Dpb11 and Rtt107 (referred to as Mus81 complex hereafter) (**Gritenaite et al., 2014**; **Princz et al., 2015**; **Princz et al., 2017**). The Mus81 complex forms exclusively during M phase and is likely involved in targeting Mus81-Mms4 to its substrates or controlling its action by other means (**Gritenaite et al., 2014**; **Princz et al., 2017**). Intriguingly, phosphorylation of Mus81-Mms4 and formation of the Mus81 complex displays features commonly associated with switch-like activation (positive feedback, multi-site phosphorylation), suggesting that with the transition to M phase cells might enter a state of increased Mus81-Mms4 function (**Pfander and Matos, 2017**; **Princz et al., 2017**) (note that function in vivo will not only be determined by enzymatic activity, but also by targeting of the enzyme to its substrate, etc). Notably, however, *mus81* mutant phenotypes suggest that the main function of Mus81-Mms4 can be attributed to the response to replication perturbation (**Xiao et al., 1998**; **Interthal and Heyer, 2000**; **Boddy et al., 2001**; **Mullen et al., 2001**; **Doe et al., 2002**; **Bastin-Shanower et al., 2003**; **Kai et al., 2005**). This raises the question, whether (i) Mus81-Mms4 may be

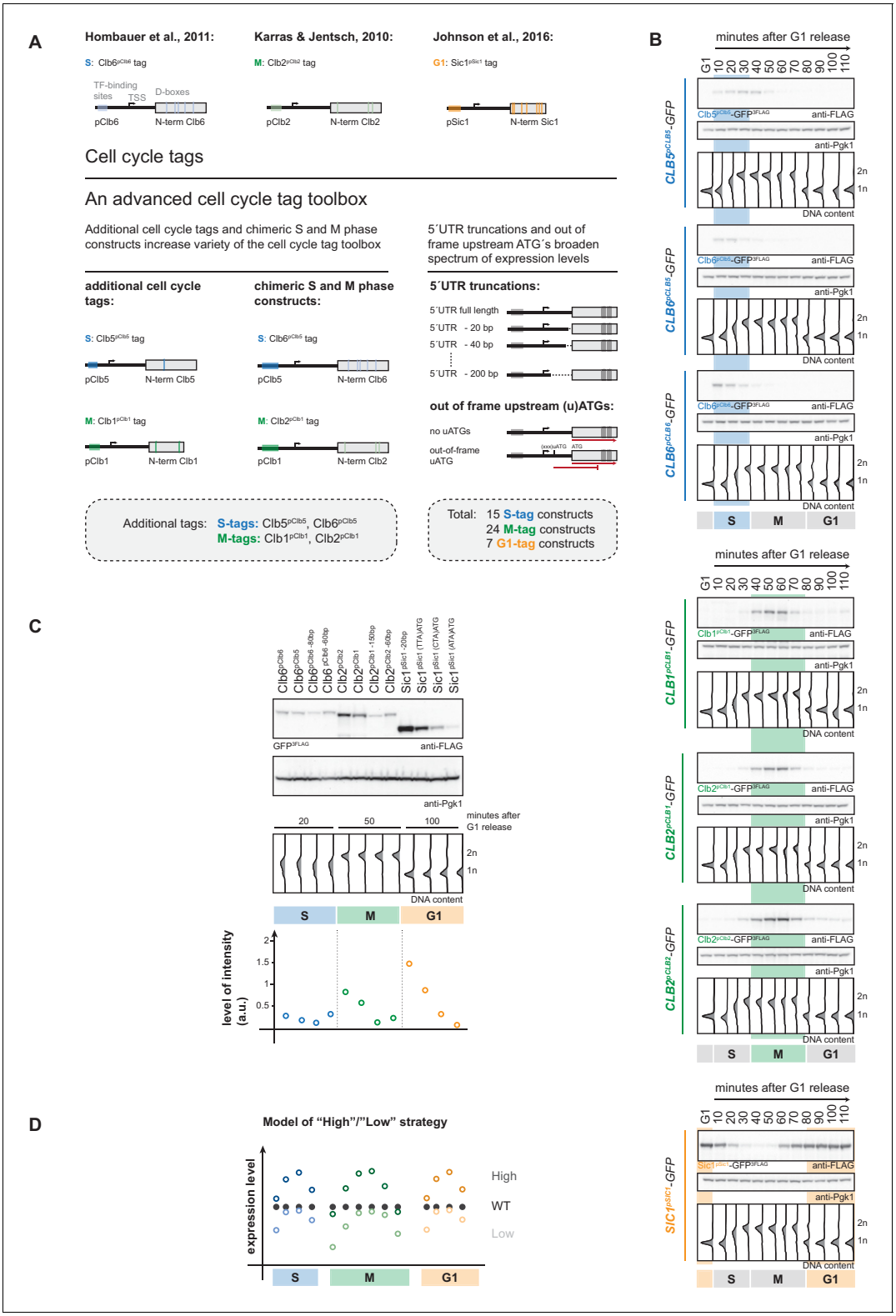

Figure 1. An advanced toolbox of cell cycle tag constructs. (**A**) Schematic representation of the applied strategies for improved cell cycle tag methodology. Upper panel: conventional cell cycle tag methodology was limited by only one construct for each cell cycle phase. Lower panel: the advanced cell cycle tag toolbox was expanded to 46 constructs. Therefore, we used new promoters and degrons from Clb5 and Clb1, chimeric promoter-degron combinations and protein expression was crippled using 5´UTR truncations and upstream out of frame ATGs. Vertical bars indicate

Figure 1 continued on next page

Figure 1 continued

location of cell cycle regulatory elements in the promoter and N-terminal degron sequence (see ***Figure 1—figure supplement 1*** for detailed description of the tagging procedure). (**B**) New cell cycle tag constructs allow cell cycle-restricted expression of GFP at varied peak expression levels. Anti-FLAG westerns of cells expressing Clb5^{pClb5}-, Clb6^{pClb5}-, Clb6^{pClb6}-, Clb1^{pClb1}-, Clb2^{pClb1}-, Clb2^{pClb2}-3FLAG-tagged versions of GFP after G1 arrest with α-factor and synchronous release through the cell cycle up to the next G1 phase. Pgk1 western was used as control and DNA content measurements indicate cell cycle progression at the individual time points below (see ***Figure 1—figure supplement 2*** for G1 release experiments of the corresponding 5´UTR truncations and for constructs containing upstream out of frame ATGs). (**C**) New promoters and degrons, chimeric promoter-degron combinations, 5'UTR truncations and upstream out of frame ATGs allow a broad spectrum of peak expression levels of cell cycle-restricted GFP. Western blot analysis of peak expression levels of cell cycle-tagged 3FLAG-GFP variants at indicated time points after G1 release (20 min = S phase, 50 min = M phase, 100 min = G1 phase). DNA content measurements below indicate cell cycle progression. Graph: peak expression levels were quantified using Image-J and signals of the individual constructs were divided by the corresponding Pgk1 sample to normalize to overall protein levels (see ***Figure 1—figure supplement 3*** for an overview of all cell cycle-tagged GFP versions in cells arrested in the corresponding cell cycle phase). (**D**) Schematic representation of the suggested cell cycle tag strategy using two sets of constructs with matching 'low' and 'high' peak expression levels. 'Low' expressing constructs (light colours) are chosen by matching peak expression levels similar to the endogenous protein but will show underexpression at cell cycle phase transitions. 'High' expressing tags generally show higher expression compared to the wildtype protein with the advantage of broader timeframes of action (timeframes in which protein levels are similar or higher than endogenous protein levels).
The online version of this article includes the following figure supplement(s) for figure 1:

Figure supplement 1. Schematic representation of the cell cycle tagging procedure.
Figure supplement 2. 5'UTR truncations and upstream out of frame ATGs do not interfere with cell cycle restriction.
Figure supplement 3. 5'UTR truncations and upstream out of frame ATGs cripple peak expression levels of cell cycle tag constructs.
Figure supplement 4. Clb6^{pClb6}- and Clb2^{pClb1}-tag induce similar peak expression levels for several cell cycle-tagged proteins.

acting in S phase directly on stalled replication forks or repair intermediates, despite a non-matching temporal regulation, or whether (ii) Mus81-Mms4 acts in M phase as post-replicative resolvase.

A second SSE with the propensity to cleave HJ structures is called Yen1 (***Ip et al., 2008***; ***Blanco et al., 2010***). Yen1 is also tightly cell cycle-controlled and becomes dephosphorylated in late M phase, specifically at the metaphase-to-anaphase transition, when CDK becomes inactivated and phosphorylation marks on Yen1 are removed by Cdc14 (***Kosugi et al., 2009***; ***Matos et al., 2011***; ***Blanco et al., 2014***; ***Eissler et al., 2014***; ***García-Luis et al., 2014***). Yen1 regulation consists of several layers and involves phosphorylation-dependent inhibition of its catalytic activity as well as phosphorylation-dependent regulation of its sub-cellular localization (***Matos et al., 2011***; ***Blanco et al., 2014***; ***Eissler et al., 2014***; ***García-Luis et al., 2014***). Furthermore, at the G1/S transition a degradation mechanism is in place to clear Yen1 from chromatin (***Talhaoui et al., 2018***). Altogether, a picture emerges whereby Yen1 is inhibited by CDK phosphorylation and becomes stimulated or activated from late M phase to the end of G1 (***Blanco et al., 2014***; ***Eissler et al., 2014***; ***García-Luis et al., 2014***). The temporal windows of high Mus81-Mms4 activity and high Yen1 activity therefore appear non-overlapping (***Matos et al., 2011***). Experimental removal of the inhibitory phosphorylation sites on Yen1 generated an allele (*YEN1-ON*), where Yen1 was found to be uncoupled from cell cycle regulation and constitutively active (***Matos et al., 2013***; ***Blanco et al., 2014***). This allele allowed to study the consequences of unrestricted activation of an SSE and showed that ectopic nuclease activity has adverse consequences in presence of replication stalling agents, suggesting that unscheduled cleavage of replication intermediates by this SSE interferes with the response to replication stalling (***Blanco et al., 2014***).

The control of SSEs in human cells involves additional features, such as the presence of two mutually exclusive MUS81 regulators (called EME1 and EME2), but the principal mechanisms of control appear to be evolutionary conserved (***Matos et al., 2011***; ***Wyatt et al., 2013***; ***Chan and West, 2014***; ***Duda et al., 2016***), suggesting that cell cycle control of SSEs is an intrinsic necessity. In this study, we take advantage of the genetic tractability of budding yeast to expand, improve and apply cell cycle tag technology with an advanced toolbox of cell cycle tag constructs to investigate the relevance of Mus81-Mms4 and Yen1 cell cycle regulation. We show that several survival and genome instability phenotypes induced by chronic or acute exposure to DNA damaging agents or other genotoxic agents are rescued by M phase restricted Mus81-Mms4, but not by a version that is confined to S phase. This suggests that for the conditions tested, the essential function of Mus81-Mms4 is as a post-replicative resolvase. Yen1 can compensate for this function, if present in constitutively active form in early M phase. We also employ cell cycle tags to reintroduce cell cycle regulation and find that premature activation of Yen1 in S phase, but also in early M phase interferes with the response

to replication fork stalling, suggesting that a temporal hierarchy of HJ-cleaving nucleases is required for optimal DNA repair.

Results

An advanced toolbox of cell cycle tags

When we started this study, three cell cycle tag constructs were available to restrict target protein expression to G1, S or M phase. The S-tag uses promoter and N-terminal degron (aa 1–195) of the S phase cyclin Clb6 and restricts expression to S phase (***Figure 1A***; ***Hombauer et al., 2011***). The M-tag (originally referred to as G2-tag; ***Karras and Jentsch, 2010***) uses promoter and N-terminal degron sequence (aa 1–180) of the M phase cyclin Clb2 and restricts expression to M phase (***Figure 1A***; ***Karras and Jentsch, 2010***). The G1-tag uses promoter and N-terminal degron of the G1 regulator Sic1 (aa 1–105) and restricts protein expression to G1 (***Figure 1A***; ***Johnson et al., 2016***). In order to overcome the limitations of these specific constructs and allow for modulation of expression levels we generated a toolbox of 46 cell cycle tag constructs. Specifically, we used a three-pronged approach to create constructs that at the same time allow varied peak expression levels and retained cell cycle restriction (***Figure 1A***): (i) we used additional promoters and N-terminal degron sequences from S phase cyclin Clb5 (aa 1–202) and from M phase cyclin Clb1 (aa 1–120); (ii) we generated chimeric S-tag and M-tag constructs (containing Clb5 promoter and Clb6 degron ($Clb6^{pClb5}$-tag) or Clb1 promoter and Clb2 degron ($Clb2^{pClb1}$-tag), respectively); (iii) in order to cripple expression from some promoters, we either truncated 5'UTRs or introduced out-of-frame ATGs, which have been shown to reduce protein expression levels by reduced mRNA stability and reduced translation rates, respectively (***Yun et al., 2012***; ***Araujo et al., 2012***; ***Dvir et al., 2013***; ***Merrick and Pavitt, 2018***).

We constructed 46 plasmids based on the pYM-N vector series (***Janke et al., 2004***) that allow the introduction of all variants of cell cycle tags by a well-established recombination-based strategy using a single pair of oligonucleotide primers and the natNT2 resistance cassette (***Figure 1—figure supplement 1***, see supplementary methods for detailed protocol). As test substrate, we subjected the GFP ORF, which was integrated in the yeast genome, to the cell cycle tagging approach and the resulting yeast strains were verified for genomic integration and expression. Next, we tested whether all constructs restricted protein expression to the desired cell cycle phases. Therefore, we arrested cells in G1 using α-factor, synchronously released them into the cell cycle and followed them to the next G1. Notably, all constructs restricted GFP-expression to the target cell cycle phase (***Figure 1B***, ***Figure 1—figure supplement 2***). When comparing the different S-tag constructs, we noticed that constructs containing the Clb6 degron sequence imposed a much sharper restriction of expression to S phase consistent with the differential regulation of Clb5 and Clb6 (***Figure 1B***; ***Kühne and Linder, 1993***; ***Schwob and Nasmyth, 1993***; ***Jackson et al., 2006***), suggesting that these constructs should be the preferred choice for an S-tag experiment.

We then took S, M and G1 phase samples (20, 50 and 100 min, respectively) from our cell cycle release experiments in order to measure peak expression levels for the individual constructs. This analysis showed that within different G1-, S- and M-tag constructs expression varied by up to 10-fold, respectively (***Figure 1C***, ***Figure 1—figure supplement 3***). Notably, none of the S-tag constructs tested gave peak expression levels in the same range as those of the previously used Clb2 M-tag and Sic1 G1-tag constructs (***Figure 1C***, ***Figure 1—figure supplement 3***), emphasizing the need for new M- and G1-tag constructs. Satisfyingly, we found that M-tag constructs containing the pClb1 promoter or the 5'UTR-truncated pClb2 promoter showed much weaker peak expression levels and tighter temporal restriction of expression at the same time (***Figure 1B–C***, ***Figure 1—figure supplements 2*** and ***3***). Similarly, for the G1-tag we found that upstream out-of-frame ATGs reduced protein expression from pSic1 constructs and also led to tighter temporal restriction of expression (***Figure 1B–C***, ***Figure 1—figure supplements 2*** and ***3***).

Therefore, these constructs from our advanced cell cycle tag toolbox will allow to titrate peak expression levels within a certain range and offer at the same time superior restriction of target protein expression to the cell cycle phase of interest. We also note that by introducing cell cycle-restricted expression, one will usually change expression of the protein of interest from a continuous, often constant expression regime to a dynamically, cell cycle phase-restricted expression regime

(*Figure 1D*). Due to this dynamic expression it may sometimes be difficult to directly compare cell cycle-tagged constructs with endogenous proteins, as well as the arising phenotypes. To mitigate this problem, we therefore developed a strategy where we conducted experiments with two sets of G1-, S- and M-tag constructs (*Figure 1D*). The first set (called 'low' hereafter) can be chosen to yield peak expression similar to the protein of interest but may show 'under-expression' at cell cycle transitions (*Figure 1D*). The second set (called 'high' hereafter) can be chosen to yield peak expression higher to the protein of interest (overexpression) but will avoid under-expression at cell cycle transitions (*Figure 1D*). Most importantly, with the presented toolbox it will be possible to use constructs, which give highly similar peak expression levels in different cell cycle phases and the respective strains are therefore phenotypically comparable. Protein expression should be tested for any new cell cycle-tagged protein, even though we observed similar trends for different proteins tested. For example, we found that S phase levels of Clb6^{pClb6}-tagged proteins were very similar to levels of Clb2^{pClb1}-tagged proteins in five (Xrs2, Rad52, Fun30, Sgs1, Yen1-ON) (*Figure 1—figure supplement 4*, *Figure 5—figure supplement 2*) out of six cases (Mus81-Mms4 being the exception). Overall, our advanced cell cycle tag toolbox therefore offers titratable expression levels, which allows for the first time a direct comparison of phenotypes arising from cell cycle restriction of a protein of interest to G1, S or M phase.

Cell cycle-restricted expression of Mus81-Mms4

To showcase the cell cycle tag toolbox, we applied it to Mus81-Mms4. Deletion of *MUS81* or *MMS4* causes phenotypes that imply Mus81-Mms4 in the cellular response to replication fork stalling (*Xiao et al., 1998*; *Interthal and Heyer, 2000*; *Boddy et al., 2001*; *Mullen et al., 2001*; *Doe et al., 2002*; *Bastin-Shanower et al., 2003*; *Kai et al., 2005*; *Saugar et al., 2013*). In contrast, Mus81-Mms4 function is specifically upregulated once cells enter M phase (*Matos et al., 2011*; *Gallo-Fernández et al., 2012*; *Matos et al., 2013*; *Saugar et al., 2013*; *Szakal and Branzei, 2013*; *Gritenaite et al., 2014*; *Princz et al., 2017*). We therefore decided to employ our toolbox to discriminate between potential S phase- and M phase-specific functions of Mus81-Mms4. In addition to the strategy outlined in *Figure 1*, we constructed cell cycle tags for both subunits of the Mus81-Mms4 heterodimer, as we reasoned that this would result in even tighter cell cycle restriction of the complex. Specifically, we found that Clb6$^{pClb6\ -80bp}$-tagged and Clb2$^{pClb1\ -150bp}$-tagged versions of Mus81-Mms4 restricted Mus81-Mms4 expression to S and M phase and resulted in very similar peak expression levels between 0.9 and 1.2-fold of the endogenous proteins (*Figure 2A*, *Figure 2—figure supplement 1A,C*). We therefore refer to these versions as S^{low}-Mus81-Mms4 (Clb6$^{pClb6\ -80bp}$-tag) and M^{low}-Mus81-Mms4 (Clb2$^{pClb1\ -150bp}$-tag), respectively. While peak expression levels are comparable to endogenous Mus81-Mms4, we observed reduced expression levels at cell cycle transitions. For example, we observed that expression of M^{low}-Mus81-Mms4 was below endogenous levels in early M phase (see *Figure 2B*, 37.5 and 45 min time points). The same trend was also observed for the nuclear fraction of Mus81-Mms4 (*Figure 2B*, right panel, *Figure 2—figure supplement 2*). Consistently, the window of time during which we could observe the M phase specific, hyperphosphorylated form of Mms4 was shorter for M^{low}-Mus81-Mms4 compared to endogenous Mus81-Mms4 (*Figure 2C*). Taken together, M^{low}-Mus81-Mms4 peak expression is comparable to endogenous Mus81-Mms4, but expression and hyperphosphorylation appears reduced in early and late M phase. To complement S^{low}-Mus81-Mms4 and M^{low}-Mus81-Mms4, we therefore also used the Clb5^{pClb6}-tagged S phase-restricted S^{high}-Mus81-Mms4, as well as Clb2^{pClb1}-tagged M phase-restricted M^{high}-Mus81-Mms4 (*Figure 2A*). Comparison of peak expression levels in S and M phase suggests that S^{high}-Mus81-Mms4 and M^{high}-Mus81-Mms4 are expressed to very similar levels, but 2 to 5-fold overexpressed compared to endogenous Mus81-Mms4 (*Figure 2—figure supplement 1B, C*). Both constructs showed expected restriction of expression to S and M phase (*Figure 2A*) and when we compared M^{high}-Mus81-Mms4 to M^{low}-Mus81-Mms4, we noticed that the M^{high}-Mus81-Mms4 did neither show underexpression in early M phase (*Figure 2B*), nor a shortened window of M phase-specific Mms4 phosphorylation (*Figure 2C*). Therefore, S^{high}-Mus81-Mms4 and M^{high}-Mus81-Mms4 constructs are expressed to similar levels, avoid under-expression at cell cycle transitions, but show overexpression compared to endogenous expression levels. The two sets of S- and M-tag constructs are therefore complementary and enable us to follow the high/low expression strategy outlined in *Figure 1D* to investigate Mus81-Mms4 phenotypes.

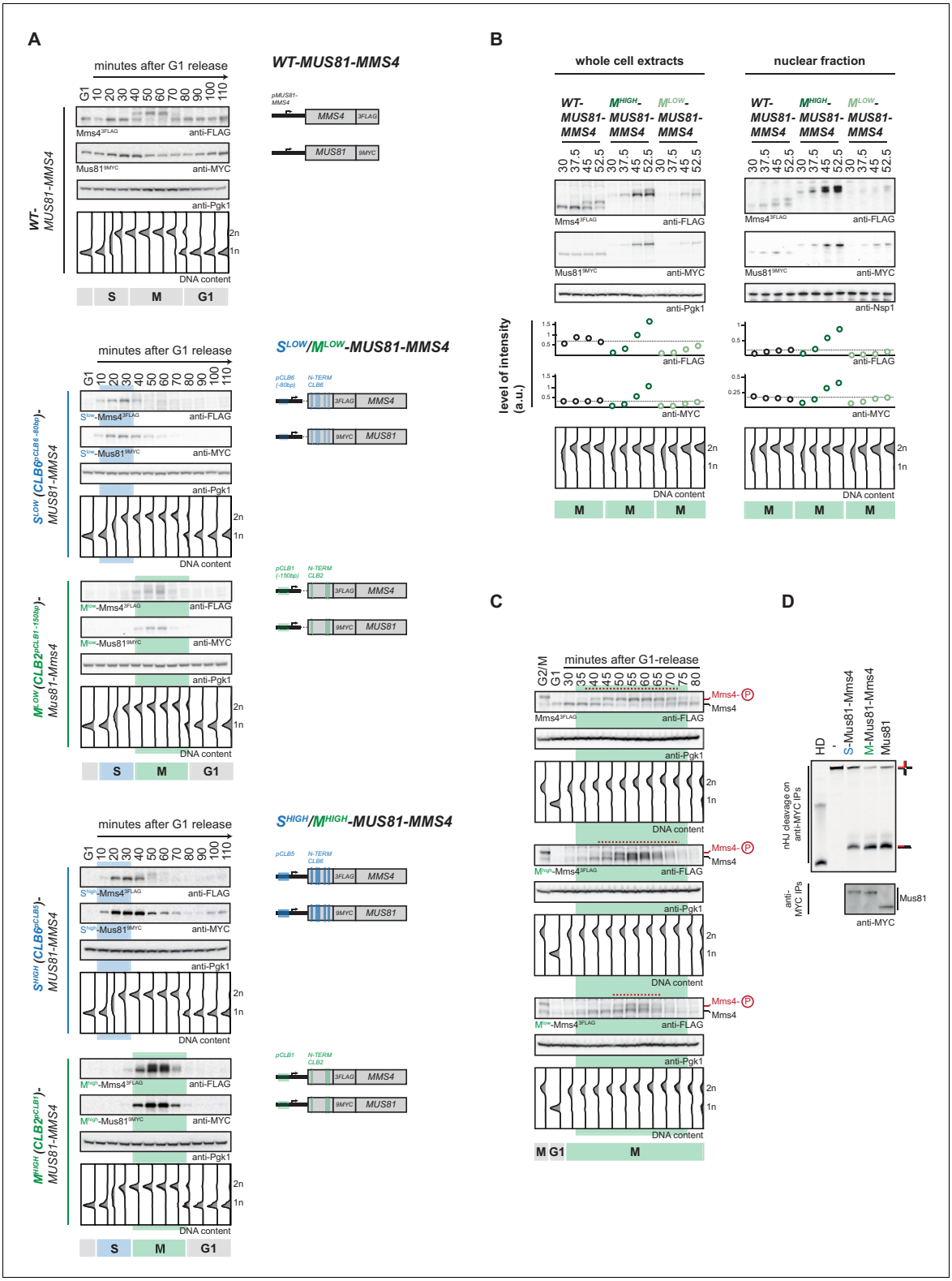

Figure 2. Cell cycle-restricted expression of Mus81-Mms4. (**A**) Restriction of Mus81-Mms4 expression to S or M phase of matched pairs of 'low' and 'high' expressing cell cycle tag constructs. (Left) Western blot and DNA content analysis of strains expressing WT, S phase-restricted (S^{low} ($Clb6^{pClb6\text{ -}80bp}$)-$S^{high}$ ($Clb6^{pClb5}$)-Mus81-Mms4) and M phase-restricted (M^{low} ($Clb2^{pClb1\text{ -}150bp}$)-$M^{high}$ ($Clb2^{pClb1}$)-Mus81-Mms4) alleles of Mus81 (9MYC-tagged)-Mms4 (3FLAG-tagged) during a single cell cycle as in ***Figure 1D*** (see ***Figure 2—figure supplement 1*** for quantification of peak expression levels of

Figure 2 continued on next page

Figure 2 continued

the S^{low}-/M^{low} -Mus81-Mms4 and S^{high}-/M^{high}-Mus81-Mms4 constructs). (Right) Schematic representation of WT, S (S^{low}-/S^{high}-Mus81-Mms4) and M phase (M^{low}-/M^{high}-Mus81-Mms4) restricted Mus81-Mms4 constructs. Blue and green bars indicate location of cell cycle regulatory elements in the promoter and N-terminal degron sequence. (**B**) Different constructs ('high' and 'low' peak expression levels) of Mus81-Mms4 lead to underexpression of the M^{low}-Mus81-Mms4 construct or to overexpression of the M^{high}-Mus81-Mms4 construct in early M phase and similar trends are seen in the nuclear fraction. Western blot analysis of protein levels in whole cell extracts (left panel) and after nuclei separation (right panel) at indicated time points after a G1-release (early M phase; see DNA content profile depicted at the bottom). While immediately with entry into M phase the M^{high}-Mus81-Mms4 construct reaches similar or higher protein levels than endogenous Mus81-Mms4, the M^{low}-Mus81-Mms4 construct shows a 10–15 min delay in reaching comparable expression levels and this holds true for both, whole cell extracts and the nuclear fraction. Expression levels were quantified using Image-J and signals of the individual time points were divided by the corresponding Pgk1 (whole cell extracts) or Nsp1 (nuclear fraction) signal to normalize to overall protein levels (graphs below contain normalized values for every construct). (see ***Figure 2—figure supplement 2*** for control western blots of the nuclear fractionation) (**C**) Different constructs ('high' and 'low' peak expression levels) of Mus81-Mms4 lead to different windows of Mus81-Mms4 phosphorylation in M^{low}-Mus81-Mms4 and M^{high}-Mus81-Mms4. Western blot analysis of the phosphorylation states of Mms4 at indicated time points after a G1-release (M phase; see DNA content profile depicted below the western blots). While M^{high}-Mus81-Mms4 shows a similar timeframe of Mms4 phosphorylation to endogenous Mus81-Mms4, M^{low}-Mus81-Mms4 is phosphorylated and stimulated during a shortened window of time only (compare red lines above the Mms4-3FLAG western blots: 15–20 min of phosphorylation in M^{low}-Mus81-Mms4 compared to 30 min in M^{high}-Mus81-Mms4 and 30–35 min in Mus81-Mms4). (**D**) N-terminal tagging does not alter Mus81-Mms4 activity. Resolution assay using a nicked HJ (nHJ) substrate and immunopurified Mus81-Mms4, S-Mus81-Mms4 and M-Mus81-Mms4 (note that WT and cell cycle-tagged proteins were expressed from pGal1-10 promoter). Myc-tagged Mus81-Mms4 was purified from cycling cells, dephosphorylated using λ-Phosphatase and incubated with the nHJ substrate for 2 hr. Upper panel: nHJ cleavage assay with heat DNA substrate (HD) as control. Lower panel: western blot analysis of Mus81-9MYC IP after nHJ cleavage assay (see ***Figure 2—figure supplement 3*** for a western blot analysis of Mms4 dephosphorylation by λ-Phosphatase).
The online version of this article includes the following figure supplement(s) for figure 2:

Figure supplement 1. Analysis of 'low' and 'high' S- and M-tagged Mus81-Mms4 peak expression levels.
Figure supplement 2. Nuclear/cytoplasmic fractionation.
Figure supplement 3. λ-Phosphatase treatment leads to efficient Mms4 dephosphorylation of WT, S- and M-Mus81-Mms4 used for activity assays.

Lastly, we also ensured that N-terminal tagging of Mus81 or Mms4 did not lead to inactivation of the Mus81-Mms4 enzymatic activity. To this end we obtained Mus81-Mms4, Clb6 (S-)-tagged Mus81-Mms4 and Clb2 (M-)-tagged Mus81-Mms4 by immuno-purification, phosphatase treated the protein to exclude cell cycle-dependent stimulatory effects and found that all versions showed nuclease activity towards a nicked Holliday junction (nHJ) model substrate (***Figure 2D***, ***Figure 2—figure supplement 3***).

Mus81-Mms4 restricted to M phase, but not S phase is sufficient for the response to genotoxic insults

To reveal phenotypes of Mus81-Mms4 cell cycle restriction, we first tested cell viability upon chronic exposure to replication stalling chemicals (MMS, CPT and HU). *mus81*Δ cells were hypersensitive to MMS and CPT and showed reduced growth on HU containing medium (***Figure 3A–B***; ***Xiao et al., 1998***; ***Interthal and Heyer, 2000***; ***Mullen et al., 2001***; ***Bastin-Shanower et al., 2003***; ***Saugar et al., 2013***). Restricting Mus81-Mms4 to S phase also gave a severe hypersensitivity to MMS and CPT: S^{low}-Mus81-Mms4 expressing cells showed similar phenotypes as *mus81*Δ (***Figure 3A***, ***Figure 3—figure supplement 1A***), while S^{high}-Mus81-Mms4 also showed pronounced hypersensitivity, but compared to *mus81*Δ (and S^{low}-Mus81-Mms4) the phenotype was less severe (***Figure 3B***). In contrast, restricting Mus81-Mms4 to M phase showed very little phenotype. Specifically, M^{high}-Mus81-Mms4 cells did not show any hypersensitivity (***Figure 3B***), while M^{low}-Mus81-Mms4 cells showed a small but detectable growth defect in the presence of high doses of MMS or CPT (***Figure 3A***). Collectively, these data suggest that Mus81-Mms4 would exhibit its dominant function in the response to genotoxic agents during M phase and not during S phase.

We interpret the slight phenotypic differences between S^{high}-Mus81-Mms4 and S^{low}-Mus81-Mms4, as well as between M^{high}-Mus81-Mms4 and M^{low}-Mus81-Mms4 (***Figure 3A–B***), to arise from leaking of S^{high}-Mus81-Mms4 into M phase (***Figure 2A***) as well as from underexpression of M^{low}-Mus81-Mms4 during early and late M phase (***Figure 2B–C***), respectively. This interpretation is supported by the facts that (i) the residual viability of S^{high}-Mus81-Mms4 depends on M phase-specific phosphorylation events (***Figure 3—figure supplement 1B–C,M*** phase specific phosphorylation is abolished by the *mms4-14A* mutant; ***Matos et al., 2011***) and (ii) the MMS and CPT sensitivity of

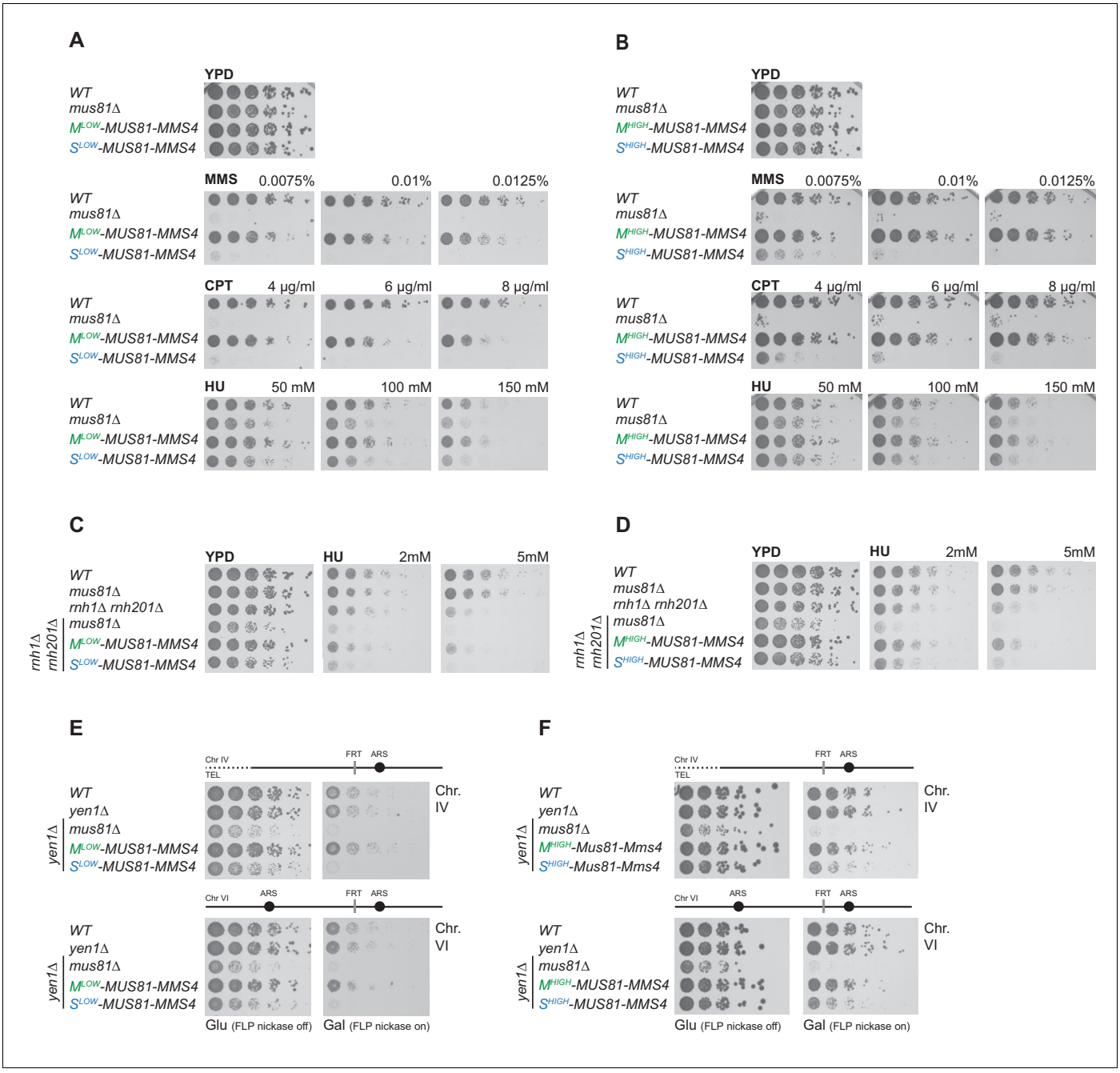

Figure 3. Mus81-Mms4 restricted to M phase, but not S phase is sufficient for the response to genotoxic insults. (**A/B**) M phase-restricted Mus81-Mms4 is sufficient to confer viability to replication fork stalling drugs. Viability of cells with M^{low} ($Clb2^{pClb1\ -150bp}$)-Mus81-Mms4/S^{low} ($Clb6^{pClb6\ -80bp}$)-Mus81-Mms4 constructs at low peak expression levels (**A**) or M^{high} ($Clb2^{pClb1}$)-Mus81-Mms4/S^{high} ($Clb6^{pClb5}$)-Mus81-Mms4 constructs at high peak expression levels (**B**) is compared to that of *WT* and *mus81Δ* cells. Strains were plated in 5-fold serial dilutions on YPD plates containing the indicated amounts of MMS, CPT or HU and incubated at 30˚C for 2 days. (**C/D**) Mitotic function of Mus81-Mms4 is sufficient to confer viability upon induction of RNA-DNA-hybrids in the absence of RNAse H enzymes and mild replication stress (HU). Cell cycle-tagged versions of Mus81-Mms4 were integrated in the *rnh1Δ rnh201Δ* background. Strains were spotted in 5-fold serial dilutions on YPD containing indicated concentrations of HU and incubated at 30˚C for 2 days. (**C**) Spotting containing M^{low}-Mus81-Mms4/S^{low}-Mus81-Mms4 cells. (**D**) Spotting of M^{high}-Mus81-Mms4/S^{high}-Mus81-Mms4 cells. (**E/F**) Repair of Flp-nickase induced DNA lesions requires the M phase function of Mus81-Mms4. Galactose-induced DNA nicking is presumed to be followed by replication run-off in S phase to form single-ended DSBs and repair by BIR (***Nielsen et al., 2009***; ***Mayle et al., 2015***). Location of the corresponding FRT sites on chromosome IV and VI are indicated relative to replication origins. Cells were spotted in 5-fold serial dilutions in presence of glucose or

Figure 3 continued on next page

Figure 3 continued

galactose (FLP-induction) and incubated at 30˚C for 2 days. (**E**) Spottings of M^{low}-Mus81-Mms4/S^{low}-Mus81-Mms4 cells. (**F**) Spottings of M^{high}-Mus81-Mms4/S^{high}-Mus81-Mms4 cells.

The online version of this article includes the following figure supplement(s) for figure 3:

Figure supplement 1. Residual S^{high}-Mus81-Mms4 function in response to genotoxic agents is explained by insufficient restriction to S phase; slight M^{low}-Mus81-Mms4 defect in response to genotoxic agents is due to underexpression during M phase, respectively.

M^{low}-Mus81-Mms4 cannot be rescued by an additional copy of S^{low}-Mus81-Mms4 (***Figure 3—figure supplement 1D–E***).

We next tested whether endogenous replication stress would require Mus81-Mms4 during M phase as well or whether S phase Mus81-Mms4 could play a role in this context. Absence of RNaseH1 and RNaseH2 generates replication stress due to defects in the removal of RNA-DNA-hybrids and defects in ribonucleotide excision repair (***Sollier and Cimprich, 2015***; ***Hamperl and Cimprich, 2016***). Mus81 orthologs were first implicated in the replication stress caused by RNaseH-deficiency because of the synthetic growth phenotype of a *mus81*Δ *rnh1*Δ *rnh201*Δ mutant in *S. pombe* (***Zhao et al., 2018***). We observe a similar synthetic growth phenotype in the corresponding budding yeast *mus81*Δ *rnh1*Δ *rnh201*Δ mutant, which was further aggravated by addition of HU in low concentrations (***Figure 3C–D***). Notably, presence of M phase-restricted versions of Mus81-Mms4 was able to rescue these phenotypes back to levels of the *rnh1*Δ *rnh201*Δ strain, while S phase-restricted versions of Mus81-Mms4 were unable to do so (***Figure 3C–D***). Furthermore, we studied the response to a site-directed protein-bound single strand break induced by a step-arrest mutant of the Flp recombinase (Flp nickase; ***Nielsen et al., 2009***; ***Mayle et al., 2015***). Previous studies have suggested that single strand breaks generated in the Flp nickase system would lead to replication run-off (replication fork breakage) and repair by break-induced replication (BIR) and that Mus81-Mms4 and Yen1 would be redundantly required for survival (***Mayle et al., 2015***). Notably, however, also in the Flp-nick system, we observed that M phase restriction of Mus81-Mms4 allowed survival similar to WT cells (***Figure 3E–F***, note the *yen1*Δ background). In contrast, the S^{low}-Mus81-Mms4 construct led to pronounced sensitivity similar to the *MUS81* deletion, while S^{high}-Mus81-Mms4 led to an intermediary phenotype (***Figure 3E–F***). Collectively, these data show that restriction of Mus81-Mms4 to S phase renders cells sensitive to various forms of replication stress, while restriction of Mus81-Mms4 to M phase does not cause a discernible phenotype, suggesting that in budding yeast the dominant function of Mus81-Mms4 in response to replication stress is post-replicative.

Mus81-Mms4 act as a post-replicative resolvase

To reveal the temporal control underlying the activity of Mus81-Mms4 in resolving recombination and/or replication structures, we turned to single cell cycle experiments. First, we used a single-cell-cycle setup to show that even after DNA damage induction, and recovery, the cell cycle restriction of Mus81-Mms4 expression to S or M phase remains intact (***Figure 4—figure supplement 1***). Consistent with the fact that in budding yeast cyclin-CDK complexes are unlikely to be directly regulated by DNA damage signals (***Zegerman and Diffley, 2009***), we observed restriction to S or M phase as expected. When we next treated cells with MMS in S phase and measured cell survival, we obtained a similar picture as in experiments with chronic exposure: M phase-restricted Mus81-Mms4 showed sensitivity similar to WT cells (***Figure 4A***). In contrast, cells expressing S phase-restricted Mus81-Mms4 showed hypersensitivity, with S^{low}-Mus81-Mms4 cells similar to the *mus81*Δ knock-out and S^{high}-Mus81-Mms4 displaying slightly better survival (***Figure 4A***). To have a physical read-out of repair, we used pulsed-field gel electrophoresis (PFGE), which resolves linear chromosomes, but not in the presence of replication and recombination structures. Intriguingly, *mus81*Δ deficiency has been shown to interfere with recovery of linear chromosomes after MMS treatment in S phase (***Ho et al., 2010***, see ***Figure 4B–C***), but it has been unclear whether this represents a direct function of Mus81 at stalled replication forks or rather a post-replicative function in resolving recombination intermediates. When we released cells from replication fork stalling with MMS in S phase, we found that cells expressing M phase-restricted Mus81-Mms4 versions recover linear chromosomes as WT cells (***Figure 4B–C***). In contrast, cells restricting Mus81-Mms4 to S phase were strongly delayed in the appearance of resolved, linear chromosomes, as were *mus81*Δ cells (***Figure 4B–C***). These data

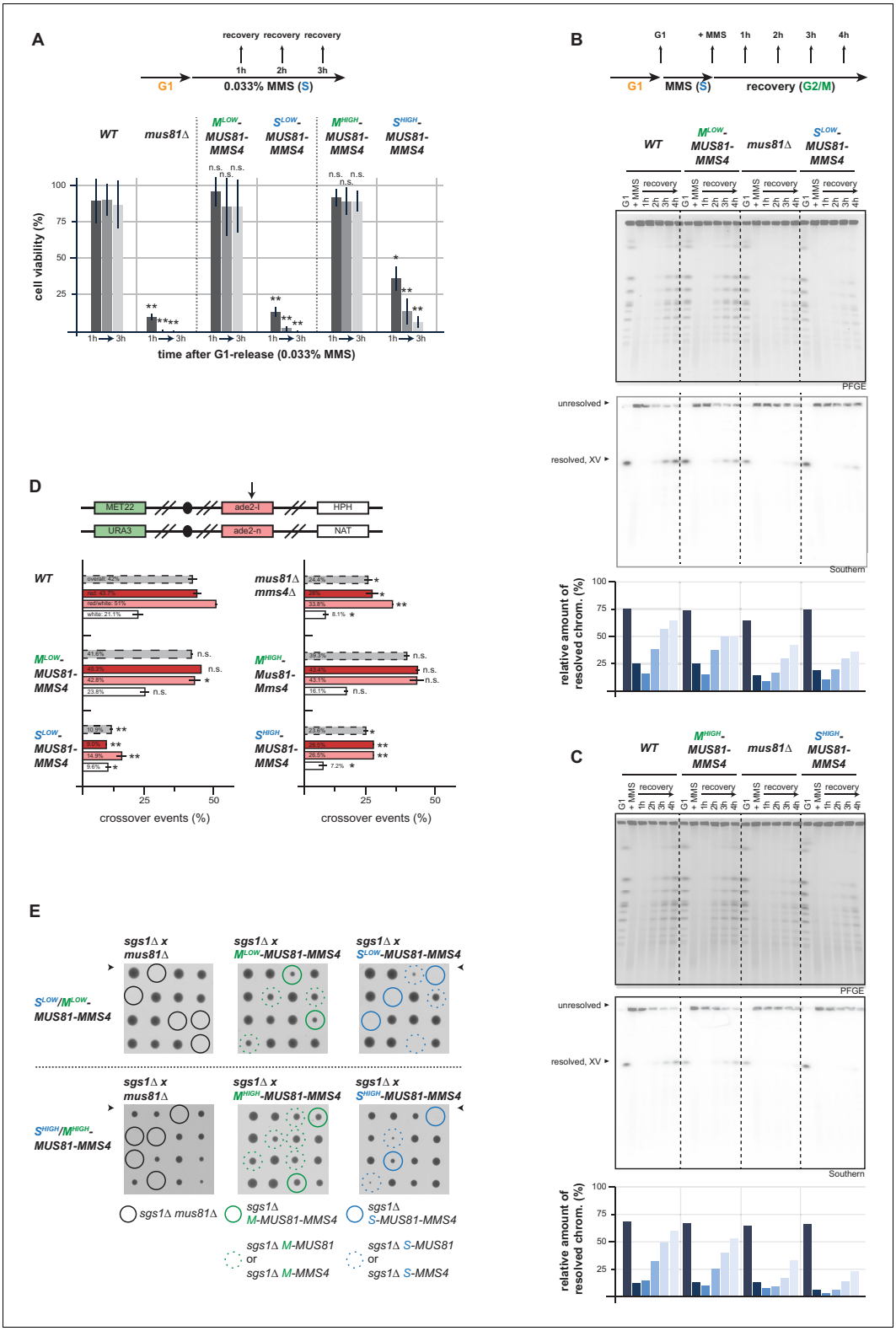

Figure 4. Mus81-Mms4 act as a post-replicative resolvase. (**A**) Viability after a pulse of MMS in S phase and subsequent replication fork stalling depends on the M phase function of Mus81-Mms4. Viability assay scoring survivors after pulses of MMS in S phase for one to three hours (upper). Cell viability (%) was determined by colony forming units normalized to untreated cells (0 hr) and is depicted as mean of biological replicates (n = 3) with error bars indicating standard deviation. Significance: n.s. p>0.05, *p<0.05, **p<0.005 as calculated by an unpaired Student´s T-test (see ***Figure 4—***

Figure 4 continued on next page

Figure 4 continued

source data 1 for underlying values and exact p-values). (B/C) Resolution of replication/repair intermediates arising in response to replication stalling in S phase requires mitotic Mus81-Mms4 function. PFGE analysis of cells recovering (1–4 hr in Nocodazole) from a pulse of MMS (0.033%, 1 hr) in S phase (see upper panel for experimental setup). PFGE gels were stained with EtBr or subjected to southern blot hybridization with a probe against the *ADE2* locus located on chromosome XV. The relative number of resolved chromosomes XV from the southern blots was quantified using ImageJ and is depicted below. (**B**) PFGE/southern analysis of M^{low}-Mus81-Mms4/S^{low}-Mus81-Mms4 cells. (**C**) PFGE/southern analysis of M^{high}-Mus81-Mms4/S^{high}-Mus81-Mms4 cells. (**D**) HR repair resulting in crossovers depends on the mitotic function of Mus81. I-SceI induced recombination assay between heterologous *ade2* alleles in diploid cells as described in ***Ho et al., 2010***. Upper panel: arrangement of marker genes on chromosomes IV used for classifying the genetic outcomes of DSB repair. The arrow indicates the I-SceI site. Bottom panel: genetic outcome of repair, with overall crossover events (grey) and crossovers among individual classes (red, red/white, white) that differ in conversion tract length. Depicted are mean values from two independent experiments each scoring 400–600 cells with the standard deviation as error bars. Significance: n.s. $p>0.05$, *$p<0.05$, **$p<0.005$ compared to WT cells by unpaired Student´s T-test (see ***Figure 4—source data 2*** for underlying values and exact p-values). (**E**) The essential requirement of Mus81 in the absence of *SGS1*-dependent dissolution occurs during M phase. Tetrad analysis of yeast diploid cells with indicated genotypes reveals synthetic lethality between *sgs1*Δ and S^{low}-/S^{high}-Mus81-Mms4 while M^{low}-/M^{high}-Mus81-Mms4 shows no discernible effect on cell growth in the background of *sgs1*Δ (see ***Figure 4—figure supplement 2*** for a growth analysis of the individual spores of the tetrad analysis with S^{high}-/M^{high}-Mus81-Mms4).

The online version of this article includes the following source data and figure supplement(s) for figure 4:

Source data 1. Average, stdv and p-values of normalized colony numbers from replicates 1–3 depicted in ***Figure 4A***.
Source data 2. Average, stdv and p-values of CO rates from two independent experiments depicted in ***Figure 4D***.
Figure supplement 1. Cell cycle tags restrict efficiently to S or M phase also after DNA damage treatment.
Figure supplement 2. Mus81 function during M phase is required in the absence of Sgs1 function.

therefore indicate that Mus81-Mms4 resolves replication or recombination structures to linear chromosomes in a post-replicative manner during M phase.

To further test if the dominant M phase function of Mus81 is that of a post-replicative resolvase, we turned to DSB repair. Specifically, we used a genetic system to study the repair products of an I-SceI induced DSB in diploid cells and score for rates by which recombination intermediates are processed by resolution enzymes generating crossovers (***Ho et al., 2010***). Cells lacking Mus81-Mms4 showed a strong reduction in the formation of crossover repair products (***Ho et al., 2010***; ***Figure 4D***). Notably, cells expressing M phase-restricted versions of Mus81-Mms4 were proficient in crossover formation as WT cells, while S phase-restricted versions of Mus81-Mms4 as well as the *MUS81* deletion showed reduced rates of crossover formation (***Figure 4D***). This shows that the M phase function of Mus81-Mms4 is linked to its role in forming crossovers, suggesting that in budding yeast a major function of Mus81-Mms4 is that of a post-replicative resolvase.

A large proportion of recombination intermediates is typically processed by the Sgs1-Top3-Rmi1 helicase-decatenase complex (***Gangloff et al., 1994***; ***Fabre et al., 2002***; ***Wu and Hickson, 2003***; ***Cejka et al., 2010***). A hallmark phenotype of *mus81*Δ mutants therefore is the synthetic lethality with *sgs1*Δ (***Kaliraman et al., 2001***; ***Mullen et al., 2001***; ***Fabre et al., 2002***; ***Bastin-Shanower et al., 2003***). A strong synthetic phenotype was observed when we restricted Mus81 expression to S phase, but no such defect was seen when we restricted Mus81 expression to M phase (***Figure 4E***, ***Figure 4—figure supplement 2***). Overall, the cell cycle tag methodology therefore makes a strong case for Mus81-Mms4 having its dominant function in response to replication perturbation by acting post-replicatively in M phase, likely as a resolvase processing HR or replication intermediates. Such an M function is consistent with M phase specific phosphorylation and stimulation (***Matos et al., 2011***; ***Gallo-Fernández et al., 2012***; ***Matos et al., 2013***; ***Saugar et al., 2013***; ***Szakal and Branzei, 2013***; ***Gritenaite et al., 2014***; ***Princz et al., 2017***), but does not exclude an S phase function outside of the tested phenotypes.

Premature activation of Yen1 from S to early M phase interferes with the response to replication stalling lesions

Why are resolvases cell cycle regulated? We and others have reasoned that high levels of resolvase activity during S phase may interfere with replication and the response to replication stalling (***Szakal and Branzei, 2013***; ***Blanco et al., 2014***; ***Duda et al., 2016***; ***Pfander and Matos, 2017***). We realized that cell cycle tags could also be used to reinstall cell cycle regulation to deregulated versions of proteins, in this case resolvases. To this end we turned to a second resolvase – Yen1, which

is cell cycle-controlled and restricted to late M phase by inhibitory cyclin-CDK phosphorylation (**Kosugi et al., 2009**; **Matos et al., 2011**; **Blanco et al., 2014**; **Eissler et al., 2014**; **García-Luis et al., 2014**). A mutant version of Yen1 called *YEN1-ON* is deficient in inhibitory CDK phosphorylation sites, constitutively active throughout the cell cycle and detrimental to cellular survival after genotoxic insults as well as during meiosis (**Blanco et al., 2014**; **Eissler et al., 2014**; **Arter et al., 2018**).

To restrict Yen1-ON to specific cell cycle phases and reveal at which cell cycle phase the detrimental effects of *YEN1-ON* manifest, we combined this allele with cell cycle tags. Specifically, we used our proposed cell cycle tag workflow (**Figure 1D**) and generated two sets of G1-S-M triples expressed at low and high levels, with similar peak expression levels within each set. Tagging of Yen1 at the N-terminus interfered with protein function and we therefore constructed C-terminal cell cycle-tagged versions of Yen1-ON (**Figure 5A**, **Figure 5—figure supplement 1**). When we screened different cell cycle tag constructs, we found that Clb6$^{pClb6\ -80bp}$-tagged, Clb2$^{pClb2\ -60bp}$-tagged and Sic1$^{pSic1\ u(ATA)AUG}$-tagged versions of Yen1-ON showed peak expression levels in S, M and G1 phase that were between 1.3 to 1.5-fold of Yen1-ON expressed from endogenous promoter (**Figure 5A**, **Figure 5—figure supplement 2A,C**) and will therefore be referred to as M^{low}-Yen1-ON, S^{low}-Yen1-ON and G1^{low}-Yen1-ON, respectively. Furthermore, Clb2^{pClb1}-tagged, Clb6^{pClb6}-tagged and Sic1$^{pSic1\ -20bp}$-tagged versions of Yen1-ON showed 2.5 to 3-fold peak expression levels compared to endogenous Yen1-ON expressed from its endogenous promoter, but similar among the different constructs (**Figure 5A**, **Figure 5—figure supplement 2B,C**), and will be referred to as M^{high}-Yen1-ON, S^{high}-Yen1-ON and G1^{high}-Yen1-ON, respectively. S^{low}-Yen1-ON and S^{high}-Yen1-ON expression peaked in S phase (20–50 min and 20–60 min after G1 release, respectively), M^{low}-Yen1-ON and M^{high}-Yen1-ON expression in M phase (50–70 min) and G1^{low}-Yen1-ON and G1^{high}-Yen1-ON started to express in late M phase (70 min, **Figure 5A**), thereby confirming cell cycle restriction of Yen1-ON expression to the expected cell cycle phases.

With cell cycle-restricted versions of Yen1-ON at hand we tested known Yen1-ON phenotypes. Deregulated Yen1-ON is able to complement phenotypes of the *MUS81* deletion mutant such as MMS hypersensitivity, suggesting that both resolvases display a degree of functional redundancy (**Blanco et al., 2014**). Notably, only the M phase-restricted version of Yen1-ON and the constitutively expressed Yen1-ON were able to rescue the MMS sensitivity of cells lacking *MUS81*, while the S phase-restricted and the G1 phase-restricted versions of Yen1-ON were unable to do so (**Figure 5B**). These data further indicate that early M phase is a window of opportunity, during which a Mus81-like resolvase must act and that Yen1-ON can take this function, if specifically activated during this time.

Conversely, *YEN1-ON* itself induces hypersensitivity towards MMS compared to WT cells (**Blanco et al., 2014**; **Figure 5C–D**). We therefore tested the cell cycle-restricted versions of Yen1-ON for MMS hypersensitivity and found that restriction of Yen1-ON expression to late M and G1 using the G1^{high}-Yen1-ON or G1^{low}-Yen1-ON construct did not yield hypersensitivity, no matter whether cells were chronically exposed to MMS (**Figure 5C**) or treated with a pulse of MMS during S phase (**Figure 5D**). This suggests that restricting Yen1-ON expression to those cell cycle phases where the protein would normally be in its dephosphorylated form is sufficient to suppress the MMS hypersensitivity phenotype. In contrast, Yen1-ON expression in S or M phase caused MMS hypersensitivity that was similar to what was observed with unrestricted expression of Yen1-ON (**Figure 5C–D**). Notably, Yen1-ON phenotypes depend strongly and in a dose-dependent manner on its expression levels (**Blanco et al., 2014**; MG Blanco, personal communication). Consistently, we saw slightly increased MMS hypersensitivity in S^{high}-Yen1-ON and M^{high}-Yen1-ON compared to S^{low}-Yen1-ON and M^{low}-Yen1-ON (**Figure 5C–D**).

Therefore, we conclude that (i) the presence of deregulated Yen1 in S phase is detrimental to the cellular response to replication stalling and that (ii) deregulated Yen1 in M phase is detrimental as well but can at the same time partially compensate for the absence of Mus81-Mms4. Overall, the cell cycle tag approach therefore demonstrated that the dominant functions of Mus81-Mms4 and Yen1 manifest in those cell cycle phases – M phase and late M/G1 phase, respectively – where the proteins also become stimulated by PTM modification/demodification.

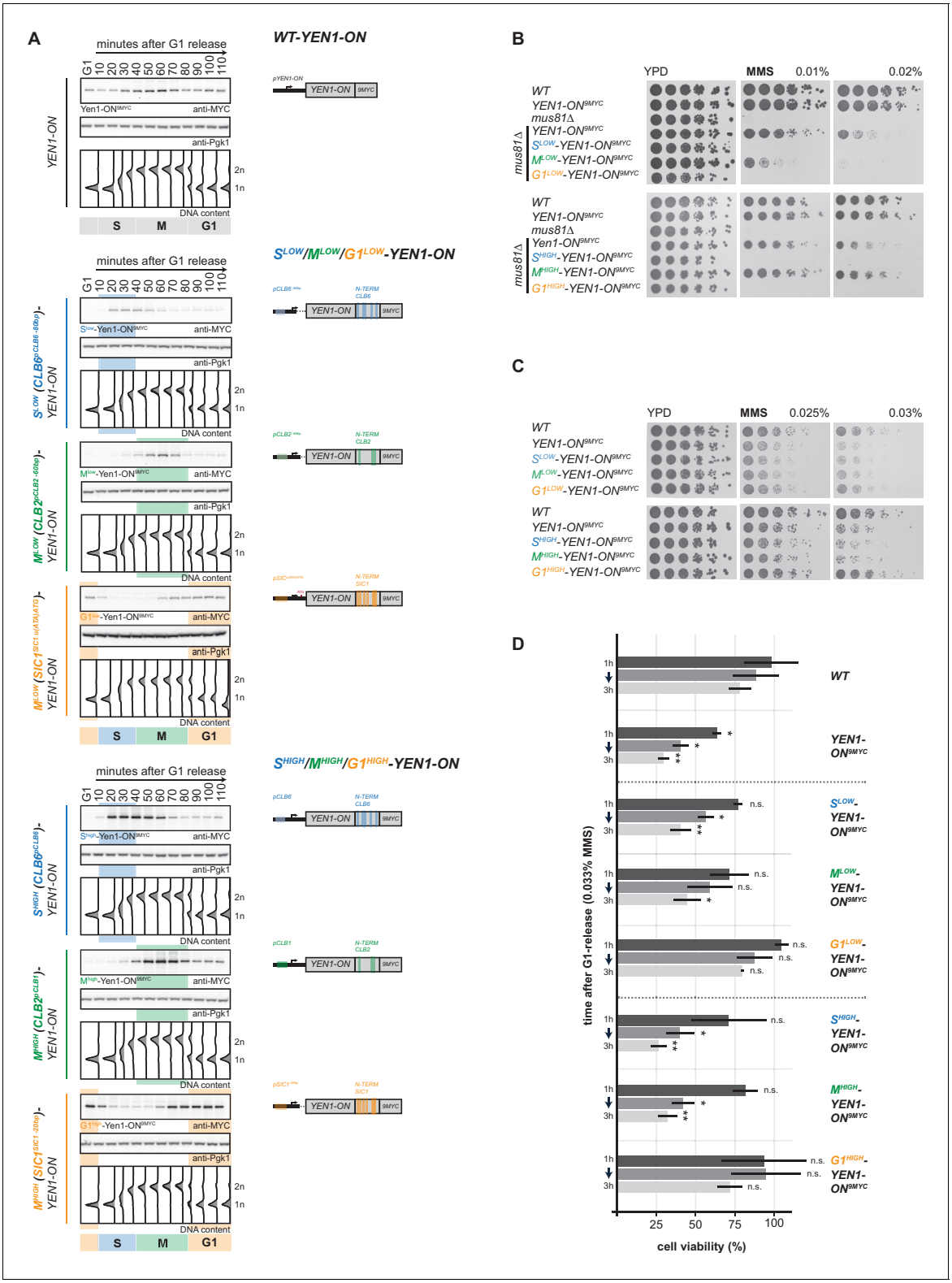

Figure 5. Premature activation of Yen1 in S or early M phase interferes with the response to replication stalling lesions. (**A**) Cell cycle-tagged Yen1-ON-9MYC constructs restrict expression of constitutively active Yen1-ON to S, M or G1 phase. (Left) Western blot analysis of strains expressing WT, S (S^{low} ($Clb6^{pClb6\ -80bp}$)-Yen1-ON^{9MYC}/S^{high} ($Clb6^{pClb6}$)-Yen1-ON^{9MYC}), M (M^{low} ($Clb2^{pClb2\ -60bp}$)-Yen1-ON^{9MYC}/M^{high} ($Clb2^{pClb1}$)-Yen1-ON^{9MYC}) and G1 ($G1^{low}$ ($Sic1^{pSic1\ u(ATA)ATG}$)-Yen1-ON^{9MYC}/$G1^{high}$ ($Sic1^{pSic1\ -20bp}$)-Yen1-ON^{9MYC}) phase-restricted Yen1-ON during synchronous cell cycle progression as in

Figure 5 continued on next page

Figure 5 continued

Figure 2A. (see ***Figure 5—figure supplement 2*** for quantification of peak expression levels for individual constructs). (Right) schematic representation of endogenously expressed and cell cycle-tagged Yen1-ON constructs. Blue, green and orange bars indicate location of cell cycle regulatory elements in the promoter and N-terminal degron sequence. (**B**), The M phase function of Yen1-ON is able to bypass Mus81 requirement after MMS induced replication fork stalling. Strains with indicated genotypes were chronically exposed to MMS as in ***Figure 3A*** (note the *mus81Δ* background). (**C–D**), Viability after MMS induced replication fork stalling decreases when Yen1-ON is restricted to S or early M phase. (**C**) Survival of indicated strains after chronic MMS exposure as in (**B**). (**D**) Viability assay after a single pulse of MMS in S phase was measured for indicated strains as in ***Figure 4A*** (see ***Figure 5—source data 1*** for underlying values and exact p-values).

The online version of this article includes the following source data and figure supplement(s) for figure 5:

Source data 1. average, stdv and p-values of normalized colony numbers from replicates 1–3 depicted in ***Figure 5D***.
Figure supplement 1. Strategy for C-terminal cell cycle tagging of Yen1-ON.
Figure supplement 2. Analysis of 'low' and 'high' S-, M- and G1-tagged Yen1-ON peak expression levels.

Discussion

An advanced toolbox of cell cycle tags

Cell cycle tags are a straightforward method to restrict protein expression to specific cell cycle phases. The toolbox of constructs presented here allows straightforward introduction of cell cycle tags at the locus of interest within the budding yeast genome using standard recombination-based techniques (***Knop et al., 1999***; ***Janke et al., 2004***). Importantly, with constructs that vary in peak expression, our cell cycle tag toolbox allows for the first time to restrict protein expression to different cell cycle phases and at similar peak expression levels. Similar peak expression levels are necessary, if one wants to compare phenotypes arising from restricting protein expression to different cell cycle phases or tries to unravel at which cell cycle phase a protein exhibits its essential function. To allow titration of expression levels, our cell cycle tag toolbox currently contains a total of 46 cell cycle tag constructs, with the upper expression limit being determined by cyclin promoters (***Figure 1***). So far, we have used these constructs to restrict expression of 13 proteins (***Figures 2–4***; JB and BP unpublished data). Based on this experience, we suggest the following experimental workflow: (i) Compare peak expression levels of cell cycle-restricted constructs to endogenously expressed protein. Here, a western blot against 3FLAG-tagged protein might be used (see ***Pfander and Diffley, 2011*** for pYM-3FLAG tagging constructs). (ii) Due to the dynamic expression regime, a given cell cycle-tagged construct is unlikely to give endogenous expression levels throughout the cell cycle phase of interest. This problem is further aggravated if experimental conditions are varied (for example: growth on liquid vs solid media, cell cycle arrest, or drug treatment activating cell cycle checkpoints). Therefore, we suggest finding triples of S-, M- and G1-tag constructs (or sometimes pairs) with similar peak expression levels. Furthermore, we advise to select two sets of triples/pairs (called 'low' and 'high' throughout the manuscript), which vary in peak expression levels and thereby allow to separate phenotypes arising from under- or overexpression from those arising from cell cycle restriction. Although expression may vary for individual proteins, combinations of constructs that regularly gave us similar peak expression levels are $Clb6^{pClb6}$ (or $Clb6^{pClb5}$), $Clb2^{pClb1}$, $Sic1^{pSic1\ -20bp}$ for the high expressing set and $Clb6^{pClb6\ -80bp}$, $Clb2^{pClb2\text{-}60bp}$ (or $Clb2^{pClb1\ -150bp}$), $Sic1^{pSic1\ u(ATA)ATG}$ for the low set. (iii) Genetics will often indicate whether N-terminal tagging is compatible with protein function as such, but an additional control for the functionality of the tagged constructs is desirable. For Mus81-Mms4 we used cleavage of DNA junctions in vitro (***Figure 2D***). Collectively these considerations are expected to allow interpretation of the cell cycle restriction experiment and reveal cell cycle stage-specific functionality of the protein of interest.

The essential function of the structure-selective nuclease Mus81-Mms4 manifests in M phase

Phenotypic analysis suggests that Mus81-Mms4 plays a major role in the response to replication stalling (***Xiao et al., 1998***; ***Interthal and Heyer, 2000***; ***Boddy et al., 2001***; ***Mullen et al., 2001***; ***Doe et al., 2002***; ***Bastin-Shanower et al., 2003***; ***Kai et al., 2005***; ***Saugar et al., 2013***). As such, it is seemingly contradictory that Mus81-Mms4 becomes post-translationally modified and stimulated in its activity only after S phase, when cells enter M phase (***Matos et al., 2011***; ***Matos et al., 2013***; ***Gallo-Fernández et al., 2012***; ***Saugar et al., 2013***; ***Szakal and Branzei, 2013***; ***Princz et al., 2017***).

Mutations abolishing Mus81-Mms4 phosphorylation showed pronounced phenotypes and M phase-specific stimulation of Mus81-Mms4 shows hallmark signs of switch-like activation (**Matos et al., 2011**; **Gallo-Fernández et al., 2012**; **Matos et al., 2013**; **Szakal and Branzei, 2013**; **Princz et al., 2017**). Nonetheless, a possible S phase function as well as the relative contribution of S and M phase phenotypes have been widely discussed (**Xiao et al., 1998**; **Boddy et al., 2000**; **Interthal and Heyer, 2000**; **Haber and Heyer, 2001**; **Kaliraman et al., 2001**; **Mullen et al., 2001**; **Doe et al., 2002**; **Fabre et al., 2002**; **Bastin-Shanower et al., 2003**; **Kai et al., 2005**; **Hanada et al., 2007**; **Shimura et al., 2008**; **Regairaz et al., 2011**; **Fu et al., 2015**; **Xing et al., 2015**; **Lemaçon et al., 2017**). In this study, we have applied the cell cycle tag approach to tackle this question and observed that restriction of Mus81-Mms4 expression to S phase induces strong phenotypes similar to those of the *MUS81* deletion, while restriction of Mus81-Mms4 to M phase allows full functionality. The essential function(s) of Mus81-Mms4 therefore appear to be specific to M phase, correlating with its M phase-specific stimulation.

Consequently, this raises the question about the mechanism underlying the Mus81-Mms4 M phase function. We think that our data are generally consistent with a model whereby Mus81-Mms4 acts as a resolvase that processes an HR intermediate (for example a HJ or a D loop (**Boddy et al., 2001**; **Kaliraman et al., 2001**; **Chen et al., 2001**; **Constantinou et al., 2002**; **Doe et al., 2002**; **Bastin-Shanower et al., 2003**; **Ciccia et al., 2003**; **Gaillard et al., 2003**; **Osman et al., 2003**; **Whitby et al., 2003**; **Fricke et al., 2005**; **Ehmsen and Heyer, 2008**; **Taylor and McGowan, 2008**; **Schwartz et al., 2012**; **Pepe and West, 2014b**)). This HR intermediate could originate from the usage of HR (or template switch replication) to bypass replication stalling lesions or DNA breaks arising in S phase (**Liberi et al., 2005**; **Branzei et al., 2008**; **Giannattasio et al., 2014**; **Branzei and Szakal, 2016**). As such, the prime function of Mus81-Mms4 would be to aid resolution of sister chromatids (**Roseaulin et al., 2008**; **Wechsler et al., 2011**; **Wyatt et al., 2013**; **Mankouri et al., 2013**; **Matos et al., 2013**; **Szakal and Branzei, 2013**; **Gritenaite et al., 2014**; **Princz et al., 2017**) and share functional overlap with STR-dependent dissolution (**Gangloff et al., 1994**; **Fabre et al., 2002**; **Wu and Hickson, 2003**; **Ira et al., 2003**).

Mus81-Mms4 might also have more than one M phase function. For example, it is possible that Mus81-Mms4 might act on replication forks that persist until M phase, similar to what has been shown for MUS81 in human cells, which acts in the MIDAS pathway to process replication forks at sites of under-replicated DNA and to thereby initiate repair by BIR (**Minocherhomji et al., 2015**; **Duda et al., 2016**). Furthermore, Mus81-Mms4 may also act at a later step in BIR to switch from an extending D-loop mechanism of DNA synthesis to a type of DNA synthesis that is more similar to canonical DNA replication, a model that has been suggested by a study in budding yeast (**Mayle et al., 2015**). Interestingly, we observed using the same experimental set-up as Mayle et al. that M phase-restricted Mus81-Mms4 is entirely sufficient for survival after induction of the Flp-nickase (**Figure 3E,F**), suggesting that a possible function of Mus81-Mms4 in BIR takes place in M phase thus bearing a similar cell cycle profile as MIDAS (**Minocherhomji et al., 2015**). In line with our conclusions, and while this manuscript was in preparation, the Pasero and Aguilera labs published a preprint showing by several approaches a post-replicative function of Mus81-Mms4 in response to replication blockage (**Pardo et al., 2019**).

We emphasize that our study can by no means rule out that Mus81-Mms4 also functions in S phase. However, at least in budding yeast we are not aware of any data in the current literature that would necessitate to evoke such an S phase function for Mus81-Mms4. This raises the question of whether budding yeast Mus81-Mms4 can serve as a paradigm for other species. The fact that human MUS81 complexes are cell cycle regulated (**Wyatt et al., 2013**; **Duda et al., 2016**) suggests that Mus81-Mms4 with its essential M phase function may indeed be a good model for the Mus81 biology in other organisms. However, we caution that additional regulatory mechanisms exist in other systems. Fission yeast Mus81-Eme1 harbours for example an additional layer of control by the DNA damage checkpoint (**Boddy et al., 2000**; **Kai et al., 2005**; **Froget et al., 2008**; **Dehé et al., 2013**). Human MUS81 has two accessory subunits (EME1 and EME2; **Ciccia et al., 2003**), which are likely differentially regulated (**Matos et al., 2011**; **Duda et al., 2016**). Indeed, there is overwhelming genetic data showing that in human cells MUS81 is required for the cellular response to replication perturbation (**Hanada et al., 2007**; **Shimura et al., 2008**; **Regairaz et al., 2011**; **Fugger et al., 2013**; **Naim et al., 2013**; **Ying et al., 2013**; **Pepe and West, 2014a**; **Xing et al., 2015**; **Fu et al., 2015**; **Minocherhomji et al., 2015**; **Lemaçon et al., 2017**). While some of these data could be

explained by a role for MUS81 as a post-replicative resolvase – similar to what is shown here for the budding yeast protein – an earlier role at stalled replication forks in S phase cannot be excluded. Perhaps the strongest case for an S phase function of human MUS81 is made by several genetic studies showing that cells depleted for MUS81 display perturbed DNA replication, a constitutive DNA damage response and defects in the response to replication perturbation (**Hanada et al., 2007**; **Shimura et al., 2008**; **Regairaz et al., 2011**; **Buisson et al., 2015**; **Fu et al., 2015**; **Xing et al., 2015**). These phenotypes could arise from a direct function at replication forks in S phase (perhaps in processing/cleavage of stalled replication forks), which would then be absent from the budding yeast system (or so far elusive). Since at this stage a possible indirect effect upon MUS81 deletion or depletion can also not be excluded, we suggest that methodologies analogous to the cell cycle tag system described here might be useful to ascertain the relative contribution of M and S phase functions in human cells.

Premature resolvase activation is detrimental to the response to replication stalling

A second and so far under-utilized application of cell cycle tags is to install de novo cell cycle regulation on a deregulated mutant protein. We demonstrated this strategy using the deregulated *YEN1-ON* allele of the Yen1 resolvase (**Blanco et al., 2014**). Specifically, we showed that the previously described MMS hypersensitivity phenotype of *YEN1-ON* cells is generated by premature activation of Yen1 in S and early M phase. These data corroborate the importance of restricting post-translational activation of Yen1 specifically to late M and G1 phase. They also argue against Yen1 having a function in S phase and raise the question about what detrimental effects premature resolvase activation might be causing.

Interestingly, these data suggest that differences between the Mus81-Mms4- and Yen1-dependent mechanisms exist and fit to both enzymes having distinct temporal activation profiles. Differential activation of Mus81-Mms4 and Yen1 could perhaps simply serve the purpose to equip cells with at least one highly active SSE at different cell cycle stages from early M to the G1/S transition (**Wild and Matos, 2016**). Furthermore, temporal activation establishes hierarchy in the corresponding resolution/dissolution mechanisms. In particular, we favour a three-tiered hierarchy for enzymes that process recombination intermediates: first, STR-dependent dissolution is fully active in S phase (**Ashton et al., 2011**; **Versini et al., 2003**; **Bizard and Hickson, 2014**; **Grigaitis et al., 2020**), second, Mus81-Mms4 gets stimulated in early M and third, Yen1 would become activated only in late M and as a measure of last resort. Such a hierarchy could be a means to counteract cross-overs and loss-of-heterozygosity in mitotically dividing cells (**Ho et al., 2010**; **Matos et al., 2013**; **Szakal and Branzei, 2013**; **Blanco et al., 2014**), but it may simply reflect differential efficiency of competing molecular mechanisms. Furthermore, it is possible that the three mechanisms are directed towards distinct substrates. In order to identify the exact nature of these substrates, molecular genetic assays will be necessary and we suggest they be carried out with very precise genetic perturbation provided by cell cycle tag methodology.

Materials and methods

Key resources table

Reagent type (species) or resource	Designation	Source or reference	Identifiers	Additional information
Antibody	anti-FLAG (rabbit-polyclonal)	Sigma	Cat# F7425, RRID:AB_439687	WB (1:2000)
Antibody	anti-FLAG M2-Peroxidase (mouse-monoclonal)	Sigma	Cat# A8592, RRID:AB_439702	WB (1:3000)
Antibody	anti-MYC (mouse-monoclonal)	Millipore	Cat# 05–724, clone 4A6, RRID:AB_11211891	WB (1:2000)

Continued on next page

Continued

Reagent type (species) or resource	Designation	Source or reference	Identifiers	Additional information
Antibody	anti-Clb2 (rabbit-polyclonal)	Santa Cruz	Cat# sc-9071, RRID:AB_667962	WB (1:500)
Antibody	anti-Hsp70 (mouse-polyclonal)	Enzo Life Sciences	Cat# ADI-SPA-822, RRID:AB_10615940	WB (1:10000)
Antibody	anti-H4 (rabbit-polyclonal)	Abcam	Cat# ab10158, RRID:AB_296888	WB (1:2000)
Antibody	anti-Nsp1 (mouse-monoclonal)	Abcam	Cat# ab4641, RRID:AB_304549	WB (1:10000)
Strain, strain background (*S. cerevisiae*)	strain background, W303	***Rothstein, 1983***		
Strain, strain background (*S. cerevisiae*)	yeast strains	This study		***Supplementary File 1***
Recombinant DNA reagent	plasmid backbone, pYM-N31	***Janke et al., 2004*** Euroscarf	P30284	
Recombinant DNA reagent	plasmid backbone, pRS303	ATCC	Cat# 77138	
Recombinant DNA reagent	plasmids	This study		***Supplementary file 1***
Sequence-based reagent	S1	***Janke et al., 2004***	PCR primers	cgtacgctgcaggtcgac
Sequence-based reagent	S4	***Janke et al., 2004***	PCR primers	catcgatgaattctctgtcg
Sequence-based reagent	yeGFP S1	This study	PCR primers	attgtaatacgactcact atagggcgaattggag ctccaccgcggtggcg gccgccgtacgctgca ggtcgac
Sequence-based reagent	yeGFP S4	This study	PCR primers	ctaattcaaccaaaattg ggacaacaccagtgaa taattcttcacctttagaca tcatcgatgaattctctgtcg
Sequence-based reagent	Mus81 S1	This study	PCR primers	caaagtttcaaaggatt gatacgaacacacattc ctagcatgaaagcatgc gtacgctgcaggtcgac
Sequence-based reagent	Mus81 S4	This study	PCR primers	caactaattcttgtaaccatt caatatataggtcttttaagtt tgatgagagttccatcgatg aattctctgtcg
Sequence-based reagent	Mms4 S1	This study	PCR primers	acaatgtatggattatgg tatagaataatagtagtc acatattgcagctagttaa cgtacgctgcaggtcgac
Sequence-based reagent	Mms4 S4	This study	PCR primers	gaatactggcatcgtttct tgaatctttgtcctcaaca aaatcaacgatctggctc atcgatgaattctctgtcg
Commercial assay or kit	In-Fusion HD Cloning	Clontech	639648	

Continued on next page

Continued

Reagent type (species) or resource	Designation	Source or reference	Identifiers	Additional information
Chemical compound, drug	Sytox-green	Invitrogen	S7020	
Chemical compound, drug	RNaseA	Sigma Aldrich	R4875	
Chemical compound, drug	ProteinaseK	Sigma Aldrich	P2308	
Chemical compound, drug	Pierce ECL Western Blotting Substrate	Thermo Fisher	2106	
Chemical compound, drug	Nocodazol	Sigma Aldrich	M1404	
Chemical compound, drug	Hydroxyurea	Sigma Aldrich	H8627	
Chemical compound, drug	MMS	Sigma Aldrich	129925	
Chemical compound, drug	Camptothecin	Sigma Aldrich	C9911	
Peptide, recombinant protein	alpha-Factor	MPIB core facility		
Other	Zymolyase Z100T	Roth	9329.2	
Other	Pulsed Field certified Agarose	BioRad	1620138	
Other	Amersham Protran Premium 0.45 um Nitrocellulose membrane	GE Healthcare	10600003	
Other	Amersham Hybond N+ Nylon membrane	GE Healthcare	RPN203B	
Other	NuPAGE Novex, 4–12% BIS-TRIS gels	Invitrogen	NP0323	
Software, algorithm	T-Test calculator	GraphPad	GraphPad, RRID:SCR_000306	http://www.graphpad.com/quickcalcs/ttest2

Yeast strains

All yeast strains are based on W303 (***Rothstein, 1983***) and constructed by genetic crossing and transformation techniques. ORF deletion as well as N-terminal cell cycle tagging was done using standard techniques (***Knop et al., 1999***; ***Janke et al., 2004***) and is described in more detail in the paragraph construction of cell cycle-tagged strains. A list of all yeast strains used in this study can be found in ***Supplementary file 1*** – Table 1.

Construction of cell cycle-tagged strains

Tagging constructs for N-terminal cell cycle tagging of genes are based on the pYM-N plasmid (***Janke et al., 2004***) and harbour the regulatory sequences of the corresponding cyclin (promoter + N-terminus) together with a 3FLAG-tag and the NAT marker sequence flanked by S1 and S4 primer

sequences (***Figure 1—figure supplement 1***). Plasmid constructs were generated using standard molecular biology techniques and truncation of the 5´UTR or insertion of upstream out of frame ATGs was achieved by site-directed mutagenesis techniques. A list of tagging constructs for N-terminal cell cycle tagging of genes can be found in ***Supplementary file 1*** - Table 2.

Amplification of the N-terminal tagging cassettes was achieved by PCR using S1 and S4 primer sequences (see Key Resources table for sequences) fused to a 55 bp sequence homologous to the promoter-gene junction of the corresponding gene (***Figure 1—figure supplement 1***) (see Key Resources table for sequences of S1, S4 primers coupled to the GFP, Mus81 and Mms4 promoter-gene junction sequences). The PCR product was transformed into competent yeast cells and correct integration of the tagging constructs was verified by genotyping PCR using two primer pairs, whereby the first tested integration of the tagging construct and the second verified deletion of the endogenous promoter sequence. Expression of the gene fusion product was then verified by western blotting (see ***Figure 1—figure supplement 1*** for a protocol of the experimental workflow).

For C-terminal cell cycle tagging of Yen1-ON, constructs were assembled together with the gene of interest within the integrative pRS303 vector backbone, linearized by restriction enzyme cutting and integrated into the HIS3 locus. Correct integration of the plasmids was checked by genotyping PCR using two primer pairs verifying integration of a single copy of the plasmid and expression of the tagged protein was verified by western blotting (see ***Figure 5—figure supplement 1*** for a protocol of the workflow).

Antibodies

Detection of proteins was achieved by using antibodies listed in the Key Resources table.

DNA content measurement

Cell cycle progression was analysed by DNA content measurements by flow cytometry. 1×10^7 – 2×10^7 cells were harvested and resuspended in 1 ml of fixation buffer (70% ethanol + 50 mM Tris pH 8). Cells were washed 1x with 1 ml of 50 mM Tris pH 8 and incubated in 520 µl of RNase solution (500 µl 50 mM Tris pH 8 + 20 µl RNase A (10 mg/ml in 10 mM Tris pH 7.5, 10 mM MgCl2) over night at 37˚C. Next, cells were treated with 220 µl proteinase K solution (200 µl 50 mM Tris pH 8 + 20 µl proteinase K (10 mg/ml in 50˚C glycerol, 10 mM Tris pH 7.5, 25 mM CaCl2) for 30 min at 50˚C. Afterwards, cells were resuspended in 500 µl 50 mM Tris pH 8, sonicated (5'', 50% Cycle, minimum power) and stained in SYTOX solution (1:1000 in Tris pH 8). Fluorescence intensity was measured at 520 nm using MACSquant Analyzer 10 (Milteny Biotech) and the data was analysed using FlowJo (FlowJo, LLC).

Acrylamide gel electrophoresis and western blotting

Separation of proteins was achieved using standard SDS-polyacrylamid gel electrophoresis in 4–12% Novex NuPage BisTris precast gels (ThermoFisher) with MOPS buffer (50 mM MOPS, 50 mM Tris-base, 0.1% SDS, 1.025 mM EDTA, adjusted to pH 7.7). Afterwards, proteins were transferred to nitrocellulose membrane (Amersham Protran Premium 0.45 µm NC) by wet blotting in western transfer buffer (48 mM Tris-base, 39 mM glycine, 0.0375% SDS, 20% methanol). Membranes were incubated with the primary antibodies (diluted at concentrations indicated in the Key resources table in milk buffer: 2.5% milk powder, 0.5% BSA, 0.5 % NP-40, 0.1% Tween-20, 50 mM Tris pH 7.5, 137 mM NaCl, 3 mM KaCl) over night at 4˚C or at room temperature for 2 hr when using mouse-anti-FLAG directly coupled to HRP. Appropriate secondary antibodies coupled to HRP were applied at room temperature for 2 hr. Washing of the membranes was performed three times for 5 min with western wash buffer (50 mM Tris pH 7.5, 137 mM NaCl, 3 mM KaCl, 0.2% NP-40) and incubated with Pierce ECL western blotting substrate (ThermoFisher) according to the manufacturer's instruction. Chemiluminescence was detected using a tabletop film processor (OPTMAX, Protec) or with an iBright FL1000 imaging system (ThermoFisher).

Preparation of whole cell extracts (alkaline lysis/TCA)

2×10^7 cells were resuspended in 1 ml of pre-cooled water and mixed with 150 µl of freshly prepared lysis solution (1.85 M NaOH, 7.5% beta-mercaptoethanol). Lysis was performed at 4˚C for 15 min and protein precipitation was achieved by adding 150 µl of 55% pre-cooled TCA solution and

incubation for 10 min. After centrifugation and aspiration of the supernatant, protein pellets were resuspended in 50 µl HU-buffer (8 M Urea, 5% SDS, 200 mM Tris pH 6.8, 1.5% dithiothreitol, traces of bromophenol blue) and incubated at 65˚C for 10 min.

Synchronization of cells, cell cycle release, viability

Generally, cell cycle arrests and releases were performed as described in ***Reusswig et al., 2016***. Cells were grown to log-phase (OD_{600}0.4–0.6) in YP + 2% glucose (YPD) prior to arrest. To arrest cells in G1, S and M phase, the cultures were supplemented with α-factor (5 µg/ml, MPIB), nocodazole (5 µg/ml, Sigma-Aldrich) and hydroxyurea (HU) (200 mM, Sigma-Aldrich) for 2 hr, respectively.

Release from G1 was performed by washing cells twice with prewarmed YP followed by resuspending cells in the same volume of prewarmed YPD. To ensure that cells run through the cell cycle only once, α-factor (5 µg/ml) was added back to the cultures 40 min after release from G1. For DNA damage treatment in S phase and analysis of fully replicated chromosomes by PFGE cells were released from G1 into prewarmed YPD containing 0.033% MMS for 1 hr. Afterwards, cells were washed twice again with prewarmed YP and resuspended in prewarmed YPD containing nocodazole (5 µg/ml).

To determine survival of MMS treatment cells were kept in MMS containing medium (0.033%) and plated in triplicates onto YPD plates at time points indicated in the figures. Colony-forming units were counted after incubation at 30˚C for 3 days. Viability experiments were performed in three independent biological replicates and the standard deviations of those experiments are represented as error bars in the corresponding bar charts. Statistical significance for the viability of individual strains compared to the wild-type was calculated using an unpaired Student´s T-test. These calculations were done using the GraphPad web-tool 'T-test calculator' (http://www.graphpad.com/quickcalcs/ttest2).

For subsequent analysis of DNA or protein content, aliquots (1 OD_{600}, approx. 1×10^7 cells) were withdrawn from the culture at indicated time points. For flow cytometric analysis, cells were resuspended in fixation buffer (70% ethanol + 50 mM Tris pH 8) and incubated at 4˚C for at least 30 min prior to further processing (see section DNA content measurement). For western analysis, cells were snap-frozen in liquid nitrogen and stored at −80˚C prior to further processing (see section alkaline lysis/TCA).

Chronic treatment with genotoxic agents

To assess viability of yeast strains on MMS, CPT and HU containing solid medium (prepared 1 day prior), cells from stationary grown over-night cultures were spotted with a starting concentration of OD_{600} 0.5 in serial dilution (1:5) and incubated at 30˚C for 2 days. All spottings were done in 2–3 biological replicates, each containing two technical replicates.

Pulsed-field gel electrophoresis (PFGE) and southern blotting

Cells were fixed and embedded in agarose plugs as described in ***Finn and Li, 2013***. Plugs were loaded on a 1% (w/v) agarose (Pulsed-field certified, BioRad) gel in 0.5 x TBE (45 mM Tris, 45 mM borate, 0.5 mM EDTA). Electrophoresis was carried out in 14˚C cold 0.5 x TBE in a CHEF DR-III system (initial switch time 60 s, final switch time 120 s, 6 V/cm, angle 120˚C, 24 hr). Afterwards, the gel was stained with 1 µg/ml ethidium-bromide in 0.5 x TBE for 1 hr and destained with deionized water. Images were taken using a VWR GenoSmart gel documentation system.

For southern blotting the DNA was nicked in 0.125 M HCl for 10 min, denatured in 1.5 M NaCl, 0.5M NaOH for 30 min and neutralized by 0.5 M Tris, 1.5 M NaCl (pH 7.5) for 30 min. The DNA was transferred onto a Hybond-N+ membrane (GE healthcare) and cross-linked with UV-light (Stratagen, auto-crosslink function). The membrane was probed with a radioactive (α−32P dCTP) labelled ADE2 fragment and imaged using a Typhoon FLA 9000 imaging system.

DSB-induced recombination assay

The DSB-induced recombination assay was performed as described previously (***Ho et al., 2010***). In brief, diploid cells were grown to log-phase (OD_{600}0.4–0.6) in liquid YPAR (YP + 40 mg/l adenine + 2% raffinose). DSB formation (I-SceI expression) was induced by adding galactose (final concentration 2%) to the cultures for 1.5 hr. Afterwards cells were plated onto YPAD (YPD + 10 mg/l adenine),

incubated for 3–4 days and replica plated onto YPAD +Hyg +Nat, YPAD + Hyg, YPAD + Nat, SC -Ura, SC -Met and SCR -ADE +Gal to classify recombination events. The different classes evaluated arise from repair of DSBs by either short tract or long tract gene conversion which produces ade2-n or ADE+ recombinants, respectively (white class: two short tract conversions; red class: two long tract conversions; red/white class: on long tract, on short tract conversion). CO events in the different classes were measured by the number of colonies that have rendered both daughter cells homozygous for the HPH and NAT marker. In each experiment 400–600 cells per strain were evaluated for the individual class of repair and the experiment was independently repeated twice. Standard deviations were calculated and included as error bars. Statistical significance for the CO rates of individual strains and classes compared to the wild-type was calculated using an unpaired Student´s T-test. These calculations were done using the GraphPad web-tool 'T-test calculator' (http://www.graphpad.com/quickcalcs/ttest2).

Mus81-Mms4 nHJ cleavage assay

Asynchronous mitotic cultures were generated by inoculating 1 l of YP-Raffinose (20 g/l bactopeptone, 10 g/l yeast extract, 20 g/l D-(+)-Raffinose) with overnight cultures, to an OD_{600} of ~0.2. After cells have grown to an exponential stage (OD_{600} ~0.5) Mus81-Mms4 expression was induced by adding 20 g/l D-(+)-Galactose to the culture. The cells were then grown for 2 hr and harvested by centrifugation.

For Myc-affinity purifications yeast pellets were resuspended in 200 µl of lysis buffer (40 mM Tris-HCl (pH 7.5 at 25˚C), 150 mM NaCl, 20 mM β-glycerolphosphate, 1 mM NaF, 0.5 mM EGTA, 0.1 mM EDTA, 15% (V/V) glycerol, 0.1% (V/V) NP-40, 1 mM DTT, 2 mM PMSF, 1x Complete Protease inhibitor cocktail (Roche)) and lysed with glass beads. Obtained lysates were cleared by centrifugation and normalized. Myc-tagged Mus81-Mms4 was then immunoprecipitated using mouse monoclonal antibodies to Myc (9E10) coupled to agarose beads (AminoLink Plus), pre-blocked with 1 mg/ml BSA in lysis buffer. Immunoprecipitations were done on a rotating wheel for 1 hr at 4˚C. Prior western blotting or DNA cleavage assays the beads were extensively washed with the wash buffer (40 mM Tris-HCl (pH 7.5 at 25˚C), 150 mM NaCl, 15% (V/V) glycerol, 0.1% (V/V) NP-40) and dephosphorylated by treating the beads with bacteriophage λ protein phosphatase (New England Biolabs) in 1x protein metallophosphatases (PMP) buffer supplemented with 1 mM $MnCl_2$. Reactions were assembled on ice and incubated at 30˚C for 15 min. The dephosphorylated Mus81-Mms4 complexes were then subjected to SDS-PAGE gel and used for DNA cleavage assays.

DNA cleavage assays on beads were adapted from previously described protocols (***Grigaitis et al., 2018***; ***Matos and West, 2017***). In short, 20 µl of reaction mixture (20 mM Tris-Ac, pH 7.5 (25˚C), 3 mM $MgAc_2$, 1 mM DTT, 100 µg/ml BSA) containing 5 nM fluorescently labeled nicked Holliday junction, prepared as previously described (***Grigaitis et al., 2018***) were added to dry aspirated anti-Myc beads, corresponding to ~20 µl of volume. Reactions were assembled on ice and initiated by transferring them to 30˚C. Reactions were performed for 2 hr at 30˚C, shaking 800 rpm, stopped by the addition of 5x STOP solution (100 mM Tris-Ac, (pH 7.5 at 25˚C), 50 mM EDTA, 2.5% (m/w) SDS, 10 mg/ml Proteinase K) and incubated for 1 hr at 37˚C, shaking 800 rpm. Subsequently 5 µl of 6x DNA loading dye (13 mM Tris-HCl (pH 8.0 at 25˚C), 40 mM EDTA, 0.32% (V/V) SDS, 250 µM Ficoll 400, 0.4 µM OrangeG) were added. Reaction mixtures were analysed on a native 10% polyacrylamide gel in 1x TBE (89 mM Tris-borate (pH 8.4 at 25˚C), 2 mM EDTA) by running the electrophoresis for 1 hr 15 min at 7.5 V/cm. The gel was then imaged with a Typhoon scanner (GE Healtcare).

Nuclear fractionation

The protocol for preparation of nuclear fractions was adapted from ***Pasero et al., 1999***. In brief, 30 ml of the synchronized cultures (at different time points after G1 release) were fixed with sodium azide (total concentration 0.1%) and harvested by centrifugation (2 min, 3500 rpm, RT). Cells were resuspended in 5 ml of 100 mM EDTA-KOH, pH 8, 10 mM DTT and incubated with constant shaking at 30˚C for 10 min. Afterwards, cells were resuspended in 2 ml of YPD/1.1 M sorbitol and 0.5 mg/ml Z100T was added (incubation for 20 min, constant shaking, 30˚C) and subsequently recovered in 2 ml YPD/1.1 M sorbitol + 0.5 mM PMSF (incubation for 10 min, constant shaking, 30˚C). Zymolyase digested cells were resuspended in 2 ml of ice cold breakage buffer (10 mM Tris-HCl, pH 7.4, 40

mM KCl, 4 mM EDTA-KOH, 0.25 mM Spermidine, 0.1 mM Spermine, 18% Ficoll, 1% beta-mercaptoethanol, 1% aprotinin, 0.5 mM PMSF, 300 µg/ml benzamidine, 1 µg/ml pepstatin A, 0.5 µg/ml leupeptin) and dounced on ice using a tight pestle (about 30 strokes) to lyse cells efficiently (Total extract sample). Lysis was verified microscopically and extracts were centrifuged to remove unbroken cells (2 x, 12 min, 5000 g, 4˚C). Finally, cleared extracts were centrifuged at high speed to separate the nuclei from the cytoplasm (15 min, 21000 g, 4˚C). The supernatant (Cytoplasmic sample) was removed, nuclei washed once by rinsing the pellet with 1 ml of cold breakage buffer and the nuclear pellet was resuspended in 100 µl 0.25 x buffer A (10 mM Tris-HCl, pH 7.4, 40 mM KCl, 4 mM EDTA-KOH, 0.25 mM Spermidine, 0.1 mM Spermine) + 0.5 mM PMSF (Nuclear sample).

Acknowledgements

We thank Uschi Schkölziger and Tobias Freimann for technical assistance, Jonathan Baxter, Lotte Bjergbaek, Gregorz Ira, Lorraine Symington and Wolfgang Zachariae for strains, constructs and protocols, Georgios I Karras for design of an early version of the Clb5-S-tag construct, Miguel G Blanco for communication of unpublished data, Miguel G Blanco, Hans Hombauer and members of the Pfander and Jentsch labs for stimulating discussion and critical reading of the manuscript. This work was supported by the Max Planck Society (to BP), by ETH Zürich and the Swiss National Science Foundation (to JM). Work in the Pfander lab is supported by grants of the Max Planck Society and by the Deutsche Forschungsgemeinschaft (DFG, German Research Foundation) – Project ID PF794/3-1; Project-ID 213249687 – SFB 1064 Deutsche Forschungsgemeinschaft (DFG, German Research Council).

Additional information

Funding

Funder	Grant reference number	Author
Schweizerischer Nationalfonds zur Förderung der Wissenschaftlichen Forschung		Joao Matos
Eidgenössische Technische Hochschule Zürich		Joao Matos
Max-Planck-Gesellschaft		Boris Pfander
Deutsche Forschungsgemeinschaft	PF794/3-1	Boris Pfander
Deutsche Forschungsgemeinschaft	213249687 – SFB 1064	Boris Pfander

The funders had no role in study design, data collection and interpretation, or the decision to submit the work for publication.

Author contributions

Julia Bittmann, Conceptualization, Formal analysis, Investigation, Methodology, Project administration, Writing - review and editing; Rokas Grigaitis, Formal analysis, Investigation, Methodology; Lorenzo Galanti, Formal analysis, Investigation, Methodology, Writing - review and editing; Silas Amarell, Investigation, Methodology; Florian Wilfling, Methodology; Joao Matos, Resources, Formal analysis, Supervision, Writing - review and editing; Boris Pfander, Conceptualization, Resources, Formal analysis, Supervision, Funding acquisition, Investigation, Methodology, Writing - original draft, Writing - review and editing

Author ORCIDs

Julia Bittmann https://orcid.org/0000-0001-6527-7383
Lorenzo Galanti http://orcid.org/0000-0003-2538-3581

Joao Matos http://orcid.org/0000-0002-3754-3709
Boris Pfander https://orcid.org/0000-0003-2180-5054

Decision letter and Author response
Decision letter https://doi.org/10.7554/eLife.52459.sa1
Author response https://doi.org/10.7554/eLife.52459.sa2

Additional files

Supplementary files

- Supplementary file 1. Yeast strains and Plasmids. Table 1. Yeast strains used in this study. Table 2. Cell cycle tagging plasmids used in this study Table 3. Other plasmids used in this study
- Transparent reporting form

Data availability

All data generated or analysed during this study are included in the manuscript and supporting files.

References

Araujo PR, Yoon K, Ko D, Smith AD, Qiao M, Suresh U, Burns SC, Penalva LOF. 2012. Before it gets started: regulating translation at the 5′ UTR. *Comparative and Functional Genomics* **2012**:1–8. DOI: https://doi.org/10.1155/2012/475731

Arter M, Hurtado-Nieves V, Oke A, Zhuge T, Wettstein R, Fung JC, Blanco MG, Matos J. 2018. Regulated Crossing-Over requires inactivation of Yen1/GEN1 resolvase during meiotic prophase I. *Developmental Cell* **45**: 785–800. DOI: https://doi.org/10.1016/j.devcel.2018.05.020

Ashton TM, Mankouri HW, Heidenblut A, McHugh PJ, Hickson ID. 2011. Pathways for Holliday junction processing during homologous recombination in *Saccharomyces cerevisiae*. *Molecular and Cellular Biology* **31**: 1921–1933. DOI: https://doi.org/10.1128/MCB.01130-10, PMID: 21343337

Bastin-Shanower SA, Fricke WM, Mullen JR, Brill SJ. 2003. The mechanism of Mus81-Mms4 cleavage site selection distinguishes it from the homologous endonuclease Rad1-Rad10. *Molecular and Cellular Biology* **23**: 3487–3496. DOI: https://doi.org/10.1128/MCB.23.10.3487-3496.2003, PMID: 12724407

Bizard AH, Hickson ID. 2014. The dissolution of double holliday junctions. *Cold Spring Harbor Perspectives in Biology* **6**:a016477. DOI: https://doi.org/10.1101/cshperspect.a016477, PMID: 24984776

Blanco MG, Matos J, Rass U, Ip SC, West SC. 2010. Functional overlap between the structure-specific nucleases Yen1 and Mus81-Mms4 for DNA-damage repair in *S. cerevisiae*. *DNA Repair* **9**:394–402. DOI: https://doi.org/10.1016/j.dnarep.2009.12.017, PMID: 20106725

Blanco MG, Matos J, West SC. 2014. Dual control of Yen1 nuclease activity and cellular localization by cdk and Cdc14 prevents genome instability. *Molecular Cell* **54**:94–106. DOI: https://doi.org/10.1016/j.molcel.2014.02.011, PMID: 24631285

Blanco MG, Matos J. 2015. Hold your horSSEs: controlling structure-selective endonucleases MUS81 and Yen1/GEN1. *Frontiers in Genetics* **6**:253. DOI: https://doi.org/10.3389/fgene.2015.00253, PMID: 26284109

Blow JJ, Tanaka TU. 2005. The chromosome cycle: coordinating replication and segregation. second in the cycles review series. *EMBO Reports* **6**:1028–1034. DOI: https://doi.org/10.1038/sj.embor.7400557, PMID: 16264427

Boddy MN, Lopez-Girona A, Shanahan P, Interthal H, Heyer WD, Russell P. 2000. Damage tolerance protein Mus81 associates with the FHA1 domain of checkpoint kinase Cds1. *Molecular and Cellular Biology* **20**:8758–8766. DOI: https://doi.org/10.1128/MCB.20.23.8758-8766.2000, PMID: 11073977

Boddy MN, Gaillard PHL, McDonald WH, Shanahan P, Yates JR, Russell P. 2001. Mus81-Eme1 are essential components of a holliday junction resolvase. *Cell* **107**:537–548. DOI: https://doi.org/10.1016/S0092-8674(01)00536-0, PMID: 11719193

Branzei D, Vanoli F, Foiani M. 2008. SUMOylation regulates Rad18-mediated template switch. *Nature* **456**:915–920. DOI: https://doi.org/10.1038/nature07587, PMID: 19092928

Branzei D, Szakal B. 2016. DNA damage tolerance by recombination: molecular pathways and DNA structures. *DNA Repair* **44**:68–75. DOI: https://doi.org/10.1016/j.dnarep.2016.05.008, PMID: 27236213

Buisson R, Boisvert JL, Benes CH, Zou L. 2015. Distinct but concerted roles of ATR, DNA-PK, and Chk1 in countering replication stress during S Phase. *Molecular Cell* **59**:1011–1024. DOI: https://doi.org/10.1016/j.molcel.2015.07.029, PMID: 26365377

Cejka P, Plank JL, Bachrati CZ, Hickson ID, Kowalczykowski SC. 2010. Rmi1 stimulates decatenation of double Holliday junctions during dissolution by Sgs1–Top3. *Nature Structural & Molecular Biology* **17**:1377–1382. DOI: https://doi.org/10.1038/nsmb.1919

Chan YW, West SC. 2014. Spatial control of the GEN1 holliday junction resolvase ensures genome stability. *Nature Communications* **5**:4844. DOI: https://doi.org/10.1038/ncomms5844, PMID: 25209024

Chen XB, Melchionna R, Denis CM, Gaillard PHL, Blasina A, Van de Weyer I, Boddy MN, Russell P, Vialard J, McGowan CH. 2001. Human Mus81-associated endonuclease cleaves Holliday junctions in vitro. *Molecular Cell* **8**:1117–1127. DOI: https://doi.org/10.1016/S1097-2765(01)00375-6, PMID: 11741546

Ciccia A, Constantinou A, West SC. 2003. Identification and characterization of the human mus81-eme1 endonuclease. *Journal of Biological Chemistry* **278**:25172–25178. DOI: https://doi.org/10.1074/jbc.M302882200, PMID: 12721304

Ciccia A, McDonald N, West SC. 2008. Structural and functional relationships of the XPF/MUS81 family of proteins. *Annual Review of Biochemistry* **77**:259–287. DOI: https://doi.org/10.1146/annurev.biochem.77.070306.102408, PMID: 18518821

Constantinou A, Chen XB, Mcgowan CH, West SC. 2002. Holliday junction resolution in human cells: two junction endonucleases with distinct substrate specificities. *The EMBO Journal* **21**:5577–5585. DOI: https://doi.org/10.1093/emboj/cdf554

Dehé PM, Coulon S, Scaglione S, Shanahan P, Takedachi A, Wohlschlegel JA, Yates JR, Llorente B, Russell P, Gaillard PH. 2013. Regulation of Mus81-Eme1 holliday junction resolvase in response to DNA damage. *Nature Structural & Molecular Biology* **20**:598–603. DOI: https://doi.org/10.1038/nsmb.2550, PMID: 23584455

Dehé PM, Gaillard PHL. 2017. Control of structure-specific endonucleases to maintain genome stability. *Nature Reviews Molecular Cell Biology* **18**:315–330. DOI: https://doi.org/10.1038/nrm.2016.177, PMID: 28327556

Doe CL, Ahn JS, Dixon J, Whitby MC. 2002. Mus81-Eme1 and Rqh1 involvement in processing stalled and collapsed replication forks. *Journal of Biological Chemistry* **277**:32753–32759. DOI: https://doi.org/10.1074/jbc.M202120200, PMID: 12084712

Duda H, Arter M, Gloggnitzer J, Teloni F, Wild P, Blanco MG, Altmeyer M, Matos J. 2016. A mechanism for controlled breakage of Under-replicated chromosomes during mitosis. *Developmental Cell* **39**:740–755. DOI: https://doi.org/10.1016/j.devcel.2016.11.017, PMID: 27997828

Dvir S, Velten L, Sharon E, Zeevi D, Carey LB, Weinberger A, Segal E. 2013. Deciphering the rules by which 5′-UTR sequences affect protein expression in yeast. *PNAS* **110**:E2792–E2801. DOI: https://doi.org/10.1073/pnas.1222534110, PMID: 23832786

Ehmsen KT, Heyer WD. 2008. *Saccharomyces cerevisiae* Mus81-Mms4 is a catalytic, DNA structure-selective endonuclease. *Nucleic Acids Research* **36**:2182–2195. DOI: https://doi.org/10.1093/nar/gkm1152, PMID: 18281703

Eissler CL, Mazón G, Powers BL, Savinov SN, Symington LS, Hall MC. 2014. The cdk/cDc14 module controls activation of the Yen1 holliday junction resolvase to promote genome stability. *Molecular Cell* **54**:80–93. DOI: https://doi.org/10.1016/j.molcel.2014.02.012, PMID: 24631283

Fabre F, Chan A, Heyer WD, Gangloff S. 2002. Alternate pathways involving Sgs1/Top3, Mus81/ Mms4, and Srs2 prevent formation of toxic recombination intermediates from single-stranded gaps created by DNA replication. *PNAS* **99**:16887–16892. DOI: https://doi.org/10.1073/pnas.252652399, PMID: 12475932

Finn KJ, Li JJ. 2013. Single-stranded annealing induced by re-initiation of replication origins provides a novel and efficient mechanism for generating copy number expansion via non-allelic homologous recombination. *PLOS Genetics* **9**:e1003192. DOI: https://doi.org/10.1371/journal.pgen.1003192, PMID: 23300490

Fricke WM, Bastin-Shanower SA, Brill SJ. 2005. Substrate specificity of the *Saccharomyces cerevisiae* Mus81-Mms4 endonuclease. *DNA Repair* **4**:243–251. DOI: https://doi.org/10.1016/j.dnarep.2004.10.001, PMID: 15590332

Fricke WM, Brill SJ. 2003. Slx1-Slx4 is a second structure-specific endonuclease functionally redundant with Sgs1-Top3. *Genes & Development* **17**:1768–1778. DOI: https://doi.org/10.1101/gad.1105203, PMID: 12832395

Froget B, Blaisonneau J, Lambert S, Baldacci G. 2008. Cleavage of stalled forks by fission yeast Mus81/Eme1 in absence of DNA replication checkpoint. *Molecular Biology of the Cell* **19**:445–456. DOI: https://doi.org/10.1091/mbc.e07-07-0728, PMID: 18032583

Fu H, Martin MM, Regairaz M, Huang L, You Y, Lin CM, Ryan M, Kim R, Shimura T, Pommier Y, Aladjem MI. 2015. The DNA repair endonuclease Mus81 facilitates fast DNA replication in the absence of exogenous damage. *Nature Communications* **6**:6746. DOI: https://doi.org/10.1038/ncomms7746, PMID: 25879486

Fugger K, Chu WK, Haahr P, Kousholt AN, Beck H, Payne MJ, Hanada K, Hickson ID, Sørensen CS. 2013. FBH1 co-operates with MUS81 in inducing DNA double-strand breaks and cell death following replication stress. *Nature Communications* **4**:1423. DOI: https://doi.org/10.1038/ncomms2395, PMID: 23361013

Gaillard PHL, Noguchi E, Shanahan P, Russell P. 2003. The endogenous Mus81-Eme1 complex resolves holliday junctions by a nick and counternick mechanism. *Molecular Cell* **12**:747–759. DOI: https://doi.org/10.1016/S1097-2765(03)00342-3, PMID: 14527419

Gallo-Fernández M, Saugar I, Ortiz-Bazán MÁ, Vázquez MV, Tercero JA. 2012. Cell cycle-dependent regulation of the nuclease activity of Mus81-Eme1/Mms4. *Nucleic Acids Research* **40**:8325–8335. DOI: https://doi.org/10.1093/nar/gks599, PMID: 22730299

Gangloff S, McDonald JP, Bendixen C, Arthur L, Rothstein R. 1994. The yeast type I topoisomerase Top3 interacts with Sgs1, a DNA helicase homolog: a potential eukaryotic reverse gyrase. *Molecular and Cellular Biology* **14**:8391–8398. DOI: https://doi.org/10.1128/MCB.14.12.8391, PMID: 7969174

García-Luis J, Clemente-Blanco A, Aragón L, Machín F. 2014. Cdc14 targets the Holliday junction resolvase Yen1 to the nucleus in early anaphase. *Cell Cycle* **13**:1392–1399. DOI: https://doi.org/10.4161/cc.28370, PMID: 24626187

Giannattasio M, Zwicky K, Follonier C, Foiani M, Lopes M, Branzei D. 2014. Visualization of recombination-mediated damage bypass by template switching. *Nature Structural & Molecular Biology* **21**:884–892. DOI: https://doi.org/10.1038/nsmb.2888, PMID: 25195051

Gonzalez-Huici V, Szakal B, Urulangodi M, Psakhye I, Castellucci F, Menolfi D, Rajakumara E, Fumasoni M, Bermejo R, Jentsch S, Branzei D. 2014. DNA bending facilitates the error-free DNA damage tolerance pathway and upholds genome integrity. *The EMBO Journal* **33**:327–340. DOI: https://doi.org/10.1002/embj.201387425, PMID: 24473148

González-Prieto R, Muñoz-Cabello AM, Cabello-Lobato MJ, Prado F. 2013. Rad51 replication fork recruitment is required for DNA damage tolerance. *The EMBO Journal* **32**:1307–1321. DOI: https://doi.org/10.1038/emboj.2013.73, PMID: 23563117

Grigaitis R, Susperregui A, Wild P, Matos J. 2018. Characterization of DNA helicases and nucleases from meiotic extracts of *S. cerevisiae*. *Mitosis and Meiosis* **144**:371–388. DOI: https://doi.org/10.1016/bs.mcb.2018.03.029

Grigaitis R, Ranjha L, Wild P, Kasaciunaite K, Ceppi I, Kissling V, Susperregui A, Peter M, Seidel R, Cejka P, Matos J. 2020. Regulatory control of RecQ helicase Sgs1/BLM during meiosis and mitosis. *Developmental Cell* **55**:3508884. DOI: https://doi.org/10.2139/ssrn.3508884

Gritenaite D, Princz LN, Szakal B, Bantele SC, Wendeler L, Schilbach S, Habermann BH, Matos J, Lisby M, Branzei D, Pfander B. 2014. A cell cycle-regulated Slx4-Dpb11 complex promotes the resolution of DNA repair intermediates linked to stalled replication. *Genes & Development* **28**:1604–1619. DOI: https://doi.org/10.1101/gad.240515.114, PMID: 25030699

Guervilly JH, Gaillard PH. 2018. SLX4: multitasking to maintain genome stability. *Critical Reviews in Biochemistry and Molecular Biology* **53**:475–514. DOI: https://doi.org/10.1080/10409238.2018.1488803, PMID: 30284473

Haber JE, Heyer WD. 2001. The fuss about Mus81. *Cell* **107**:551–554. DOI: https://doi.org/10.1016/S0092-8674(01)00593-1, PMID: 11733053

Hamperl S, Cimprich KA. 2016. Conflict resolution in the genome: how transcription and replication make it work. *Cell* **167**:1455–1467. DOI: https://doi.org/10.1016/j.cell.2016.09.053, PMID: 27912056

Hanada K, Budzowska M, Davies SL, van Drunen E, Onizawa H, Beverloo HB, Maas A, Essers J, Hickson ID, Kanaar R. 2007. The structure-specific endonuclease Mus81 contributes to replication restart by generating double-strand DNA breaks. *Nature Structural & Molecular Biology* **14**:1096–1104. DOI: https://doi.org/10.1038/nsmb1313, PMID: 17934473

Ho CK, Mazón G, Lam AF, Symington LS. 2010. Mus81 and Yen1 promote reciprocal exchange during mitotic recombination to maintain genome integrity in budding yeast. *Molecular Cell* **40**:988–1000. DOI: https://doi.org/10.1016/j.molcel.2010.11.016, PMID: 21172663

Hombauer H, Srivatsan A, Putnam CD, Kolodner RD. 2011. Mismatch repair, but not heteroduplex rejection, is temporally coupled to DNA replication. *Science* **334**:1713–1716. DOI: https://doi.org/10.1126/science.1210770, PMID: 22194578

Hung SH, Wong RP, Ulrich HD, Kao CF. 2017. Monoubiquitylation of histone H2B contributes to the bypass of DNA damage during and after DNA replication. *PNAS* **114**:E2205–E2214. DOI: https://doi.org/10.1073/pnas.1612633114, PMID: 28246327

Hustedt N, Durocher D. 2017. The control of DNA repair by the cell cycle. *Nature Cell Biology* **19**:1–9. DOI: https://doi.org/10.1038/ncb3452

Interthal H, Heyer WD. 2000. MUS81 encodes a novel helix-hairpin-helix protein involved in the response to UV- and methylation-induced DNA damage in *Saccharomyces cerevisiae*. *Molecular and General Genetics MGG* **263**:812–827. DOI: https://doi.org/10.1007/s004380000241, PMID: 10905349

Ip SC, Rass U, Blanco MG, Flynn HR, Skehel JM, West SC. 2008. Identification of Holliday junction resolvases from humans and yeast. *Nature* **456**:357–361. DOI: https://doi.org/10.1038/nature07470, PMID: 19020614

Ira G, Malkova A, Liberi G, Foiani M, Haber JE. 2003. Srs2 and Sgs1-Top3 suppress crossovers during double-strand break repair in yeast. *Cell* **115**:401–411. DOI: https://doi.org/10.1016/S0092-8674(03)00886-9, PMID: 14622595

Jackson LP, Reed SI, Haase SB. 2006. Distinct mechanisms control the stability of the related S-phase cyclins Clb5 and Clb6. *Molecular and Cellular Biology* **26**:2456–2466. DOI: https://doi.org/10.1128/MCB.26.6.2456-2466.2006, PMID: 16508019

Janke C, Magiera MM, Rathfelder N, Taxis C, Reber S, Maekawa H, Moreno-Borchart A, Doenges G, Schwob E, Schiebel E, Knop M. 2004. A versatile toolbox for PCR-based tagging of yeast genes: new fluorescent proteins, more markers and promoter substitution cassettes. *Yeast* **21**:947–962. DOI: https://doi.org/10.1002/yea.1142, PMID: 15334558

Jessop L, Lichten M. 2008. Mus81/Mms4 endonuclease and Sgs1 helicase collaborate to ensure proper recombination intermediate metabolism during meiosis. *Molecular Cell* **31**:313–323. DOI: https://doi.org/10.1016/j.molcel.2008.05.021, PMID: 18691964

Johnson C, Gali VK, Takahashi TS, Kubota T. 2016. PCNA retention on DNA into G2/M phase causes genome instability in cells lacking Elg1. *Cell Reports* **16**:684–695. DOI: https://doi.org/10.1016/j.celrep.2016.06.030, PMID: 27373149

Kahli M, Osmundson JS, Yeung R, Smith DJ. 2019. Processing of eukaryotic okazaki fragments by redundant nucleases can be uncoupled from ongoing DNA replication *in vivo*. *Nucleic Acids Research* **47**:1814–1822. DOI: https://doi.org/10.1093/nar/gky1242, PMID: 30541106

Kai M, Boddy MN, Russell P, Wang TS. 2005. Replication checkpoint kinase Cds1 regulates Mus81 to preserve genome integrity during replication stress. *Genes & Development* **19**:919–932. DOI: https://doi.org/10.1101/gad.1304305, PMID: 15805465

Kaliraman V, Mullen JR, Fricke WM, Bastin-Shanower SA, Brill SJ. 2001. Functional overlap between Sgs1-Top3 and the Mms4-Mus81 endonuclease. *Genes & Development* **15**:2730–2740. DOI: https://doi.org/10.1101/gad.932201, PMID: 11641278

Karras GI, Fumasoni M, Sienski G, Vanoli F, Branzei D, Jentsch S. 2013. Noncanonical role of the 9-1-1 clamp in the error-free DNA damage tolerance pathway. *Molecular Cell* **49**:536–546. DOI: https://doi.org/10.1016/j.molcel.2012.11.016, PMID: 23260657

Karras GI, Jentsch S. 2010. The RAD6 DNA damage tolerance pathway operates uncoupled from the replication fork and is functional beyond S phase. *Cell* **141**:255–267. DOI: https://doi.org/10.1016/j.cell.2010.02.028, PMID: 20403322

Knop M, Siegers K, Pereira G, Zachariae W, Winsor B, Nasmyth K, Schiebel E. 1999. Epitope tagging of yeast genes using a PCR-based strategy: more tags and improved practical routines. *Yeast* **15**:963–972. DOI: https://doi.org/10.1002/(SICI)1097-0061(199907)15:10B<963::AID-YEA399>3.0.CO;2-W, PMID: 10407276

Kosugi S, Hasebe M, Tomita M, Yanagawa H. 2009. Systematic identification of cell cycle-dependent yeast nucleocytoplasmic shuttling proteins by prediction of composite motifs. *PNAS* **106**:10171–10176. DOI: https://doi.org/10.1073/pnas.0900604106, PMID: 19520826

Kühne C, Linder P. 1993. A new pair of B-type cyclins from *Saccharomyces cerevisiae* that function early in the cell cycle. *The EMBO Journal* **12**:3437–3447. DOI: https://doi.org/10.1002/j.1460-2075.1993.tb06018.x, PMID: 8253070

Lafuente-Barquero J, Luke-Glaser S, Graf M, Silva S, Gómez-González B, Lockhart A, Lisby M, Aguilera A, Luke B. 2017. The Smc5/6 complex regulates the yeast Mph1 helicase at RNA-DNA hybrid-mediated DNA damage. *PLOS Genetics* **13**:e1007136. DOI: https://doi.org/10.1371/journal.pgen.1007136, PMID: 29281624

Lemaçon D, Jackson J, Quinet A, Brickner JR, Li S, Yazinski S, You Z, Ira G, Zou L, Mosammaparast N, Vindigni A. 2017. MRE11 and EXO1 nucleases degrade reversed forks and elicit MUS81-dependent fork rescue in BRCA2-deficient cells. *Nature Communications* **8**:860. DOI: https://doi.org/10.1038/s41467-017-01180-5, PMID: 29038425

Liberi G, Maffioletti G, Lucca C, Chiolo I, Baryshnikova A, Cotta-Ramusino C, Lopes M, Pellicioli A, Haber JE, Foiani M. 2005. Rad51-dependent DNA structures accumulate at damaged replication forks in sgs1 mutants defective in the yeast ortholog of BLM RecQ helicase. *Genes & Development* **19**:339–350. DOI: https://doi.org/10.1101/gad.322605, PMID: 15687257

Lockhart A, Pires VB, Bento F, Kellner V, Luke-Glaser S, Yakoub G, Ulrich HD, Luke B. 2019. RNase H1 and H2 are differentially regulated to process RNA-DNA hybrids. *Cell Reports* **29**:2890–2900. DOI: https://doi.org/10.1016/j.celrep.2019.10.108, PMID: 31775053

Mankouri HW, Huttner D, Hickson ID. 2013. How unfinished business from S-phase affects mitosis and beyond. *The EMBO Journal* **32**:2661–2671. DOI: https://doi.org/10.1038/emboj.2013.211, PMID: 24065128

Matos J, Blanco MG, Maslen S, Skehel JM, West SC. 2011. Regulatory control of the resolution of DNA recombination intermediates during meiosis and mitosis. *Cell* **147**:158–172. DOI: https://doi.org/10.1016/j.cell.2011.08.032, PMID: 21962513

Matos J, Blanco MG, West SC. 2013. Cell-cycle kinases coordinate the resolution of recombination intermediates with chromosome segregation. *Cell Reports* **4**:76–86. DOI: https://doi.org/10.1016/j.celrep.2013.05.039, PMID: 23810555

Matos J, West SC. 2014. Holliday junction resolution: regulation in space and time. *DNA Repair* **19**:176–181. DOI: https://doi.org/10.1016/j.dnarep.2014.03.013, PMID: 24767945

Matos J, West SC. 2017. Analysis of Structure-Selective endonuclease activities from yeast and human extracts. *Methods in Enzymology* **591**:271–286. DOI: https://doi.org/10.1016/bs.mie.2017.03.005, PMID: 28645372

Mayle R, Campbell IM, Beck CR, Yu Y, Wilson M, Shaw CA, Bjergbaek L, Lupski JR, Ira G. 2015. DNA REPAIR Mus81 and converging forks limit the mutagenicity of replication fork breakage. *Science* **349**:742–747. DOI: https://doi.org/10.1126/science.aaa8391, PMID: 26273056

Menolfi D, Delamarre A, Lengronne A, Pasero P, Branzei D. 2015. Essential roles of the Smc5/6 complex in replication through natural pausing sites and endogenous DNA damage tolerance. *Molecular Cell* **60**:835–846. DOI: https://doi.org/10.1016/j.molcel.2015.10.023, PMID: 26698660

Merrick WC, Pavitt GD. 2018. Protein synthesis initiation in eukaryotic cells. *Cold Spring Harbor Perspectives in Biology* **10**:a033092. DOI: https://doi.org/10.1101/cshperspect.a033092, PMID: 29735639

Minocherhomji S, Ying S, Bjerregaard VA, Bursomanno S, Aleliunaite A, Wu W, Mankouri HW, Shen H, Liu Y, Hickson ID. 2015. Replication stress activates DNA repair synthesis in mitosis. *Nature* **528**:286–290. DOI: https://doi.org/10.1038/nature16139, PMID: 26633632

Mullen JR, Kaliraman V, Ibrahim SS, Brill SJ. 2001. Requirement for three novel protein complexes in the absence of the Sgs1 DNA helicase in*Saccharomyces cerevisiae*. *Genetics* **157**:103–118. PMID: 11139495

Muñoz IM, Hain K, Déclais AC, Gardiner M, Toh GW, Sanchez-Pulido L, Heuckmann JM, Toth R, Macartney T, Eppink B, Kanaar R, Ponting CP, Lilley DM, Rouse J. 2009. Coordination of structure-specific nucleases by human SLX4/BTBD12 is required for DNA repair. *Molecular Cell* **35**:116–127. DOI: https://doi.org/10.1016/j.molcel.2009.06.020, PMID: 19595721

Naim V, Wilhelm T, Debatisse M, Rosselli F. 2013. ERCC1 and MUS81-EME1 promote sister chromatid separation by processing late replication intermediates at common fragile sites during mitosis. *Nature Cell Biology* **15**:1008–1015. DOI: https://doi.org/10.1038/ncb2793, PMID: 23811686

Nielsen I, Bentsen IB, Lisby M, Hansen S, Mundbjerg K, Andersen AH, Bjergbaek L. 2009. A Flp-nick system to study repair of a single protein-bound nick in vivo. *Nature Methods* **6**:753–757. DOI: https://doi.org/10.1038/nmeth.1372, PMID: 19749762

Oh SD, Lao JP, Taylor AF, Smith GR, Hunter N. 2008. RecQ helicase, Sgs1, and XPF family endonuclease, Mus81-Mms4, resolve aberrant joint molecules during meiotic recombination. *Molecular Cell* **31**:324–336. DOI: https://doi.org/10.1016/j.molcel.2008.07.006, PMID: 18691965

Osman F, Dixon J, Doe CL, Whitby MC. 2003. Generating crossovers by resolution of nicked Holliday junctions: a role for Mus81-Eme1 in meiosis. *Molecular Cell* **12**:761–774. DOI: https://doi.org/10.1016/s1097-2765(03)00343-5, PMID: 14527420

Pardo B, Moriel-Carretero M, Vicat T, Aguilera A, Pasero P. 2019. A new role of the Mus81 nuclease for replication completion after fork restart. *bioRxiv*. DOI: https://doi.org/10.1101/785501

Pasero P, Duncker BP, Gasser SM. 1999. In vitro DNA replication in yeast nuclear extracts. *Methods* **18**:368–376. DOI: https://doi.org/10.1006/meth.1999.0794, PMID: 10454998

Pepe A, West SC. 2014a. MUS81-EME2 promotes replication fork restart. *Cell Reports* **7**:1048–1055. DOI: https://doi.org/10.1016/j.celrep.2014.04.007, PMID: 24813886

Pepe A, West SC. 2014b. Substrate specificity of the MUS81-EME2 structure selective endonuclease. *Nucleic Acids Research* **42**:3833–3845. DOI: https://doi.org/10.1093/nar/gkt1333, PMID: 24371268

Pfander B, Diffley JF. 2011. Dpb11 coordinates Mec1 kinase activation with cell cycle-regulated Rad9 recruitment. *The EMBO Journal* **30**:4897–4907. DOI: https://doi.org/10.1038/emboj.2011.345, PMID: 21946560

Pfander B, Matos J. 2017. Control of Mus81 nuclease during the cell cycle. *FEBS Letters* **591**:2048–2056. DOI: https://doi.org/10.1002/1873-3468.12727, PMID: 28640495

Princz LN, Gritenaite D, Pfander B. 2015. The Slx4-Dpb11 scaffold complex: coordinating the response to replication fork stalling in S-phase and the subsequent mitosis. *Cell Cycle* **14**:488–494. DOI: https://doi.org/10.4161/15384101.2014.989126, PMID: 25496009

Princz LN, Wild P, Bittmann J, Aguado FJ, Blanco MG, Matos J, Pfander B. 2017. Dbf4-dependent kinase and the Rtt107 scaffold promote Mus81-Mms4 resolvase activation during mitosis. *The EMBO Journal* **36**:664–678. DOI: https://doi.org/10.15252/embj.201694831, PMID: 28096179

Rass U, Compton SA, Matos J, Singleton MR, Ip SC, Blanco MG, Griffith JD, West SC. 2010. Mechanism of Holliday junction resolution by the human GEN1 protein. *Genes & Development* **24**:1559–1569. DOI: https://doi.org/10.1101/gad.585310, PMID: 20634321

Regairaz M, Zhang YW, Fu H, Agama KK, Tata N, Agrawal S, Aladjem MI, Pommier Y. 2011. Mus81-mediated DNA cleavage resolves replication forks stalled by topoisomerase I-DNA complexes. *The Journal of Cell Biology* **195**:739–749. DOI: https://doi.org/10.1083/jcb.201104003, PMID: 22123861

Renaud-Young M, Lloyd DC, Chatfield-Reed K, George I, Chua G, Cobb J. 2015. The NuA4 complex promotes translesion synthesis (TLS)-mediated DNA damage tolerance. *Genetics* **199**:1065–1076. DOI: https://doi.org/10.1534/genetics.115.174490, PMID: 25701288

Reusswig KU, Zimmermann F, Galanti L, Pfander B. 2016. Robust replication control is generated by temporal gaps between licensing and firing phases and depends on degradation of firing factor Sld2. *Cell Reports* **17**:556–569. DOI: https://doi.org/10.1016/j.celrep.2016.09.013, PMID: 27705801

Roseaulin L, Yamada Y, Tsutsui Y, Russell P, Iwasaki H, Arcangioli B. 2008. Mus81 is essential for sister chromatid recombination at broken replication forks. *The EMBO Journal* **27**:1378–1387. DOI: https://doi.org/10.1038/emboj.2008.65, PMID: 18388861

Rothstein RJ. 1983. One-step gene disruption in yeast. *Methods in Enzymology* **101**:202–211. DOI: https://doi.org/10.1016/0076-6879(83)01015-0, PMID: 6310324

Saugar I, Vázquez MV, Gallo-Fernández M, Ortiz-Bazán MÁ, Segurado M, Calzada A, Tercero JA. 2013. Temporal regulation of the Mus81-Mms4 endonuclease ensures cell survival under conditions of DNA damage. *Nucleic Acids Research* **41**:8943–8958. DOI: https://doi.org/10.1093/nar/gkt645, PMID: 23901010

Saugar I, Jiménez-Martín A, Tercero JA. 2017. Subnuclear relocalization of Structure-Specific endonucleases in response to DNA damage. *Cell Reports* **20**:1553–1562. DOI: https://doi.org/10.1016/j.celrep.2017.07.059, PMID: 28813668

Schwartz EK, Wright WD, Ehmsen KT, Evans JE, Stahlberg H, Heyer WD. 2012. Mus81-Mms4 functions as a single heterodimer to cleave nicked intermediates in recombinational DNA repair. *Molecular and Cellular Biology* **32**:3065–3080. DOI: https://doi.org/10.1128/MCB.00547-12, PMID: 22645308

Schwartz EK, Heyer WD. 2011. Processing of joint molecule intermediates by structure-selective endonucleases during homologous recombination in eukaryotes. *Chromosoma* **120**:109–127. DOI: https://doi.org/10.1007/s00412-010-0304-7, PMID: 21369956

Schwob E, Nasmyth K. 1993. CLB5 and CLB6, *a new pair of B cyclins involved in DNA replication in Saccharomyces cerevisiae*. *Genes & Development* **7**:1160–1175. DOI: https://doi.org/10.1101/gad.7.7a.1160, PMID: 8319908

Shimura T, Torres MJ, Martin MM, Rao VA, Pommier Y, Katsura M, Miyagawa K, Aladjem MI. 2008. Bloom's syndrome helicase and Mus81 are required to induce transient double-strand DNA breaks in response to DNA replication stress. *Journal of Molecular Biology* **375**:1152–1164. DOI: https://doi.org/10.1016/j.jmb.2007.11.006, PMID: 18054789

Siler J, Xia B, Wong C, Kath M, Bi X. 2017. Cell cycle-dependent positive and negative functions of Fun30 chromatin remodeler in DNA damage response. *DNA Repair* **50**:61–70. DOI: https://doi.org/10.1016/j.dnarep.2016.12.009, PMID: 28089177

Sollier J, Cimprich KA. 2015. Breaking bad: r-loops and genome integrity. *Trends in Cell Biology* **25**:514–522. DOI: https://doi.org/10.1016/j.tcb.2015.05.003, PMID: 26045257

Szakal B, Branzei D. 2013. Premature Cdk1/Cdc5/Mus81 pathway activation induces aberrant replication and deleterious crossover. *The EMBO Journal* **32**:1155–1167. DOI: https://doi.org/10.1038/emboj.2013.67, PMID: 23531881

Talhaoui I, Bernal M, Mullen JR, Dorison H, Palancade B, Brill SJ, Mazón G. 2018. Slx5-Slx8 ubiquitin ligase targets active pools of the Yen1 nuclease to limit crossover formation. *Nature Communications* **9**:5016. DOI: https://doi.org/10.1038/s41467-018-07364-x, PMID: 30479332

Taylor ER, McGowan CH. 2008. Cleavage mechanism of human Mus81-Eme1 acting on Holliday-junction structures. *PNAS* **105**:3757–3762. DOI: https://doi.org/10.1073/pnas.0710291105, PMID: 18310322

Versini G, Comet I, Wu M, Hoopes L, Schwob E, Pasero P. 2003. The yeast Sgs1 helicase is differentially required for genomic and ribosomal DNA replication. *The EMBO Journal* **22**:1939–1949. DOI: https://doi.org/10.1093/emboj/cdg180, PMID: 12682026

Wechsler T, Newman S, West SC. 2011. Aberrant chromosome morphology in human cells defective for Holliday junction resolution. *Nature* **471**:642–646. DOI: https://doi.org/10.1038/nature09790, PMID: 21399624

Whitby MC, Osman F, Dixon J. 2003. Cleavage of model replication forks by fission yeast Mus81-Eme1 and budding yeast Mus81-Mms4. *Journal of Biological Chemistry* **278**:6928–6935. DOI: https://doi.org/10.1074/jbc.M210006200, PMID: 12473680

Wild P, Matos J. 2016. Cell cycle control of DNA joint molecule resolution. *Current Opinion in Cell Biology* **40**:74–80. DOI: https://doi.org/10.1016/j.ceb.2016.02.018, PMID: 26970388

Wu L, Hickson ID. 2003. The bloom's syndrome helicase suppresses crossing over during homologous recombination. *Nature* **426**:870–874. DOI: https://doi.org/10.1038/nature02253, PMID: 14685245

Wyatt HD, Sarbajna S, Matos J, West SC. 2013. Coordinated actions of SLX1-SLX4 and MUS81-EME1 for Holliday junction resolution in human cells. *Molecular Cell* **52**:234–247. DOI: https://doi.org/10.1016/j.molcel.2013.08.035, PMID: 24076221

Xiao W, Chow BL, Milo CN. 1998. Mms4, a putative transcriptional (co)activator, protects *Saccharomyces cerevisiae* cells from endogenous and environmental DNA damage. *Molecular and General Genetics MGG* **257**:614–623. DOI: https://doi.org/10.1007/s004380050689, PMID: 9604884

Xing M, Wang X, Palmai-Pallag T, Shen H, Helleday T, Hickson ID, Ying S. 2015. Acute MUS81 depletion leads to replication fork slowing and a constitutive DNA damage response. *Oncotarget* **6**:37638–37646. DOI: https://doi.org/10.18632/oncotarget.5497

Ying S, Minocherhomji S, Chan KL, Palmai-Pallag T, Chu WK, Wass T, Mankouri HW, Liu Y, Hickson ID. 2013. MUS81 promotes common fragile site expression. *Nature Cell Biology* **15**:1001–1007. DOI: https://doi.org/10.1038/ncb2773, PMID: 23811685

Yun Y, Adesanya TM, Mitra RD. 2012. A systematic study of gene expression variation at single-nucleotide resolution reveals widespread regulatory roles for uAUGs. *Genome Research* **22**:1089–1097. DOI: https://doi.org/10.1101/gr.117366.110, PMID: 22454232

Zegerman P, Diffley JF. 2009. DNA replication as a target of the DNA damage checkpoint. *DNA Repair* **8**:1077–1088. DOI: https://doi.org/10.1016/j.dnarep.2009.04.023, PMID: 19505853

Zhao H, Zhu M, Limbo O, Russell P. 2018. RNase H eliminates R-loops that disrupt DNA replication but is nonessential for efficient DSB repair. *EMBO Reports* **19**:e45335. DOI: https://doi.org/10.15252/embr.201745335, PMID: 29622660

RESEARCH ARTICLE

Figures and figure supplements

An advanced cell cycle tag toolbox reveals principles underlying temporal control of structure-selective nucleases

Julia Bittmann *et al*

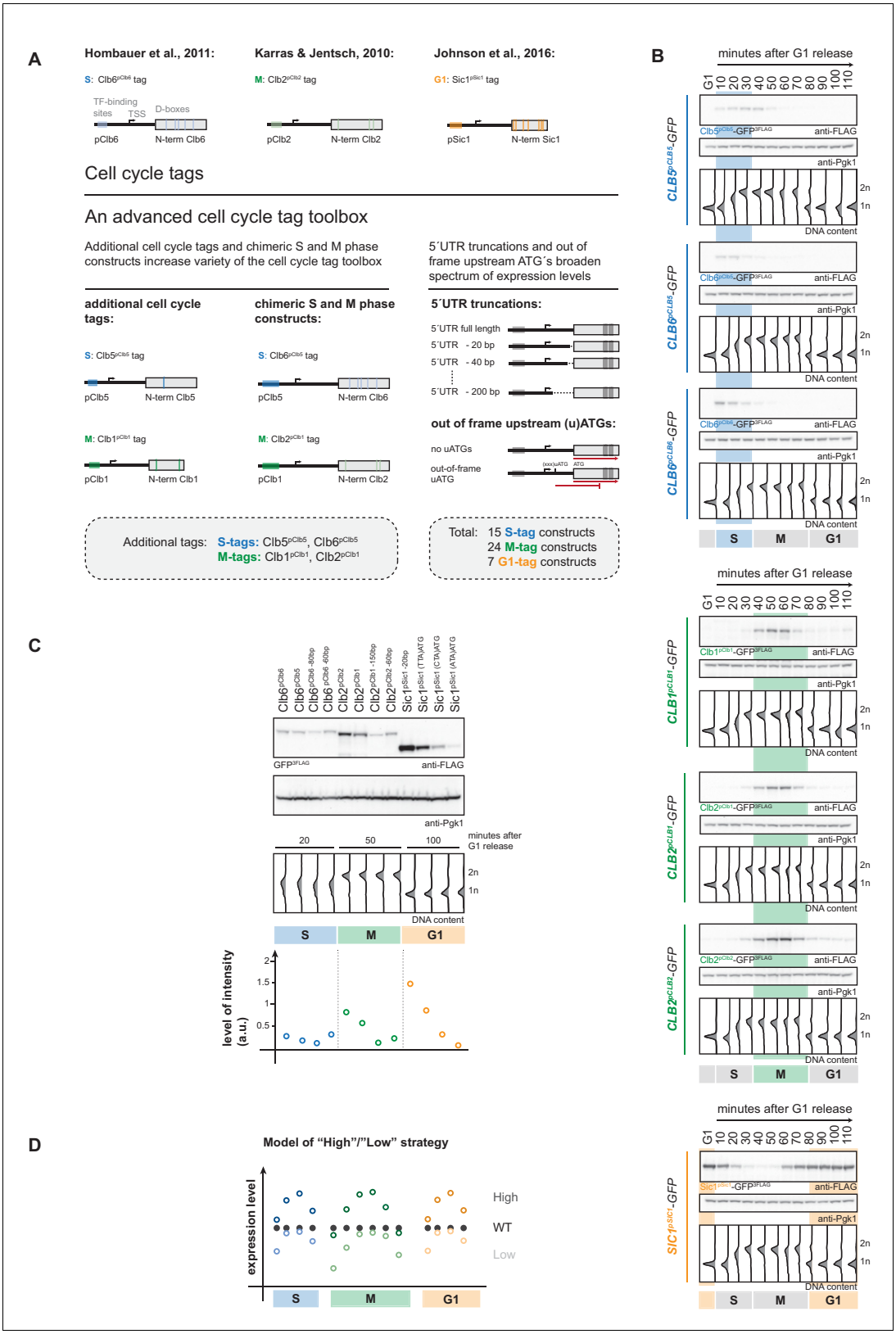

Figure 1. An advanced toolbox of cell cycle tag constructs. (**A**) Schematic representation of the applied strategies for improved cell cycle tag methodology. Upper panel: conventional cell cycle tag methodology was limited by only one construct for each cell cycle phase. Lower panel: the

Figure 1 continued on next page

Figure 1 continued

advanced cell cycle tag toolbox was expanded to 46 constructs. Therefore, we used new promoters and degrons from Clb5 and Clb1, chimeric promoter-degron combinations and protein expression was crippled using 5´UTR truncations and upstream out of frame ATGs. Vertical bars indicate location of cell cycle regulatory elements in the promoter and N-terminal degron sequence (see ***Figure 1—figure supplement 1*** for detailed description of the tagging procedure). (**B**) New cell cycle tag constructs allow cell cycle-restricted expression of GFP at varied peak expression levels. Anti-FLAG westerns of cells expressing Clb5^{pClb5}-, Clb6^{pClb5}-, Clb6^{pClb6}-, Clb1^{pClb1}-, Clb2^{pClb1}-, Clb2^{pClb2}-3FLAG-tagged versions of GFP after G1 arrest with α-factor and synchronous release through the cell cycle up to the next G1 phase. Pgk1 western was used as control and DNA content measurements indicate cell cycle progression at the individual time points below (see ***Figure 1—figure supplement 2*** for G1 release experiments of the corresponding 5´UTR truncations and for constructs containing upstream out of frame ATGs). (**C**) New promoters and degrons, chimeric promoter-degron combinations, 5'UTR truncations and upstream out of frame ATGs allow a broad spectrum of peak expression levels of cell cycle-restricted GFP. Western blot analysis of peak expression levels of cell cycle-tagged 3FLAG-GFP variants at indicated time points after G1 release (20 min = S phase, 50 min = M phase, 100 min = G1 phase). DNA content measurements below indicate cell cycle progression. Graph: peak expression levels were quantified using Image-J and signals of the individual constructs were divided by the corresponding Pgk1 sample to normalize to overall protein levels (see ***Figure 1—figure supplement 3*** for an overview of all cell cycle-tagged GFP versions in cells arrested in the corresponding cell cycle phase). (**D**) Schematic representation of the suggested cell cycle tag strategy using two sets of constructs with matching 'low' and 'high' peak expression levels. 'Low' expressing constructs (light colours) are chosen by matching peak expression levels similar to the endogenous protein but will show underexpression at cell cycle phase transitions. 'High' expressing tags generally show higher expression compared to the wildtype protein with the advantage of broader timeframes of action (timeframes in which protein levels are similar or higher than endogenous protein levels).

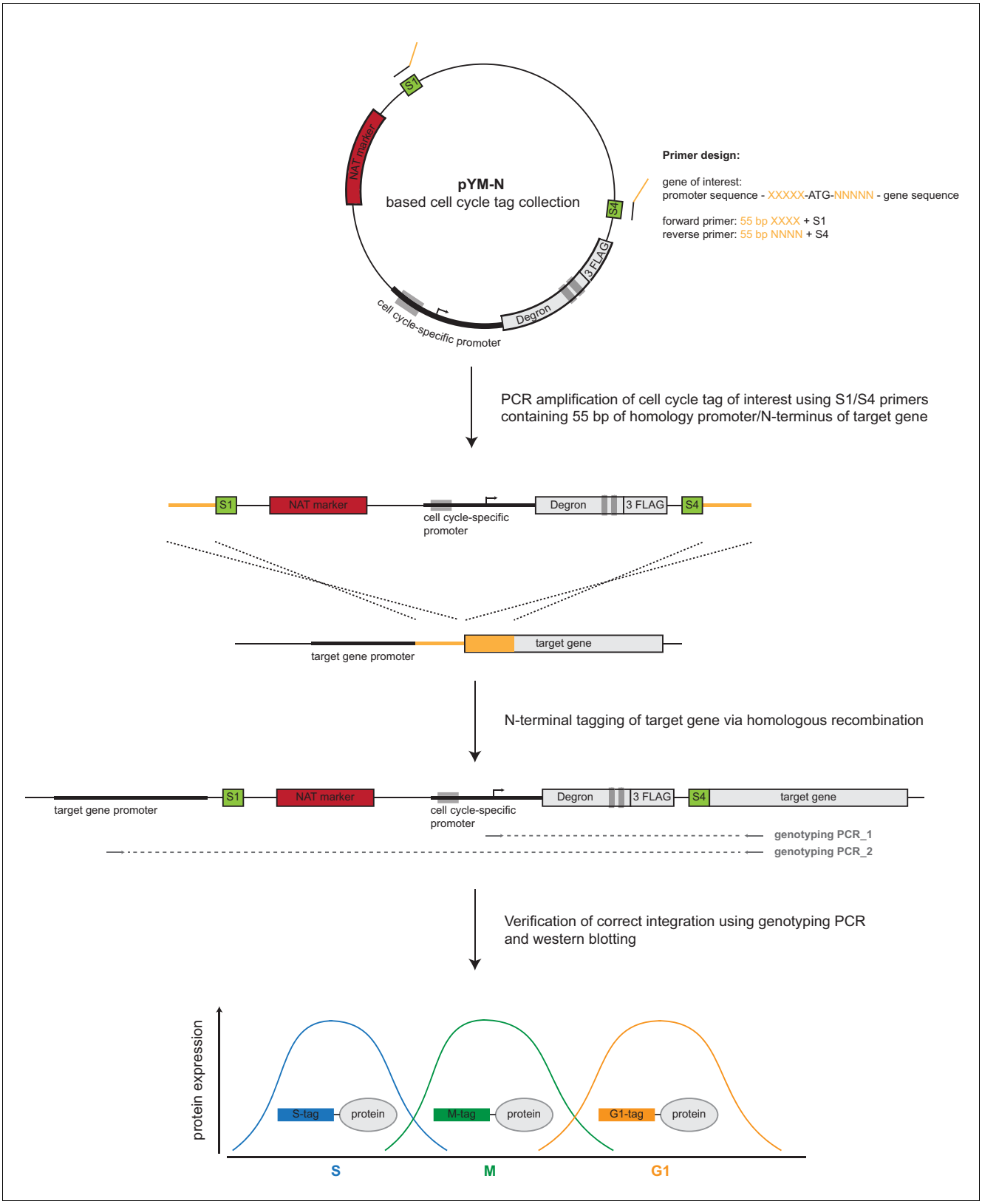
pYM-N
based cell cycle tag collection
S1
NAT marker
S4
3 FLAG
Degron
cell cycle-specific promoter
Primer design:
gene of interest:
promoter sequence - XXXXX-ATG-NNNNN - gene sequence
forward primer: 55 bp XXXX + S1
reverse primer: 55 bp NNNN + S4
PCR amplification of cell cycle tag of interest using S1/S4 primers containing 55 bp of homology promoter/N-terminus of target gene
target gene promoter
target gene
N-terminal tagging of target gene via homologous recombination
genotyping PCR_1
genotyping PCR_2
Verification of correct integration using genotyping PCR and western blotting
protein expression
S-tag
protein
M-tag
G1-tag
S
M
G1

Figure 1—figure supplement 1. Schematic representation of the cell cycle tagging procedure. A construct from the pYM-N-based (***Janke et al., 2004***) collection of cell cycle tags is used as a template for PCR amplification and homologous recombination-based tagging of a gene of interest. A detailed description of the workflow can be found in Materials and methods (construction of cell cycle-tagged strains).

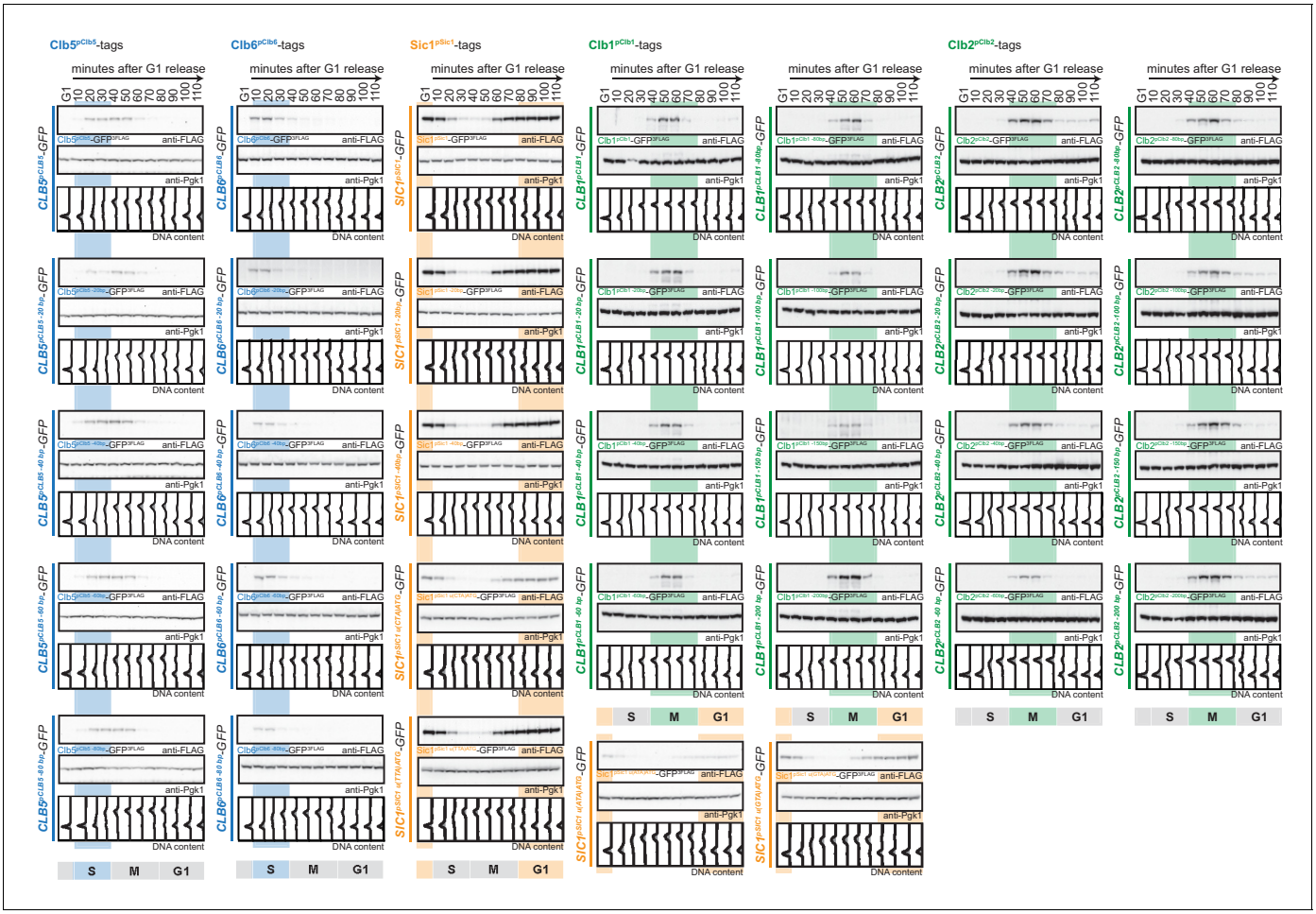

Figure 1—figure supplement 2. 5'UTR truncations and upstream out of frame ATGs do not interfere with cell cycle restriction. Western blot analysis of Clb5^{pClb5}-, Clb6^{pClb6}-, Clb1^{pClb1}-, Clb2^{pClb2}- and Sic1^{pSic1}-tagged GFP expressed from 33 constructs with truncated 5'UTR or upstream out of frame ATGs during a single cell cycle. Cells were arrested in G1 and synchronously released to the cell cycle up to the next G1 as in ***Figure 1B***. Anti-FLAG western shows cell cycle-tagged constructs, anti-Pgk1 western is used as control. Bottom: DNA content measurement by flow cytometry.

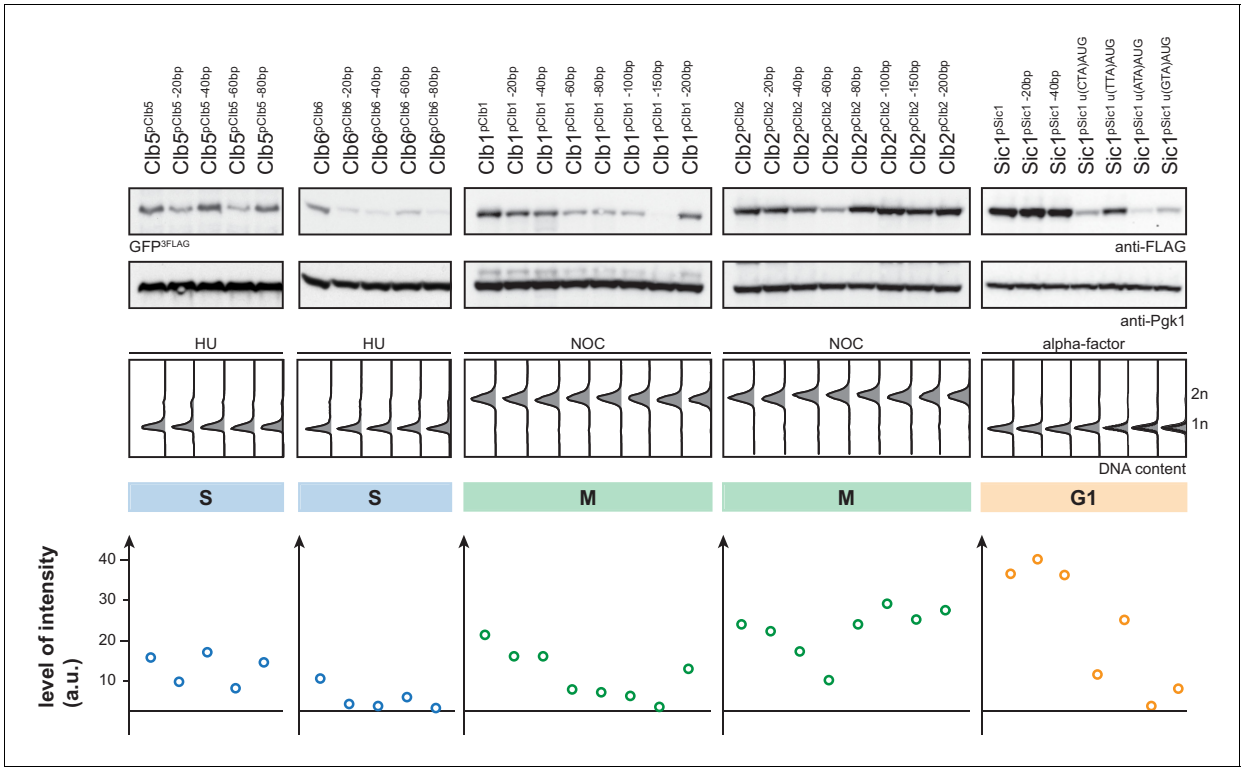

Figure 1—figure supplement 3. 5'UTR truncations and upstream out of frame ATGs cripple peak expression levels of cell cycle tag constructs. Western blot analysis of Clb5^{pClb5}-, Clb6^{pClb6}, Clb1^{pClb1}-, Clb2^{pClb2}- and Sic1^{pSic1}-tagged GFP expressed from constructs with truncated 5'UTR and upstream out of frame ATGs in HU (S), NOC (M) and α-factor (G1) arrested cells. Middle: DNA content measurements of corresponding samples by flow cytometry. Bottom: Expression levels were quantified using Image-J.

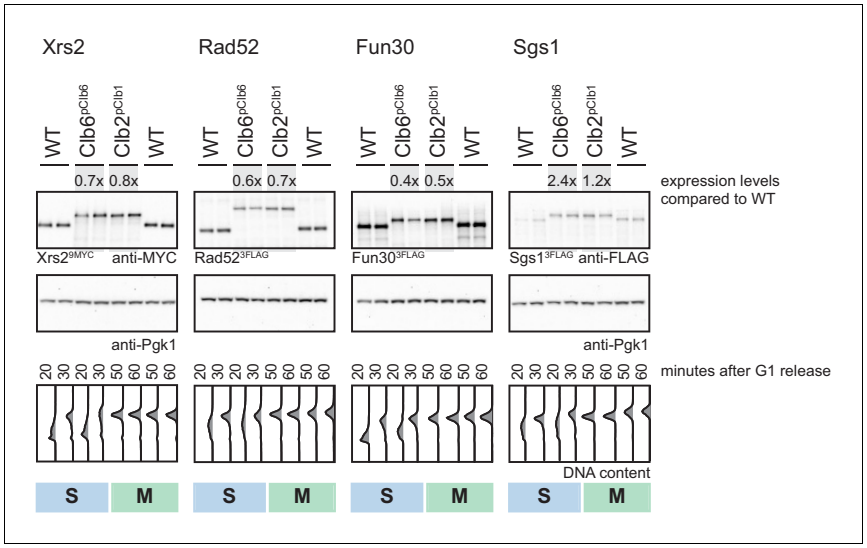

Figure 1—figure supplement 4. Clb6^{pClb6}- and Clb2^{pClb1}-tag induce similar peak expression levels for several cell cycle-tagged proteins. Clb6^{pClb6} (S)- and Clb2^{pClb1} (M)-tagged Xrs2, Rad52, Fun30 and Sgs1 show similar peak expression levels. Western blot analysis of peak expression levels at indicated time points after G1 release. Expression levels were quantified using Image-J and signals of the individual constructs were divided by the corresponding Pgk1 sample to normalize to overall protein levels. Normalized protein levels of Clb6^{pClb6} and Clb2^{pClb1}-tagged Xrs2, Rad52, Fun30 and Sgs1 were compared to WT expression at the corresponding time point (fold difference) and the two analysed time points (20 and 30 min time points for S phase and the 50 and 60 min time points for M phase) for each construct were averaged to result in a mean fold difference that is indicated above the western blots. Bottom: DNA content analysis by flow cytometry.

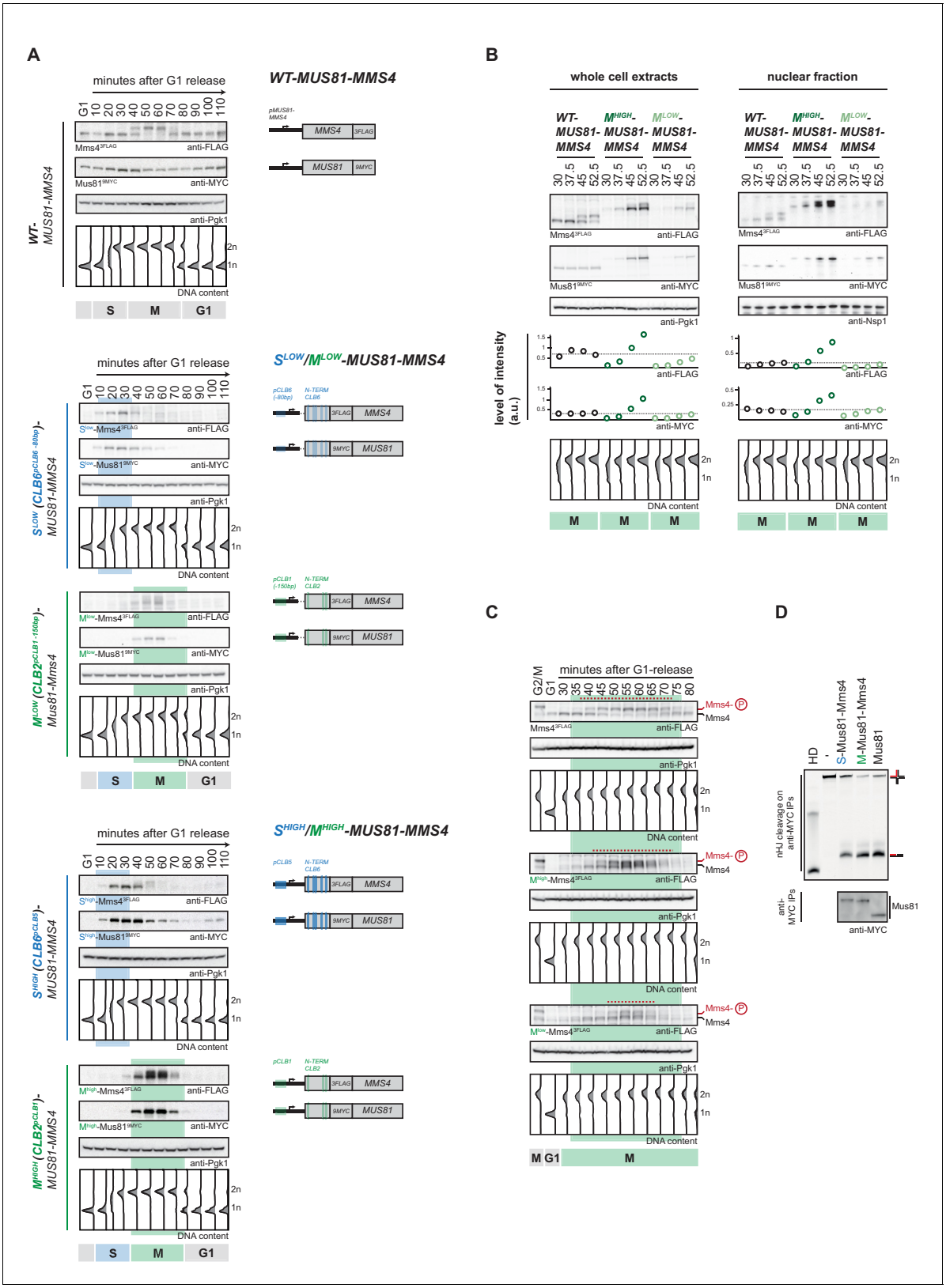

Figure 2. Cell cycle-restricted expression of Mus81-Mms4. (**A**) Restriction of Mus81-Mms4 expression to S or M phase of matched pairs of 'low' and 'high' expressing cell cycle tag constructs. (Left) Western blot and DNA content analysis of strains expressing WT, S phase-restricted (S^{low} ($Clb6^{pClb6}$ -

Figure 2 continued on next page

Figure 2 continued

^{80bp})-/S^{high} (Clb6^{pClb5})-Mus81-Mms4) and M phase-restricted (M^{low} (Clb2$^{pClb1\ -150bp}$)-/M^{high} (Clb2^{pClb1})-Mus81-Mms4) alleles of Mus81 (9MYC-tagged)-Mms4 (3FLAG-tagged) during a single cell cycle as in ***Figure 1D*** (see ***Figure 2—figure supplement 1*** for quantification of peak expression levels of the S^{low}-/M^{low} -Mus81-Mms4 and S^{high}-/M^{high}-Mus81-Mms4 constructs). (Right) Schematic representation of WT, S (S^{low}-/S^{high}-Mus81-Mms4) and M phase (M^{low}-/M^{high}-Mus81-Mms4) restricted Mus81-Mms4 constructs. Blue and green bars indicate location of cell cycle regulatory elements in the promoter and N-terminal degron sequence. (**B**) Different constructs ('high' and 'low' peak expression levels) of Mus81-Mms4 lead to underexpression of the M^{low}-Mus81-Mms4 construct or to overexpression of the M^{high}-Mus81-Mms4 construct in early M phase and similar trends are seen in the nuclear fraction. Western blot analysis of protein levels in whole cell extracts (left panel) and after nuclei separation (right panel) at indicated time points after a G1-release (early M phase; see DNA content profile depicted at the bottom). While immediately with entry into M phase the M^{high}-Mus81-Mms4 construct reaches similar or higher protein levels than endogenous Mus81-Mms4, the M^{low}-Mus81-Mms4 construct shows a 10–15 min delay in reaching comparable expression levels and this holds true for both, whole cell extracts and the nuclear fraction. Expression levels were quantified using Image-J and signals of the individual time points were divided by the corresponding Pgk1 (whole cell extracts) or Nsp1 (nuclear fraction) signal to normalize to overall protein levels (graphs below contain normalized values for every construct). (see ***Figure 2—figure supplement 2*** for control western blots of the nuclear fractionation) (**C**) Different constructs ('high' and 'low' peak expression levels) of Mus81-Mms4 lead to different windows of Mus81-Mms4 phosphorylation in M^{low}-Mus81-Mms4 and M^{high}-Mus81-Mms4. Western blot analysis of the phosphorylation states of Mms4 at indicated time points after a G1-release (M phase; see DNA content profile depicted below the western blots). While M^{high}-Mus81-Mms4 shows a similar timeframe of Mms4 phosphorylation to endogenous Mus81-Mms4, M^{low}-Mus81-Mms4 is phosphorylated and stimulated during a shortened window of time only (compare red lines above the Mms4-3FLAG western blots: 15–20 min of phosphorylation in M^{low}-Mus81-Mms4 compared to 30 min in M^{high}-Mus81-Mms4 and 30–35 min in Mus81-Mms4). (**D**) N-terminal tagging does not alter Mus81-Mms4 activity. Resolution assay using a nicked HJ (nHJ) substrate and immunopurified Mus81-Mms4, S-Mus81-Mms4 and M-Mus81-Mms4 (note that WT and cell cycle-tagged proteins were expressed from pGal1-10 promoter). Myc-tagged Mus81-Mms4 was purified from cycling cells, dephosphorylated using λ-Phosphatase and incubated with the nHJ substrate for 2 hr. Upper panel: nHJ cleavage assay with heat DNA substrate (HD) as control. Lower panel: western blot analysis of Mus81-9MYC IP after nHJ cleavage assay (see ***Figure 2—figure supplement 3*** for a western blot analysis of Mms4 dephosphorylation by λ-Phosphatase).

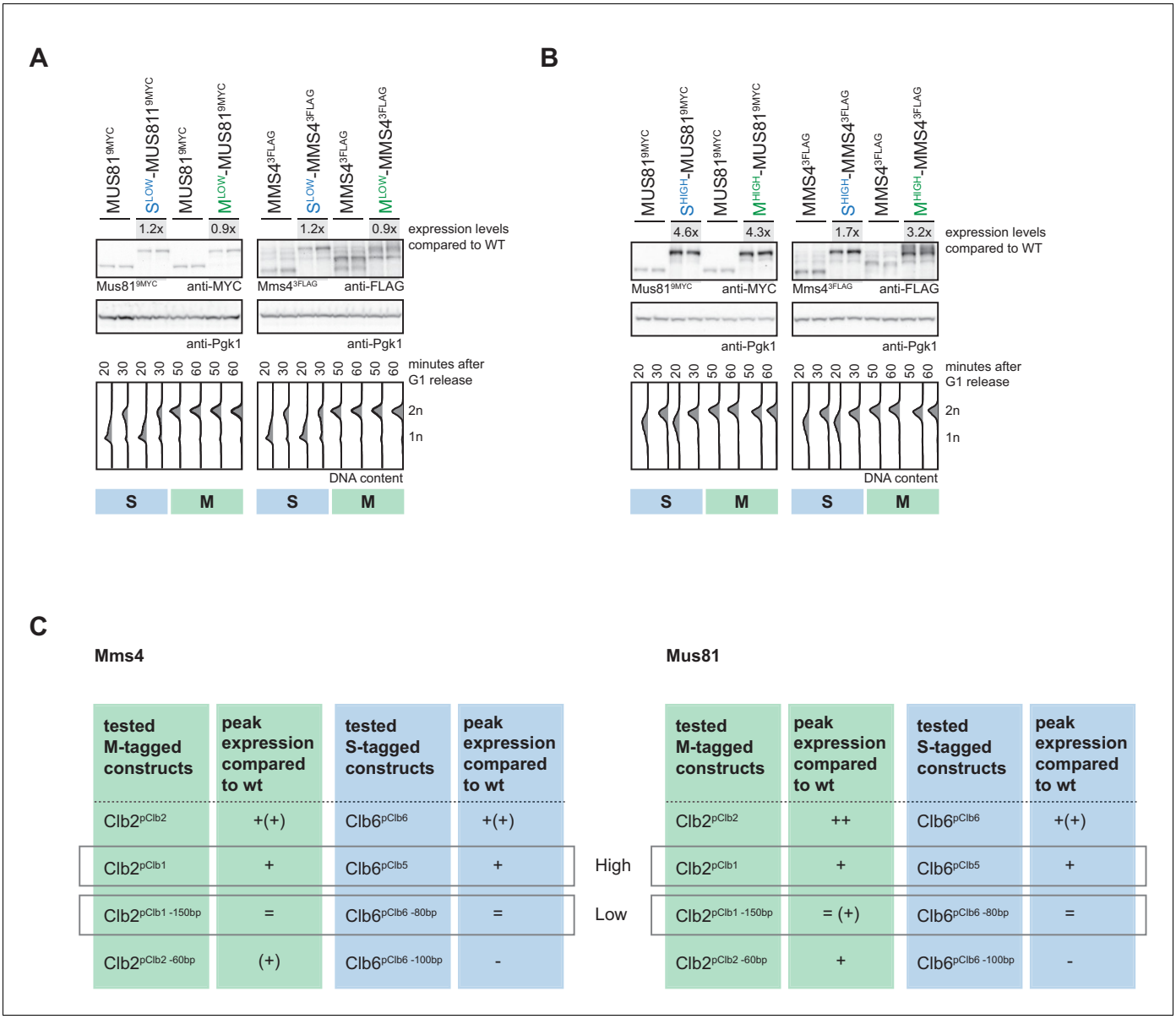

Figure 2—figure supplement 1. Analysis of 'low' and 'high' S- and M-tagged Mus81-Mms4 peak expression levels. (**A/B**) Sets of S^{low}-Mus81-Mms4 ($Clb6^{pClb6\ -80bp}$)/M^{low}-Mus81-Mms4 ($Clb2^{pClb1\ -150bp}$) (**A**) and S^{high}-Mus81-Mms4 ($Clb6^{pClb5}$)/M^{high}-Mus81-Mms4 ($Clb2^{pClb1}$) (**B**) display similar peak expression levels. Western blot analysis of peak expression levels at individual time points after G1 release. Expression levels were quantified using Image-J and signals at the individual time points were divided by the corresponding Pgk1 sample to normalize to overall protein levels. Normalized protein levels of S^{low}-/M^{low}-Mus81-Mms4 and S^{high}-/M^{high}-Mus81-Mms4 were compared to wt expression at the corresponding time point (fold difference) and the two analysed time points (20 and 30 min time points for S phase and 50 and 60 min time points for M phase) for each construct were averaged to result in a mean fold difference that is indicated above the western blots. Bottom: DNA content measurement by flow cytometry. (**C**) Summary of peak expression levels of various cell cycle-tagged Mus81/Mms4 constructs. Depicted are relations of peak expression values in comparison to WT, which lead to selection of 'high' and 'low' expressing constructs.

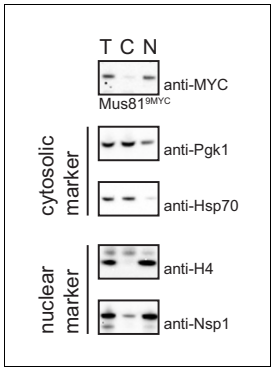

Figure 2—figure supplement 2. Nuclear/cytoplasmic fractionation. Western blot analysis of different fractions obtained after nuclei separation of a representable sample from the experiment in ***Figure 2B*** shows efficient separation into cytoplasmic and nuclear fractions. Pgk1 and chaperone Hsp70 serve as cytosolic markers, histone H4 and the nuclear pore complex protein NSP1 serve as nuclear markers.
T = total lysate, C = cytoplasmic fraction, N = nuclear fraction.

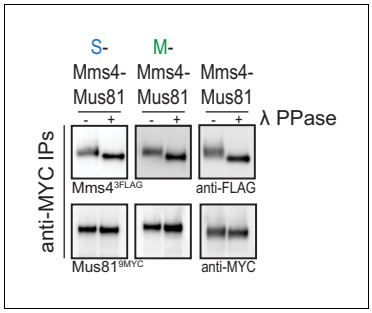

Figure 2—figure supplement 3. λ-Phosphatase treatment leads to efficient Mms4 dephosphorylation of WT, S- and M-Mus81-Mms4 used for activity assays. Western blot analysis of Mms4 shows efficient dephosphorylation of Mms4 after λ-Phosphatase treatment of WT, S- and M-Mus81-Mms4 preparations used in activity assays (see ***Figure 2D*** for activity assay done with S-, M- and WT Mus81-Mms4).

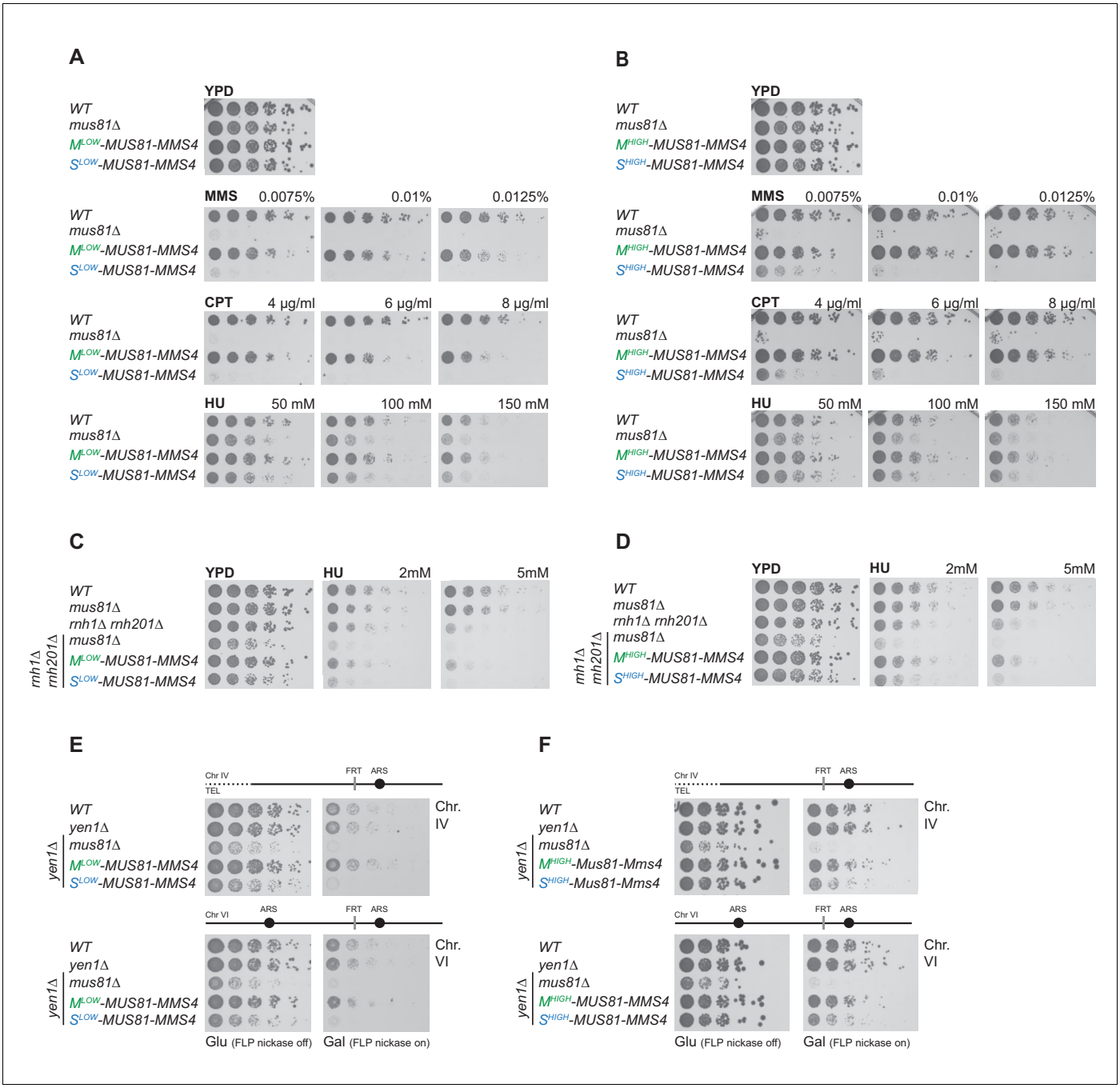

Figure 3. Mus81-Mms4 restricted to M phase, but not S phase is sufficient for the response to genotoxic insults. (**A/B**) M phase-restricted Mus81-Mms4 is sufficient to confer viability to replication fork stalling drugs. Viability of cells with M^{low} ($Clb2^{pClb1\ -150bp}$)-Mus81-Mms4/S^{low} ($Clb6^{pClb6\ -80bp}$)-Mus81-Mms4 constructs at low peak expression levels (**A**) or M^{high} ($Clb2^{pClb1}$)-Mus81-Mms4/S^{high} ($Clb6^{pClb5}$)-Mus81-Mms4 constructs at high peak expression levels (**B**) is compared to that of *WT* and *mus81Δ* cells. Strains were plated in 5-fold serial dilutions on YPD plates containing the indicated amounts of MMS, CPT or HU and incubated at 30°C for 2 days. (**C/D**) Mitotic function of Mus81-Mms4 is sufficient to confer viability upon induction of RNA-DNA-hybrids in the absence of RNAse H enzymes and mild replication stress (HU). Cell cycle-tagged versions of Mus81-Mms4 were integrated in the *rnh1Δ rnh201Δ* background. Strains were spotted in 5-fold serial dilutions on YPD containing indicated concentrations of HU and incubated at 30°C for 2 days. (**C**) Spotting containing M^{low}-Mus81-Mms4/S^{low}-Mus81-Mms4 cells. (**D**) Spotting of M^{high}-Mus81-Mms4/S^{high}-Mus81-Mms4 cells. (**E/F**) Repair of Flp-nickase induced DNA lesions requires the M phase function of Mus81-Mms4. Galactose-induced DNA nicking is presumed to be followed by replication run-off in S phase to form single-ended DSBs and repair by BIR (***Nielsen et al., 2009***; ***Mayle et al., 2015***). Location of the corresponding FRT sites on chromosome IV and VI are indicated relative to replication origins. Cells were spotted in 5-fold serial dilutions in presence of glucose or

Figure 3 continued on next page

Figure 3 continued

galactose (FLP-induction) and incubated at 30°C for 2 days. (**E**) Spottings of M^{low}-Mus81-Mms4/S^{low}-Mus81-Mms4 cells. (**F**) Spottings of M^{high}-Mus81-Mms4/S^{high}-Mus81-Mms4 cells.

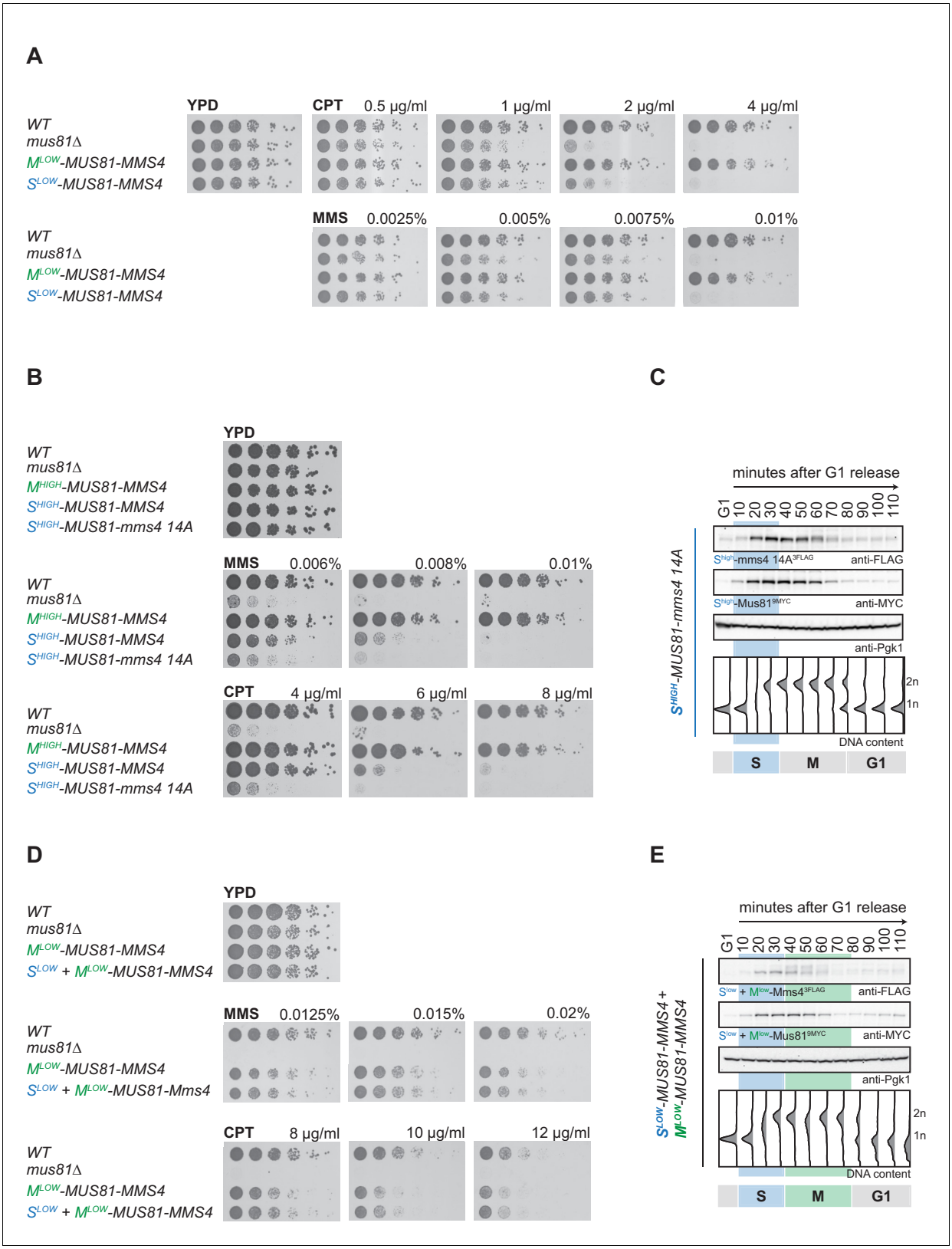

Figure 3—figure supplement 1. Residual S^{high}-Mus81-Mms4 function in response to genotoxic agents is explained by insufficient restriction to S phase; slight M^{low}-Mus81-Mms4 defect in response to genotoxic agents is due to underexpression during M phase, respectively. (**A**) S^{low}-Mus81-Mms4

Figure 3—figure supplement 1 continued on next page

Figure 3—figure supplement 1 continued

cells show comparable DNA damage sensitivity to *mus81*Δ even at low CPT and MMS concentrations. Indicated strains were chronically exposed to CPT and MMS as in ***Figure 3A/B***. (**B/C**) Residual Mms4 phosphorylation is responsible for the observed difference between *mus81*Δ and S^{high}-Mus81-Mms4. While S^{high}-Mus81-Mms4 cells show better survival after MMS and CPT treatment compared to *mus81*Δ cells, additional removal of phosphorylation sites targeted during M phase (mms4 14A) from the S^{high}-Mus81-Mms4 construct (S^{high}-Mus81-mms4 14A) lead to a phenotype comparable to *mus81*Δ indicating this residual functionality comes from leakage of the S^{high} tagged protein in M phase (S^{high}-Mus81-mms4 14A). (**B**) Spotting of indicated strains as in ***Figure 3A/B***. (**C**) Western blot analysis of the S^{high}-Mus81-mms4 14A construct at indicated time points after G1 release as in ***Figure 1D***. (**D/E**) The observed survival defect of M^{low}-Mus81-Mms4 cells upon exposure with high MMS and CPT concentrations is not derived from a missing S phase function, but rather from underexpression of the M^{low}-Mus81-Mms4 construct. Additional expression of S^{low}-Mus81-Mms4 as a second copy together with M^{low}-Mus81-Mms4 (S^{low}+M^{low}-Mus81-Mms4) does not rescue the defect of M^{low}-Mus81-Mms4 cells at high MMS and CPT concentrations and thereby rules out a contribution of S phase Mus81-Mms4. (**D**) Spotting of indicated strains as in ***Figure 3A/B***. (**E**) Western blot analysis of cells expressing both S^{low}-Mus81-Mms4 and M^{low}-Mus81-Mms4 (S^{low}+M^{low}-Mus81-Mms4) constructs at indicated time points after G1 release as in ***Figure 1D***.

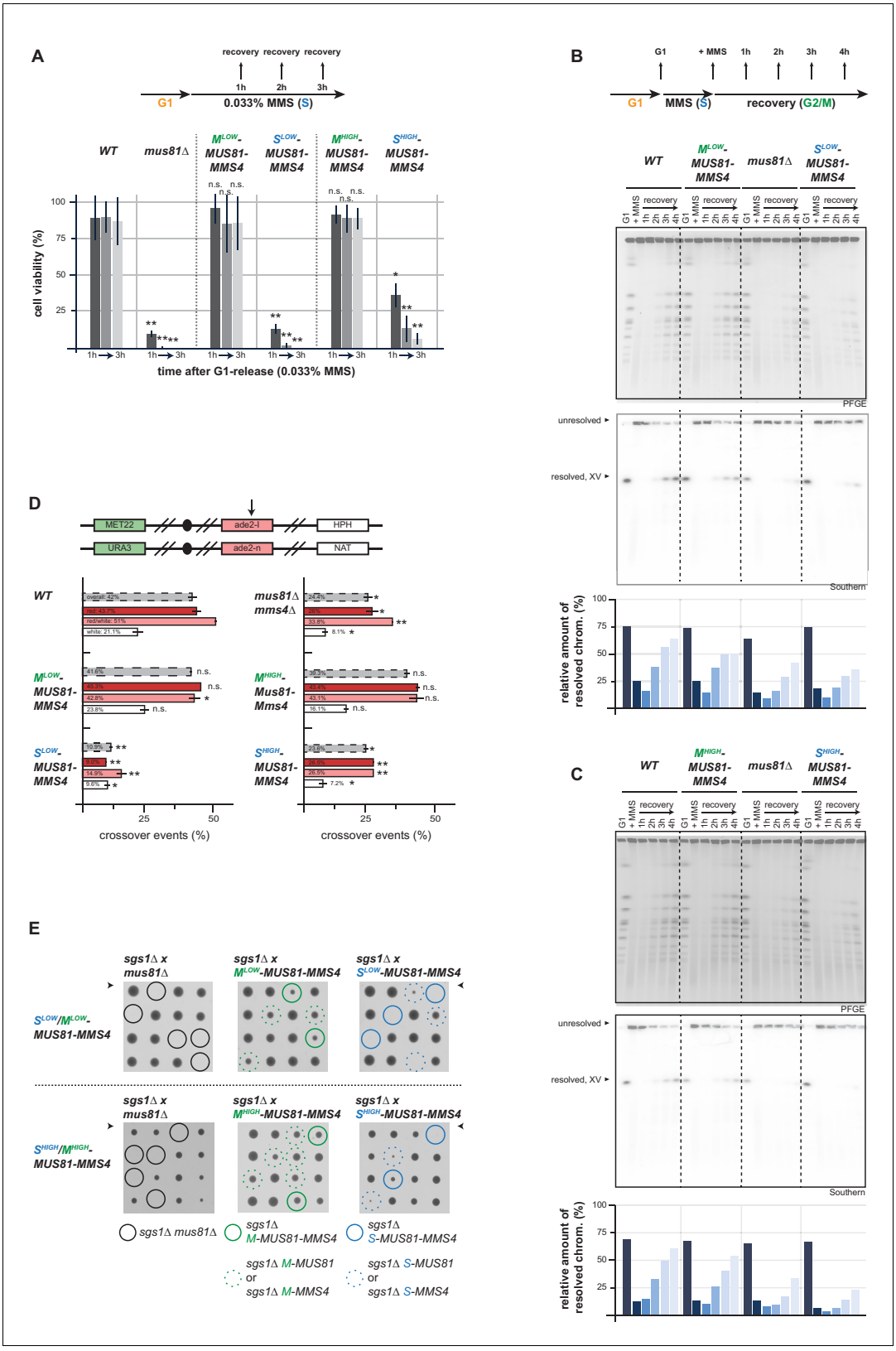

Figure 4. Mus81-Mms4 act as a post-replicative resolvase. (**A**) Viability after a pulse of MMS in S phase and subsequent replication fork stalling depends on the M phase function of Mus81-Mms4. Viability assay scoring survivors after pulses of MMS in S phase for one to three hours (upper). Cell

Figure 4 continued on next page

Figure 4 continued

viability (%) was determined by colony forming units normalized to untreated cells (0 hr) and is depicted as mean of biological replicates (n = 3) with error bars indicating standard deviation. Significance: n.s. p>0.05, *p<0.05, **p<0.005 as calculated by an unpaired Student´s T-test (see ***Figure 4—source data 1*** for underlying values and exact p-values). (B/C) Resolution of replication/repair intermediates arising in response to replication stalling in S phase requires mitotic Mus81-Mms4 function. PFGE analysis of cells recovering (1–4 hr in Nocodazole) from a pulse of MMS (0.033%, 1 hr) in S phase (see upper panel for experimental setup). PFGE gels were stained with EtBr or subjected to southern blot hybridization with a probe against the *ADE2* locus located on chromosome XV. The relative number of resolved chromosomes XV from the southern blots was quantified using ImageJ and is depicted below. (**B**) PFGE/southern analysis of M^{low}-Mus81-Mms4/S^{low}-Mus81-Mms4 cells. (**C**) PFGE/southern analysis of M^{high}-Mus81-Mms4/S^{high}-Mus81-Mms4 cells. (**D**) HR repair resulting in crossovers depends on the mitotic function of Mus81. I-SceI induced recombination assay between heterologous *ade2* alleles in diploid cells as described in ***Ho et al., 2010***. Upper panel: arrangement of marker genes on chromosomes IV used for classifying the genetic outcomes of DSB repair. The arrow indicates the I-SceI site. Bottom panel: genetic outcome of repair, with overall crossover events (grey) and crossovers among individual classes (red, red/white, white) that differ in conversion tract length. Depicted are mean values from two independent experiments each scoring 400–600 cells with the standard deviation as error bars. Significance: n.s. p>0.05, *p<0.05, **p<0.005 compared to WT cells by unpaired Student´s T-test (see ***Figure 4—source data 2*** for underlying values and exact p-values). (**E**) The essential requirement of Mus81 in the absence of *SGS1*-dependent dissolution occurs during M phase. Tetrad analysis of yeast diploid cells with indicated genotypes reveals synthetic lethality between *sgs1*Δ and S^{low}-/S^{high}-Mus81-Mms4 while M^{low}-/M^{high}-Mus81-Mms4 shows no discernible effect on cell growth in the background of *sgs1*Δ (see ***Figure 4—figure supplement 2*** for a growth analysis of the individual spores of the tetrad analysis with S^{high}-/M^{high}-Mus81-Mms4).

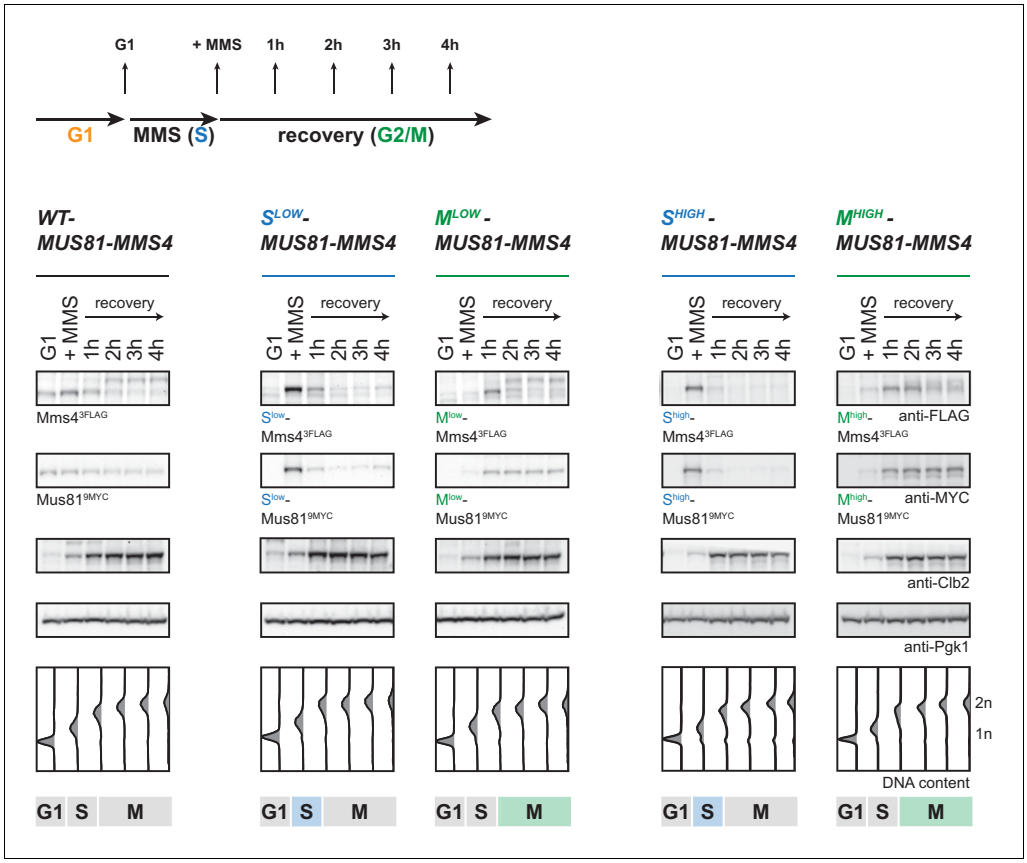

Figure 4—figure supplement 1. Cell cycle tags restrict efficiently to S or M phase also after DNA damage treatment. Western blot analysis of WT cells (left), of cells expressing S^{low}-Mus81-Mms4 or M^{low}-Mus81-Mms4 (middle) and of cells expressing S^{high}-Mus81-Mms4 or M^{high}-Mus81-Mms4 (right) S- and M-tagged Mus81-Mms4 recovering from a pulse of MMS (0.033%, 1 hr) as in ***Figure 4B/C***. Rise in Clb2 levels are coincidental with entry into M phase. Pgk1 serves as control.

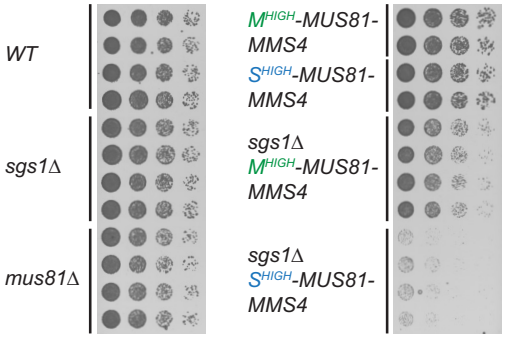

Figure 4—figure supplement 2. Mus81 function during M phase is required in the absence of Sgs1 function. Growth assay of yeast haploid cells with the indicated genotypes derived from the tetrad analysis of S^{high}-/M^{high}-Mus81-Mms4 in ***Figure 4E*** including very slow growing S^{high}-/M^{high}-Mus81-Mms4 *sgs1*Δ haploids. Four strains of indicated genotypes were spotted in 5-fold serial dilutions and growth was analysed after incubation of 1.5 days at 30°C on YPD plates.

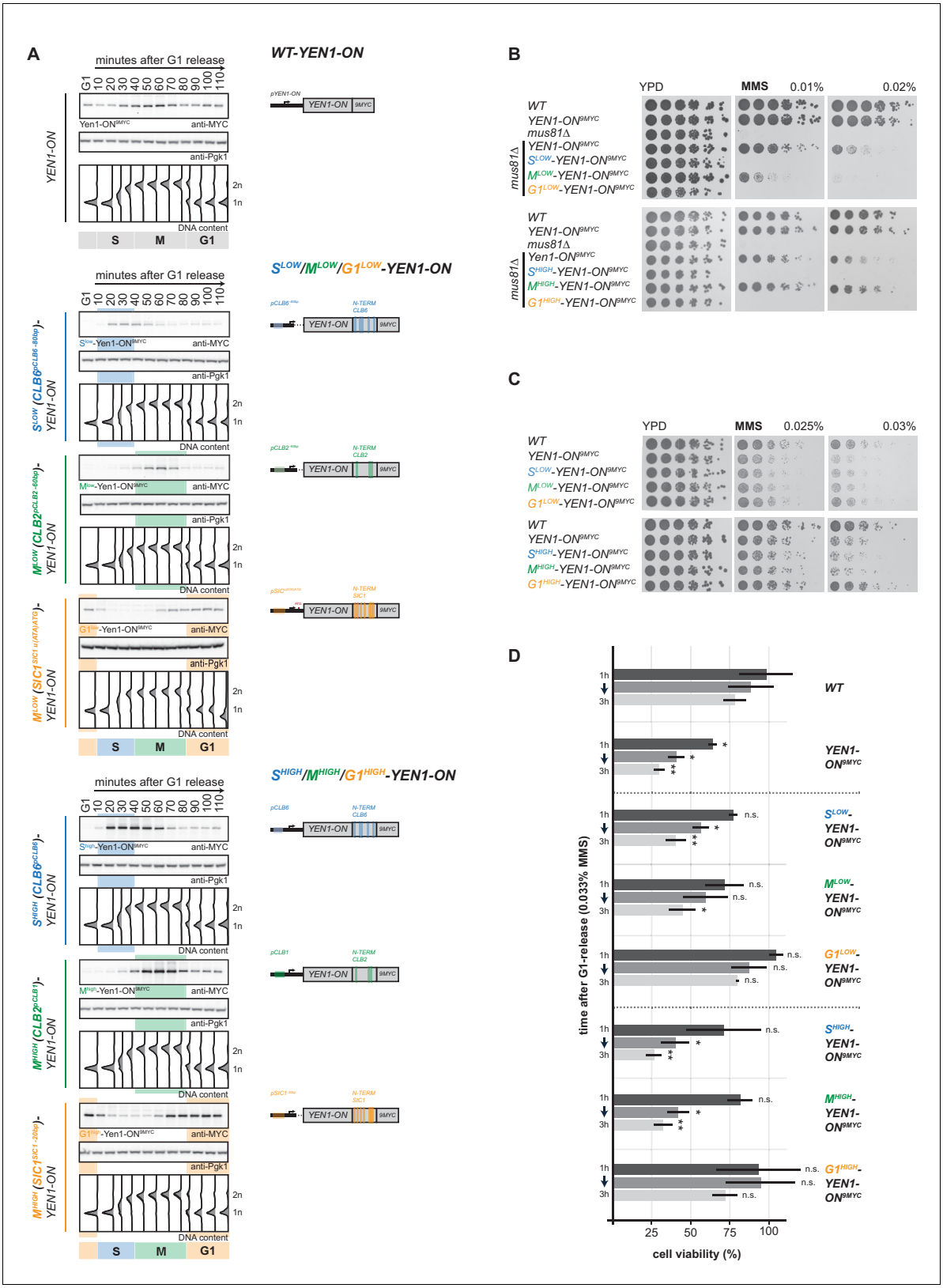

Figure 5. Premature activation of Yen1 in S or early M phase interferes with the response to replication stalling lesions. (**A**) Cell cycle-tagged Yen1-ON-9MYC constructs restrict expression of constitutively active Yen1-ON to S, M or G1 phase. (Left) Western blot analysis of strains expressing WT, S (S^{low}

Figure 5 continued on next page

Figure 5 continued

($Clb6^{pClb6\ -80bp}$)-Yen1-ON^{9MYC}/S^{high} ($Clb6^{pClb6}$)-Yen1-ON^{9MYC}), M (M^{low} ($Clb2^{pClb2\ -60bp}$)-Yen1-ON^{9MYC}/M^{high} ($Clb2^{pClb1}$)-Yen1-$ON^{9MYC)}$ and G1 ($G1^{low}$ ($Sic1^{pSic1\ u(ATA)ATG}$)-Yen1-ON^{9MYC}/$G1^{high}$ ($Sic1^{pSic1\ -20bp}$)-Yen1-ON^{9MYC}) phase-restricted Yen1-ON during synchronous cell cycle progression as in ***Figure 2A***. (see ***Figure 5—figure supplement 2*** for quantification of peak expression levels for individual constructs). (Right) schematic representation of endogenously expressed and cell cycle-tagged Yen1-ON constructs. Blue, green and orange bars indicate location of cell cycle regulatory elements in the promoter and N-terminal degron sequence. (**B**), The M phase function of Yen1-ON is able to bypass Mus81 requirement after MMS induced replication fork stalling. Strains with indicated genotypes were chronically exposed to MMS as in ***Figure 3A*** (note the *mus81*Δ background). (**C–D**), Viability after MMS induced replication fork stalling decreases when Yen1-ON is restricted to S or early M phase. (**C**) Survival of indicated strains after chronic MMS exposure as in (**B**). (**D**) Viability assay after a single pulse of MMS in S phase was measured for indicated strains as in ***Figure 4A*** (see ***Figure 5—source data 1*** for underlying values and exact p-values).

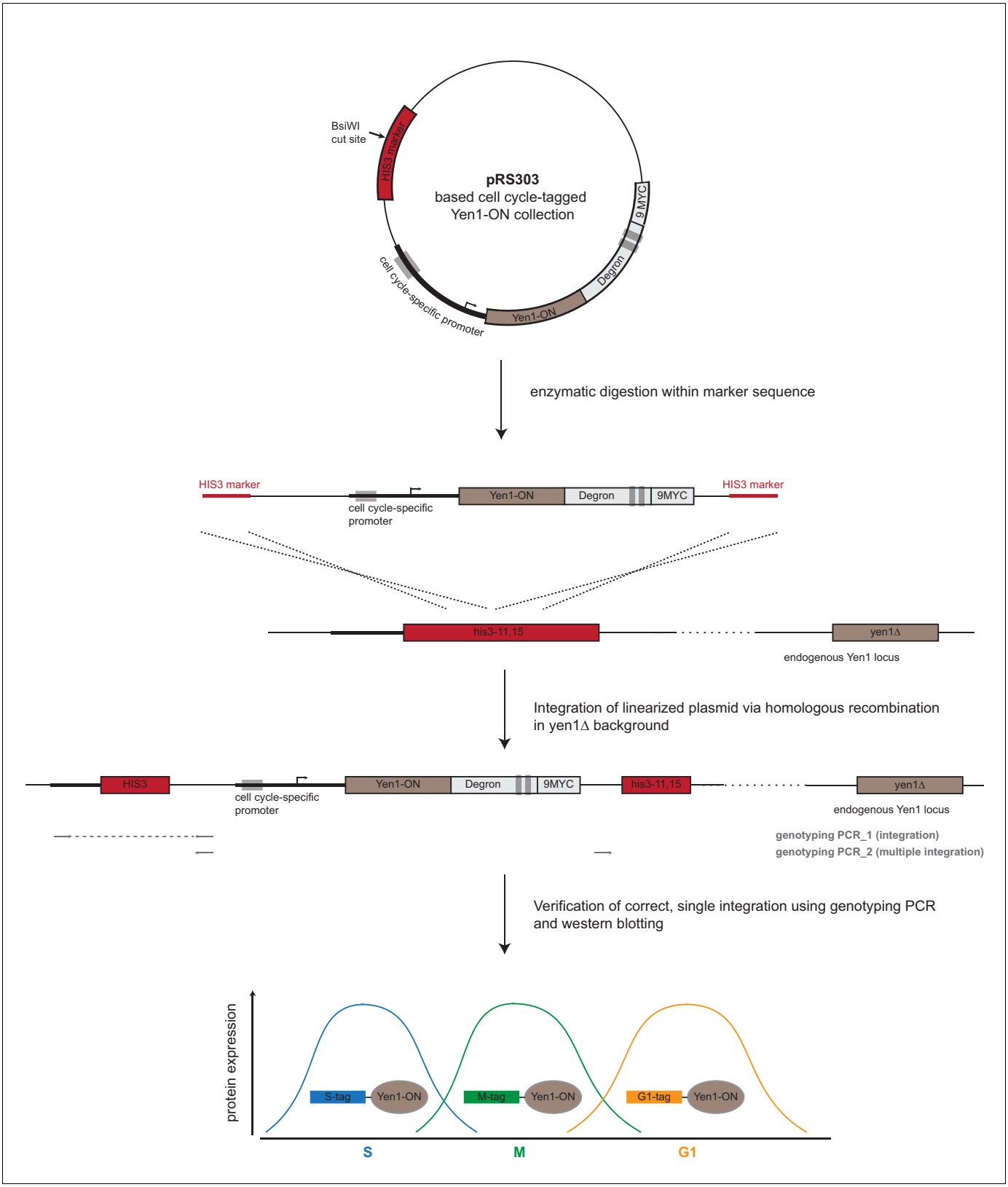

Figure 5—figure supplement 1. Strategy for C-terminal cell cycle tagging of Yen1-ON. In order to generate Yen1-ON alleles expressed under cell cycle-regulated promoters and with C-terminal degrons, Yen1-ON constructs were generated in pRS303 integrative vectors. Cell cycle-tagged Yen1-ON

Figure 5—figure supplement 1 continued on next page

Figure 5—figure supplement 1 continued

constructs were linearized and integrated at the *his3-11,15* locus via homologous recombination. A detailed description of the workflow can be found in Materials and methods (construction of cell cycle-tagged strains).

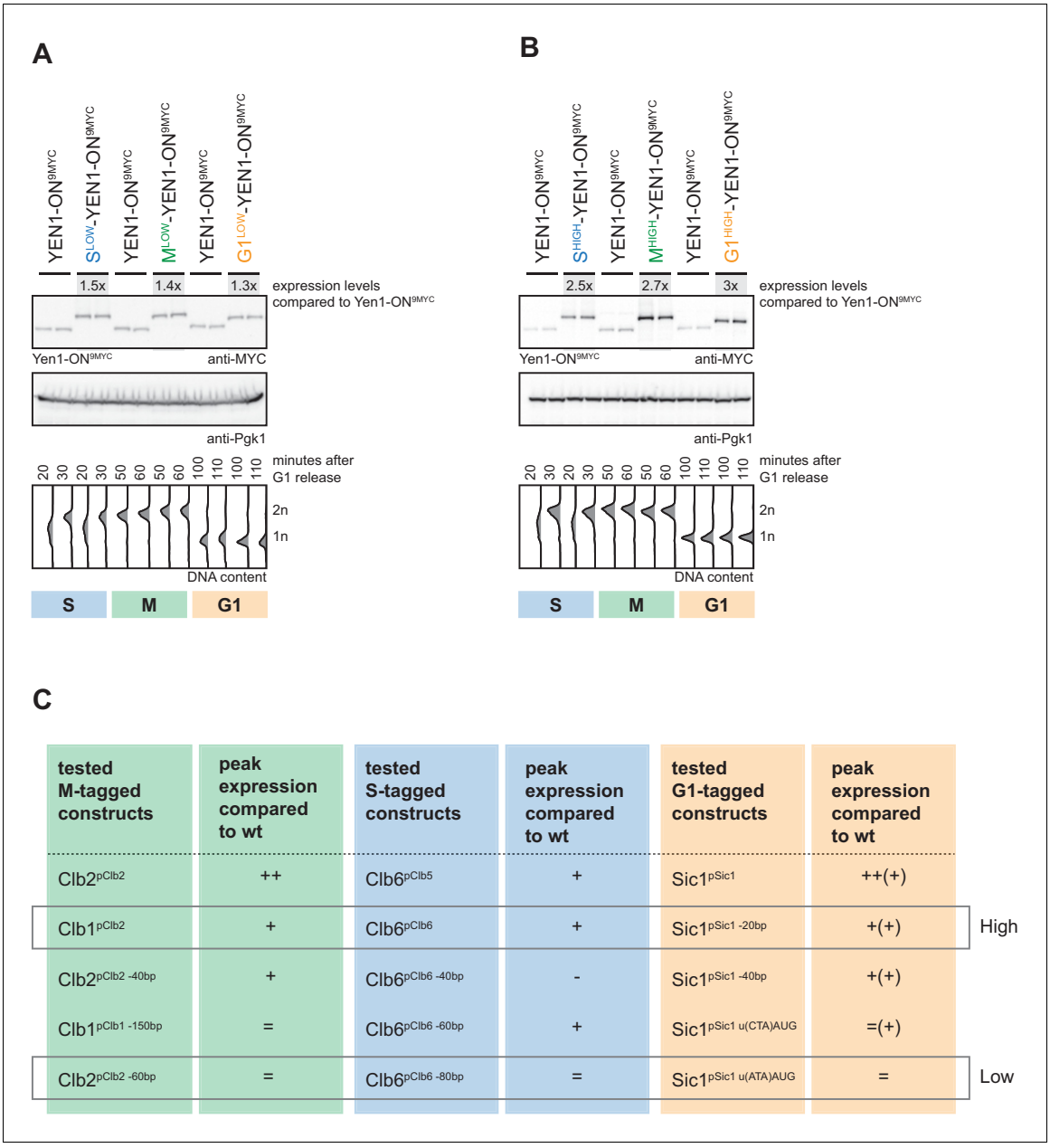

Figure 5—figure supplement 2. Analysis of 'low' and 'high' S-, M- and G1-tagged Yen1-ON peak expression levels. (**A/B**) Sets of S^{low} ($Clb6^{pClb6\ -80bp}$)-, M^{low} ($Clb2^{pClb2\ -60bp}$)- and $G1^{low}$ ($Sic1^{pSic1\ u(ATA)ATG}$)-Yen1-ON (**A**) and S^{high} ($Clb6^{pClb6}$)-, M^{high} ($Clb2^{pClb1}$)- and $G1^{high}$ ($Sic1^{pSic1\ -20bp}$)-Yen1-ON (**B**) display similar peak expression levels in S, M and G1 phase, respectively. Western blot analysis of peak expression levels of cell cycle-tagged Yen1-ON-9MYC variants at individual time points after G1 release (20,30 min = S; 50,60 min = M; 100,110 = G1) as controlled by DNA content measurement by flow cytometry (lower). Peak expression levels were quantified using Image-J and signals of the individual constructs were divided by the corresponding Pgk1 sample to normalize to overall protein levels. Normalized peak expression levels were compared to WT expression at the corresponding time point (fold difference) and the two analysed time points were averaged for each construct to result in a mean fold difference that is indicated above the western blots. (**C**) Summary of peak expression levels of various tested cell cycle-tagged Yen1-ON constructs. Depicted are relations of peak expression values in comparison to WT, which lead to selection of 'high' and 'low' expressing constructs.

Publication 2 | Princz et al., (2017) EMBO J

Princz, L.N., Wild, P., **Bittmann, J.**, Aguado, F.J., Blanco, M.G., Matos, J., Pfander, B. Dbf4-dependent kinase and the Rtt107 scaffold promote Mus81-Mms4 resolvase activation during mitosis. EMBO J (2017) 36: 664-678 DOI: 10.15252/embj.201694831

Article

TRANSPARENT PROCESS OPEN ACCESS

THE EMBO JOURNAL

Dbf4-dependent kinase and the Rtt107 scaffold promote Mus81-Mms4 resolvase activation during mitosis

Lissa N Princz[1], Philipp Wild[2], Julia Bittmann[1], F Javier Aguado[3], Miguel G Blanco[3], Joao Matos[2] & Boris Pfander[1,*]

Abstract

DNA repair by homologous recombination is under stringent cell cycle control. This includes the last step of the reaction, disentanglement of DNA joint molecules (JMs). Previous work has established that JM resolving nucleases are activated specifically at the onset of mitosis. In case of budding yeast Mus81-Mms4, this cell cycle stage-specific activation is known to depend on phosphorylation by CDK and Cdc5 kinases. Here, we show that a third cell cycle kinase, Cdc7-Dbf4 (DDK), targets Mus81-Mms4 in conjunction with Cdc5—both kinases bind to as well as phosphorylate Mus81-Mms4 in an interdependent manner. Moreover, DDK-mediated phosphorylation of Mms4 is strictly required for Mus81 activation in mitosis, establishing DDK as a novel regulator of homologous recombination. The scaffold protein Rtt107, which binds the Mus81-Mms4 complex, interacts with Cdc7 and thereby targets DDK and Cdc5 to the complex enabling full Mus81 activation. Therefore, Mus81 activation in mitosis involves at least three cell cycle kinases, CDK, Cdc5 and DDK. Furthermore, tethering of the kinases in a stable complex with Mus81 is critical for efficient JM resolution.

Keywords cell cycle; genome stability; homologous recombination; joint molecule resolution; post-translational modification
Subject Categories Cell Cycle; DNA Replication, Repair & Recombination
DOI 10.15252/embj.201694831 | Received 22 May 2016 | Revised 15 December 2016 | Accepted 19 December 2016 | Published online 18 January 2017
The EMBO Journal (2017) 36: 664–678

Introduction

Many DNA transactions are under cell cycle control to adjust them to cell cycle phase-specific features of chromosomes (Branzei & Foiani, 2008). Homologous recombination (HR) is cell cycle-regulated at several steps including the first, DNA end resection, and the last, JM removal (Heyer *et al*, 2010; Ferretti *et al*, 2013; Mathiasen & Lisby, 2014; Matos & West, 2014). Given that JMs provide stable linkages between sister chromatids, they will interfere with chromosome segregation and therefore need to be disentangled before sister chromatid separation during mitosis. Accordingly, JM resolvases, such as budding yeast Mus81-Mms4 (Interthal & Heyer, 2000; Schwartz *et al*, 2012) or Yen1 (Ip *et al*, 2008), become activated during mitosis (Matos *et al*, 2011, 2013; Gallo-Fernández *et al*, 2012; Szakal & Branzei, 2013; Blanco *et al*, 2014; Eissler *et al*, 2014). In contrast, the alternative JM removal pathway, JM dissolution by the Sgs1-Top3-Rmi1 complex, is thought to be constantly active throughout the cell cycle (Mankouri *et al*, 2013; Bizard & Hickson, 2014). The activation of JM resolvases in mitosis therefore leads to a shift in the balance between JM removal pathways, with dissolution being preferred outside of mitosis, but JM resolution becoming increasingly important in mitosis (Matos *et al*, 2011, 2013; Gallo-Fernández *et al*, 2012; Dehé *et al*, 2013; Saugar *et al*, 2013; Szakal & Branzei, 2013; Wyatt *et al*, 2013). It has been hypothesized that JM resolvases are downregulated at cell cycle stages other than mitosis in order to counteract crossover-induced loss of heterozygosity or to prevent over-active resolvases from interfering with S phase by, for example, cleaving stalled replication forks (Gallo-Fernández *et al*, 2012; Szakal & Branzei, 2013; Blanco *et al*, 2014).

Budding yeast Mus81-Mms4 has previously been shown to be targeted by two cell cycle kinases, cyclin-dependent kinase Cdc28 (CDK) and the yeast polo-kinase Cdc5 (Matos *et al*, 2011, 2013; Gallo-Fernández *et al*, 2012; Szakal & Branzei, 2013). The corresponding Mms4 phosphorylation events were shown to correlate with and to be required for activation of Mus81-Mms4 in mitosis. In 2014, we showed that in mitosis Mus81-Mms4 also forms a complex with Slx4-Slx1 and the scaffold proteins Dpb11 and Rtt107 (Gritenaite *et al*, 2014). Interestingly, mass spectrometric analysis of this complex (Gritenaite *et al*, 2014) revealed that Cdc5 and a third cell cycle kinase Dbf4-Cdc7 (Dbf4-dependent kinase, DDK) are also a stable part of this protein assembly (see Appendix Fig S1A). Here,

1 Max Planck Institute of Biochemistry, DNA Replication and Genome Integrity, Martinsried, Germany
2 Institute of Biochemistry, Eidgenössische Technische Hochschule, Zürich, Switzerland
3 Department of Biochemistry and Molecular Biology, Center for Research in Molecular Medicine and Chronic Diseases, Universidade de Santiago de Compostela, Santiago de Compostela, Spain
*Corresponding author. Tel: +49 89 85783050; Fax: +49 89 85783022; E-mail: bpfander@biochem.mpg.de

we investigate the role of DDK in Mus81-Mms4 regulation and find that DDK can phosphorylate Mms4 and that DDK and Cdc5 target Mus81-Mms4 in an interdependent manner. Moreover, we show that Rtt107 promotes the association of both kinases with the Mus81-Mms4 complex. The DDK-dependent regulation of Mus81-Mms4 is critical for Mus81 activity thus revealing DDK as a novel regulator of homologous recombination.

Results

Mus81-Mms4 is a DDK phosphorylation target

The cell cycle regulation of JM resolution by Mus81-Mms4 is intricate and involves phosphorylation by the cell cycle kinases CDK and Cdc5 (Matos *et al*, 2011, 2013; Gallo-Fernández *et al*, 2012; Szakal & Branzei, 2013) as well as complex formation with the scaffold proteins Dpb11, Slx4 and Rtt107 (Gritenaite *et al*, 2014). To study this protein complex, we performed an analysis of Mms4^{3FLAG} interactors in mitosis by SILAC-based quantitative mass spectrometry (Gritenaite *et al*, 2014) and found in addition to Dpb11, Slx4, Rtt107 and Cdc5, also Cdc7 and Dbf4 as specific interactors of Mms4 (Appendix Fig S1A). We verified that Cdc7 binds to Mus81-Mms4 in an Mms4^{3FLAG} pull down from mitotic cells analysed by Western blots (Fig 1A). The fact that Mus81-Mms4 binds to DDK suggested that it might be involved in the phosphorylation cascade that occurs on Mms4 and controls Mus81 activity in mitosis. Accordingly, we found that purified DDK was able to phosphorylate both subunits of purified Mus81-Mms4 *in vitro* (Fig 1B, lane 3). When we furthermore compared the DDK-dependent

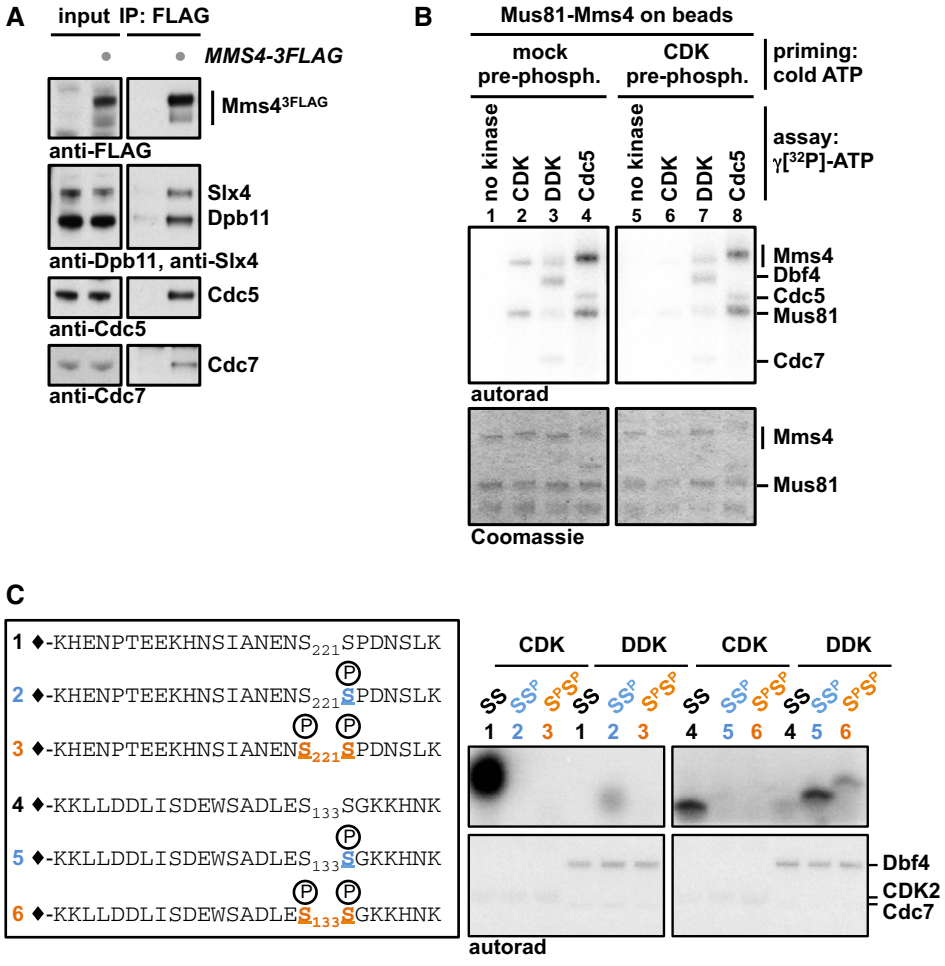

Figure 1. Dbf4-dependent kinase (DDK) binds to the Mus81-Mms4 complex in mitosis and can phosphorylate Mms4 at (S/T)(S/T) motifs.

A Cdc7 and Cdc5 are specifically enriched in Mms4^{3FLAG} co-IPs from cells arrested in mitosis (with nocodazole). Under the same conditions, Mus81-Mms4 associates with scaffold proteins such as Dpb11 and Slx4 (Appendix Fig S1A and Gritenaite *et al*, 2014).

B DDK can phosphorylate Mus81-Mms4 *in vitro*. Purified, immobilized Mus81-Mms4 is incubated in an *in vitro* kinase assay with purified CDK2/cycA^{N170} (a model CDK), DDK or Cdc5 (lanes 1–4). Additionally, Mus81-Mms4 is incubated with respective kinases after a non-radioactive priming step with CDK (lanes 5–8).

C DDK phosphorylates Mms4 peptides at (S/T)(S/T) motifs and is enhanced by priming phosphorylation. Mms4 peptides including (S/T)(S/T) motifs (221/222; 133/134) were synthesized in different phosphorylation states (depicted in left panel) and incubated in an *in vitro* kinase assay with either CDK or DDK. CDK targets unphosphorylated Mms4 peptides 1 and (to a weaker extent) 4 consistent with its substrate specificity (Mok *et al*, 2010), while DDK primarily targets Mms4 peptides 2 and 5, which harbour a priming phosphorylation at the C-terminal (S/T) site (see Appendix Fig S1B for in-gel running behaviour of peptides).

phosphorylation signal to Mms4 phosphorylation by CDK and Cdc5 (Fig 1B, lanes 2–4), we observed different degrees of phosphorylation shifts indicating that the three kinases phosphorylate Mms4 at distinct sites and/or to different degrees. DDK target sites on other proteins have been studied in detail, and in several cases, DDK was found to target (S/T)(S/T) motifs, where phosphorylation was stimulated by a priming phosphorylation usually on the second (S/T) (Masai *et al*, 2006; Montagnoli *et al*, 2006; Randell *et al*, 2010; Lyons *et al*, 2013). Intriguingly, Mms4 contains 15 of these motifs and we therefore tested whether these could be targeted by DDK and would depend on priming phosphorylation. We therefore turned to a peptide-based assay where Mms4 phosphorylation states are precisely defined. To this end, we synthesized peptides corresponding to two (S/T)(S/T) motifs of Mms4. We chose two representative motifs: S222, as it harbours a minimal CDK consensus motif (S/T)P, and S134, as it contains a non-(S/T)P consensus for CDK [(S/T)X(K/R)(K/R) (Suzuki *et al*, 2015)]. For each of these motifs, we generated peptides in three different phosphorylation states: non-phosphorylated, phosphorylated at the second serine and doubly phosphorylated (Fig 1C and Appendix Fig S1B). When using such peptides as substrates in *in vitro* kinase reactions, we saw that CDK targeted specifically only the second serine in each peptide, although much stronger for S222 than for S134, consistent with these residues matching CDK consensus motifs (Fig 1C). In contrast, DDK showed only little activity towards the non-phosphorylated peptides, but was strongly stimulated when the second residue in the (S/T)(S/T) motif was in a phosphorylated state (Fig 1C). DDK may thus be stimulated by priming phosphorylation in order to efficiently phosphorylate Mms4 on (S/T)(S/T) sites. However, using the full-length protein as a phosphorylation substrate, we did not obtain evidence for a stimulatory effect on DDK by prior CDK phosphorylation (Fig 1B and Appendix Fig S1C), perhaps because over the whole 15 (S/T)(S/T) motifs CDK phosphorylation plays a minor role. We also did not reveal any priming activity of either CDK or DDK for Mms4 phosphorylation by Cdc5 (Fig 1B and Appendix Fig S1D). Overall, the data in Fig 1 thus identify Mus81-Mms4 as an interaction partner and potential substrate of DDK.

Mus81-Mms4 is phosphorylated by a mitotic Cdc5-DDK complex

DDK is present and active throughout S phase and mitosis until anaphase when the Dbf4 subunit is degraded by APC/C^{Cdc20} (Cheng *et al*, 1999; Weinreich & Stillman, 1999; Ferreira *et al*, 2000). We therefore tested at which cell cycle stage DDK would associate with Mus81-Mms4 using cells synchronously progressing through the cell cycle. Figure 2A shows that DDK did not associate with Mus81-Mms4 in S phase, but only once cells had reached mitosis. Strikingly, DDK binding therefore coincided with binding of Cdc5, Slx4 and Dpb11 and most notably the appearance of the hyperphosphorylated form of $Mms4^{3FLAG}$ (Fig 2A).

Given this late timing of the association, we tested in co-immunoprecipitation (co-IP) experiments whether DDK binding to Mus81-Mms4 would depend on CDK or Cdc5 activity. Using analog-sensitive mutant yeast strains for CDK [*cdc28-as1* (Bishop *et al*, 2000)] and for Cdc5 [*cdc5-as1* (Snead *et al*, 2007)], we observed that inhibition of these kinases in mitotically arrested cells strongly reduced the hyperphosphorylation shift of Mms4 (see also Matos *et al*, 2013) and compromised the association with DDK (Fig 2B and C, and Appendix Fig S2A–C). Notably, both conditions also interfered with Cdc5 binding (Fig 2B and C, and Appendix Fig S2A), suggesting that the association of DDK may follow a similar regulation as Cdc5.

Next, we tested whether conversely DDK is involved in Mms4 phosphorylation. To bypass the essential function of DDK in DNA replication, we used the $mcm5^{bob1\text{-}1}$ allele (Hardy *et al*, 1997), which allowed us to test a *cdc7*Δ mutant. Using Western blot and SILAC-based mass spectrometry as a read-out of $Mms4^{3FLAG}$ co-IPs from cells arrested in mitosis, we found that Cdc5 association with Mus81-Mms4 was strongly reduced in the *cdc7*Δ mutant strain (Fig 2D and E). Moreover, we observed that $Mms4^{3FLAG}$ phosphorylation as indicated by mobility shift was decreased in the absence of DDK, although not to the same extent as upon CDK or Cdc5 inhibition (Fig 2D and Appendix Fig S2C). Additionally, as an alternative way to deregulate DDK, we used the *cdc7-1* temperature-sensitive mutant. Even with WT cells, we observed that elevated temperature (38°C) leads to a slight reduction in Cdc5 binding to Mus81-Mms4. However, in *cdc7-1* mutant cells, incubation at 38°C leads to the complete disappearance of Cdc5 binding to Mus81-Mms4 (Appendix Fig S2D). Therefore, we conclude from these data that DDK and Cdc5 bind to Mus81-Mms4 in an interdependent fashion.

Interestingly, Cdc5 was previously shown to interact with DDK via a non-consensus polo-box binding site within Dbf4 (Miller *et al*, 2009; Chen & Weinreich, 2010). The proposed model based on genetic experiments suggested that DDK binding antagonizes mitotic functions of Cdc5. However, the catalytic activity of Cdc5 was not inhibited in this complex (Miller *et al*, 2009) and we reason that DDK may simply target Cdc5 to a specific set of substrates. Since the Cdc5 binding site was mapped to the N-terminal portion of Dbf4 (Miller *et al*, 2009), we tested whether N-terminal truncations of Dbf4 would affect DDK or Cdc5 association with Mus81-Mms4. While the *dbf4-ΔN66* truncation lacking the first 66 amino acids (including a D-box motif) did not influence DDK or Cdc5 binding to $Mms4^{3FLAG}$, the *dbf4-ΔN109* truncation, which additionally lacks the Cdc5 binding motif (Miller *et al*, 2009), showed strongly decreased DDK and Cdc5 binding to Mus81-Mms4 (Fig 2F). Additionally, also mitotic hyperphosphorylation of Mms4 was diminished when DDK and Cdc5 could not interact with each other (Fig 2F). Overall, these data strongly suggest that Cdc5 and DDK interact with and target Mus81-Mms4 in an interdependent manner. Furthermore, it is currently unclear whether collaboration of DDK and Cdc5 is a widespread phenomenon that may affect other Cdc5 substrates as well, given that mitotic phosphorylation of two candidate Cdc5 substrates, Ulp2 and Scc1 (Alexandru *et al*, 2001), was affected to varying degree by the *cdc7*Δ mutation (Appendix Fig S2E).

Given the known cell cycle regulation of Cdc5 and DDK (Shirayama *et al*, 1998; Cheng *et al*, 1999; Weinreich & Stillman, 1999; Ferreira *et al*, 2000; Mortensen *et al*, 2005), the limiting factor for the temporal regulation of this complex and its restriction to mitosis is expected to be Cdc5 and not DDK, which is present already throughout S phase. Consistently, we observed that forced expression of Cdc5 (using the galactose-inducible *GAL* promoter) in cells that were arrested in S phase by hydroxyurea (HU) led to the premature occurrence of Mms4

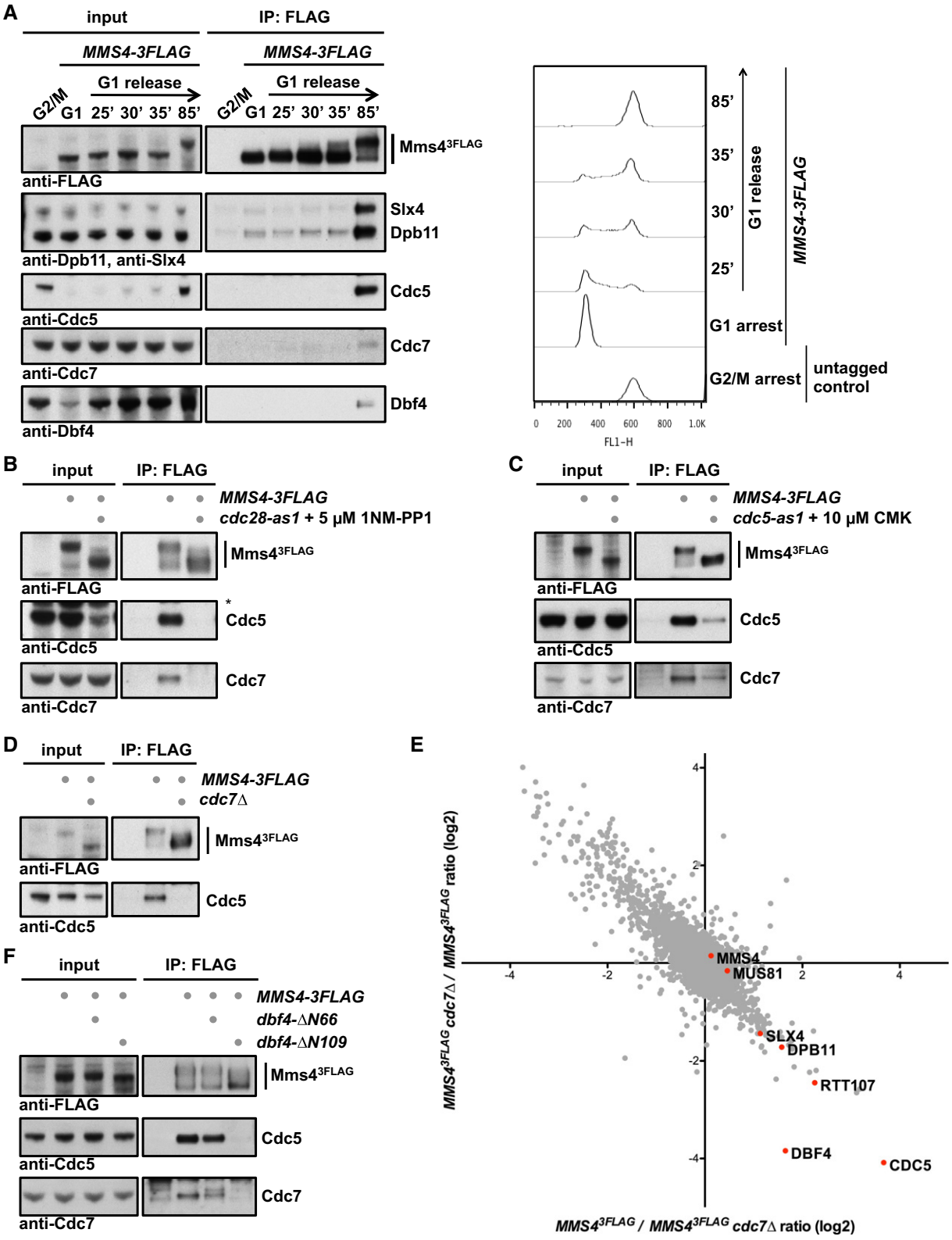

Figure 2.

hyperphosphorylation (Fig EV1A; Matos *et al*, 2013), suggesting that S-phase DDK is in principle competent for Cdc5 binding and joint substrate phosphorylation.

Furthermore, we performed additional experiments that addressed the regulation of Mus81-Mms4 by the DNA damage response. In M-phase-arrested cells, association of DDK and

Figure 2. DDK and Cdc5 target Mus81-Mms4 in an interdependent manner.

A DDK stably associates with Mus81-Mms4 in mitosis, but not in S phase or G1. Mms4^{3FLAG} pull down experiment (left panel, as in Fig 1A) from cells arrested in G1 (with alpha-factor) or in cells progressing synchronously through S phase until mitosis (arrest with nocodazole) reveals that DDK binds specifically in mitosis concomitant with the raise in Cdc5 levels and Cdc5 binding to Mus81-Mms4. A nocodazole-arrested untagged strain was used as a control. Right panel shows measurements of DNA content by FACS from the respective samples.

B CDK activity is required for DDK and Cdc5 association with Mus81-Mms4. Mms4^{3FLAG} pull down as in (A), but in mitotic WT or *cdc28-as1* mutant cells treated with 5 μM 1NM-PP1 for 1 h. Additional Western blots of this experiment are shown in Appendix Fig S5B, including as a control the identical anti-FLAG Western blot.

C Cdc5 activity is required for DDK association with Mus81-Mms4. Mms4^{3FLAG} pull down as in (A), but with mitotically arrested WT or *cdc5-as1* mutant cells treated with 10 μM CMK for 1 h.

D, E DDK is required for Cdc5 binding to Mus81-Mms4 in mitosis and the mitotic Mms4 phospho-shift. (D) Mms4^{3FLAG} pull down using mitotically arrested cells as in (A), but using a *bob1-1* background (all samples), where the DDK subunit Cdc7 could be deleted. (E) SILAC-based quantification of Mms4^{3FLAG} pull downs in mitotically arrested *bob1-1* vs. *bob1-1 cdc7*Δ cells. Plotted are the H/L ratios of two independent experiments including label switch.

F The Cdc5 binding region on Dbf4 is required for interaction of DDK and Cdc5 with Mus81-Mms4 and for efficient Mms4 phosphorylation. Mms4^{3FLAG} pull down as in (A), but using mitotically arrested cells expressing N-terminal truncation mutants of Dbf4 lacking aa2–66 (including a D-box motif) or 2–109 [additionally including the Cdc5 binding site (Miller *et al*, 2009)].

Cdc5 with Mus81-Mms4 was reduced after induction of DNA damage with phleomycin (Appendix Fig S2F), but this treatment was not sufficient to induce a significant reduction in the Mms4 phosphorylation shift. Interestingly, when we forced Cdc5 expression in S-phase cells and compared normal S-phase cells to cells treated with hydroxyurea (HU), we observed that the Mms4 phosphorylation shift was less pronounced in the presence of hydroxyurea (HU) (Fig EV1B). These data are therefore consistent with the current view that DNA damage, specifically the DNA damage checkpoint, negatively influences Mus81 resolution activity (Szakal & Branzei, 2013; Gritenaite *et al*, 2014). Since DDK is known to be targeted and inhibited by the DNA damage checkpoint (Weinreich & Stillman, 1999; Lopez-Mosqueda *et al*, 2010; Zegerman & Diffley, 2010), it could become particularly critical to regulate Mms4 phosphorylation after DNA damage.

Even though DDK and Cdc5 seem to target Mus81-Mms4 in unison, we tested whether it was possible to resolve differences on the level of individual phosphorylation sites. Therefore, we analysed Mms4 phosphorylation sites in M-phase cells after Cdc5 inhibition (Fig 3A and C) or *CDC7* deletion (Fig 3B and D) by SILAC-based mass spectrometry. We also applied two different experimental set-ups that used either endogenously expressed Mus81-Mms4 (Fig 3A and B) or overexpressed Mus81-Mms4 (Fig 3C and D), as the latter set-up allowed much better coverage of Mms4 phosphopeptides in higher order phosphorylation states (peptides harbouring > 1 phosphorylated site). Cdc5 inhibition or lack of DDK led to overlapping, but distinct changes in Mms4 phosphorylation sites, suggesting that each kinase phosphorylates specific sites on Mms4. After Cdc5 inhibition, phosphorylation of many sites was reduced and among those were sites that match to a putative Cdc5 consensus [(D/E/N)X(S/T), blue, Fig 3A and C; Mok *et al*, 2010]. Overall, *CDC7* affected Mms4 phosphorylation less than Cdc5 inhibition, but nonetheless, we found widespread changes in the phosphorylation of (S/T)(S/T) motifs (Fig 3B and D). (S/T)(S/T) motifs were found less abundantly in the doubly phosphorylated state (Fig 3D, red), while conversely these motifs were found more abundantly in the state where only the second (S/T) was singly phosphorylated (Fig 3B and D, yellow), as expected for a substrate–product relation. These data are thus consistent with phosphorylation of the second (S/T) priming for phosphorylation at the preceding (S/T) (Appendix Table S1 and Appendix Fig S3).

DDK phosphorylation is required for activation of Mus81-Mms4 during mitosis

Phosphorylation of Mms4 by CDK and Cdc5 has previously been shown to be required for the upregulation of Mus81-Mms4 activity during mitosis (Matos *et al*, 2011, 2013; Gallo-Fernández *et al*, 2012; Szakal & Branzei, 2013). Based on our finding that hyperphosphorylation of Mms4 was impaired in the absence of DDK (Fig 2D and Appendix Fig S2C), we predicted that also Mus81-Mms4 activity would be influenced. Therefore, we tested the activity of endogenous Mus81^{9myc}-Mms4^{3FLAG} immunopurified from G2/M arrested cells (approx. 5 fmol) on a nicked Holliday junction (nHJ) substrate (500 fmol) using an assay related to those in (Matos *et al*, 2011, 2013; Gritenaite *et al*, 2014). Notably, the activity of the endogenous purified Mus81-Mms4 from G2/M cells exceeded the activity of recombinant Mus81-Mms4 (subjected to a dephosphorylation step during the purification), indicating that it is the mitotically activated form (Appendix Fig S4A). Moreover, the activity of endogenous purified Mus81-Mms4 was not influenced by 350 mM NaCl salt washes. This indicates that the presence of accessory, salt-labile factors such as Rtt107 or Cdc5 in the reaction is unlikely to contribute to Mus81 activity (Appendix Fig S4B and C).

Importantly, when we used this assay to test immunopurified Mus81^{9myc}-Mms4^{3FLAG} from mitotic cells lacking DDK (*cdc7*Δ or *dbf4*Δ), we observed a reduced activity compared to Mus81^{9myc}-Mms4^{3FLAG} from WT cells (Fig 4A and Appendix Fig S4D; also observed with an RF substrate, Appendix Fig S4E). In order to exclude that indirect effects of the *CDC7* deletion may cause the reduction in Mus81 activity, we furthermore created an Mms4 mutant that specifically lacks candidate DDK phosphorylation sites. We chose to mutate (S/T)(S/T) motifs (SS motifs in particular) and created an *mms4-8A* mutant that harboured eight S to A exchanges at the N-terminal (S/T) of the motifs (see Appendix Fig S3A). This mutant appeared less phosphorylated in mitosis as judged by a less pronounced phosphorylation shift (Fig 4B). Furthermore, we observed a reduction in the association of DDK and Cdc5 with the Mus81-Mms4-8A complex in pull-down experiments (Fig 4B), suggesting that phosphorylation of Mms4 also plays a role in tethering these kinases. Notably, Mus81^{9myc}-Mms4^{3FLAG}-8A from mitotic cells showed a moderate but reproducible reduction in resolution activity on nHJ substrates compared to WT Mus81^{9myc}-Mms4^{3FLAG} (Fig 4C and Appendix Fig

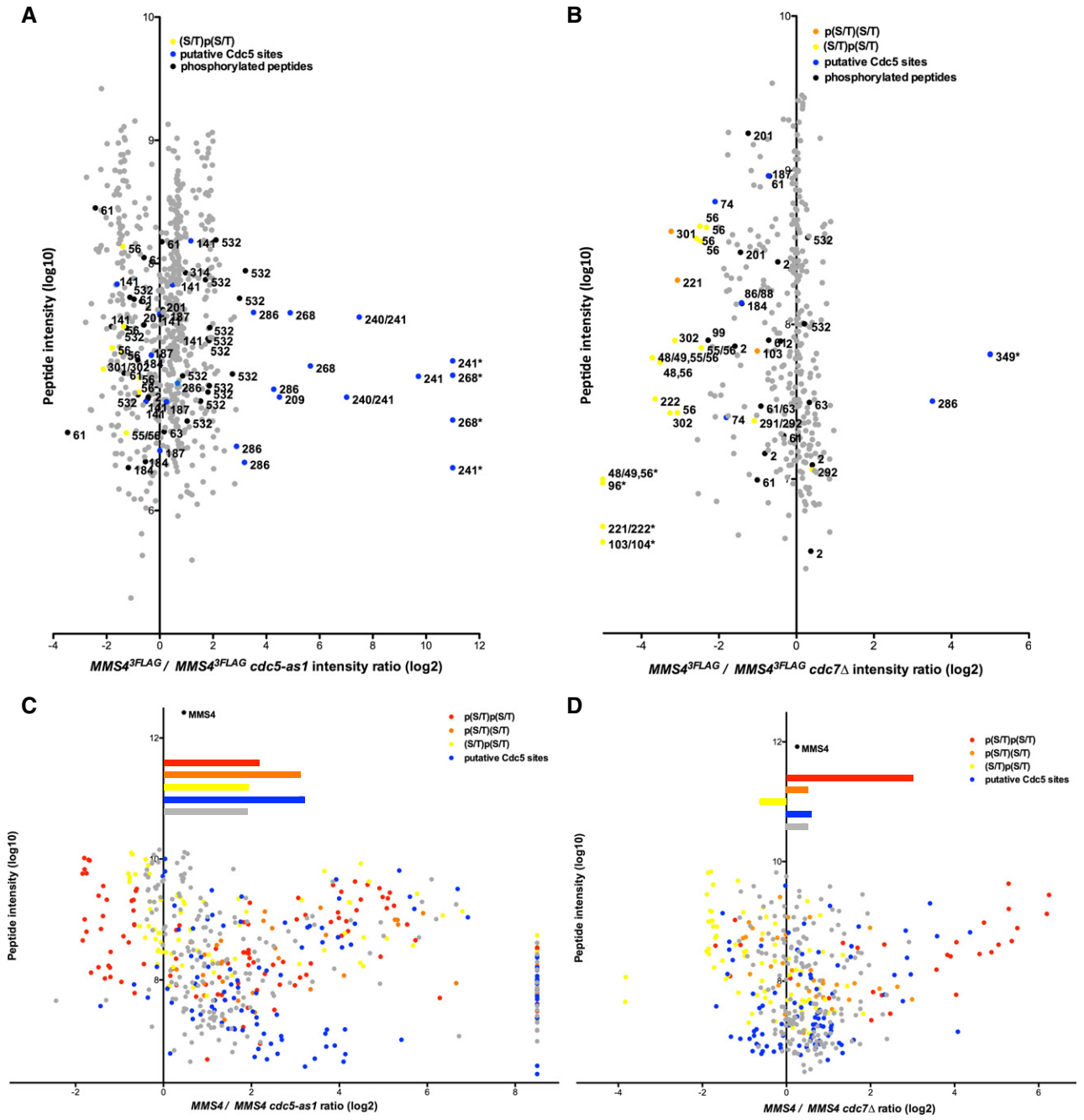

Figure 3. Analysis of Mms4 phosphorylation sites reveals Cdc5 and DDK target sites, as well as the interdependence between the two.
Changes of the abundance of phosphorylated Mms4 peptides after Cdc5 inhibition (as in Fig 2C) (A, C) or in the absence of Cdc7 (B, D) in mitotically arrested cells.

A, B Depicted are SILAC-based intensity ratios of individual MS evidences for peptides of endogenously expressed Mms4. Evidences of non-phosphorylated Mms4 peptides are shown in grey; evidences of phosphorylated peptides are shown in black, yellow, orange or blue. Blue colour indicates putative Cdc5 phosphorylation as defined by the (D/E/N)X(S/T) consensus (and additionally S268, which was also very strongly deregulated upon Cdc5 inhibition). Yellow or orange colours mark singly phosphorylated (S/T)(S/T) motifs, with orange marking p(S/T)(S/T) and yellow marking (S/T)p(S/T). Numbers indicate the phosphorylated residue in the depicted peptide. An asterisk marks peptide evidences that contained measured intensity values exclusively in the heavy or light sample. For doubly phosphorylated peptides, the two phospho-sites are separated by a comma. For singly phosphorylated (S/T)(S/T) motifs, peptide ion fragmentation was in some cases unable to unambiguously identify the phosphorylated residue. In these cases, possible phosphorylation sites are indicated as "a/b". Note that doubly phosphorylated (S/T)(S/T) sites were not reproducibly identified under conditions of endogenous Mus81-Mms4 expression.

C, D As in panels (A, B) but using Mus81-Mms4 expressed from a high-copy promoter. Depicted are SILAC-based H/L ratios of individual MS evidences for phosphorylated peptides only. Peptides were sorted into categories according to their phosphorylation status: putative DDK target sites ((S/T)(S/T) motifs) were differentiated into the categories p(S/T)p(S/T) (red), p(S/T)(S/T) (orange) or (S/T)p(S/T) (yellow). Phosphorylated peptides matching the Cdc5 consensus site are coloured in blue. All other phosphorylated peptides are marked in grey. Bars depict the mean of the ratios of the respective category. Overall, Mms4 H/L ratio is shown on top.

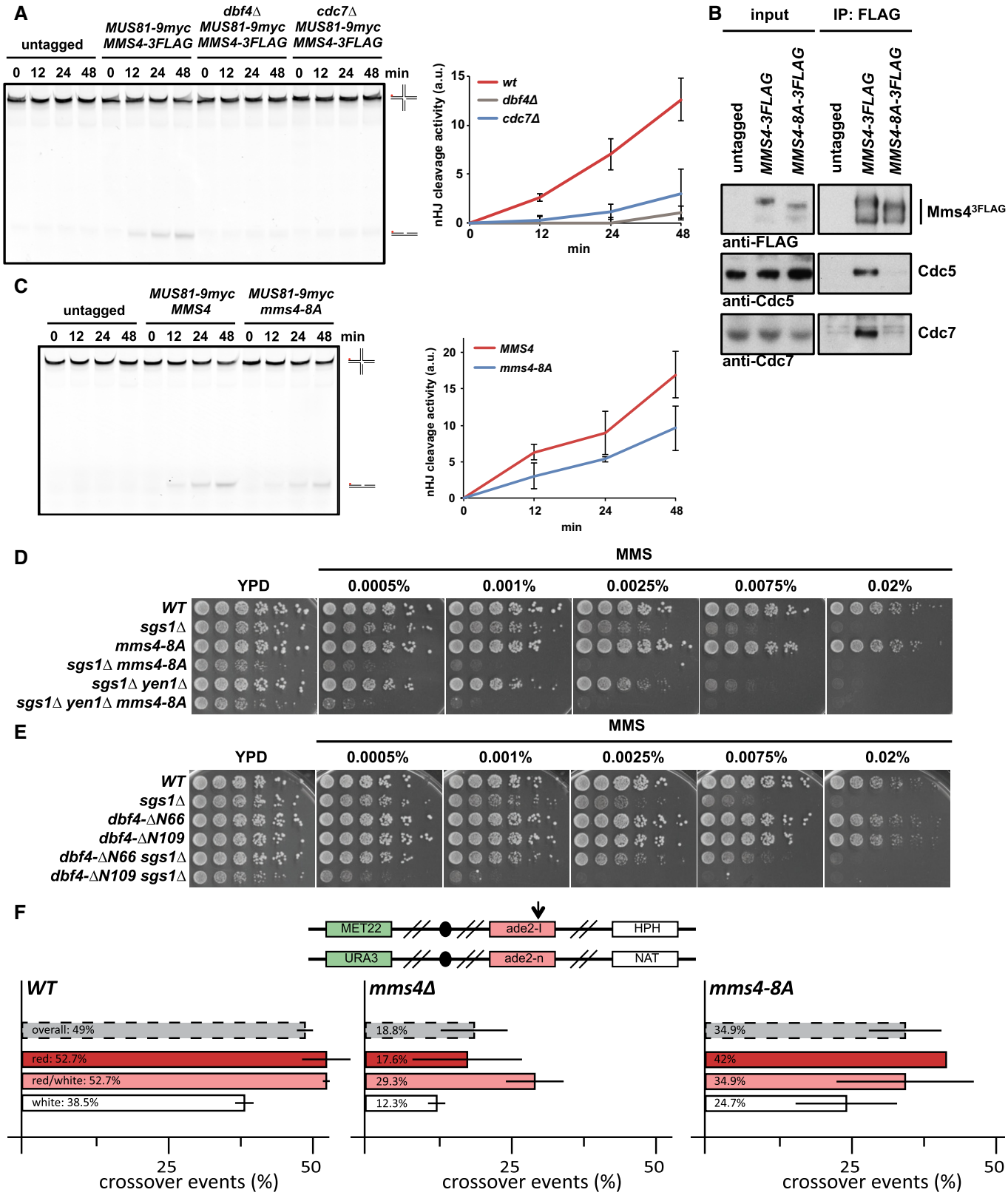

Figure 4.

S4F). These data thus indicate that DDK targets Mus81-Mms4 and that (S/T)(S/T) phosphorylation events are essential for full activation of Mus81 in mitosis.

Additionally, we investigated the relevance of the *mms4-8A* mutation *in vivo*. In comparison with *mus81*Δ or *mms4*Δ mutants, the *mms4-8A* mutant showed a hypomorphic phenotype. For

Figure 4. DDK phosphorylation controls activation of Mus81-Mms4 resolvase activity in mitosis.

A DDK is required for mitotic activation of Mus81-Mms4. Resolution assay using a nicked Holliday junction (nHJ) substrate and Mus81^{9myc}-Mms4^{3FLAG} purified from mitotically arrested *bob1-1* (DDK-WT^{+}), *bob1-1 dbf4*Δ and *bob1-1 cdc7*Δ strains or untagged control cells. Right panel: quantification of cleavage products. See Appendix Fig S4D for Western blots samples of anti-myc IPs. Left panel: representative gel image.

B A defect in the phosphorylation of Mms4 (S/T)(S/T) sites causes reduced association of Cdc5 and DDK with Mus81-Mms4 and reduced phosphorylation of Mms4. Mms4^{3FLAG} pull down as in Fig 1A, but using mitotically arrested WT and *mms4-8A* mutant cells, which harbour 8 serine to alanine exchanges at (S/T)(S/T) motifs (detailed in Appendix Fig S3).

C Reduced (S/T)(S/T) phosphorylation of Mms4 generates a defect in Mus81-Mms4 activity. Resolution assay as in (A), but comparing mitotic Mus81-Mms4 from untagged, WT and *mms4-8A* strains (see Appendix Fig S4F for Western blot samples of anti-myc IPs).

D, E The *mms4-8A* mutation and lack of the Cdc5-DDK interaction (*dbf4-ΔN109*) lead to hypersensitivity towards MMS specifically in the *sgs1*Δ background. Shown is the growth of indicated strains in fivefold serial dilution on plates containing MMS at indicated concentrations after 2 days at 30°C.

F The *mms4-8A* mutant leads to a reduction in crossover formation. Recombination assay between heterologous *ade2* alleles in diploid cells as described in Ho *et al* (2010). The top panel indicates markers on both copies of chromosome XV that are used to determine genetic outcomes of DSB repair. Arrow indicates the I-SceI cut site. Bottom panel indicates rates of crossover events (%) overall (grey) and in the individual classes (red, red/white, white) that differ in gene conversion tract length. Error bars indicate standard deviation of two independent experiments, each scoring 400–600 colonies per strain.

Data information: (A, C) Depicted are means from three independent experiments, error bars correspond to standard deviation.

example, it did neither significantly increase the MMS hypersensitivity of a *yen1*Δ mutant, nor did it confer synthetic lethality with mutants defective in STR function, such as *sgs1*Δ, even though the *mms4-8A sgs1*Δ double mutant displayed a slow growth phenotype (Figs 4D and EV2A). Importantly, however, we did observe a strongly increased hypersensitivity towards MMS, when we tested an *mms4-8A sgs1*Δ double mutant and compared it to an *sgs1*Δ single mutant (Fig 4D). The *mms4-8A* mutation thus leads to a phenotype that is very similar to other activation-deficient *MMS4* mutants in budding and fission yeast (Gallo-Fernández *et al*, 2012; Dehé *et al*, 2013; Matos *et al*, 2013). Remarkably, the MMS hypersensitivity phenotype of the *mms4-8A* mutant was highly similar to that of the Cdc5 binding-deficient *dbf4-ΔN109* mutant (Figs 4E and EV2B), which also showed reduced survival when combined with *sgs1*Δ (Fig 4E). These data are therefore consistent with DDK functioning to stimulate JM resolution via Mms4 hyperphosphorylation.

It is likely that the *mms4-8A* mutant is only partially deficient in DDK phosphorylation, since Mms4 contains overall 15 (S/T)(S/T) sites and DDK may phosphorylate the protein on non-(S/T)(S/T) sites as well. We therefore note that an *mms4-12A* mutant, harbouring four additional S to A exchanges on (S/T)(S/T) motifs, showed further increased MMS sensitivity in the *mms4-12A sgs1*Δ mutant, when compared to the *mms4-8A sgs1*Δ mutant, even though there were only minor additional effects on either the Mms4 mitotic phosphorylation shift or JM resolution activity (Fig EV2C–E).

In order to directly assess whether DDK phosphorylation was required for Mus81 function during JM resolution, we tested the influence of the *mms4-8A* mutant in a genetic crossover assay (Ho *et al*, 2010). In this system, a site-specific DSB is induced in diploid cells and repair products can be measured by the arrangement of markers and colony sectoring (Fig 4F, upper panel). In this assay, *mus81*Δ and *mms4*Δ mutants show a reduction in CO products and a proportional increase in NCO products (Fig 4F; Ho *et al*, 2010), as would be expected from a defect in JM resolution and the accompanying shift of repair pathways towards JM dissolution. The *mms4-8A* mutant shows a similar, albeit weaker defect in the formation of CO products (Fig 4F), suggesting that the defect in Mus81 activation in mitosis results in an overall defect in JM resolution. We therefore conclude that DDK—in conjunction with Cdc5—acts directly on Mms4 and that these phosphorylation events are required for efficient Mus81-dependent JM resolution in mitosis.

The Dpb11-Mms4 interaction is not required for DDK-Cdc5-dependent activation of Mus81-Mms4

It is noteworthy that the association of DDK and Cdc5 with Mus81-Mms4 coincides with the formation of the Mus81-Mms4 complex with scaffold proteins such as Slx4, Dpb11 and Rtt107, which come together in mitosis (Fig 2A). Therefore, we asked whether the scaffold proteins Dpb11, Slx4 or Rtt107 would be required to target DDK and Cdc5 to Mus81-Mms4. In order to investigate the influence of Dpb11, we searched for an *MMS4* mutant that was deficient in the interaction with Dpb11. When we used a two-hybrid approach to map the Dpb11 interaction site on Mms4, we found that Mms4 constructs comprising aa 1–212 or 101–230 interacted with Dpb11, while constructs comprising aa 1–195 or 176–230 showed no or reduced interaction (Appendix Fig S5A). This suggested that the Dpb11 binding site may be located between aa 101–212 of Mms4. Consistently, we observed that the Mms4-S201A mutation abolished binding to Dpb11 in yeast two-hybrid and co-IP (Fig 5A and B), while the Mms4-S184A mutation reduced it (Fig 5A). Serine 201 and 184 are therefore likely candidates for phospho-sites bound and read by Dpb11. Serine 201 matches the full CDK consensus motif (S/T)PxK, while serine 184 matches the minimal CDK consensus motif (S/T)P. Indeed, we find that CDK inhibition reduced the Dpb11 interaction with Mus81-Mms4 (Appendix Fig S5B) consistent with a requirement of CDK phosphorylation for a robust interaction between Dpb11 and Mms4.

When we investigated the phenotype of the *mms4-SS184,201AA* mutant, we found that it showed enhanced hypersensitivity to MMS specifically in the *sgs1*Δ mutant background, consistent with a role of Dpb11 in JM resolution after MMS damage (Fig 5C). We also noted that the phenotype of this *MMS4* variant differed from that induced by Dpb11 binding-deficient version of Slx4 [*slx4-S486A* (Gritenaite *et al*, 2014; Ohouo *et al*, 2012)]. This could suggest that these mutants are able to separate different Dpb11 functions such as a mitotic function in conjunction with Mus81-Mms4 and an S-phase function, which Slx4 and Dpb11 might have independently of Mus81-Mms4 (Ohouo *et al*, 2012; Gritenaite *et al*, 2014; Cussiol *et al*, 2015; Princz *et al*, 2015). However, it also needs to be considered that Slx4 and Mus81-Mms4 may be connected by more than one scaffold protein (see below).

Importantly, however, we did not observe a defect in the association of DDK or Cdc5 with Mus81-Mms4, when we performed

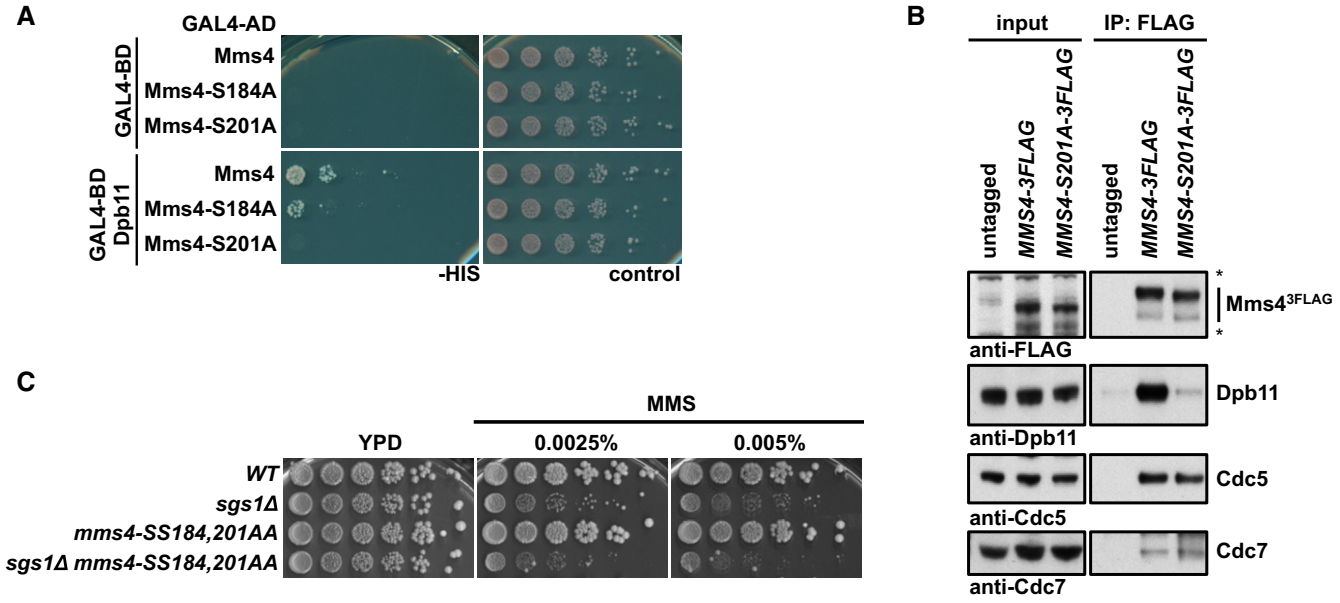

Figure 5. The interaction between Mms4 and Dpb11 is dispensable for binding of Cdc5 and DDK and mitotic Mus81-Mms4 activation.

A, B Serine 201 of Mms4 is required for Dpb11 binding, but not for interaction with DDK and Cdc5. (A) Two-hybrid interaction analysis using Gal4-BD-Dpb11 with Gal4-AD-Mms4, Gal4-AD-Mms4-S184A and Gal4-AD-Mms4-S201A constructs. (B) Mms4^{3FLAG} pull downs from mitotically arrested cells as in Fig 1A, but using WT or *S201A* variants of Mms4^{3FLAG}. Asterisks mark cross-reactive bands.

C The Dpb11 binding-deficient allele *mms4-SS184,201AA* leads to a MMS hypersensitivity specifically in the *sgs1*Δ background. Spotting assay as in Fig 4D.

Mms4-S201A^{3FLAG} pull downs and compared them to a WT Mms4^{3FLAG} pull down (Fig 5B). Furthermore, we only observed a very minor defect in the *in vitro* resolution of nHJ substrates, when we purified Mus81-Mms4 from mitotically arrested *mms4-S201A* cells (Appendix Fig S5C). We therefore reason that Dpb11 is most likely not involved in promoting Mms4 phosphorylation or DDK-Cdc5-dependent activation of Mus81-Mms4.

The Rtt107 scaffold recruits DDK and Cdc5 to Mus81-Mms4

Having excluded a role of Dpb11 in the recruitment of DDK and Cdc5, we next tested a possible involvement of the Rtt107 scaffold protein. Indeed, when we used an *rtt107*Δ mutant in IP and SILAC-based IP-MS experiments, we observed that DDK and Cdc5 binding to Mus81-Mms4 was strongly reduced (Fig 6A and Appendix Fig S6A). Interestingly, Rtt107 bound to DDK and Cdc5 even under conditions where Rtt107 binding to Mus81-Mms4 was abolished (*mus81*Δ, Appendix Fig S6B). This suggests that Rtt107 may form a subcomplex with DDK and Cdc5. Consistently, we found that Rtt107 bound to Cdc7 in a two-hybrid assay (Fig 6B). These data therefore suggest that Rtt107 mediates binding of DDK and Cdc5 to the Mus81-Mms4 complex, most likely via a Cdc7 interaction site on Rtt107.

During our co-IP studies, we furthermore found that the location of Rtt107 in the mitotic Mus81-Mms4 complex was different than expected. Given that Slx4 was required to bridge between Rtt107 and Dpb11 (Ohouo *et al*, 2010) and that Mms4 and Dpb11 seemingly interact directly (Gritenaite *et al*, 2014 and Fig 5A and B), we initially expected that Slx4 and Dpb11 would be required to mediate the interaction between Rtt107 and Mus81-Mms4. Surprisingly, we found that an *slx4*Δ mutant did not influence DDK or Cdc5 binding to Mus81-Mms4 and thereby differed from *rtt107*Δ (Fig 6A). Therefore, we tested if Rtt107 could bind to Mus81-Mms4 independently of Slx4 or Dpb11. Indeed, we found that the Mus81-Mms4 interaction to Rtt107 was not influenced by the *slx4*Δ mutant (Fig 6C) or the Dpb11 binding-deficient *mms4-S201A* allele (Fig 6D), indicating that Rtt107 binding to the Mus81-Mms4 complex occurs independently of the other scaffold proteins. In contrast, our data also show that its binding is strongly dependent on kinases and Mms4 phosphorylation, since Rtt107 binding was strongly reduced in the absence of DDK (Fig 2E), after Cdc5 inhibition (Appendix Fig S2A) or in the *mms4-8A* phosphorylation site mutant (Fig EV3).

Therefore, these data provide novel insight into the role of Rtt107 in Mus81-Mms4 regulation. First, it shows that Rtt107 mediates the association of DDK and Cdc5 kinases with Mus81-Mms4. Second, it also suggests that Rtt107 may bind directly to Mus81-Mms4 and that this binding is dependent on Mms4 phosphorylation and the cell cycle kinases DDK and Cdc5, although an alternative model whereby Rtt107 indirectly promotes DDK and Cdc5 to tightly associate with Mus81-Mms4 cannot be ruled out entirely. The fact that Rtt107 promotes the interaction of Mus81-Mms4 with the kinases, yet in turn requires the kinases and Mms4 phosphorylation for interaction, suggests that Rtt107 may be acting after initial Mms4 phosphorylation has occurred and at this late stage tethers the kinases, thus promoting phosphorylation of otherwise inefficiently phosphorylated sites.

Rtt107 stimulates Mms4 hyperphosphorylation in order to enhance Mus81-Mms4 activity in mitosis

Given Rtt107's involvement in tethering DDK and Cdc5 to the Mus81-Mms4 complex, we asked whether Rtt107 would mediate

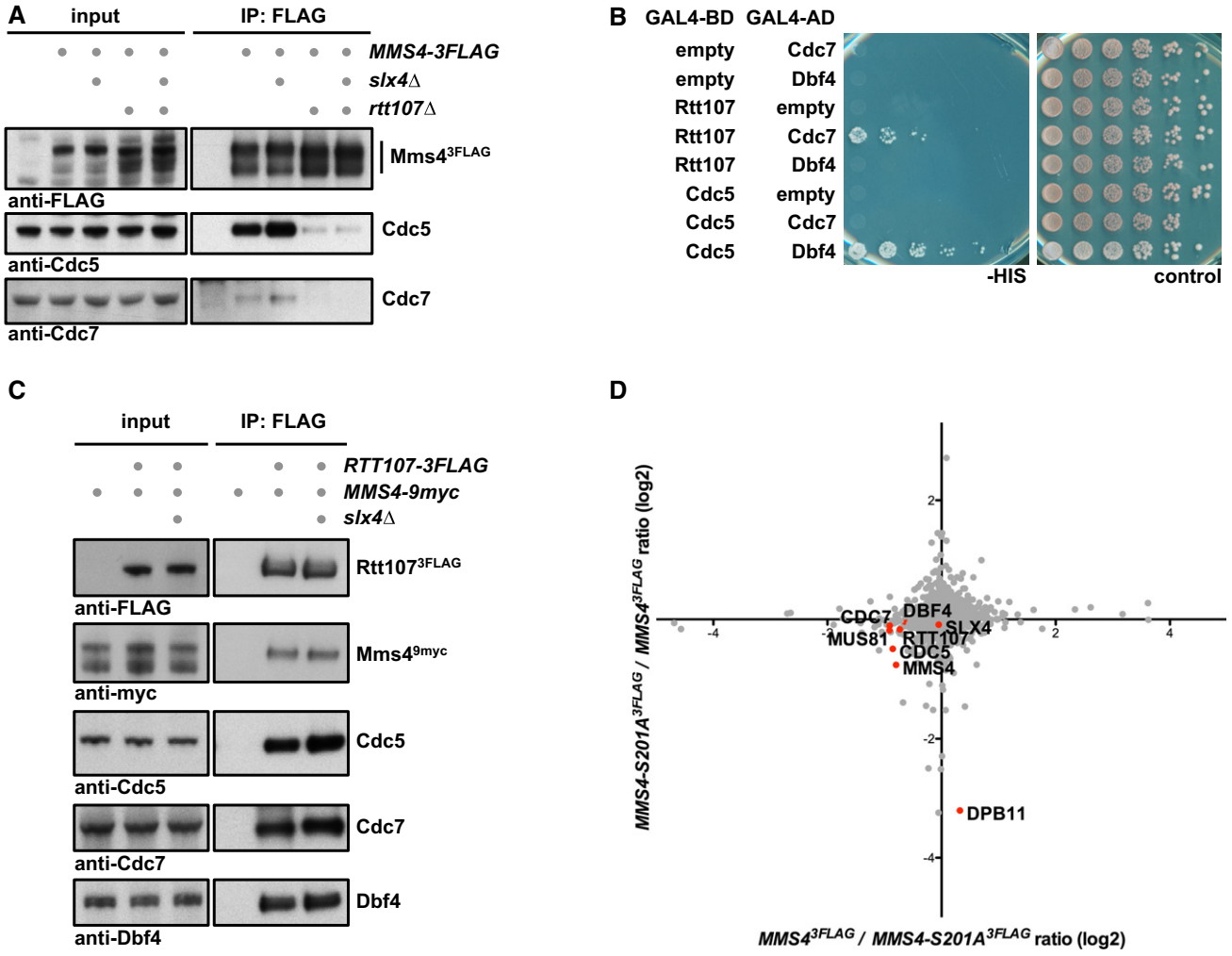

Figure 6. The Rtt107 scaffold tethers DDK and Cdc5 to Mus81-Mms4 independently of Slx4 and Dpb11.

A Rtt107, but not Slx4, is required for DDK and Cdc5 interaction with Mus81-Mms4. Mms4^{3FLAG} pull downs from mitotically arrested cells as in Fig 1A, but specifically comparing interactions of Mus81-Mms4 in WT, *slx4Δ*, *rtt107Δ* and *slx4Δ rtt107Δ* mutant backgrounds.

B Rtt107 interacts with Cdc7. Two-hybrid interaction was tested using Gal4-BD-Rtt107 constructs and Gal4-AD-Cdc7 or Gal4-AD-Dbf4 constructs. Interaction between Gal4-BD-Cdc5 and Gal4-AD-Dbf4 serves as positive control.

C Rtt107 interacts with Mus81-Mms4, DDK and Cdc5 independently of Slx4. Rtt107^{3FLAG} co-IPs from untagged control, WT or *slx4Δ* cells arrested in mitosis were probed for indicated proteins.

D Rtt107 interacts with Mus81-Mms4 independently of the Mms4-Dpb11 interaction. SILAC-based Mms4^{3FLAG} pull down in WT and *mms4-S201A* cells reveals changes in the Dpb11 association, but not in Rtt107, Slx4, Cdc5 or DDK binding. Plotted are the H/L ratios of two experiments including label switch.

mitotic hyperphosphorylation of Mms4 and concomitant activation of the Mus81 nuclease. We observed only a minor effect on the mitotic phospho-shift of Mms4 when using *rtt107Δ* mutants (Fig 6A and Appendix Fig S2C). However, as it is still unclear which phosphorylation sites contribute to the Mms4 phospho-shift, we investigated the effect of *rtt107Δ* on individual phosphorylation sites in our mass spectrometry data. Appendix Fig S7A and B shows SILAC-based comparisons of Mms4 phosphorylation sites in WT and *rtt107Δ* cells, expressing Mus81-Mms4 from endogenous (Appendix Fig S7A) or high-copy promoters (Appendix Fig S7B). The overexpression set-up allowed us to quantify phosphorylation at (S/T)(S/T) motifs, and we found that double phosphorylation of several of these sites was reduced (Appendix Fig S7B), although the change was much smaller compared to cells lacking DDK. On the other hand, while we could not detect higher order phosphorylated Mms4 peptides using endogenous Mus81-Mms4, we could detect an effect of Rtt107 on several other sites (T209, S241 and S268, and to a lesser extent S286; Appendix Fig S7A), which were also deregulated after Cdc5 inhibition (Fig 3A and C). These data are thus consistent with Rtt107 promoting efficient DDK and Cdc5 phosphorylation of Mms4.

Therefore, we tested whether Rtt107 would affect the mitotic activation of Mus81-Mms4. We immunopurified Mus81^{9myc}-Mms4^{3FLAG} from WT and *rtt107Δ* cells that were arrested in mitosis and found that Mus81-Mms4 activity on a nHJ substrate was reduced in the *rtt107Δ* background (Fig 7A and Appendix Fig S7C). Furthermore, in the background of deficient DDK (*cdc7Δ bob1-1*), additional mutation of *rtt107Δ* did not lead to a further defect in

Mus81-mediated cleavage (Appendix Fig S7D). Therefore, we conclude that Rtt107 is required for full mitotic activation of Mus81-Mms4 and that it works at least in part through cell cycle kinases such as DDK.

In order to test whether such a defect in Mus81-Mms4 activation would translate into a shifted balance of JM removal pathways, we measured rates of crossover and non-crossover formation in the absence of Rtt107. We observed a reduction in crossover rates in the *rtt107*Δ mutant indicating a shift in the balance of JM removal pathways (Fig 7B). The decrease was mostly visible in one class of recombinants (Fig 7B, "red") and is smaller compared to the phenotype of a *mus81*Δ or a *mms4-8A* mutant (Ho *et al*, 2010; Fig 4F), consistent with a stimulatory but non-essential role of the Rtt107 scaffold in Mus81-Mms4 function. These data thus provide the first mechanistic insight of how the interaction of the mitotic Mus81-Mms4 complex with the scaffold proteins influences Mus81 function, as Rtt107 facilitates DDK and Cdc5 tethering, full mitotic phosphorylation of Mms4 and activation of Mus81-Mms4.

Discussion

Activation of Mus81-Mms4 during mitosis is critical for the response to DNA damage, in particular to process repair intermediates that may arise from DSBs and stalled replication forks (Matos *et al*, 2011, 2013; Gallo-Fernández *et al*, 2012; Saugar *et al*, 2013; Szakal

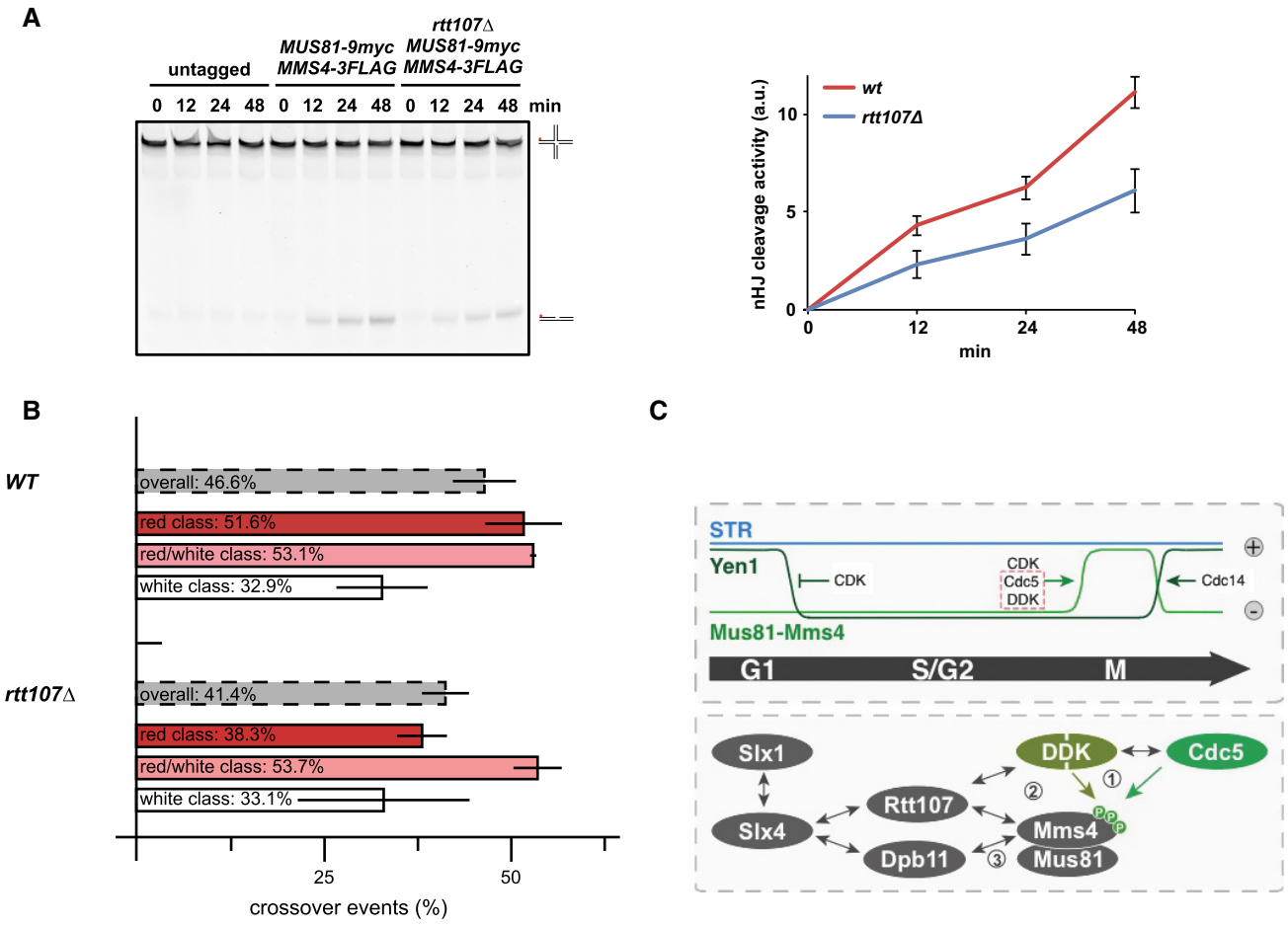

Figure 7. Rtt107 is required for efficient Mus81-Mms4 activation in mitosis.

A Mus81-Mms4 purified from mitotic *rtt107*Δ cells is less active compared to Mus81-Mms4 from WT cells. *In vitro* resolution activity of Mus81^{9myc}-Mms4^{3FLAG} purified from WT or *rtt107*Δ cells is tested on a nHJ substrate (see Appendix Fig S7C for control Western blot). Right panel: quantification of cleavage products from three independent experiments (mean ± SD). Left panel: representative gel picture.

B The *rtt107*Δ mutant leads to a reduction in crossover formation. Recombination assay as in Fig 4F. Note that the *rtt107*Δ mutant particularly affects crossover formation in the red class (long conversion tracts), while no significant defect could be observed in the red/white and white class (mean ± SD).

C Hypothetical model of Mus81-based JM resolution. Upper panel: cell cycle regulation of JM removal pathways, indicating Mus81 activation in mitosis. Lower panel: physical interactions of Mus81-Mms4 and its regulatory complex in mitotic cells. Grey arrows indicate physical interactions; green arrows specifically indicate kinase–substrate interactions. Genetic data indicate a hierarchy of molecular events leading to Mus81 activation. (1) DDK, Cdc5 and CDK (not shown) phosphorylate Mms4. (2) Rtt107 binds to DDK and Cdc5 and—in a phosphorylation-dependent manner—associates with Mus81-Mms4. This interaction is either direct or could potentially depend on bridging effects by DDK and Cdc5. Rtt107 promotes the stable interaction of DDK and Cdc5 with Mus81-Mms4 and thus full phosphorylation of Mms4 and Mus81 activation. (3) Upon Mms4 phosphorylation, two scaffold proteins, Rtt107 and Dpb11, bind independently to Mus81-Mms4. Both proteins can also bind to Slx4 enabling two alternative connections of Slx4 with Mus81-Mms4.

& Branzei, 2013). Previously, this regulation was shown to critically depend on phosphorylation by the cell cycle kinases CDK and Cdc5 (Matos *et al*, 2011, 2013; Gallo-Fernández *et al*, 2012; Saugar *et al*, 2013; Szakal & Branzei, 2013), but also involve the formation of a multi-protein complex comprising several scaffold proteins (Gritenaite *et al*, 2014). Here, we not only identify a new cell cycle kinase to be crucial for this regulation—DDK—but moreover show that the two regulatory pathways—cell cycle kinase phosphorylation and scaffold complex formation—are connected by Rtt107 (see Fig 7C for a hypothetical model). Rtt107 association depends on active cell cycle kinases and Mms4 phosphorylation, but in turn Rtt107 is required for stable DDK and Cdc5 association with the Mus81-Mms4 complex, as well as full phosphorylation of Mms4 and mitotic activation of Mus81. This study thus extends our mechanistic understanding of the regulatory framework that controls cell cycle-regulated JM resolution.

Interestingly, our work shows that for its function as a regulator of Mus81-Mms4 DDK must act interdependently and as a complex with Cdc5. DDK and Cdc5 have been shown to interact physically (Miller *et al*, 2009; Chen & Weinreich, 2010), but until now DDK was viewed to antagonize mitotic functions of Cdc5 (Miller *et al*, 2009). In contrast, in meiosis I DDK and Cdc5 are known to cooperate in order to promote chromosome segregation and jointly phosphorylate the monopolin and cohesin subunits Lrs4 and Rec8, respectively, as well as the meiotic regulator Spo13 (Matos *et al*, 2008). We now provide the first example for a joint DDK and Cdc5 substrate in the mitotic cell cycle, suggesting that cooperation between DDK and Cdc5 could be a more widespread phenomenon than previously anticipated. The apparent antagonism between DDK and Cdc5 in the regulation of mitotic exit (Miller *et al*, 2009), a canonical Cdc5 function, could be explained if DDK targeted Cdc5 to a specialized subset of substrates rather than to substrates involved in mitotic exit. It is also interesting to note that we could detect significant DDK binding to Mus81-Mms4 only after cells finished S phase (Fig 2A). Therefore, the role of DDK in Mms4 phosphorylation is clearly post-replicative and further challenges a simplified view of DDK as an S-phase kinase (Matos *et al*, 2008). It will therefore be interesting to see whether additional DDK substrates during mitosis can be identified and whether DDK collaborates with Cdc5 for their phosphorylation as well.

Mus81-Mms4 has previously been shown to be cell cycle-regulated and Mms4 to be a critical CDK and Cdc5 phosphorylation target (Matos *et al*, 2011; Gallo-Fernández *et al*, 2012). We add DDK to this already complex regulation. Our data clearly show that phosphorylation of (S/T)(S/T) motifs is critical for Mus81-Mms4 function. The hypomorphic phenotype of the *mms4-8A* mutant (Fig 4C, D and F) is likely due to additional DDK phosphorylation sites either on Mms4 or perhaps even on Mus81. Importantly, DDK does not appear to establish the timing of Mms4 phosphorylation in mitosis, as Cdc5 still seems to be the limiting factor for this temporal control in undisturbed cell cycles (Fig EV1B). However, the fact that activation of Mus81-Mms4 depends on the activity of several kinases makes it a coincidence detector that integrates the activity of several cell cycle regulators. Therefore, it can be envisioned that there are specific cellular conditions under which DDK activity becomes limiting for Mus81-Mms4 activation. Notably, DNA damage checkpoint kinases are known to phosphorylate DDK and counteract its function during S phase (Weinreich & Stillman, 1999; Lopez-Mosqueda *et al*, 2010; Zegerman & Diffley, 2010). Therefore, it can be speculated that the checkpoint acts as a negative regulator of Mus81-Mms4 activation via inhibition of DDK. Such regulation could therefore explain how the presence of DNA damage restricts Mus81 activity towards replication intermediates (Matos *et al*, 2011, 2013; Saugar *et al*, 2013; Szakal & Branzei, 2013; Gritenaite *et al*, 2014), suggesting that cell cycle and checkpoint pathways converge in the regulation of Mus81.

A second layer of Mus81 regulation relies on the formation of a multi-protein complex, which assembles specifically in mitosis and contains Mus81-Mms4, DDK, Cdc5 and Slx4 as well as the scaffold proteins Dpb11 and Rtt107 (Gritenaite *et al*, 2014). We are only beginning to understand the mechanism whereby this scaffold complex influences Mus81 function. Here, we show that Rtt107, but not Dpb11 or Slx4, promotes the stable association of DDK and Cdc5 with Mus81-Mms4 (Fig 6), suggesting that one function of the multi-protein complex is to promote efficient Mus81-Mms4 phosphorylation. Conversely, our new data as well as our previous work (Gritenaite *et al*, 2014) show that phosphorylation by cell cycle kinases also regulates the formation of the multi-protein complex. In particular, Rtt107 association with Mus81-Mms4 depends strongly on DDK and Cdc5 (Fig 2E and Appendix Fig S2A). A direct interaction of Rtt107 with Mus81-Mms4 seems the most plausible interpretation of our data, although we currently cannot exclude that Rtt107 may facilitate the interaction of DDK and Cdc5 with Mus81-Mms4 without a direct interaction. A possible phosphorylation dependence of Rtt107 binding to the complex could thus originate from Mms4 phosphorylation generating a binding site for Rtt107 [e.g. for Rtt107 BRCT domains (Li *et al*, 2012)].

Importantly, Rtt107 is in turn required for stable binding of DDK and Cdc5 (Fig 6A and Appendix Fig S6A). Via tethering the kinases, Rtt107 regulates the phosphorylation of specific Mms4 sites and is required for full Mus81 activation (Fig 7A and Appendix Fig S7A and B). The interdependence between Rtt107 and Cdc5/DDK phosphorylation therefore suggests that Rtt107 may be part of a signal amplification mechanism, which ensures efficient Mus81-Mms4 phosphorylation and activation. Mechanistically, Rtt107-dependent stimulation of Mms4 phosphorylation thus resembles a kinase priming mechanism. It is entirely possible that other kinase priming mechanisms for either Cdc5 or DDK are at work in the Mms4 phosphorylation cascade, although the *in vitro* kinase assays with full-length proteins did not provide support for such a mechanism (Fig 1B, and Appendix Fig S1C and D). Altogether, it seems plausible to speculate that Rtt107-dependent and Rtt107-independent amplification mechanisms are involved in generating a switch-like activation of Mus81 in mitosis.

Furthermore, Rtt107 can also bind to Slx4 (Ohouo *et al*, 2010). There are thus two BRCT-containing scaffold proteins—Dpb11 (Gritenaite *et al*, 2014) and Rtt107—that could bridge between Mus81-Mms4 and Slx4. Interestingly, our data with different *mms4* mutants suggest that either one of these BRCT scaffold proteins is sufficient to connect Slx4 and Mus81-Mms4 [Figs 6D and EV3; note that the *rtt107*Δ mutant (Appendix Fig S6A) is difficult to interpret in this regard as it also leads to defects in Slx4 phosphorylation and the Slx4-Dpb11 interaction (Ohouo *et al*, 2010)]. This redundancy may thus explain the modest phenotype of the *mms4-S201A* mutant that is deficient in the Mms4-Dpb11 interaction (Fig 5C).

Several aspects of Mus81-Mms4 regulation are conserved throughout eukaryotic evolution. The HJ resolution activity of

Mus81-Eme1 in mammalian cells is cell cycle-regulated (Matos *et al*, 2011; Wyatt *et al*, 2013). Mus81-Eme1 furthermore binds to Slx4 and forms multi-protein complexes (Fekairi *et al*, 2009; Muñoz *et al*, 2009; Svendsen *et al*, 2009; Castor *et al*, 2013; Wyatt *et al*, 2013), albeit these complexes may have a different organization to that in yeast. Therefore, it will be interesting to explore in the future if in human cells DDK is also required for activation of Mus81-Eme1 and if this mechanism may contribute to the anti-tumorigenic activity of DDK inhibitors (Montagnoli *et al*, 2008).

Materials and Methods

All yeast strains are based on W303 and were constructed using standard methods. Plasmids were constructed using the In-Fusion HD cloning kit (Clontech Laboratories), and mutations were introduced by site-directed mutagenesis. A summary of all yeast strains used in this study can be found in the Appendix Table S2.

Cell cycle synchronization was achieved using alpha-factor (G1), hydroxyurea (S), or nocodazole (mitosis). DNA content was measured by flow cytometry with a BD FACSCalibur system using SYTOX green to stain DNA.

Co-immunoprecipitations of yeast extracts were performed on anti-FLAG agarose resin (Sigma) for 2 h with head-over-tail rotation at 4°C as previously described (Gritenaite *et al*, 2014). After bead washing, proteins were eluted by 3X FLAG-peptide (Sigma), precipitated and separated on 4–12% Bis-Tris gels. For SILAC-based mass spectrometry, cells were labelled with heavy-isotope-labelled lysine (Lys6 or Lys8), and proteins were digested with Lys-C. Mass spectrometry data were analysed using MaxQuant (Cox & Mann, 2008).

Yeast two-hybrid assays, genetic interaction assays, *in vitro* kinase assays and peptide binding assays were performed as described previously (Pfander & Diffley, 2011; Gritenaite *et al*, 2014).

Nuclease assays were done as described (Matos *et al*, 2011, 2013). Briefly, Mus81^{9myc} was immunopurified from mitotically arrested cells and mixed with 5′-Cy3-end-labelled nicked Holliday junctions. After incubation at 30°C for the indicated times, the reaction was stopped by proteinase K and SDS for 1 h at 37°C. Products were separated by 10% PAGE, and cleavage efficiency was normalized to the level of immunoprecipitated Mus81^{9myc}. Unspecific nHJ cleavage in untagged controls was subtracted in the quantifications.

DSB-induced recombination assays were performed as described (Ho *et al*, 2010). Diploids harbouring I-SceI under the control of the *GAL* promoter were grown in adenine-rich raffinose medium and arrested in mitosis. Nuclease expression was induced by addition of galactose for 2.5 h. Cells were plated on YPAD and replica plated on YPAD + Hyg + Nat, YPAD + Hyg, YPAD + Nat, SC-Met, SC-Ura and SCR-ADE + Gal media after 3–4 days to classify recombination events.

Detailed experimental procedures are available in the Appendix.

Data availability

Mass spectrometric datasets are available at EBI PRIDE. DDK and the Rtt107 scaffold promote Mus81-Mms4 resolvase activation during mitosis (2015). PXD005356.

Expanded View for this article is available online.

Acknowledgements

We thank U. Kagerer for technical assistance, D. Gritenaite for early contributions to the project, N. Nagaraj and the proteomics laboratory of the MPIB core facility for proteomics analysis, the MPIB core facility for peptide synthesis and sequencing, J. Diffley and L. Symington for antibodies, plasmid constructs and strains, S. Jentsch, Z. Storchova, C. Biertümpfel and members of the Jentsch and Pfander labs for stimulating discussion and critical reading of the manuscript. Work in the Pfander laboratory is supported by the Max-Planck Society and the German Research Council (DFG). Work in the Matos laboratory is supported by ETH Zürich and the Swiss National Science Foundation (Grants 31003A_153058 and 155823). Work in the Blanco laboratory is co-financed by Ministerio de Economía y Competitividad and FEDER (RYC-2012-10835 and BFU2013-41554-P). Philipp Wild is supported by an EMBO long-term fellowship (ALTF 475-2015). F. Javier Aguado is supported by a PhD fellowship from the I2C Program of Xunta de Galicia (ED481A-2015/011).

Author contributions

PW and JM performed *in vitro* resolution assays of Figs 4A and C, 7A, and EV2E, and Appendix Figs S4A, C, E, and S7D and analysed the data. FJA and MGB provided recombinant purified Mus81-Mms4 used in Fig 1B, and Appendix Figs S1C and D, and S4A. All other experiments were performed and analysed by LNP, JB and BP. BP wrote the paper and all authors commented on the manuscript.

Conflict of interest

The authors declare that they have no conflict of interest.

References

Alexandru G, Uhlmann F, Mechtler K, Poupart MA, Nasmyth K (2001) Phosphorylation of the cohesin subunit Scc1 by Polo/Cdc5 kinase regulates sister chromatid separation in yeast. *Cell* 105: 459 – 472

Bishop AC, Ubersax JA, Petsch DT, Matheos DP, Gray NS, Blethrow J, Shimizu E, Tsien JZ, Schultz PG, Rose MD, Wood JL, Morgan DO, Shokat KM (2000) A chemical switch for inhibitor-sensitive alleles of any protein kinase. *Nature* 407: 395 – 401

Bizard AH, Hickson ID (2014) The dissolution of double Holliday junctions. *Cold Spring Harb Perspect Biol* 6: a016477

Blanco MG, Matos J, West SC (2014) Dual control of Yen1 nuclease activity and cellular localization by Cdk and Cdc14 prevents genome instability. *Mol Cell* 54: 94 – 106

Branzei D, Foiani M (2008) Regulation of DNA repair throughout the cell cycle. *Nat Rev Mol Cell Biol* 9: 297 – 308

Castor D, Nair N, Déclais A-C, Lachaud C, Toth R, Macartney TJ, Lilley DMJ, Arthur JSC, Rouse J (2013) Cooperative control of Holliday junction resolution and DNA repair by the SLX1 and MUS81-EME1 nucleases. *Mol Cell* 52: 221 – 233

Chen YC, Weinreich M (2010) Dbf4 regulates the Cdc5 polo-like kinase through a distinct non-canonical binding interaction. *J Biol Chem* 285: 41244 – 41254

Cheng L, Collyer T, Hardy CF (1999) Cell cycle regulation of DNA replication initiator factor Dbf4p. *Mol Cell Biol* 19: 4270 – 4278

Cox J, Mann M (2008) MaxQuant enables high peptide identification rates, individualized p.p.b.-range mass accuracies and proteome-wide protein quantification. *Nat Biotechnol* 26: 1367 – 1372

Cussiol JR, Jablonowski CM, Yimit A, Brown GW, Smolka MB (2015) Dampening DNA damage checkpoint signalling via coordinated BRCT domain interactions. *EMBO J* 34: 1704 – 1717

Dehé P-M, Coulon S, Scaglione S, Shanahan P, Takedachi A, Wohlschlegel JA, Yates JR, Llorente B, Russell P, Gaillard P-HL (2013) Regulation of Mus81–Eme1 Holliday junction resolvase in response to DNA damage. *Nat Struct Mol Biol* 20: 598 – 603

Eissler CL, Mazón G, Powers BL, Savinov SN, Symington LS, Hall MC (2014) The Cdk/Cdc14 module controls activation of the Yen1 Holliday junction resolvase to promote genome stability. *Mol Cell* 54: 80 – 93

Fekairi S, Scaglione S, Chahwan C, Taylor ER, Tissier A, Coulon S, Dong M-Q, Ruse C, Yates JR, Russell P, Fuchs RP, McGowan CH, Gaillard P-HL (2009) Human SLX4 is a Holliday junction resolvase subunit that binds multiple DNA repair/recombination endonucleases. *Cell* 138: 78 – 89

Ferreira MF, Santocanale C, Drury LS, Diffley JF (2000) Dbf4p, an essential S phase-promoting factor, is targeted for degradation by the anaphase-promoting complex. *Mol Cell Biol* 20: 242 – 248

Ferretti LP, Lafranchi L, Sartori AA (2013) Controlling DNA-end resection: a new task for CDKs. *Front Genet* 4: 1 – 7

Gallo-Fernández M, Saugar I, Ortiz-Bazán MÁ, Vázquez MV, Tercero JA (2012) Cell cycle-dependent regulation of the nuclease activity of Mus81-Eme1/Mms4. *Nucleic Acids Res* 40: 8325 – 8335

Gritenaite D, Princz LN, Szakal B, Bantele SCS, Wendeler L, Schilbach S, Habermann BH, Matos J, Lisby M, Branzei D, Pfander B (2014) A cell cycle-regulated Slx4-Dpb11 complex promotes the resolution of DNA repair intermediates linked to stalled replication. *Genes Dev* 28: 1604 – 1619

Hardy CF, Dryga O, Seematter S, Pahl PM, Sclafani RA (1997) mcm5/cdc46-bob1 bypasses the requirement for the S phase activator Cdc7p. *Proc Natl Acad Sci USA* 94: 3151 – 3155

Heyer W-D, Ehmsen KT, Liu J (2010) Regulation of homologous recombination in eukaryotes. *Annu Rev Genet* 44: 113 – 139

Ho CK, Mazón G, Lam AF, Symington LS (2010) Mus81 and Yen1 promote reciprocal exchange during mitotic recombination to maintain genome integrity in budding yeast. *Mol Cell* 40: 988 – 1000

Interthal H, Heyer WD (2000) MUS81 encodes a novel helix-hairpin-helix protein involved in the response to UV- and methylation-induced DNA damage in *Saccharomyces cerevisiae*. *Mol Gen Genet* 263: 812 – 827

Ip SCY, Rass U, Blanco MG, Flynn HR, Skehel JM, West SC (2008) Identification of Holliday junction resolvases from humans and yeast. *Nature* 456: 357 – 361

Li X, Liu K, Li F, Wang J, Huang H, Wu J, Shi Y (2012) Structure of C-terminal tandem BRCT repeats of Rtt107 protein reveals critical role in interaction with phosphorylated histone H2A during DNA damage repair. *J Biol Chem* 287: 9137 – 9146

Lopez-Mosqueda J, Maas NL, Jonsson ZO, DeFazio-Eli LG, Wohlschlegel J, Toczyski DP (2010) Damage-induced phosphorylation of Sld3 is important to block late origin firing. *Nature* 467: 479 – 483

Lyons NA, Fonslow BR, Diedrich JK, Yates JR, Morgan DO (2013) Sequential primed kinases create a damage-responsive phosphodegron on Eco1. *Nat Struct Mol Biol* 20: 194 – 201

Mankouri HW, Huttner D, Hickson ID (2013) How unfinished business from S-phase affects mitosis and beyond. *EMBO J* 32: 2661 – 2671

Masai H, Taniyama C, Ogino K, Matsui E, Kakusho N, Matsumoto S, Kim JM, Ishii A, Tanaka T, Kobayashi T, Tamai K, Ohtani K, Arai K-I (2006) Phosphorylation of MCM4 by Cdc7 kinase facilitates its interaction with Cdc45 on the chromatin. *J Biol Chem* 281: 39249 – 39261

Mathiasen DP, Lisby M (2014) Cell cycle regulation of homologous recombination in *Saccharomyces cerevisiae*. *FEMS Microbiol Rev* 38: 172 – 184

Matos J, Lipp JJ, Bogdanova A, Guillot S, Okaz E, Junqueira M, Shevchenko A, Zachariae W (2008) Dbf4-dependent CDC7 kinase links DNA replication to the segregation of homologous chromosomes in meiosis I. *Cell* 135: 662 – 678

Matos J, Blanco MG, Maslen S, Skehel JM, West SC (2011) Regulatory control of the resolution of DNA recombination intermediates during meiosis and mitosis. *Cell* 147: 158 – 172

Matos J, Blanco MG, West SC (2013) Cell-cycle kinases coordinate the resolution of recombination intermediates with chromosome segregation. *Cell Rep* 4: 76 – 86

Matos J, West SC (2014) Holliday junction resolution: regulation in space and time. *DNA Repair (Amst)* 19: 176 – 181

Miller CT, Gabrielse C, Chen Y-C, Weinreich M (2009) Cdc7p-Dbf4p regulates mitotic exit by inhibiting polo kinase. *PLoS Genet* 5: 1 – 13

Mok J, Kim PM, Lam HYK, Piccirillo S, Zhou X, Jeschke GR, Sheridan DL, Parker SA, Desai V, Jwa M, Cameroni E, Niu H, Good M, Remenyi A, Ma J-LN, Sheu Y-J, Sassi HE, Sopko R, Chan CSM, De Virgilio C *et al* (2010) Deciphering protein kinase specificity through large-scale analysis of yeast phosphorylation site motifs. *Sci Signal* 3: ra12

Montagnoli A, Valsasina B, Brotherton D, Troiani S, Rainoldi S, Tenca P, Molinari A, Santocanale C (2006) Identification of Mcm2 phosphorylation sites by S-phase-regulating kinases. *J Biol Chem* 281: 10281 – 10290

Montagnoli A, Valsasina B, Croci V, Menichincheri M, Rainoldi S, Marchesi V, Tibolla M, Tenca P, Brotherton D, Albanese C, Patton V, Alzani R, Ciavolella A, Sola F, Molinari A, Volpi D, Avanzi N, Fiorentini F, Cattoni M, Healy S *et al* (2008) A Cdc7 kinase inhibitor restricts initiation of DNA replication and has antitumor activity. *Nat Chem Biol* 4: 357 – 365

Mortensen EM, Haas W, Gygi M, Gygi SP, Kellogg DR (2005) Cdc28-dependent regulation of the Cdc5/Polo kinase. *Curr Biol* 15: 2033 – 2037

Muñoz IM, Hain K, Déclais A-C, Gardiner M, Toh GW, Sanchez-Pulido L, Heuckmann JM, Toth R, Macartney T, Eppink B, Kanaar R, Ponting CP, Lilley DMJ, Rouse J (2009) Coordination of structure-specific nucleases by human SLX4/BTBD12 Is required for DNA repair. *Mol Cell* 35: 116 – 127

Ohouo PY, de Oliveira FMB, Almeida BS, Smolka MB (2010) DNA damage signaling recruits the Rtt107-Slx4 scaffolds via Dpb11 to mediate replication stress response. *Mol Cell* 39: 300 – 306

Ohouo PY, de Oliveira FMB, Liu Y, Ma CJ, Smolka MB (2012) DNA-repair scaffolds dampen checkpoint signalling by counteracting the adaptor Rad9. *Nature* 493: 120 – 124

Pfander B, Diffley JFX (2011) Dpb11 coordinates Mec1 kinase activation with cell cycle-regulated Rad9 recruitment. *EMBO J* 30: 4897 – 4907

Princz LN, Gritenaite D, Pfander B (2015) The Slx4-Dpb11 scaffold complex: coordinating the response to replication fork stalling in S-phase and the subsequent mitosis. *Cell Cycle* 14: 488 – 494

Randell JCW, Fan A, Chan C, Francis LI, Heller RC, Galani K, Bell SP (2010) Mec1 is one of multiple kinases that prime the Mcm2-7 helicase for phosphorylation by Cdc7. *Mol Cell* 40: 353 – 363

Saugar I, Vazquez MV, Gallo-Fernandez M, Ortiz-Bazan MA, Segurado M, Calzada A, Tercero JA (2013) Temporal regulation of the Mus81-Mms4 endonuclease ensures cell survival under conditions of DNA damage. *Nucleic Acids Res* 41: 8943 – 8958

Schwartz EK, Wright WD, Ehmsen KT, Evans JE, Stahlberg H, Heyer WD (2012) Mus81-Mms4 functions as a single heterodimer to cleave nicked intermediates in recombinational DNA repair. *Mol Cell Biol* 32: 3065 – 3080

Shirayama M, Zachariae W, Ciosk R, Nasmyth K (1998) The Polo-like kinase Cdc5p and the WD-repeat protein Cdc20p/fizzy are regulators and substrates of the anaphase promoting complex in *Saccharomyces cerevisiae*. *EMBO J* 17: 1336 – 1349

Snead JL, Sullivan M, Lowery DM, Cohen MS, Zhang C, Randle DH, Taunton J, Yaffe MB, Morgan DO, Shokat KM (2007) A coupled chemical-genetic and bioinformatic approach to polo-like kinase pathway exploration. *Chem Biol* 14: 1261 – 1272

Suzuki K, Sako K, Akiyama K, Isoda M, Senoo C, Nakajo N, Sagata N (2015) Identification of non-Ser/Thr-Pro consensus motifs for Cdk1 and their roles in mitotic regulation of C2H2 zinc finger proteins and Ect2. *Sci Rep* 5: 7929

Svendsen JM, Smogorzewska A, Sowa ME, O'Connell BC, Gygi SP, Elledge SJ, Harper JW (2009) Mammalian BTBD12/SLX4 assembles a Holliday junction resolvase and is required for DNA repair. *Cell* 138: 63 – 77

Szakal B, Branzei D (2013) Premature Cdk1/Cdc5/Mus81 pathway activation induces aberrant replication and deleterious crossover. *EMBO J* 32: 1155 – 1167

Weinreich M, Stillman B (1999) Cdc7p-Dbf4p kinase binds to chromatin during S phase and is regulated by both the APC and the RAD53 checkpoint pathway. *EMBO J* 18: 5334 – 5346

Wyatt HDM, Sarbajna S, Matos J, West SC (2013) Coordinated actions of SLX1-SLX4 and MUS81-EME1 for Holliday junction resolution in human cells. *Mol Cell* 52: 234 – 247

Zegerman P, Diffley JFX (2010) Checkpoint-dependent inhibition of DNA replication initiation by Sld3 and Dbf4 phosphorylation. *Nature* 467: 474 – 478

Appendix – Table of Contents

- **Appendix Figure Legends**
- **Appendix Figures**
- **Appendix Table S1**
- **Appendix Supplementary Materials and Methods (including Appendix Table S2)**
- **Appendix References**

Appendix Figure Legends:

Figure S1:

Mus81-Mms4 forms a complex in mitosis with kinases and scaffold proteins, and is a target to phosphorylation by these kinases.

(A) SILAC-based quantification of Mms4^{3FLAG} pulldowns in untagged vs *MMS4^{3FLAG}* cells after G2/M arrest with nocodazole. H/L ratios from two label-switch experiments without ratio count cut-off are plotted. #, as the only protein of the analysis Dpb11 displayed exclusively peptides that were derived from the Mms4^{3FLAG} IP samples, but not the control samples. This experiment is already shown as Fig. S8A in Gritenaite *et al.*, 2014.

(B) Coomassie staining to show running behaviour of peptides used in Fig. 1C. Peptides 1-3 shift down upon increasing phosphorylation, whereas peptides 4-6 display an up-shift.

(C) Kinetic *in vitro* kinase assay. Purified, immobilized Mus81-Mms4 is either mock treated or treated with CDK in a non-radioactive priming step, and incubated with purified DDK (upper panel) or Cdc5 (lower panel). Samples were taken after indicated time points.

(D) Mus81-Mms4 *in vitro* phosphorylation is independent of DKK and/or CDK pre-phosphorylation. Purified, immobilized Mus81-Mms4 is incubated in an *in vitro* kinase assay with purified CDK2/cycA^{N170} (a model CDK), DDK or Cdc5 (lanes 1-4). Additionally, Mus81-Mms4 is incubated with respective kinases after a non-radioactive priming step with DDK (lanes 5-8) or CDK and DDK (lanes 9-12).

Figure S2:

DDK and Cdc5 target Mus81-Mms4 in an interdependent manner.

(A) Formation of the Mus81-Mms4 complex depends on Cdc5 activity. SILAC-based quantification of Mms4^{3FLAG} pulldowns in *WT* vs *cdc5-as1* cells after mitotic arrest with nocodazole and additional treatment with 15 μM CMK for 1 h. Plotted are the H/L ratios of two label-switch experiments.

(B) CDK activity is required for Mms4 hyperphosphorylation. Whole-cell extracts of *WT* and *cdc28-as1* cells arrested in mitosis, titrated with 1NM-PP1 as indicated.

(C) Phosphorylation shift of Mms4 in whole-cell extracts of mitotically arrested *WT* and mutant cells.

(D) Cdc5 association with Mus81-Mms4 is dependent on DDK activity. Mms4^{3FLAG} pulldown as in Fig. 1A. Cells were cultivated and arrested in mitosis at RT. Inhibition of

DDK was achieved by using the *cdc7-1* allele and shifting cells to permissive temperature (38 °C) for the indicated time.

(E) Effect of DDK and Cdc5 mutants on Cdc5 substrates. Phosphorylation of Cdc5 substrates Ulp2 and Scc1 (and as control Mms4) was tested, indicated by their phosphorylation shift in 7% Tris-Acetate gels in untagged, *WT*, *cdc5-as1* and *cdc7Δ* backgrounds. Western blot analysis of Ulp2^{9myc} and Scc1^{9myc} whole-cell extracts from alpha-factor- (G1) or nocodazole-arrested (G2/M) cells. Cdc5 was inhibited by treatment with 15 µM CMK for 1 h.

(F) DDK and Cdc5 association to Mus81-Mms4 is reduced when the DNA damage checkpoint is triggered by DNA damage induction. Mms4^{3FLAG} pulldown as in Fig. 1A, but in G2/M-arrested cells that were untreated or treated with 50 µg/ml phleomycin.

Figure S3:

Summary of Mms4 phosphorylation sites. Shown is the Mms4 primary amino acid sequence. Colours indicate phosphorylation sites on endogenous Mms4 that were affected in SILAC-based mass spectrometry experiments (Fig. 3A-B) by Cdc5 inhibition (blue), *CDC7* deletion (red) or in both backgrounds (green). Serine to alanine exchanges in the *mms4-8A* mutant are boxed. Additional serine to alanine exchanges in the *mms4-12A* mutant are boxed with a dashed line.

Figure S4:

DDK phosphorylation controls activation of Mus81-Mms4 resolvase activity in mitosis.

(A) Endogenous Mus81^{3FLAG}-Mms4 purified from mitotically arrested cells shows increased activity compared to non-phosphorylated recombinant protein expressed in yeast. Left panel: Western blot analysis for quantification of bead-bound protein levels of Mus81 (endogenous and recombinant) compared to increasing amounts of soluble recombinant Mus81. Approx. 5 fmol Mus81^{3FLAG} -Mms4 are used in the assay to cleave 500 fmol nHJ substrate. Right panel: Resolution assay using a nicked HJ substrate and comparing Mus81^{3FLAG}-Mms4 purified from mitotically arrested cells with recombinant, dephosphorylated Mus81^{3FLAG}-Mms4 in similar protein concentration.

(B,C) Interaction of Mus81-Mms4 with other complex factors such as Rtt107 and Cdc5 is salt-labile, but their absence does not influence Mus81-Mms4 activity.

(B) Mms4^{3FLAG} pulldown as in Fig. 1A from mitotically arrested cells, but proteins were washed on beads with either low salt (150 mM NaCl) or high salt buffer (350 mM NaCl).

(C) Left panel: Resolution assay using a nHJ substrate and Mus81^{9myc}-Mms4^{3FLAG} purified from mitotically arrested cells under low salt (150 mM NaCl) or high salt (350 mM NaCl) conditions. Right panel: Western blots samples of anti-myc IPs.

(D,F) Western blot analysis of Mus81^{9myc} IP samples that were used as inputs for the *in vitro* resolution assays of Fig. 4A and C, respectively.

(E) DDK is required for mitotic activation of Mus81-Mms4. Resolution assay using a replication fork (RF) substrate and Mus81^{9myc}-Mms4^{3FLAG} purified from mitotically arrested *bob1-1 (DDK+)* and *bob1-1 cdc7Δ* strains or untagged control cells. Lower panel: Western blots samples of anti-myc IPs.

Figure S5:

Dpb11 interacts with the N-terminal region of Mms4 and its binding is dependent on CDK activity.

(A) Dpb11 binds to a minimal interacting fragment of Mms4 comprising the residues 101-230. Two-hybrid analysis of GAL4-BD fused to Dpb11 and GAL4-AD fusions with Mms4 or Mms4 fragment constructs (left panel). Expression of constructs was verified by western blot analysis (right panel).

(B) CDK activity is required for Dpb11 and Slx4 association with Mus81-Mms4. Mms4^{3FLAG} pulldown as in Fig. 1A, but in G2/M-arrested *WT* and *cdc28-as1* mutant cells treated with 5 μM 1NM-PP1 for 1 h. This figure is from the same experiment as Fig. 2B and therefore as control includes the identical anti-Flag western.

(C) A defect in the Dpb11-Mms4 interaction introduces only a minor defect in Mus81 activation. Resolution assay using a nicked HJ substrate and Mus81^{9myc}-Mms4^{3FLAG} purified from mitotically arrested *WT* or *mms4-S201A* cells. Right panel: Western blots samples of anti-myc IPs.

Figure S6:

The Rtt107 scaffold tethers DDK and Cdc5 to Mus81-Mms4.

(A) Formation of the Mus81-Mms4 complex depends on Rtt107. SILAC-based quantification of Mms4^{3FLAG} pulldowns in *WT* vs *rtt107Δ* cells. Plotted are the H/L ratios of two experiments including label-switch.

(B) Rtt107 binding to Cdc5 and DDK is not affected by the presence of Mus81-Mms4. Rtt107^{3FLAG} pulldown as in Fig. 1A, but in G2/M-arrested *WT* and *mus81Δ* cells.

Figure S7:

Rtt107 is required for efficient Mus81-Mms4 activation in mitosis.

(A,B) Rtt107 influences the phosphorylation of specific Cdc5-dependent phosphorylation sites. SILAC-based MS analysis of Mms4 phosphorylation after purification of endogenously expressed Mus81-Mms4^{3FLAG} **(A)** or of Mus81^{3FLAG}-Mms4$^{His10\text{-}Strep2}$ expressed from the *pGAL1-10* promoter **(B)**.

(C) Western blot analysis of Mus81^{9myc} IP samples that were used as inputs for the *in vitro* for resolution assay of Fig. 7A.

(D) *RTT107* deletion does not lead to a further reduction in Mus81 activity in the *cdc7Δ* background. Resolution assay using a nicked HJ substrate and Mus81^{9myc}-Mms4^{3FLAG} purified from mitotically arrested *bob1-1 cdc7Δ* or *bob1-1 cdc7Δ rtt107Δ* cells. Lower panel: Western blots samples of anti-myc IPs.

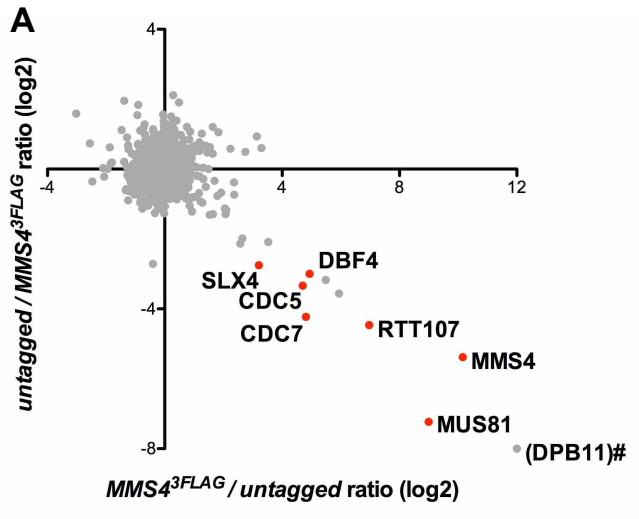
A
4
-4
4
8
12
-4
-8
untagged / MMS4^3FLAG ratio (log2)
DBF4
SLX4
CDC5
CDC7
RTT107
MMS4
MUS81
(DPB11)#
MMS4^3FLAG / untagged ratio (log2)

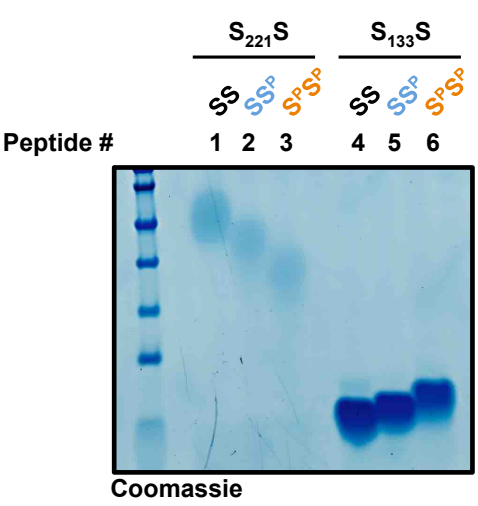
B
S221S
S133S
SS
SSP
SPSP
SS
SSP
SPSP
Peptide #
1 2 3
4 5 6
Coomassie

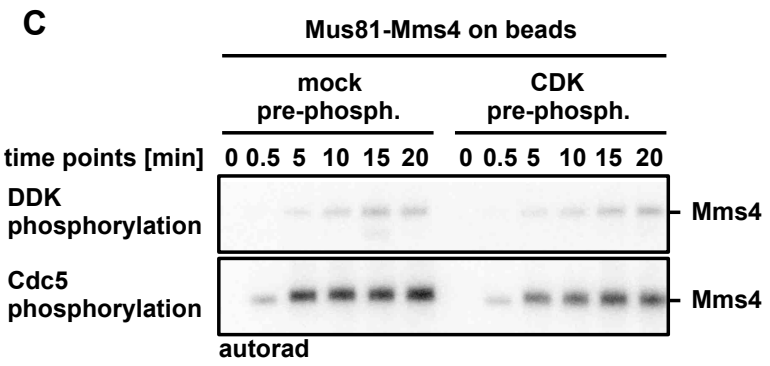
C
Mus81-Mms4 on beads
mock pre-phosph.
CDK pre-phosph.
time points [min]
0 0.5 5 10 15 20
0 0.5 5 10 15 20
DDK phosphorylation
Cdc5 phosphorylation
Mms4
Mms4
autorad

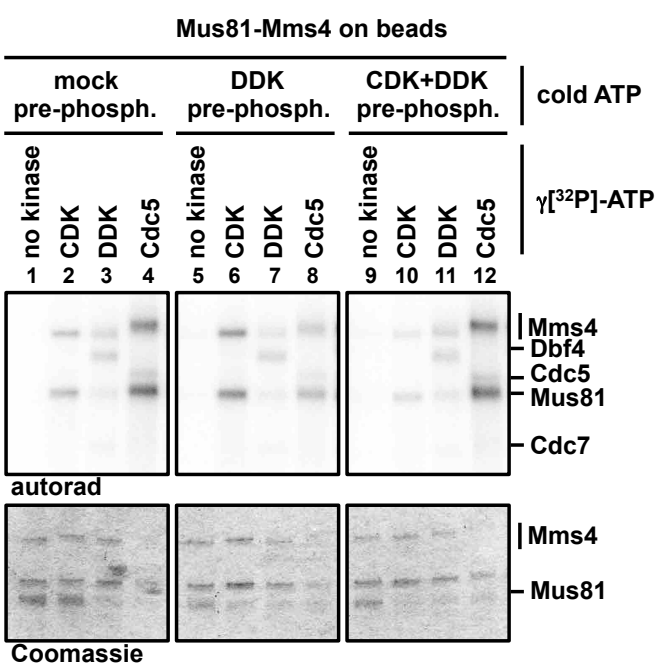
D
Mus81-Mms4 on beads
mock pre-phosph.
DDK pre-phosph.
CDK+DDK pre-phosph.
cold ATP
γ[32P]-ATP
no kinase
CDK
DDK
Cdc5
1 2 3 4
5 6 7 8
9 10 11 12
Mms4
Dbf4
Cdc5
Mus81
Cdc7
autorad
Mms4
Mus81
Coomassie

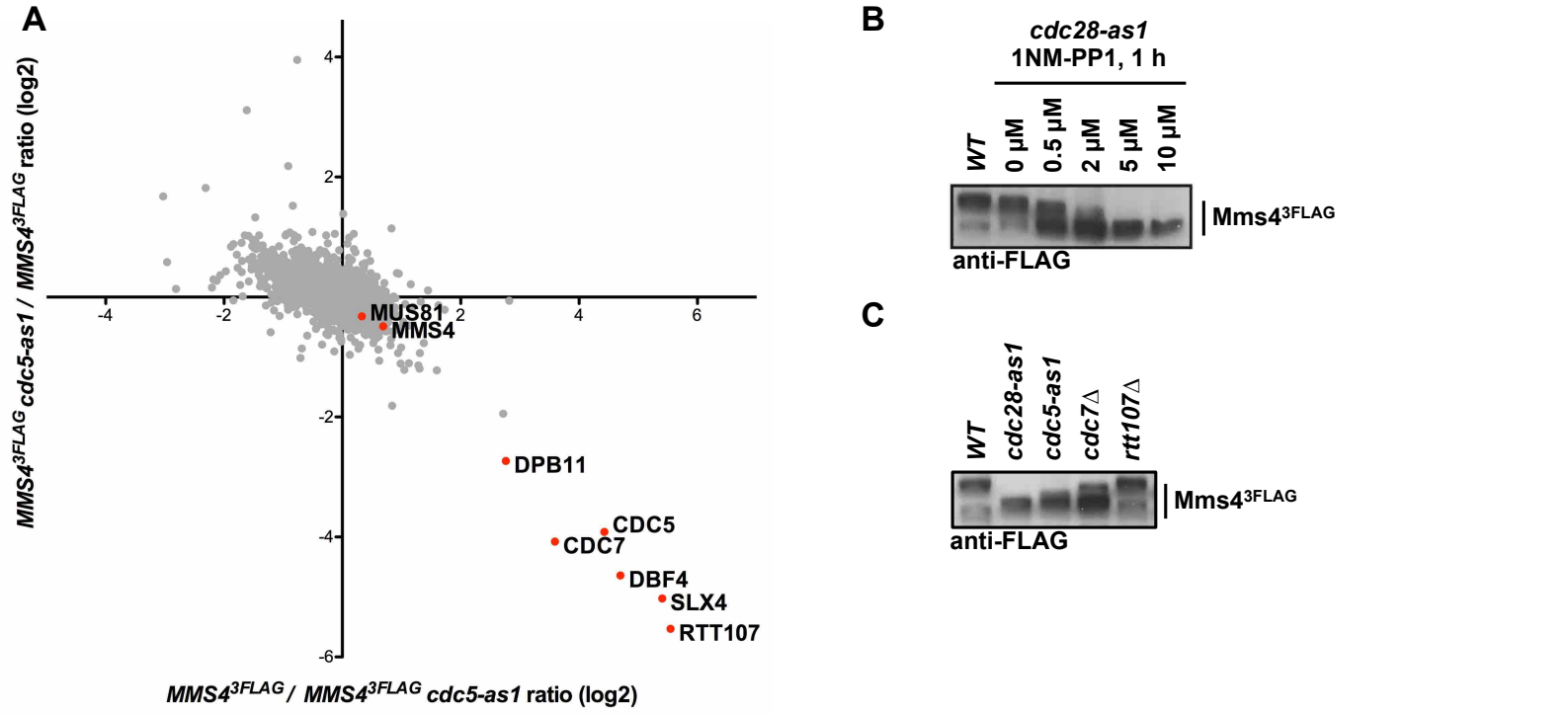

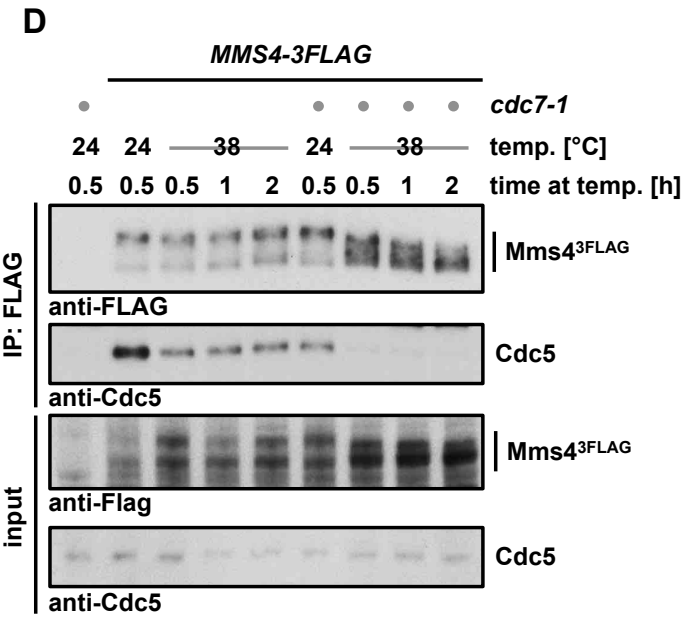

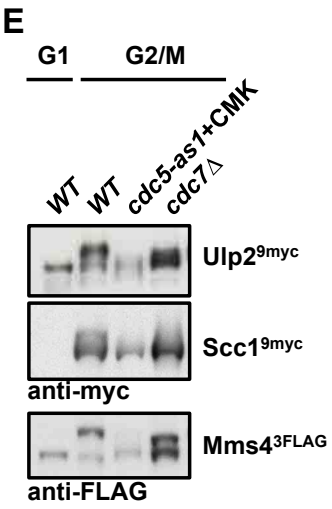

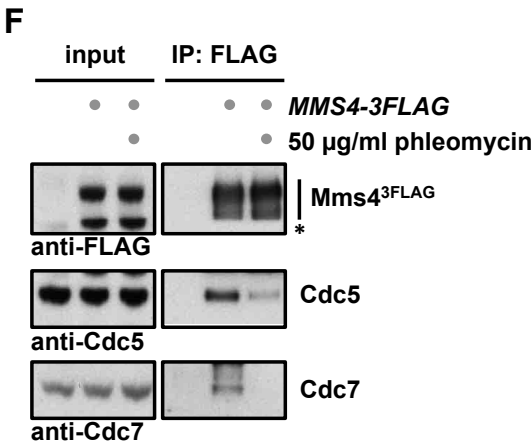

Appendix Figure S2 Legend

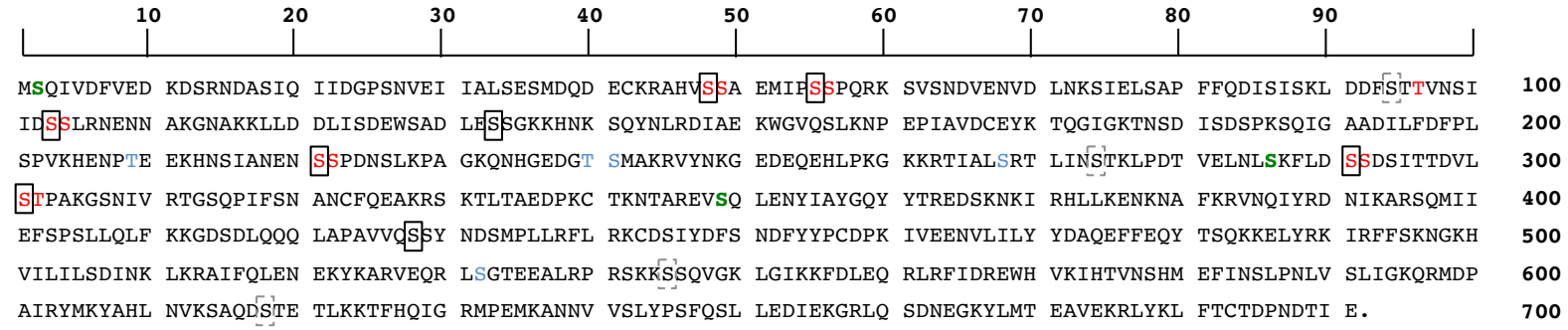

Appendix Figure S3 Legend

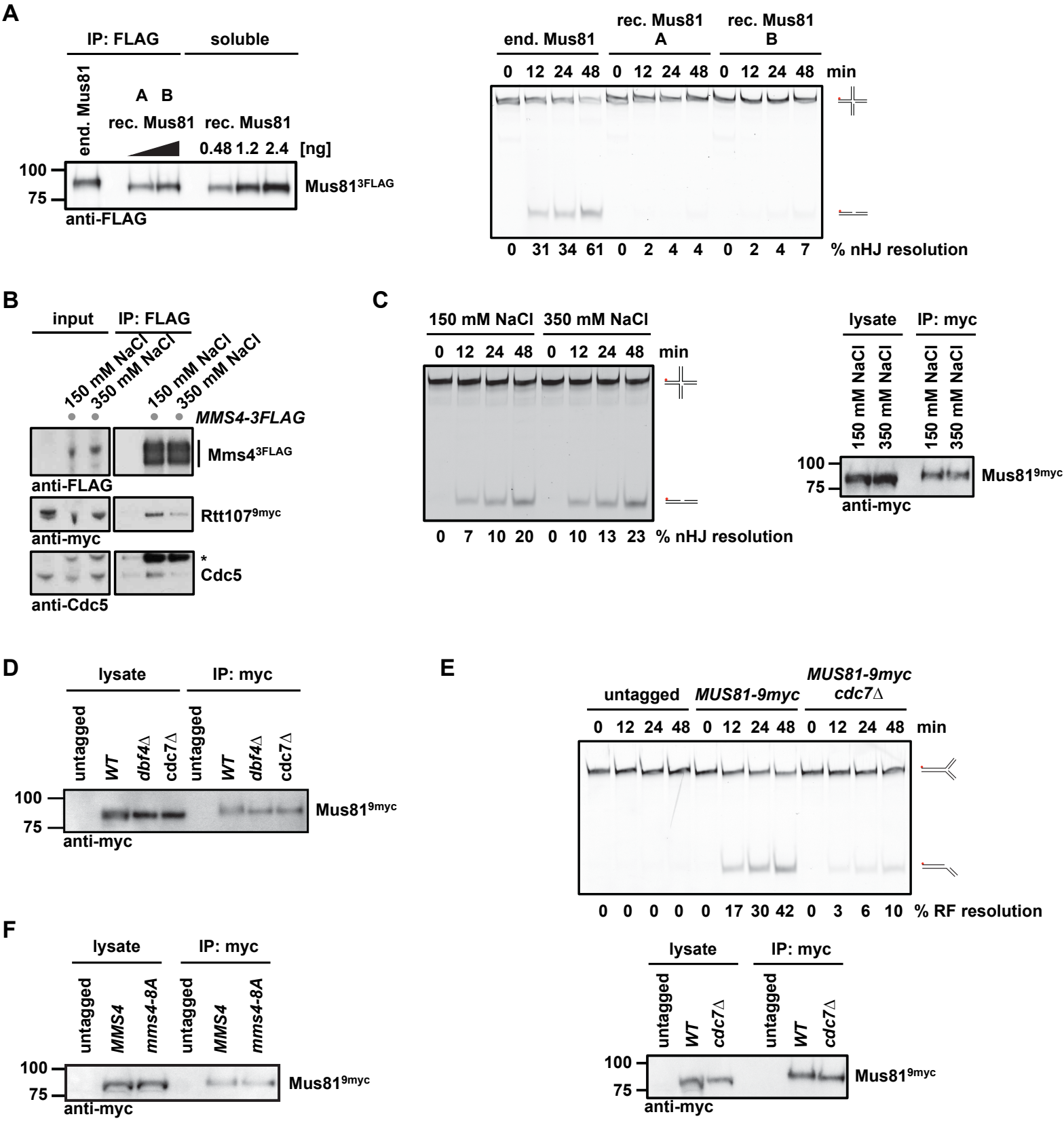

Appendix Figure S4 Legend

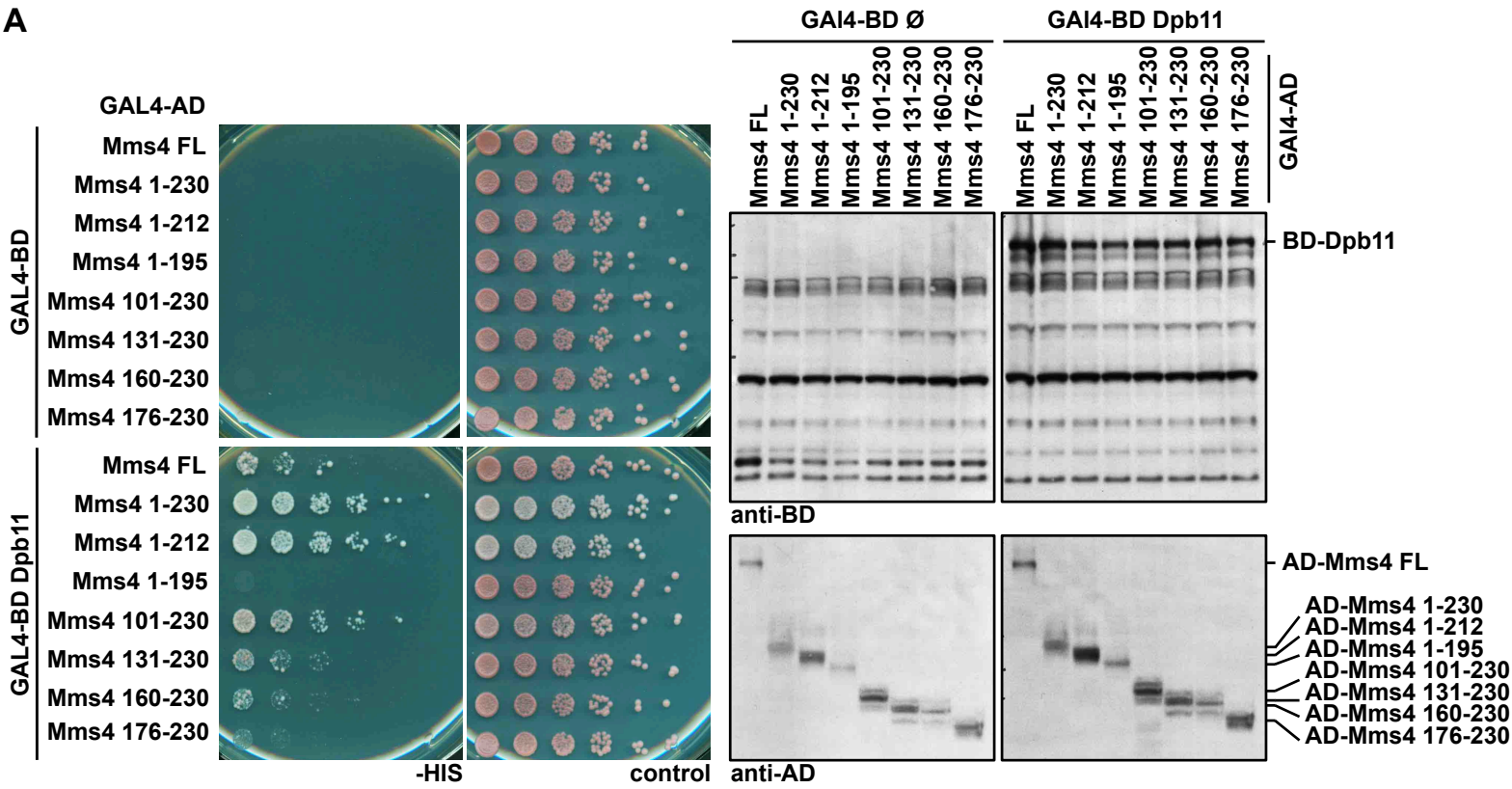

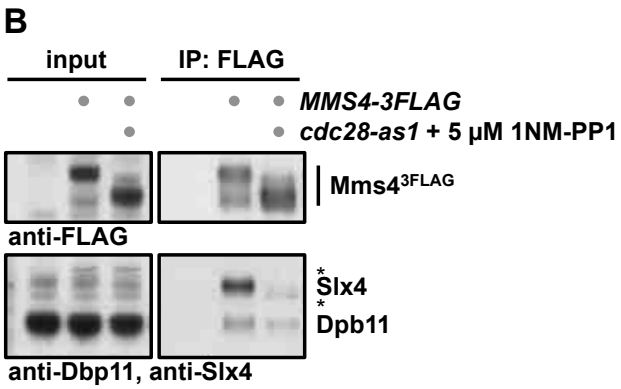

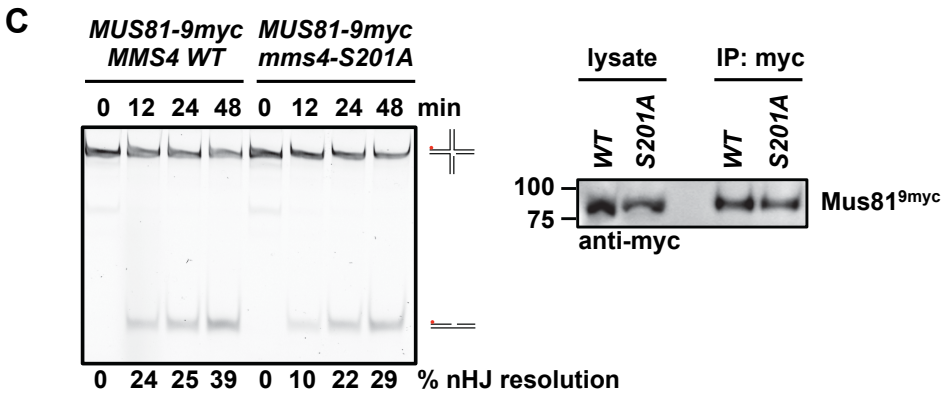

Appendix Figure S5 Legend

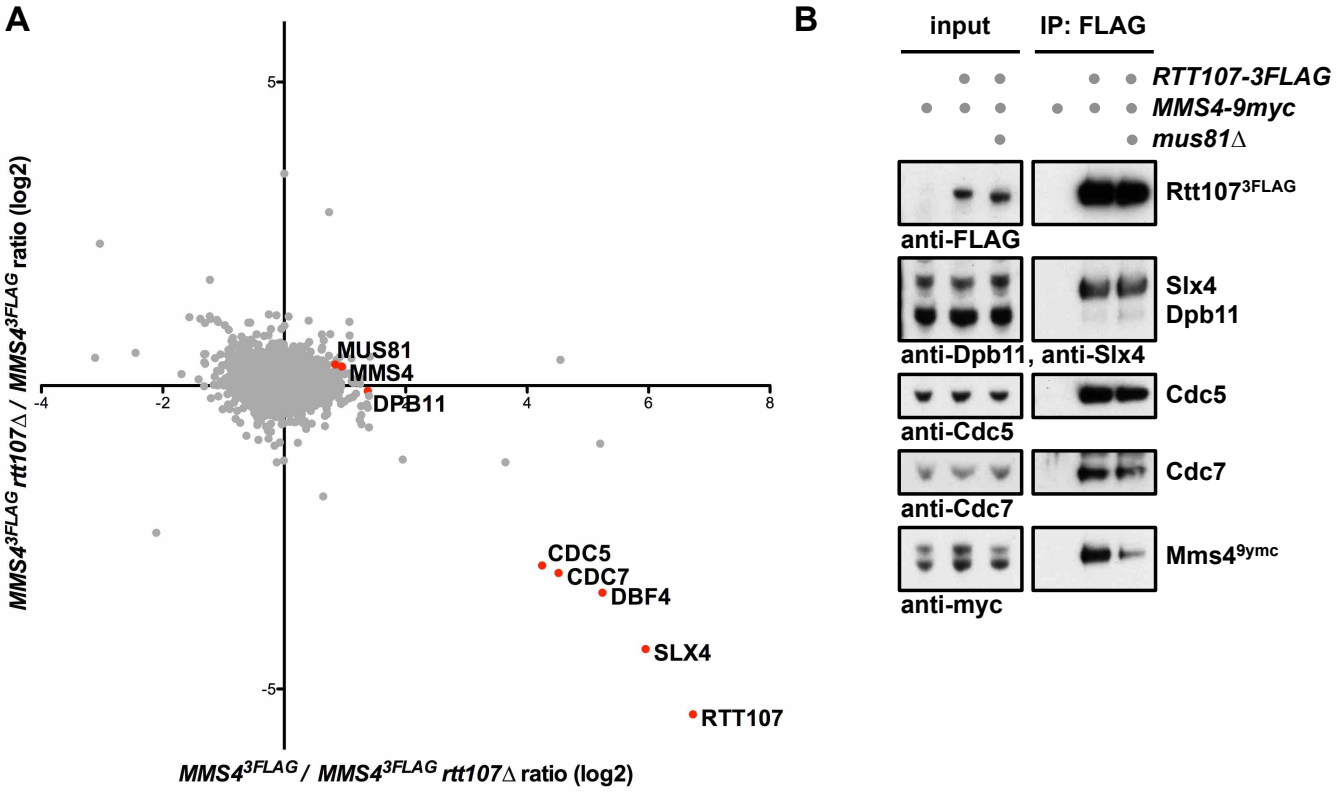

Appendix Figure S6 Legend

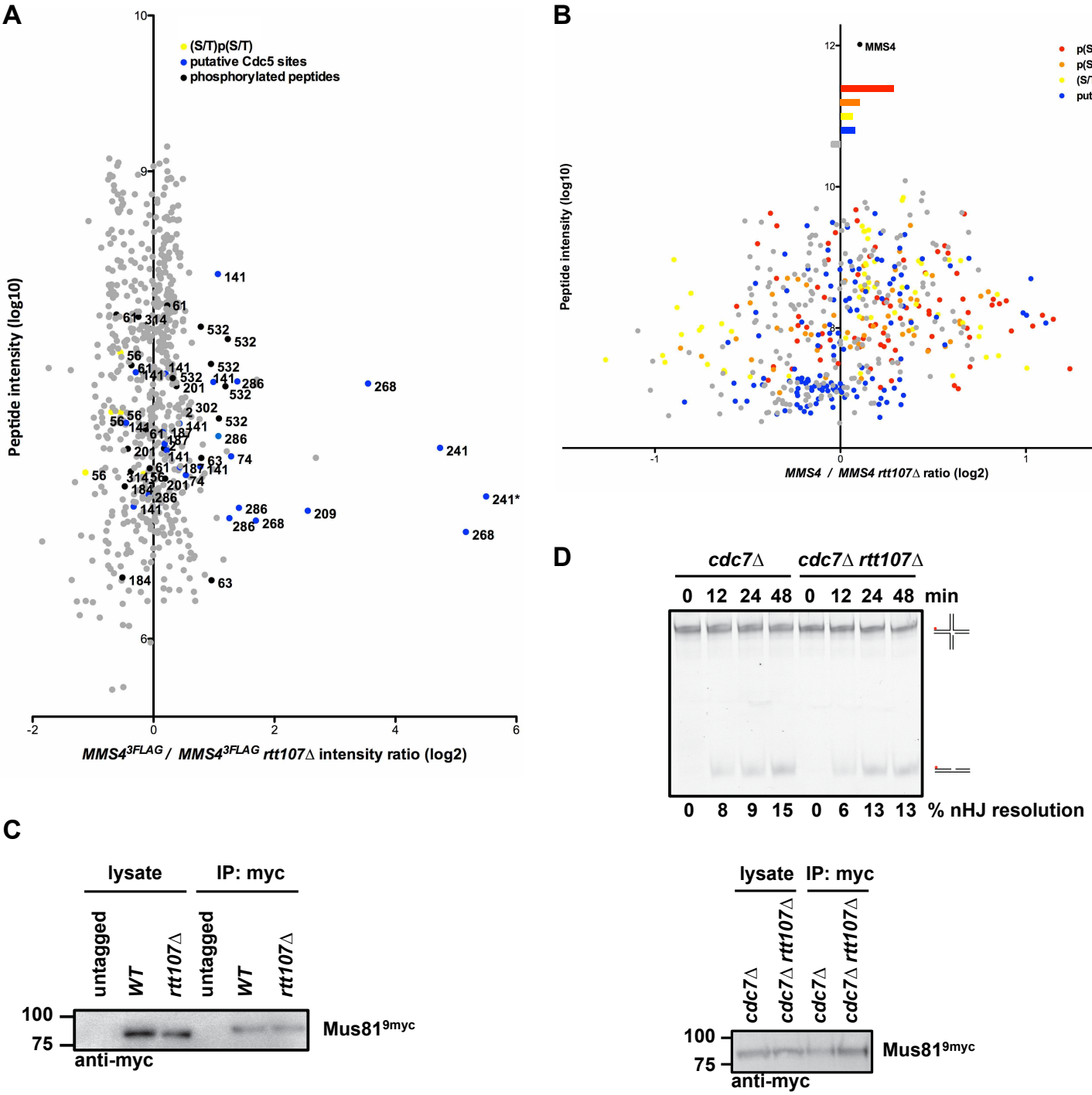

Appendix Figure S7 Legend

Appendix Table S1. Mms4 phosphorylation sites and their regulation by DDK or Cdc5 as detected by SILAC-based quantitative mass spectrometry (Fig. 3)

Mus81-Mms4 endogenous	Mus81-Mms4 overexpressed
2	2
48	48
49	49
55	55
56	56
61	61
63	63
74	74
86	78**
88*	86
94**	88**
96	94
99	95
103	96
104	99
124**	103
128**	104
133**	124
134**	128
141**	133
156**	134
184*	141
187	156
201	187
209**	201
221*	222*
222*	264
240**	268
241**	274*
268**	280*
286	286
291	291
292	292
294	294
296**	297
297**	301
301	302
302	314
314**	330**
330**	349
349	366
366**	396**
396**	532
532	542

* not measured in *cdc5-as1*
** not measured in *cdc7Δ*
phosphorylation sites affected in *cdc5-as1*
phosphorylation sites affected in *cdc7Δ*
phosphorylation sites affected in *cdc5-as1* and *cdc7Δ* backgrounds

Appendix Supplementary Materials and Methods

Yeast strains and construction

All yeast strains are based on W303 (Thomas & Rothstein, 1989). Genotypes are listed below. All biochemical experiments were performed in a W303-1A *pep4Δ* background. The genetic experiments in Fig. 4D-E, 5C, and EV2A,B,D were performed in a W303 *RAD5+* background to exclude any effect from a partial defect of the *rad5-535* allele. Two-hybrid analyses were performed in the strain PJ69-7A (James *et al.*, 1996).

S. cerevisiae strains were prepared by genetic crosses and transformation techniques. Deletion of particular genes and endogenous protein tagging were performed as described (Knop *et al.*, 1999). Correct integrations were checked by genotyping PCR. Denaturing cell extracts were prepared by alkaline lysis and TCA precipitation. The *mms4* alleles were generated using site-directed mutagenesis and integrated as linear plasmids at the TRP1 locus.

Appendix Table S2. Yeast strains used in this study

Strain	Full genotype	Relevant genotype	Source
MGBY3294	MATa *ade2-1 his3-11 leu2-3,112 trp1Δ2 can1-100 pep4::KanMX bar1::hph-NT1 ura3-52::GAL1,10p-FLAG3-MUS81/GST-His10-Strep2-MMS4::URA3*	*pGAL-FLAG3-MUS81-GST-His10-Strep2-MMS4*	This study (Blanco lab)
YBP388	MATa *ade2-1 ura3-1 his3-11,15 trp1-1 can1-100 leu2-3,112::pep4::LEU2*	*pep4*	Klein lab
YDG208	MATa *RAD5+ ade2-1 ura3-1 leu2-3,112 his3-11,15 trp1-1 can1-100*		This study
YDG291	MATa *RAD5+ ade2-1 ura3-1 leu2-3,112 his3-11,15 trp1-1 can1-100 yen1::hph-NT1*	*yen1*	Gritenaite et al., 2014
YDG329	MATa *RAD5+ ade2-1 ura3-1 leu2-3,112 his3-11,15 trp1-1 can1-100 sgs1::hph-NT1*	*sgs1*	Gritenaite et al., 2014
YDG355	MATa *RAD5+ ade2-1 ura3-1 his3-11,15 trp1-1 can1-100 mms4::hph-NT1 leu2-3,112::mms4-SS184,201AA::LEU2*	*mms4-SS184,201AA*	Gritenaite et al., 2014
YDG356	MATa *RAD5+ ade2-1 ura3-1 trp1-1 can1-100 mms4::hph-NT1 leu2-3,112::mms4-SS184,201AA::LEU2 his3-11,15::sgs1::HIS3Mx4*	*mms4-SS184,201AA sgs1*	Gritenaite et al., 2014
YDG376	MATa *RAD5+ ade2-1 ura3-1 leu2-3,112 his3-11,15 trp1-1 can1-100 yen1::hph-NT1 sgs1::nat-NT2*	*yen1 sgs1*	Gritenaite et al., 2014

YJB82	Mata/Matalpha *ade2-1/ade2-1 ura3-1/ura3-1 leu2-3,112/leu2-3,112 his3-11,15/his3-11,15 trp1-1/trp1-1 can1-100/can1-100 ade2-n/ade2-I LYS2/lys2::Gal-ISceI his3::NATMX/his3::HPHMX4 met22::kIURA3/MET22*	*diploid*	This study
YJB84	Mata/Matalpha *ade2-1/ade2-1 ura3-1/ura3-1 leu2-3,112/leu2-3,112 his3-11,15/his3-11,15 trp1-1/trp1-1 can1-100/can1-100 ade2-n/ade2-I LYS2/lys2::Gal-ISceI his3::NATMX/his3::HPHMX4 met22::kIURA3/MET22 rtt107::KanMX/rtt107::KanMX*	*diploid rtt107*	This study
YJB86	Mata/Matalpha *ade2-1/ade2-1 ura3-1/ura3-1 leu2-3,112/leu2-3,112 his3-11,15/his3-11,15 trp1-1/trp1-1 can1-100/can1-100 ade2-n/ade2-I LYS2/lys2::Gal-ISceI his3::NATMX/his3::HPHMX4 met22::::kIURA3/MET22 mms4::KanMX/mms4::KanMX trp1-1:pRS304-Mms4-SSSSSSSS48,55,103,133,221,291,301,428AAAAAAAA:TRP1/trp1-1:pRS304-Mms4-SSSSSSSS48,55,103,133,221,291,301,428AAAAAAAA:TRP1*	*diploid mms4-SSSSSSSS48,55,103,133,221,291,301,428AAAAAAAA*	This study
YLP015	MATa *ade2-1 ura3-1 his3-11,15 can1-100 trp1-1::bar1::TRP1 leu2-3,112::pep4::LEU2 lys1::nat-NT2*	*lys1*	Gritenaite et al., 2014
YLP063	MATa *RAD5+ ade2-1 ura3-1 leu2-3,112 trp1-1 can1-100 cdc5-as1 his3-11,15::pep4::HIS3Mx4 MMS4-3FLAG::hph-NT1*	*MMS4-3FLAG cdc5-as1*	Gritenaite et al., 2014
YLP065	MATa *ade2-1 ura3-1 his3-11,15 can1-100 trp1-1::bar1::TRP1 leu2-3,112::pep4::LEU2 lys1::nat-NT2 MMS4-3FLAG::hph-NT1*	*lys1 MMS4-3FLAG*	This study
YLP070	MATa *ade2-1 ura3-1 leu2-3,112 can1-100 his3-11,15::pep4::HIS3Mx4 lys1::nat-NT2 mms4::KanMx trp1-1::mms4-S184A::TRP1 MMS4-3FLAG::hph-NT1*	*lys1 mms4-S184A-3FLAG*	This study
YLP074	MATa *ade2-1 ura3-1 leu2-3,112 can1-100 his3-11,15::pep4::HIS3Mx4 lys1::nat-NT2 mms4::KanMx trp1-1::mms4-S201A::TRP1 MMS4-3FLAG::hph-NT1*	*lys1 mms4-S201A-3FLAG*	This study
YLP078	MATa *ade2-1 ura3-1 leu2-3,112 trp1-1 can1-100 his3-11,15::pep4::HIS3Mx4 MMS4-3FLAG::hph-NT1 slx4::KanMx*	*MMS4-3FLAG slx4*	Gritenaite et al., 2014

YLP092	MATa *ade2-1 ura3-1 his3-11,15 trp1-1 can1-100 leu2-3,112::pep4::LEU2 RTT107-9myc::hph-NT1*	*RTT107-9myc*	This study
YLP100	MATa *ade2-1 ura3-1 trp1-1 leu2-3,112 can1-100 his3-11,15::bob1-1::HIS3Mx4 pep4::hph-NT1*	*bob1-1*	This study
YLP111	MATa *ade2-1 ura3-1 trp1-1 leu2-3,112 can1-100 his3-11,15::bob1-1::HIS3Mx4 pep4::hph-NT1 MMS4-3FLAG::KanMx4*	*bob1-1 MMS4-3FLAG*	This study
YLP113	MATa *ade2-1 ura3-1 trp1-1 leu2-3,112 can1-100 his3-11,15::bob1-1::HIS3Mx4 pep4::hph-NT1 cdc7::nat-NT2 MMS4-3FLAG::KanMx4*	*bob1-1 cdc7 MMS4-3FLAG*	This study
YLP121	MATa *RAD5+ ade2-1 ura3-1 leu2-3,112 trp1-1 can1-100 cdc5-as1 his3-11,15::pep4::HIS3Mx4 lys1::nat-NT2 MMS4-3FLAG::hph-NT1*	*lys1 MMS4-3FLAG cdc5-as1*	This study
YLP126	MATa *ade2-1 leu2-3,112 trp1-1 can1-100 his3-11,15::bob1-1::HIS3Mx4 pep4::hph-NT1 cdc7::nat-NT2 MMS4-3FLAG::KanMx4 ura3-1::lys1::URA3*	*lys1 bob1-1 cdc7 MMS4-3FLAG*	This study
YLP128	MATa *ade2-1 ura3-1 leu2-3,112 trp1-1 can1-100 his3-11,15::pep4::HIS3Mx4 cdc7-1*	*cdc7-1*	This study
YLP132	MATa *ade2-1 ura3-1 leu2-3,112 trp1-1 can1-100 his3-11,15::pep4::HIS3Mx4 cdc7-1 MMS4-3FLAG::KanMx*	*cdc7-1 MMS4-3FLAG*	This study
YLP156	MATa *ade2-1 ura3-1 leu2-3,112 trp1-1 can1-100 his3-11,15::pep4::HIS3Mx4 MMS4-3FLAG::hph-NT1 RTT107-9myc::nat-NT2*	*MMS4-3FLAG RTT107-9myc*	This study
YLP164	MATa *ade2-1 ura3-1 leu2-3,112 can1-100 MMS4-3FLAG::hph-NT1 his3-11,15::pep4::HIS3Mx4 rtt107::KanMx trp1-1::lys1::TRP1*	*lys1 MMS4-3FLAG rtt107*	This study
YLP277	MATa *ade2-1 ura3-1 trp1-1 leu2-3,112 can1-100 MMS4-3FLAG::hph-NT1 his3-11,15::pep4::HIS3Mx4 SCC1-9myc*	*MMS4-3FLAG SCC1-9myc*	This study
YLP279	MATa RAD5+ *ade2-1 ura3-1 trp1-1 leu2-3,112 can1-100 cdc5-as1 MMS4-3FLAG::hph-NT1 his3-11,15::pep4::HIS3 SCC1-9myc::KanMx*	*MMS4-3FLAG SCC1-9myc cdc5-as1*	This study
YLP287	MATa *ade2-1 ura3-1 leu2-3,112 can1-100 his3-11,15::pep4::HIS3Mx4 mms4::KanMx trp1-1::mms4-S201A::TRP1 MMS4-3FLAG::hph-NT1 RTT107-9myc::nat-NT2*	*mms4-S201A-3FLAG RTT107-9myc*	This study

YLP339	MATa *RAD5+ ade2-1 ura3-1 leu2-3,112 his3-11,15 can1-100 mms4::hph-NT1 trp1-1::mms4-SSSSSSSS48,55,103,133,221,291,301,428AAAAAAAA::TRP1*	*mms4-SSSSSSSS48,55,103,133,221,291,301,428AAAAAAAA*	This study
YLP341	MATa *RAD5+ ade2-1 ura3-1 leu2-3,112 his3-11,15 can1-100 mms4::hph-NT1 trp1-1::mms4-SSSSSSSS48,55,103,133,221,291,301,428AAAAAAAA::TRP1 sgs1::nat-NT2*	*mms4-SSSSSSSS48,55,103,133,221,291,301,428AAAAAAAA sgs1*	This study
YLP350	MATa *RAD5+ ade2-1 ura3-1 leu2-3,112 his3-11,15 can1-100 mms4::hph-NT1 trp1-1::mms4-SSSSSSSS48,55,103,133,221,291,301,428AAAAAAAA::TRP1 yen1::KanMx*	*mms4-SSSSSSSS48,55,103,133,221,291,301,428AAAAAAAA yen1*	This study
YLP351	MATa *RAD5+ ade2-1 ura3-1 leu2-3,112 his3-11,15 can1-100 mms4::hph-NT1 trp1-1::mms4-SSSSSSSS48,55,103,133,221,291,301,428AAAAAAAA::TRP1 sgs1::nat-NT2 yen1::KanMx*	*mms4-SSSSSSSS48,55,103,133,221,291,301,428AAAAAAAA sgs1 yen1*	This study
YLP344	MATa *ade2-1 ura3-1 leu2-3,112 trp1-1 can1-100 MMS4-3FLAG::hph-NT1 his3-11,15::pep4::HIS3Mx4 dbf4-ΔN66::KanMx*	*MMS4-3FLAG dbf4-ΔN66*	This study
YLP345	MATa *ade2-1 ura3-1 leu2-3,112 trp1-1 can1-100 MMS4-3FLAG::hph-NT1 his3-11,15::pep4::HIS3Mx4 dbf4-ΔN109::KanMx*	*MMS4-3FLAG dbf4-ΔN109*	This study
YLP356	MATa *ade2-1 ura3-1 leu2-3,112 can1-100 mms4::KanMx his3-11,15::pep4::HIS3 trp1-1::mms4-SSSSSSSS48,55,103,133,221,291,301,428AAAAAAAA::TRP1 MMS4-3FLAG::hph-NT1*	*mms4-SSSSSSSS48,55,103,133,221,291,301,428AAAAAAAA-3FLAG*	This study
YLP360	MATa *ade2-1 ura3-1 leu2-3,112 his3-11,15 trp1-1 can1-100 MMS4-3FLAG::hph-NT1 cdc28-as1*	*MMS4-3FLAG cdc28-as1*	This study
YLP367	MATa *ade2-1 ura3-1 leu2-3,112 can1-100 mms4::KanMx his3-11,15::pep4::HIS3Mx4 trp1-1:: MMS4::TRP1 MMS4-3FLAG::hph-NT1 MUS81-9myc::nat-NT2*	*MMS4-3FLAG MUS81-9myc*	This study

YLP368	MATa *ade2-1 ura3-1 leu2-3,112 can1-100 mms4::KanMx his3-11,15::pep4::HIS3Mx4 trp1-1::mms4-SSSSSSSS48,55,103,133,221,291,301,428AAAAAAAA::TRP1 MMS4-3FLAG::hph-NT1 MUS81-9myc::nat-NT2*	*mms4-SSSSSSSS48,55,103,133,221,291,301,428AAAAAAAA-3FLAG MUS81-9myc*	This study
YLP369	MATa *RAD5+ ade2-1 ura3-1 leu2-3,112 his3-11,15 trp1-1 can1-100 dbf4-ΔN66::KanMx*	*dbf4-ΔN66*	This study
YLP370	MATa *RAD5+ ade2-1 ura3-1 leu2-3,112 his3-11,15 trp1-1 can1-100 dbf4-ΔN109::KanMx*	*dbf4-ΔN109*	This study
YLP371	MATa *RAD5+ ade2-1 ura3-1 leu2-3,112 his3-11,15 trp1-1 can1-100 dbf4-ΔN66::KanMx sgs1::hph-NT1*	*dbf4-ΔN66 sgs1*	This study
YLP372	MATa *RAD5+ ade2-1 ura3-1 leu2-3,112 his3-11,15 trp1-1 can1-100 dbf4-ΔN109::KanMx sgs1::hph-NT1*	*dbf4-ΔN109 sgs1*	This study
YLP374	MATa *RAD5+ ade2-1 ura3-1 leu2-3,112 his3-11,15 trp1-1 can1-100 dbf4-ΔN66::KanMx yen1::hph-NT1*	*dbf4-ΔN66 yen1*	This study
YLP375	MATa *RAD5+ ade2-1 ura3-1 his3-11,15 trp1-1 leu2-3,112 can1-100 dbf4-ΔN109::KanMx yen1::hph-NT1*	*dbf4-ΔN109 yen1*	This study
YLP438	MATa *ade2-1 ura3-1 trp1-1 leu2-3,112 can1-100 MMS4-3FLAG::hph-NT1 his3-11,15::pep4::HIS3 ULP2-9myc::KanMx*	*MMS4-3FLAG ULP2-9myc*	This study
YLP439	MATa RAD5+ *ade2-1 ura3-1 trp1-1 leu2-3,112 can1-100 cdc5-as1 MMS4-3FLAG::hph-NT1 his3-11,15::pep4::HIS3 ULP2-9myc::KanMx*	*MMS4-3FLAG ULP2-9myc cdc5-as1*	This study
YLP442	MATa *ade2-1 ura3-1 leu2-3,112 can1-100 mms4::KanMx his3-11,15::pep4::HIS3 trp1-1::mms4-SSSSSSSS48,55,103,133,221,291,301,428AAAAAAAA::TRP1 MMS4-3FLAG::hph-NT1 lys1::nat-NT2*	*lys1 mms4-SSSSSSSS48,55,103,133,221,291,301,428AAAAAAAA-3FLAG*	This study
YLP444	MATa *ade2-1 ura3-1 leu2-3,112 can1-100 mms4::KanMx his3-11,15::pep4::HIS3 trp1-1::mms4- S201A::TRP1 MMS4-3FLAG::hph-NT1 MUS81-9myc::nat-NT2*	*mms4-S201A-3FLAG MUS81-9myc*	This study
YLP445	MATa *ade2-1 ura3-1 leu2-3,112 can1-100 trp1-1::MUS81-9myc::TRP1 his3-11,15::bob1-1::HIS3 pep4::hph-NT1 MMS4-3FLAG::KanMx cdc7::nat-NT2 rtt107::kIURA*	*bob1-1 MUS81-9myc cdc7 rtt107*	This study
YLP458	MATa *ade2-1 his3-11,15 can1-100 trp1-1::bar1::TRP1 leu2-3,112::pep4::LEU2 lys1::nat-NT2 ura3-1::pRS306-pGAL1,10-FLAG3-MUS81-His-Strep-MMS4::URA3*	*lys1 pGAL-FLAG3-MUS81-His10-Strep2-MMS4*	This study

YLP459	MATa *ade2-1 trp1-1 leu2-3,112 can1-100 his3-11,15::bob1-1::HIS3 pep4::hph-NT1 lys1::nat-NT2 ura3-1::pRS306-pGAL1,10-FLAG3-MUS81-His-Strep-MMS4::URA3*	*lys1 pGAL-FLAG3-MUS81-His10-Strep2-MMS4*	This study
YLP461	MATa *ade2-1 ura3-1 leu2-3,112 can1-100 mms4::KanMx his3-11,15::pep4::HIS3 trp1-1::mms4-SSSSSSSSSSSS48,55,94,103,133,221,274,291,301,428,545,618AAAAAAAAAAAA::TRP1 MMS4-3FLAG::hph-NT1*	*mms4-SSSSSSSSSSSS48,55,94,103,133,221,274,291,301,428,545,618AAAAAAAAAAAA-3FLAG*	This study
YLP462	MATa *RAD5+ ade2-1 ura3-1 leu2-3,112 his3-11,15 can1-100 mms4::hph-NT1 trp1-1::mms4-SSSSSSSSSSSS48,55,94,103,133,221,274,291,301,428,545,618AAAAAAAAAAAA::TRP1*	*mms4-SSSSSSSSSSSS48,55,94,103,133,221,274,291,301,428,545,618AAAAAAAAAAAA*	This study
YLP463	MATa *RAD5+ ade2-1 ura3-1 leu2-3,112 his3-11,15 can1-100 mms4::hph-NT1 trp1-1::mms4-SSSSSSSS48,55,94,103,133,221,274,291,301,428,545,618AAAAAAAA::TRP1 sgs1::nat-NT2*	*mms4-SSSSSSSSSSSS48,55,94,103,133,221,274,291,301,428,545,618AAAAAAAAAAAA sgs1*	This study
YLP465	MATa *ade2-1 ura3-1 leu2-3,112 can1-100 his3-11,15::bob1-1::HIS3Mx4 pep4::hph-NT1 cdc7::nat-NT2 MMS4-3FLAG::KanMx4 trp1-1::ULP2-9myc::TRP1*	*bob1-1 cdc7 MMS4-3FLAG ULP2-9myc*	This study
YLP466	MATa *ade2-1 ura3-1 leu2-3,112 can1-100 his3-11,15::bob1-1::HIS3Mx4 pep4::hph-NT1 cdc7::nat-NT2 MMS4-3FLAG::KanMx4 trp1-1::SCC1-9myc::TRP1*	*bob1-1 cdc7 MMS4-3FLAG SCC1-9myc*	This study
YLP468	MATa *ade2-1 ura3-1 leu2-3,112 can1-100 mms4::KanMx his3-11,15::pep4::HIS3 trp1-1::mms4-SSSSSSSSSSSS48,55,94,103,133,221,274,291,301,428,545,618AAAAAAAAAAAA::TRP1 MMS4-3FLAG::hph-NT1 MUS81-9myc::nat-NT2*	*mms4-SSSSSSSSSSSS48,55,94,103,133,221,274,291,301,428,545,618AAAAAAAAAAAA-3FLAG MUS81-9myc*	This study
YLP469	MATa *RAD5+ ade2-1 leu2-3,112 trp1-1 can1-100 cdc5-as1 his3-11,15::pep4::HIS3Mx4 lys1::nat-NT2 ura3-1::GAL1,10p-FLAG3-MUS81/His10-Strep2-MMS4::URA3*	*lys1 cdc5-as1 pGAL-FLAG3-MUS81-His10-Strep2-MMS4*	This study
YLP470	MATa *ade2-1 leu2-3,112 trp1-1 can1-100 his3-11,15::bob1-1::HIS3Mx4 pep4::hph-NT1 cdc7::KanMx lys1::nat-NT2 ura3-1::GAL1,10p-FLAG3-MUS81/His10-Strep2-MMS4::URA3*	*lys1 bob1-1 cdc7 pGAL-FLAG3-MUS81-His10-Strep2-MMS4*	This study

YLP471	MATa *ade2-1 his3-11,15 trp1-1 can1-100 leu2-3,112::pep4::LEU2 rtt107::KanMx lys1::nat-NT2 ura3-1::GAL1,10p-FLAG3-MUS81/His10-Strep2-MMS4::URA3*	*lys1 rtt107 pGAL-FLAG3-MUS81-His10-Strep2-MMS4*	This study
YML1601	MATa *his3Δ1 leu2Δ0 met15Δ0 ura3Δ0 ADE2 MMS4-9myc::KanMx trp1-1::pGAL1-CDC5-GFP::TRP1*	*MMS4-9myc pGAL-CDC5-GFP*	Matos et al., 2013
YML3304	MATa *ade2-1 ura3-1 leu2-3,112 can1-100 trp1-1::MUS81-9myc::TRP1 his3-11,15::bob1-1::HIS3 pep4::hph-NT1 MMS4-3FLAG::KanMx dbf4::nat-NT2*	*bob1-1 MUS81-9myc dbf4*	This study (Matos lab)
YML3306	MATa *ade2-1 ura3-1 leu2-3,112 can1-100 trp1-1::MUS81-9myc::TRP1 his3-11,15::bob1-1::HIS3 pep4::hph-NT1 MMS4-3FLAG::KanMx cdc7::nat-NT2*	*bob1-1 MUS81-9myc cdc7*	This study (Matos lab)
YML3447	MATa *ade2-1 ura3-1 leu2-3,112 can1-100 trp1-1::MUS81-9myc::TRP1 his3-11,15::bob1-1::HIS3 pep4::hph-NT1 MMS4-3FLAG::nat-NT2 rtt107::KanMx*	*bob1-1 MUS81-9myc rtt107*	This study (Matos lab)
YSS3	MATa *ade2-1 ura3-1 trp1-1 leu2-3,112 can1-100 MMS4-3FLAG::hph-NT1 his3-11,15::pep4::HIS3Mx4*	*MMS4-3FLAG*	Gritenaite et al., 2014
YFZ020	MATa *ade2-1 ura3-1 trp1-1 can1-100 his3-11,15::pRS303-CDC5-3FLAG-pGAL1-GAL4::HIS3Mx4 leu2-3,112::pep4::LEU2*	*pGAL-CDC5-3FLAG*	This study
YFZ021	MATa *ade2-1 ura3-1 trp1-1 can1-100 his3-11,15::pRS303-DBF4-CDC7-pGAL1-GAL4::HIS3Mx4 pep4::hph-NT1 DBF4-3FLAG::KanMx leu2-3,112::CDC7-9myc::LEU2*	*pGAL-DBF4-3FLAG-CDC7-9myc*	This study

Antibodies

Proteins were detected using specific antibodies: rabbit-anti-Dpb11 (BPF19, Pfander lab), rabbit-anti-Slx4 (2057, Pfander lab), goat-anti-Cdc5 (sc-6733, Santa Cruz), rabbit-anti-Cdc7 (Diffley lab), rabbit-anti-Clb2 (sc-9071, Santa Cruz), goat-anti-Dbf4 (sc-5705; Santa Cruz), rabbit-anti-FLAG (F7425, Sigma), mouse-anti-myc (05-724, clone 4A6; Millipore), mouse-anti-Gal4-AD (TA-C10; Santa Cruz), mouse-anti-Gal4-BD (RK5C1; Santa Cruz).

FACS analysis

$1x10^7$ - $2x10^7$ cells were harvested by centrifugation and resuspended in 70% ethanol + 50 mM Tris pH 7.8. After centrifugation cells were washed with 1 ml 50 mM Tris pH 7.8 (Tris buffer) followed by resuspending in 520 µl RNase solution (500 µl 50 mM Tris pH 7.8 + 20 µl RNase A (10 mg/ml in 10 mM Tris pH 7.5, 10 mM $MgCl_2$) and incubation for 4

h at 37 °C. Next, cells were treated with proteinase K (200 µl Tris buffer + 20 µl proteinase K (10 mg/ml in 50% glycerol, 10 mM Tris pH 7.5, 25 mM $CaCl_2$) and incubated for 30' at 50 °C. After centrifugation cells were resuspended in 500 µl Tris buffer. Before measuring the DNA content, samples were sonified (5''; 50% CYCLE; minimum POWER) and stained by SYTOX solution (999 µl Tris buffer + 1 µl SYTOX). Measurement was performed using FL1 channel 520 for SYTOX-DNA by BD FACSCalibur system.

Acrylamide gel electrophoresis and western blot analysis

Protein samples were separated by standard SDS-polyacrylamide gel electrophoresis in 4-12% Novex NuPAGE Bis-Tris precast gels (ThermoFisher) with MOPS buffer (50 mM MOPS, 50 mM Tris-base, 1.025 mM EDTA, 0.1% SDS, adjusted to pH 7.7). To resolve phosphorylation shifts of Mms4 in Fig. EV1, and of $Ulp2^{9myc}$ or $Scc1^{9myc}$ (Fig. S2E), protein samples were separated in 7% Novex NuPAGE Tris-Acetate precast gel (ThermoFisher) with Tris-Acetate buffer (50 mM Tris-base, 50 mM Tricine, 0.1% SDS, adjusted to pH 8.24).

After electrophoresis, proteins were transferred to a nitrocellulose membrane (Amersham Protran Premium 0.45 µM NC) using a tank blotting system. Membranes were incubated with primary antibodies at 4 °C overnight. Incubation with appropriate secondary antibodies coupled to horseradish peroxidase (HRP) was performed at room temperature for 3 h. Membranes were washed five times for 5 min with western wash buffer (50 mM Tris pH 7.5, 137 mM NaCl, 3 mM KCl, 0.2 % NP-40) and incubated with Pierce ECL western blotting substrate (ThermoFisher) according to the instructions of the manufacturer. Chemiluminescence was detected with a tabletop film processor (OPTMAX, Protec).

Yeast Two-Hybrid analysis

The plasmids used for yeast two-hybrid analysis in this study were based on pGAD-C1 and pGBD-C1. To assay for an interaction between the proteins, respective plasmids were transformed into competent PJ69-7A cells. Transformants were spotted in serial dilution (1:5) either on SC-Leu-Trp plates (control) or on SC-Leu-Trp-His plates (selection) and incubated at 30 °C for 2-3 days. Cells from the control plates were then grown in SC-Leu-Trp to log-phase to take samples for subsequent analysis of the expression of the AD-/BD-fusion proteins by western blot.

Preparation of whole-cell extracts (alkaline lysis/TCA)

Cell pellets were re-suspended in 1 ml pre-cooled H_2O and incubated with 150 µl of freshly prepared lysis solution (1.85 M NaOH, 7.5% beta-mercaptoethanol) at 4 °C for 15 min. Then, the lysate was admixed with 150 µl 55% trichloroacetic acid (TCA) and incubated at 4 °C for 10 min. After centrifugation and careful aspiration of the supernatant, the precipitated proteins were re-suspended in 50 µl HU-buffer (8 M urea, 5% SDS, 200 mM Tris pH 6.8, 1.5% dithiothreitol, traces of bromophenol blue) and incubated at 65 °C for 10 min.

Synchronization of cells

Logarithmic growing cells were synchronized in mitosis by nocodazole (5 µg/ml), in S-phase by HU (200 mM), or in G1-phase by α-factor (5-10 µg/ml). Release from G1 synchronization into S-phase was performed by washing twice in pre-warmed YPD, and suspending cells in pre-warmed YPD with nocodazole, with HU or without chemical.

Drug treatment

DNA damage in liquid cultures was induced by addition of phleomycin to a final concentration of 50 µg/ml.

For solid media, concentrations of methyl methanesulfonate (MMS) were as indicated in the figures. Cells from stationary grown ON cultures were spotted in serial dilution (1:5) and incubated at 30 °C for 2-3 days.

Interaction assays

After cell growth under the indicated conditions, yeast extracts were obtained by freezer mill lysis (Spex Sample Prep) in lysis buffer (100 mM Hepes pH 7.6, 200 mM KOAc, 0.1% NP-40, 10% glycerol, 2 mM b-ME, 100 mM ocadaic acid, 10 mM NaF, 20 mM b-glycerophosphate, 400 µM PMSF, 4 µM aprotinin, 4 mM benzamidin, 400 µM leupeptin, 300 µM pepstatin A). Co-IP was performed for 2 hours with head-over-tail rotation at 4 °C using anti-FLAG agarose resin (Sigma). Non-specific background was removed by six washes and bound proteins were eluted by incubation with 0.5 mg/ml 3X FLAG-peptide (Sigma). The TCA-precipitated eluates were resolved on 4-12% NuPAGE gradient gels (Invitrogen), and analyzed by standard Western blotting techniques.

SILAC-based quantitative mass-spectrometry

For Co-IP experiments followed by mass spectrometry analysis, cells deficient in lysine biosynthesis were grown in synthetic complete (SC) medium supplemented with normal

lysine ("light" medium) or heavy-isotope-labeled lysine (Lys6 or Lys8; "heavy" medium) from Cambridge Isotope Laboratories and arrested in G2/M phase with nocodazole. In SILAC experiments with high-copy expression of *MUS81-MMS4*, overexpression was induced by addition of 2% galactose for 2 h after nocodazole arrest.

Lysates were prepared by harvesting cells in equal amounts after growth under the indicated conditions. After co-IP, eluted proteins from light and heavy cultures were pooled, TCA precipitated and separated on a 4-12% NuPAGE Bis-Tris gel (Invitrogen). The gel was stained with GelCode Blue (Thermo Scientific). The gel lane was excided into ten slices and peptides were analyzed by LC-MS/MS after in-gel Lys-C digestion. Samples were measured on an LTQ-Orbitrap and analyzed using MaxQuant (Cox & Mann, 2008).

For analysis of proteins (Fig. S1A, 2E, S2A, EV3A, 6D, S6A), log2 values of H/L ratios from two label-switch experiments without ratio count cut-off were plotted against each other.

For analysis of phosphorylation sites from endogenous protein levels (Fig. 3A-B, S7A), H/L ratios for Mms4 peptides were calculated from the corresponding H and L intensities of MS evidences and plotted in their log2 values against the log10 values of the peptide's overall intensity. Evidences of non-phosphorylated Mms4 peptides are shown in grey, evidences of phosphorylated peptides are shown in black. Phosphorylated peptides were sorted into categories according to their phosphorylation status. Putative DDK target sites were differentiated into the categories pSpS (red), pSS (orange) or SpS (yellow), in which the respective residues of the (S/T)(S/T) motif were phosphorylated (detected phosphorylation probability >0.7). Phosphorylated peptides matching the Cdc5 consensus site are coloured in blue. Numbers indicate the phosphorylated residue in the depicted peptide. An asterisk marks peptide evidences that contained measured intensity values exclusively in the H or L sample. Their ratio value was set to a fixed value.

For analysis of phosphorylation sites from overexpressed *MUS81-MMS4* (Fig. 3C-D, S7B), log2 values of H/L ratios of Mms4 peptides were plotted against the log10 values of the peptide's intensity. Depicted are phosphorylated peptides only. Peptides were sorted into categories according to their phosphorylation status. Putative DDK target sites were differentiated into the categories pSpS (red), pSS (orange) or SpS (yellow), in which the respective residues of the (S/T)(S/T) motif were phosphorylated (detected phosphorylation probability >0.7). Phosphorylated peptides matching the Cdc5 consensus site are coloured in blue. All other phosphorylated peptides are marked in grey. Bars depict the mean of the ratios of the respective category.

Protein purification

CDK was expressed in *E. coli* BL21 pRIL cells (Agilent). Mus81-Mms4, DDK and Cdc5 were overexpressed in *S. cerevisiae* from a galactose-inducible GAL1-10 promoter. All purification steps were performed on ice or at 4 °C.

Purification of Mus81-Mms4 from S. cerevisiae

^{FLAG3}*MUS81* and $^{GST\text{-}HIS10\text{-}STREP2}$*MMS4* were cloned under the control of the *GAL1,10* bidirectional promoter in a pRS306 derivative plasmid. The resulting vector was linearized with StuI and integrated at the *ura3-1* locus of a W303 *pep4Δ* strain.

The resulting MGBY3294 strain was grown in YP+2% raffinose to mid-log phase at 25 °C and protein expression was induced by addition of 2% galactose. Cells (10 liters at ~2-4x10^7 cells/ml) were harvested, washed and resuspended in a small volume of A500 buffer (40 mM Tris-HCl pH 7.5, 500 mM NaCl, 20% glycerol, 0.1% NP-40, 1 mM DTT) containing phosphatase and protease inhibitors and mechanically disrupted. The frozen lysate was resuspended in 2 volumes of A500, cleared by ultracentrifugation and incubated with anti-FLAG M2 agarose beads (Sigma) for 1 h at 4 °C. After extensive washing of the beads in A500, Mus81-Mms4 was dephosphorylated by treatment with 10,000 units of lambda phosphatase (New England Biolabs) for 30 min at room temperature. Beads were washed in A500 buffer and Mus81-Mms4 was then eluted with 3 volumes of A500 supplemented with 0.5 mg/ml 3X FLAG-peptide (Sigma). The eluate was then adjusted to 5 mM imidazole and proteins were loaded onto a Ni-NTA column (Qiagen). The column was washed with A500 buffer containing increasing concentrations of imidazole up to 50 mM, and finally Mus81-Mms4 was eluted with A500 containing 300 mM imidazole. The eluate was dialyzed extensively against A500, and stored in aliquots at -80 °C. Protein concentrations were determined using the Bradford assay (BioRad) and on Coomassie-stained PAGE gels using BSA as the standard, which also confirmed absence of phosphorylation-dependent electrophoretic migration shifts. Control experiments confirmed the absence of non-specific endo- or exonuclease activities.

Purification of bacterially expressed CDK2/cycA$^{\Delta N170}$

To generate CDK2/cycA$^{\Delta N170}$ complex, ^{GST}CDK2 and ^{His6}cycA$^{\Delta N170}$ were expressed separately. Bacteria with either expression plasmids were grown in 1 l LB medium supplemented with antibiotics to mid-log phase. Both cultures were cooled down on ice for 5 min to increase chaperone expression followed by addition of 1 mM IPTG and incubation for 20 h at 20 °C. Cells were pelleted and resuspended in 40 ml lysis buffer

(300 mM NaCl, 20 mM HEPES pH 7.6, 5 mM β-mercaptoethanol, 0.01% NP-40, 100 µM AEBSF, 1x complete protease inhibitor cocktail EDTA-free) followed by lysis with an EmulsiFlex-C3 system for three rounds at 1,000 bar. Cell debris was spun down at 140,000 g for 45 min. To allow complex formation between both subunits, extracts were pooled and incubated for 45 min. For glutathione affinity chromatography, 1 ml bed volume of equilibrated Glutathione Sepharose beads were added to the extract and incubated for 2 h. Beads were then washed four times with 25 CV Wash Buffer B2 (300 mM NaCl, 20 mM HEPES pH 7.6, 5 mM β-mercaptoethanol, 0.01% NP-40) before elution was achieved by protease cleavage. For this purpose, beads were resuspended in 1 CV wash buffer (150 mM NaCl, 20 mM HEPES pH 7.6, 5 mM β-mercaptoethanol, 0.01% NP-40) and incubated together with 250 U GST-PreScission protease (MPIB Core Facility) for 18 h. The eluate was then adjusted to 300 mM NaCl and 6 mM imidazole for subsequent Ni-NTA affinity chromatography. Here, a bed volume of 1 ml equilibrated Ni-NTA Agarose (Qiagen) was added to the eluate and incubated for 1 h. Beads were subsequently washed four times with 15 CV wash buffer (300 mM NaCl) + 6 mM imidazole and five times with 2 CV wash buffer (300 mM NaCl) + 6 mM imidazole + 5% glycerol. Elution was then performed with wash buffer (300 mM NaCl) + 250 mM imidazole. Fractions containing CDK were pooled and dialyzed by stirring two times against 300 volumes of dialysis buffer (150 mM NaCl, 50 mM HEPES pH 7.6, 0.1% NP-40, 2 mM β-mercaptoethanol, 10% glycerol) for 4 h in a Slide-A-Lyzer Dialysis Casette (Thermo Scientific). Dialysed material was recovered, aliquoted, snap-frozen and stored at -80 °C.

Purification of Cdc5 from S. cerevisiae

YFZ020 was grown in 10 l YP medium + 2% raffinose at 30 °C until mid-log phase before expression was induced by addition of 2% galactose. After 4 h of induction, yeast cells were harvested and washed twice with 250 ml 1 M Sorbitol + 25 mM HEPES pH 7.6. The pellet was resuspended in 1 volume of lysis buffer (500 mM NaCl, 100 mM HEPES pH 7.6, 0.1% NP-40, 10% glycerol, 2 mM β-mercaptoethanol, 400 µM PMSF, 4 µM aprotinin, 4 mM benzamidin, 400 µM leupeptin, 300 µM pepstatin A, 4x complete protease inhibitor cocktail, EDTA-free) and frozen drop-wise in liquid nitrogen. Frozen cell drops were crushed using a freezer/mill system (Spex Sample Prep). Cell powder was thawed on ice and centrifuged at >185,000 g for 1 h. The clear phase was recovered and incubated with 1 ml bed volume of anti-FLAG M2 resin (Sigma) equilibrated in lysis buffer. After 2 h of incubation, the resin was washed five times with 10 CV of wash buffer (500 mM NaCl, 100 mM HEPES pH 7.6, 0.1% NP-40, 10% glycerol, 2 mM β-

mercaptoethanol). Two elution steps were performed by adding 1 CV 0.5 mg/mL 3FLAG peptide in wash buffer and incubation for 30 min. Obtained fractions were pooled, brought to a conductivity of 10 mS/cm (100 mM salt) and subjected to anion exchange chromatography using a MonoQ 5/50 GL column with a salt gradient of 0.1-1 M NaCl over 20 CV. $Cdc5^{3FLAG}$ eluted at a conductivity of ~15 mS/cm. Kinase containing fractions were aliquoted, snap-frozen and stored at -80 °C.

Purification of DDK from S. cerevisiae

DDK was purified as described by Gros *et al.* with modifications (Gros *et al.* 2014). YFZ021 cells were grown in 10 l YP medium + 2% raffinose at 30 °C until mid-log phase before expression was induced by addition of 2% galactose. After 4 h of incubation, yeast cells were harvested and washed twice with 250 ml 1 M Sorbitol + 25 mM HEPES pH 7.6. The pellet was resuspended in 1 volume of lysis buffer (400 mM NaCl, 100 mM HEPES pH 7.6, 0.1% NP-40, 10% glycerol, 2 mM β-mercaptoethanol, 400 µM PMSF, 4 µM aprotinin, 4 mM benzamidin, 400 µM leupeptin, 300 µM pepstatin A, 4x complete protease inhibitor cocktail EDTA-free) and frozen drop-wise in liquid nitrogen. Frozen cell drops were crushed using a freezer/mill system. Cell powder was thawed on ice and centrifuged at >185,000 g for 1 h. The clear phase was recovered and incubated with 1 ml bed volume of anti-FLAG M2 resin (equilibrated in lysis buffer). After incubation for 2 h at 4 °C, the resin was washed six times with 2 CV wash buffer (400 mM NaCl, 100 mM HEPES pH 7.6, 0.1% NP-40, 10% glycerol, 2 mM β-mercaptoethanol). For λ-phosphatase treatment, beads were resuspended in 1 CV wash buffer + 2 mM $MnCl_2$ + 900 U λ-phosphatase (New England Biolabs) and incubated for 1 h at 30 °C in a tabletop thermoshaker. Beads were recovered and bound DDK was eluted twice with 1 CV 0.5 mg/ml 3FLAG peptide in wash buffer for 30 min. Elutions were pooled, concentrated using a Vivaspin 500 MWCO 50.000 (GE healthcare) and fractionated by size exclusion chromatography using a Superdex 200 GL 10/300 column (GE healthare, equilibrated in wash buffer) over 1.2 CV. DDK containing fractions were pooled, brought to a conductivity of 10 mS/cm (100 mM salt) and fractionated by anion exchange chromatography using a MonoQ 5/50 GL column with a salt gradient of 0.1-1 M NaCl over 20 CV. DDK containing fractions eluted at ~24-26 mS/cm and were aliquoted, snap frozen and stored at -80 °C.

In vitro kinase assays

Sequential kinase assays with purified Mus81-Mms4

Kinase assays were performed as described previously (Pfander & Diffley, 2011; Mordes *et al.*, 2008) with minor modifications.

Per reaction 20 pmol Mus81-Mms4 were used as substrate for 10 pmol kinase (CDK2/cyclinA$^{\Delta N170}$, DDK and/or Cdc5) in a 50 µL reaction volume containing 5 µg BSA. For sequential phosphorylation reactions Mus81-Mms4 was immobilized to Glutathione Sepharose 4B resin (GE Healthcare) for 1 h at 4 °C shaking. Beads were washed twice with binding buffer-100 (100 mM Hepes pH 7.6, 100 mM KOAc, 10% glycerol, 0.02% NP-40, 2 mM β-mercaptoethanol) and once with kinase buffer (10 mM HEPES pH 7.6, 100 mM KOAc, 50 mM β-glycerophosphate, 10 mM $MgCl_2$, 2 mM β-mercaptoethanol), and aliquoted. Residual buffer was removed.

Priming phosphorylation reactions were performed by addition of 10 pmol (of each) kinase and started by addition of 2 or 10 mM (Fig. 1B, S1C) ATP. For samples without priming reaction the equivalent volume of added kinase was substituted by kinase buffer. After 30 min at 30 °C in a tabletop shaker beads were washed twice with binding buffer-200 (100 mM Hepes pH 7.6, 200 mM KOAc, 10% glycerol, 0.02% NP-40, 2 mM β-mercaptoethanol), once with binding buffer-100 and once with kinase buffer.

The consecutive kinase reaction was performed by addition of 10 pmol kinase and started by addition of 1 mM ATP + 5 µCi γ[^{32}P]-ATP (PerkinElmer). After incubation for 30 min shaking at 30 °C reactions were stopped by addition of Laemmli sample buffer followed by boiling at 95 °C.

For kinetic analysis of the phosphorylation reactions (Fig. S1C), the second kinase reaction was upscaled to 100 µl and 20 µl samples were taken at indicated time points.

Proteins were separated on NuPAGE Novex 12% Bis-Tris gels (ThermoFisher) and analyzed by autoradiography using a Typhoon FLA 9500 imager (GE healthcare).

Kinase assays using synthetic Mms4 peptides

Kinase reactions were performed with 25 µg desthiobiotin-labelled Mms4 peptide and 10 pmol kinase in kinase buffer (10 mM HEPES pH 7.6, 10 mM β-glycerophosphate, 10 mM $MgCl_2$, 5 mM $Mg(OAc)_2$, 2 mM β-mercaptoethanol) with 100 mM KOAc in a 50 µL reaction volume containing 5 µg BSA. Reactions were started by addition of 1 mM ATP + 5 µCi γ[^{32}P]-ATP. After incubation for 30 min shaking at 30 °C reactions were stopped by addition of Laemmli sample buffer followed by boiling at 95 °C. Proteins were separated on NuPAGE Novex 12% Bis-Tris gels (ThermoFisher) in MES buffer and analyzed by autoradiography using a Typhoon FLA 9500 imager (GE healthcare).

Nuclease assays

5'-Cy3-end-labelled oligonucleotides were used to prepare synthetic nicked Holliday Junctions (nHJ) as described (Rass & West, 2008). Nuclease assays were carried out with immunopurified Mus81^{9myc} of Mus81^{3FLAG} (Fig. S4A) from cells arrested in mitosis with nocodazole. The anti-myc/anti-FLAG immunoprecipitates were extensively washed and mixed with 10 µl reaction buffer (50 mM Tris-HCl pH 7.5, 3 mM $MgCl_2$) containing 30 ng 5'-Cy3-end-labelled nHJs or RFs [11]. Reactions were incubated for the indicated times with gentle rotation at 30 °C and stopped by addition of 5 µl 10 mg/ml proteinase K and 2% SDS, and further incubation at 37 °C for 1 h. Loading buffer was added and fluorophore-labelled products were separated by 10% PAGE, and analyzed using a Typhoon scanner. Substrate cleavage was normalized using the level of immunoprecipitated Mus81^{9myc} as reference.

DSB-induced recombination assay

The DSB-induced recombination assay was performed as described previously (Ho *et al.*, 2010). In brief, diploids were grown in liquid YPAR (YPR + 40 mg/l Adenine) until the cultures reached an OD_{600} of 0.5. Cells were arrested with nocodazole and I-SceI expression was induced by adding galactose to a final concentration of 2%. After 2.5 h cells were plated onto YPAD (YPD + 10 mg/l Adenine), incubated for 3-4 days and then replica plated onto YPAD+Hyg+Nat, YPAD+Hyg, YPAD+Nat, SC-Met, SC-Ura, and SCR-ADE+Gal media to classify recombination events. The different classes depicted arise from repair of DSBs by either short tract or long tract gene conversion which produces ade2-n or ADE+ recombinants, respectively (white class: two short tract conversions; red class: two long tract conversions; red/white class: one short and one long tract conversion). Within the distinct classes CO events are measured by the number of colonies that have rendered both daughter cells homozygous for the HPH and NAT marker.

Appendix References

Cox J & Mann M (2008) MaxQuant enables high peptide identification rates, individualized p.p.b.-range mass accuracies and proteome-wide protein quantification. *Nat Biotechnol* **26**(12)**:** 1367-1372

Gritenaite D, Princz LN, Szakal B, Bantele SCS, Wendeler L, Schilbach S, Habermann BH, Matos J, Lisby M, Branzei D & Pfander B (2014) A cell cycle-regulated Slx4-Dpb11 complex promotes the resolution of DNA repair intermediates linked to stalled replication. *Genes Dev* **28:** 1604–1619

Gros J, Devbhandari S & Remus D (2014) Origin plasticity during budding yeast DNA replication *in vitro*. *EMBO J* **33**(6)**:** 621-636

Ho CK, Mazón G, Lam AF & Symington LS (2010) Mus81 and Yen1 promote reciprocal exchange during mitotic recombination to maintain genome integrity in budding yeast. *Mol Cell* **40:** 988–1000

James P, Halladay J & Craig EA (1996) Genomic libraries and a host strain designed for highly efficient two-hybrid selection in yeast. *Genetics* **144:** 1425-1436

Knop M, Siegers K, Pereira G, Zachariae W, Winsor B, Nasmyth K & Schiebel E (1999) Epitope Tagging of Yeast Genes using a PCR-based Strategy: More Tags and Improved Practical Routines. *Yeast* **15:** 963-972

Mordes DA, Nam EA & Cortez D (2008) Dpb11 activated the Mec1-Ddc2 complex. *Proc Natl Acad Sci U S A* **105**(48)**:** 18730-18734

Pfander B & Diffley JFX (2011) Dpb11 coordinates Mec1 kinase activation with cell cycle-regulated Rad9 recruitment. *EMBO J.* **30:** 4897–4907

Rass U & West SC (2006) Synthetic junctions as tools to identify and characterise Holliday junction resolvases. *Meth Enzymol* **408:** 485-501

Thomas BJ & Rothstein R (1989) Elevated recombination rates in transcriptionally active DNA. *Cell* **56:** 619-630

Expanded View Figures

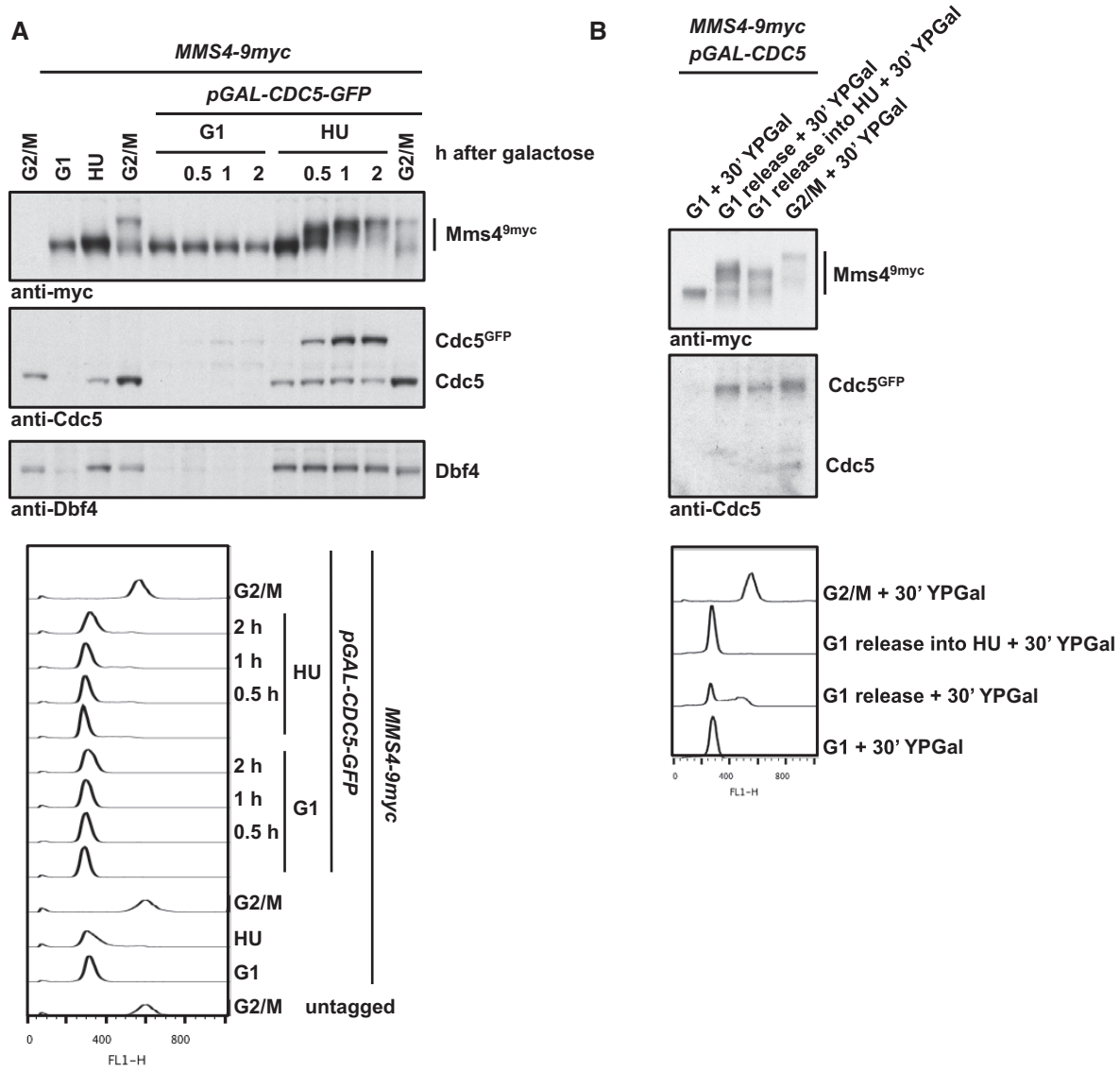

Figure EV1. Cdc5 restricts Mms4 hyperphosphorylation to mitosis.

A Overexpression of *CDC5* in S phase results in premature Mms4 hyperphosphorylation. Western blot analysis of $Mms4^{9myc}$, Cdc5 and Dbf4 from whole-cell extracts (upper panel) and FACS data (lower panel). Cells were arrested in G1 (with alpha-factor), S phase (with HU) or G2/M phase (with nocodazole). After arrest, $CDC5^{GFP}$ overexpression was induced by addition of 2% galactose for the indicated time to cells harbouring an additional copy of GFP-tagged *CDC5* under the *GAL1* promoter. Samples were run in 7% Tris-acetate gels.

B Mms4 hyperphosphorylation by *CDC5* overexpression in S phase is reduced in HU-treated cells. Western blot analysis of $Mms4^{9myc}$ and Cdc5 from precipitated whole-cell extracts (upper panel) and FACS data (lower panel) of cells arrested in G1 (with alpha factor) or G2/M phase (with nocodazole), or released to S phase (with or without HU). $CDC5^{GFP}$ overexpression was induced for 30 min by addition of 2% galactose to cells harbouring an additional copy of GFP-tagged *CDC5* under the *GAL1* promoter. Note that upon *CDC5* overexpression cells are partially defective in bulk replication. Samples were run in 7% Tris-acetate gels.

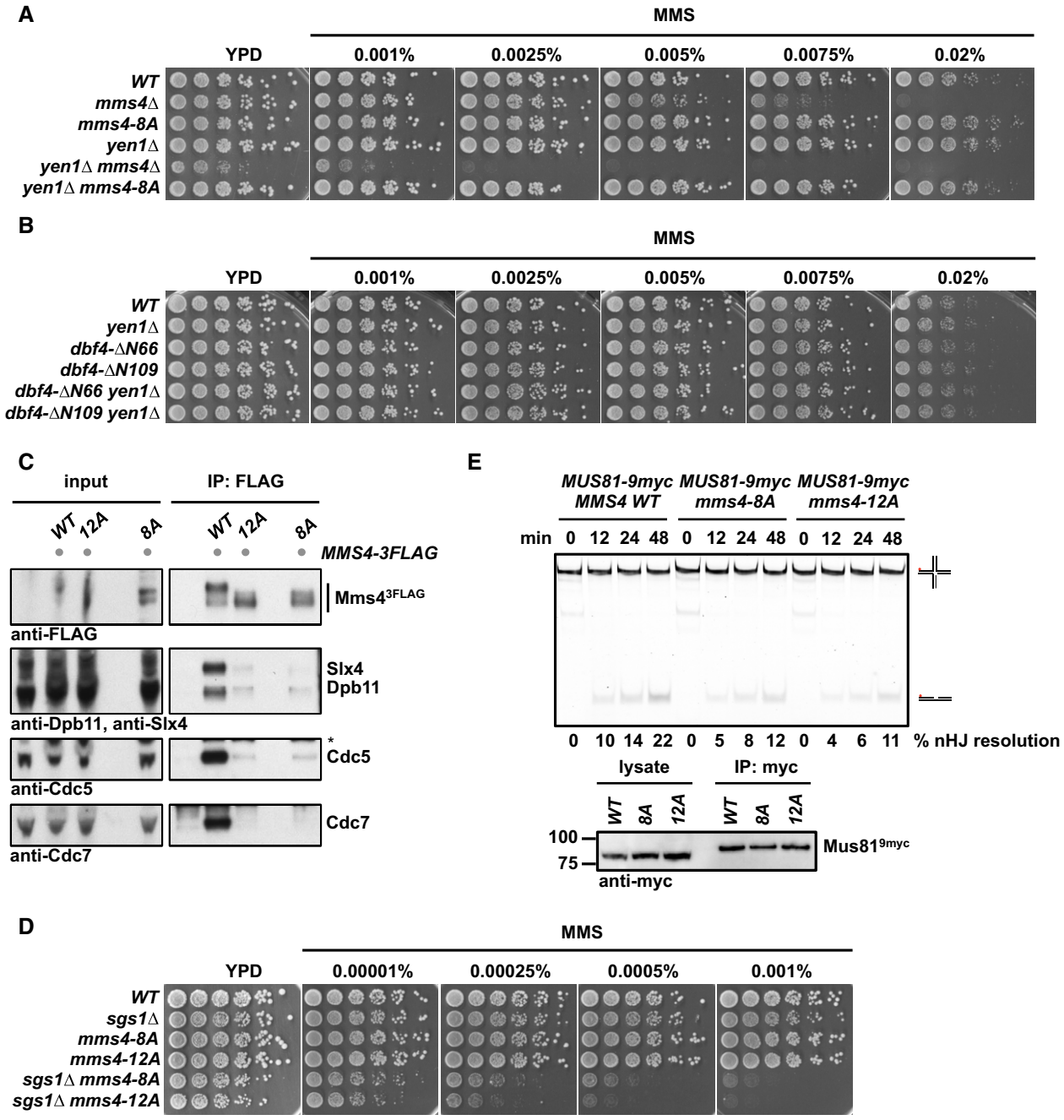

Figure EV2. Phenotypic analysis of Mms4 variants deficient in (S/T)(S/T) phosphorylation sites.

A, B The *mms4-8A* mutation or lack of Cdc5-DDK interaction does not lead to a synthetic hypersensitivity towards MMS in the *yen1*Δ background. Spotting assay as in Fig 4D and E.

C–E Additional mutation of 4 additional (S/T)(S/T) motifs in the background of the *mms4-8A* mutant (*mms4-12A*) leads to a reduction in the Mms4 phosphorylation shift (C), increases the hypersensitivity to MMS in the *sgs1*Δ background (D) and shows a slightly but not significantly decreased activity of Mus81-Mms4 (E). (C) $Mms4^{3FLAG}$ pull down as in Fig 1A, but in G2/M-arrested cells in untagged, WT, *mms4-12A* and *mms4-8A* backgrounds. Asterisk marks a cross-reactive band. (D) Spotting assay as in Fig 4D and E. (E) Resolution assay using a nHJ substrate and $Mus81^{9myc}$-$Mms4^{3FLAG}$ purified from mitotically arrested WT, *mms4-8A* or *mms4-12A* cells. Lower panel: Western blot samples of anti-myc IPs.

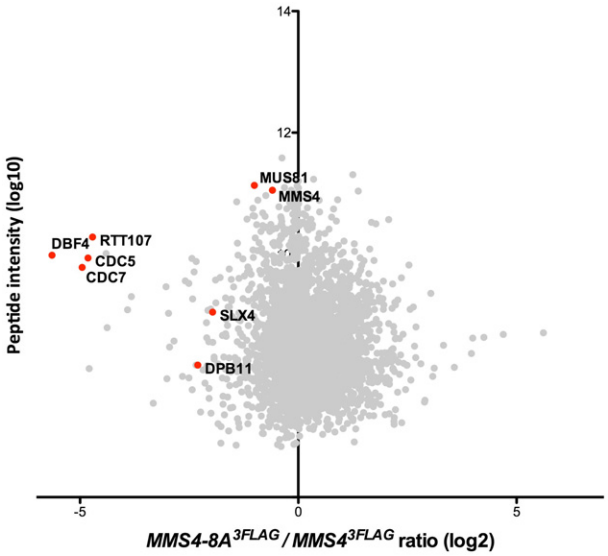

Figure EV3. A defect in the phosphorylation of Mms4 (S/T)(S/T) sites (*mms4-8A*) causes reduced association of Cdc5, DDK and Rtt107 with Mus81-Mms4.

SILAC-based quantification of $Mms4^{3FLAG}$ pull downs in WT vs. *mms4-8A* cells. Plotted are the H/L ratios against peptide intensity

Discussion

The resolution of JM structures during HR involves the enzymatic activity of the SSEs Mus81-Mms4 and Yen1 which are regulated in a cell cycle-specific manner. This cell cycle regulation is implicated by phosphorylation and dephosphorylation events on Mus81-Mms4 and Yen1 which leads to upregulation of the catalytic activity specifically during M-phase (Matos et al., 2011, Gallo-Fernandez et al., 2012, Matos et al., 2013, Szakal and Branzei, 2013, Blanco et al., 2014, Eissler et al., 2014, Garcia-Luis et al., 2014, Blanco and Matos, 2015). On the one hand this clear upregulation of the catalytic activity in M-phase is thought to protect cells from unwanted cleavage of replication fork structures during S-phase (Matos et al., 2013, Blanco et al., 2014, Szakal and Branzei, 2013). On the other hand, the involvement of Mus81-Mms4 during the resolution of structures arising from replication perturbation in S-phase is still questioning when the function of Mus81-Mms4 is required (Xiao et al., 1998, Boddy et al., 2001, Interthal and Heyer, 2000, Haber and Heyer, 2001, Kaliraman et al., 2001, Mullen et al., 2001, Doe et al., 2002, Fabre et al., 2002, Bastin-Shanower et al., 2003, Kai et al., 2005, Hanada et al., 2007, Shimura et al., 2008, Regairaz et al., 2011, Fu et al., 2015, Xing et al., 2015, Lemacon et al., 2017).

Here, I will discuss our attempts to address this discrepancy between the implications of Mus81-Mms4 in S-phase and the apparent upregulation of the catalytic activity in M-phase as well as highlight the advancements of our knowledge regarding Mus81-Mms4 regulation made by this study. More specifically, I have implemented an advanced toolbox of cell cycle tags for studying cell cycle regulation of different proteins – including Mus81-Mms4. This toolbox of cell cycle tags allowed me to clearly attribute the essential function of the SSE to M-phase and thus expand our knowledge about the timing of Mus81-Mms4 function (Bittmann et al., 2020). Furthermore, I contributed to the discovery of an additional layer of regulation occurring on Mus81-Mms4 in M-phase (Princz et al., 2017) and I will discuss a model for the connection of these regulatory mechanisms with the observed function of Mus81-Mms4 during M-phase.

1 Cell cycle tags as valuable tool to study cell cycle regulation

1.1 The limitations of previous cell cycle tag systems

Cell cycle tags can be a valuable tool to study cell cycle regulation of proteins and we have therefore chosen them to analyse the possible functions of Mus81-Mms4 in S- and M-phase. Generally, cell cycle tags allow to limit the expression of a protein of interest to a specific cell cycle phase. Fused to the protein of interest, cell cycle tags lead to cell cycle-regulated expression and degradation of that protein. Specifically, cell cycle-restricted expression is achieved by the use of regulatory elements of a protein with cycling abundance, like a cyclin or the CDK inhibitor Sic1 (Fig. 1A, (Bittmann et al., 2020); (Karras and Jentsch, 2010, Hombauer et al., 2011, Johnson et al.,

2016)). Using these regulatory elements (the 5´UTR + the N-terminal degrons) in form of cell cycle tags has allowed to successfully transmit the cell cycle-specific expression of cyclins or Sic1 to other proteins (Karras and Jentsch, 2010, Hombauer et al., 2011, Johnson et al., 2016).

Previous to this study, three cell cycle tags have been applied to limit protein expression to either S-, M- or G1-phase. These three tags use the regulatory elements of the S-phase cyclin Clb6, the M-phase cyclin Clb2 and the G1 regulator Sic1, respectively (Karras and Jentsch, 2010, Hombauer et al., 2011, Johnson et al., 2016). Although these constructs in principal restrict the expression of the fused protein to the intended cell cycle phase (Fig. 1C, (Bittmann et al., 2020); (Karras and Jentsch, 2010, Hombauer et al., 2011, Johnson et al., 2016)), we observed that these three constructs resulted in very different peak expression levels when fused to the same protein (**Figure 7**) (Fig. 1B, (Bittmann et al., 2020)).

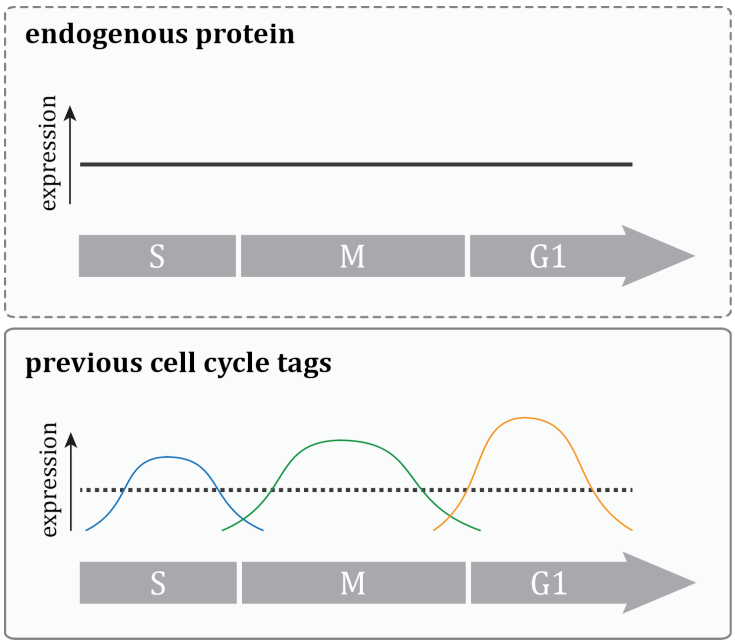

Figure 7: Problems of the cell cycle tag methodology. In contrast to the endogenous protein (upper) which is expressed throughout the cell cycle, a cell cycle-tagged version of that protein (lower) is restricted to a certain cell cycle phase. Previously, three cell cycle tags were developed for S-, M- and G1-phase, respectively, which showed different expression levels among each other and did not allow to adjust expression levels, for example to endogenous protein levels (dotted line, lower).

This fact made it impossible to compare phenotypes arising from the restriction to different cell cycle phases and thereby excluded the complementary use of cell cycle tags in different cell cycle phases. Indeed, studies applying cell cycle tags often focused on the use of a single cell cycle tag only (Karras and Jentsch, 2010, Karras et al., 2013, Gonzalez-Prieto et al., 2013, Renaud-Young et al., 2015, Hung et al., 2017, Lafuente-Barquero et al., 2017, Kahli et al., 2019). However, this initial approach was severely limited as it can only address the involvement of a certain protein in one specific cell cycle phase but cannot formerly rule out or validate that the protein is required (or not) in another cell cycle phase. The interpretation of results obtained with one single cell cycle tag construct is therefore extremely difficult and would profit from

complementary data derived from additional cell cycle tag constructs restricting to other cell cycle phases. Additionally, the limited number of a single cell cycle tag per cell cycle phase did not allow to adjust peak expression levels, for example to the level of the endogenous protein. As the expression level of a cell cycle-tagged protein is dictated by the corresponding cell cycle tag, cell cycle-restricted expression with the Clb6-, Clb2- and Sic1-tag can lead to over- or under-expression compared to the endogenous protein levels (**Figure 7**). In this case an observed phenotype can be the consequence of either the differing protein level or the restriction of the protein to a certain cell cycle phase and is therefore difficult to be interpreted.

In summary, the limiting number of three cell cycle tags with fixed expression levels extremely minimized the potential of the cell cycle tag system and we therefore attempted to overcome these limitations by introducing an increased number of cell cycle tags which would allow to restrict expression with adjusted protein levels. The flexibility in the adaption of expression levels would thereby not only allow to derive complementary data in different cell cycle phases but also to compare the effects of the restriction to the endogenous scenario.

1.2 An advanced cell cycle tag toolbox

To achieve an increase in the number of cell cycle tags and concomitantly in the range of expression levels (i) we included additional promoter and degron sequences from the S-phase cyclin Clb5 and the M-phase cyclin Clb1, (ii) we created chimeric fusions between promoter and degron sequences of different S- and M-phase cyclins (for example Clb5 promoter together with the Clb6 degron) and (iii) we introduced truncations and upstream out-of-frame ATGs into the promoter sequences to influence protein expression by reduced mRNA stability and reduced translation rates, respectively (Fig. 1A, (Bittmann et al., 2020)). Together these attempts resulted in an advanced toolbox of 46 cell cycle tag constructs that allow to restrict target protein expression to S-, M- and G1-phase and now for the first time with a broad range of peak expression levels.

In principal, these modifications to the cell cycle tag technology now permit to overcome the limitations described before for the initial set of cell cycle tags. Specifically, the large number of cell cycle tags and the concomitant variation of protein levels allows to (i) compare phenotypes arising from the restriction to different cell cycle phases and (ii) adjust expression levels to endogenous protein levels.

Another important aspect to consider in the context of expression is the dynamic nature introduced by the cell cycle-restricted expression. In contrast to the endogenous scenario where the protein of interest is usually expressed steadily throughout the cell cycle, expression from a cell cycle tag involves the production and degradation of the protein in a relatively short timeframe. A cell cycle-tagged protein is therefore not expressed with constant level throughout that cell cycle phase but will display reduced expression at the borders of the cell cycle phase

compared to its peak expression during that cell cycle phase. The overall adaptation of expression levels therefore poses an inherent problem: while adjustment of peak expression levels to the endogenous protein level will result in under-expression at cell cycle transitions, adjustment of levels at cell cycle transitions will lead to constant over-expression during that cell cycle phase (**Figure 8**, upper).

To complement for that problem, we decided to make use of the flexibility of the advanced cell cycle tag toolbox and perform cell cycle tag experiments with two complementary sets of cell cycle tags (**Figure 8**, lower). The first set of tags is chosen to result in peak expression comparable to endogenous protein levels ("low"). This will entail under-expression at cell cycle transitions and thus limit the timeframe of action to a short fraction of the corresponding cell cycle phase. Therefore, a second set of cell cycle tags is chosen to result in overall higher expression levels compared to the endogenous protein ("high"). This will lead to constant over-expression during that cell cycle phase but have the advantage of a timeframe of action that spans the whole cell cycle phase (**Figure 8**, lower).

The validity of this strategy becomes apparent with the example of the Mus81-Mms4 endonuclease. In order to achieve cell cycle-restricted "low" and "high" expression, we have created two sets of cell cycle-restricted Mus81-Mms4 variants: S^{low}-Mus81-Mms4/M^{low}-Mus81-Mms4 ("low") and S^{high}-Mus81-Mms4/M^{high}-Mus81-Mms4 ("high") (Fig. 2A, (Bittmann et al., 2020)). In addition to the differences resulting from S- and M-phase restriction (e.g. pronounced MMS sensitivity of S^{low}/S^{high} vs. no/little sensitivity of M^{low}/M^{high}; Fig. 3A,B, (Bittmann et al., 2020)), "low" and "high" sets of tags display similar, but non-identical phenotypes (e.g. degree of MMS sensitivity S^{low} vs. S^{high} and M^{low} vs. M^{high}; Fig. 3A,B, (Bittmann et al., 2020)). The different tendencies between the "low" and "high" set of tags underline the importance of using two complementary sets of cell cycle tags to facilitate interpretations originating from over- or under-expression during the restricted cell cycle phase. In detail, when using the "low" set of cell cycle tags we observed a slight DNA damage sensitivity for M^{low}-Mus81-Mms4 (Fig. 3A, 4B, 4E, (Bittmann et al., 2020)) (note that defects in Mus81-Mms4 function lead to DNA damage sensitivity). As we did not observe such a defect when using M^{high}-Mus81-Mms4 (Fig. 3B, D, F, 4C-E, (Bittmann et al., 2020)), we set out to understand how this defect in M^{low}-Mus81-Mms4 is caused and performed further control experiments which showed that this defect is due to under-expression of M^{low}-Mus81-Mms4 in M-phase. Without these control experiments and the complementary M^{high}-Mus81-Mms4 we would have interpreted the observed DNA damage sensitivity of M^{low}-Mus81-Mms4 as insufficient function of Mus81-Mms4 during M-phase. Consequently, we would have suggested an additional function of Mus81-Mms4 in other cell cycle phases (e.g S-phase). Using both "low" and "high" expressing constructs thus helped to avoid misinterpretations based on expression levels.

Taken together, the large number of cell cycle tags included in the advanced cell cycle tag toolbox allows to titrate expression levels within a certain range and thereby to choose sets of cell cycle tags with similar expression in the different cell cycle phases. Moreover, it allows to choose constructs according to the "low"/"high" strategy. I expect that these measures will greatly facilitate the interpretation of cell cycle tag experiments and thus provide a valuable tool to study cell cycle regulation of different proteins.

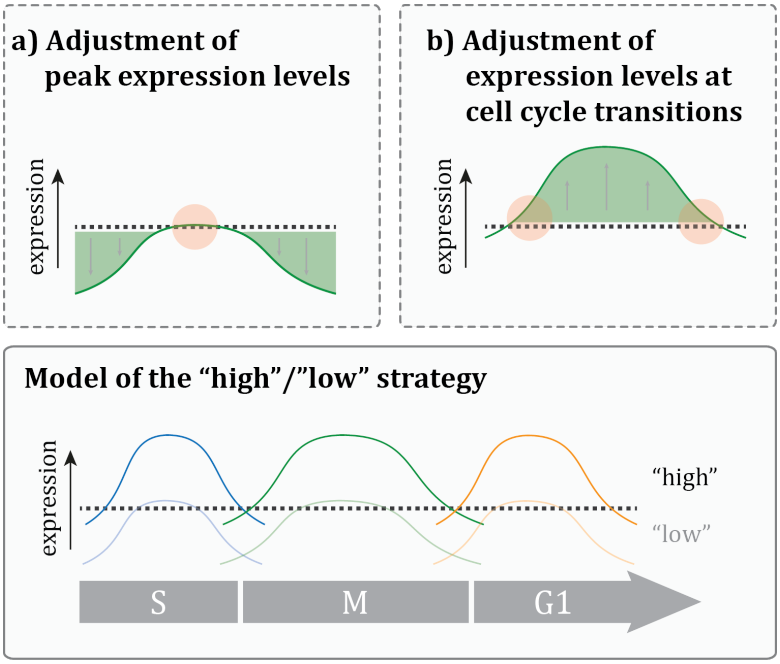

Figure 8: The "high"/"low" strategy of the advanced cell cycle tag toolbox. Considering the dynamic nature of expression from a cell cycle tag, expression levels will not be constant throughout the restricted cell cycle phase. While (a) adjustment of peak expression levels to endogenous protein levels (dotted line) will lead to under-expression at cell cycle transitions, (b) adjustment of expression levels at cell cycle transitions will lead to constant over-expression compared to endogenous protein levels. The suggested strategy for the use of cell cycle tags therefore includes two sets of constructs with matching "low" and "high" expression levels (lower). "Low" expressing tags are chosen to result in peak expression levels similar to endogenous protein levels but will show under-expression at cell cycle transitions. "High" expressing tags are chosen to result in constant over-expression throughout the cell cycle phase which consequently broadens the timeframe of action.

2 The function of Mus81-Mms4 is restricted to M-phase

2.1 Replication perturbation requires late response by Mus81-Mms4

With the advancements of the new cell cycle tag toolbox we were able to efficiently restrict expression and function of the Mus81-Mms4 SSE to S- and M-phase (Fig. 2A, (Bittmann et al., 2020)). For the first time, this allowed us to separate possible functions of Mus81-Mms4 in S- and M-phase and analyse during which of the two cell cycle phases Mus81-Mms4 would be required. Most of the functions of Mus81-Mms4 are connected with the response to replication perturbation during S-phase (Xiao et al., 1998, Interthal and Heyer, 2000, Boddy et al., 2001, Mullen et al., 2001, Doe et al., 2002, Bastin-Shanower et al., 2003, Kai et al., 2005, Saugar et al., 2013, Ho et al., 2010). As such, the upregulation of the catalytic activity Mus81-Mms4 undergoes during M-phase (Matos

et al., 2011, Matos et al., 2013, Gallo-Fernandez et al., 2012, Schwartz et al., 2012, Gritenaite et al., 2014) appears counterintuitive at first glance. Using our cell cycle-restricted alleles of *MUS81-MMS4* in a variety of functional assays analysing the response of Mus81-Mms4 to replication fork stalling (Fig. 3, 4A-C, (Bittmann et al., 2020)), we could clearly attribute the essential function of Mus81-Mms4 to M-phase. Throughout our genetic and physical assays, S-tagged Mus81-Mms4 showed phenotypes similar to a *MUS81* deletion, while M-tagged Mus81-Mms4 behaved like *WT* (Fig. 3, 4A-C, (Bittmann et al., 2020)). The involvement of Mus81-Mms4 during the response to stalled replication forks is thus timely uncoupled and matches with the timeframe of its high catalytic activity.

Given the observed functional overlap of M-tagged Mus81-Mms4 with Sgs1 (Fig. 3E, (Bittmann et al., 2020)), we conclude that our data are well described by a model where Mus81-Mms4 functions as a post-replicative resolvase. The resolvase function of Mus81-Mms4 generally constitutes an alternative or back-up pathway for the dissolution of JM structures by the STR complex (Kaliraman et al., 2001, Mullen et al., 2001, Wechsler et al., 2011, Wyatt et al., 2013). As a consequence, double mutants hampering the function of both pathways like the simultaneous deletion of *MUS81* and *SGS1* are inviable (Kaliraman et al., 2001, Mullen et al., 2001, Fabre et al., 2002, Bastin-Shanower et al., 2003). The strong synthetic phenotype observed for S-tagged Mus81-Mms4 in the background of *SGS1* (Fig. 3E, (Bittmann et al., 2020)) thus indicates the requirement of the resolution function of Mus81-Mms4 and simultaneously places this function into M-phase. The absence of *SGS1* has furthermore been shown to result in enhanced CO rates (Gangloff et al., 1994, Ira et al., 2003) which generally depend on the resolvase function of SSEs like Mus81-Mms4 (Ho et al., 2010). Interestingly, in the context of DSB repair we could show that the production of COs by Mus81-Mms4 happens during M-phase and does not require a function of Mus81-Mms4 during S-phase (Fig. 3D, (Bittmann et al., 2020)) thereby providing further evidence for a role as post-replicative resolvase. The structures requiring resolution by Mus81-Mms4 appear to arise during HR-dependent repair of stalled replication forks based on our observations made in the context of replication fork stalling by MMS, HU, CPT or transcription-replication conflicts (Fig. 3A-D, 4A-C, (Bittmann et al., 2020)). As described previously, we observed that Mus81-Mms4 is required for the response to lesions induced by these agents but can do so sufficiently in M-phase judged by the *WT*-like behaviour of M-tagged Mus81-Mms4 and the *MUS81* deletion-like phenotype of S-tagged Mus81-Mms4 (Fig. 3A-D, 4A-C, (Bittmann et al., 2020)). Replication fork stalling has been shown to induce JMs like D-loops or HJs in an HR-dependent manner (Liberi et al., 2005, Branzei et al., 2008, Giannattasio et al., 2014, Branzei and Szakal, 2016) thereby providing a possible substrate for the mitotic function of Mus81-Mms4. While Mus81-Mms4 was generally implicated in the resolution of such replication derived JMs before (Xiao et al., 1998, Interthal and Heyer, 2000, Boddy et al., 2001, Mullen et al., 2001, Doe et

al., 2002, Bastin-Shanower et al., 2003, Kai et al., 2005, Saugar et al., 2013, Ho et al., 2010), we can now attribute this function of Mus81-Mms4 to M-phase.

In addition to its function during resolution, Mus81-Mms4 has also been implicated in the process of break-induced replication (BIR) (Munoz-Galvan et al., 2012, Roseaulin et al., 2008, Mayle et al., 2015). BIR constitutes an HR-dependent pathway that is involved in the repair of single-ended DSBs. Single-ended DSBs can arise due to the breakage of replication forks and the single DSB end can serve as entry point for the initiation of a conservative mode of replication which proceeds via a migrating D-loop during BIR (Kramara et al., 2018). This conservative mode of replication is associated with a high level of mutagenicity and bears the risk of LOH as large parts of the template chromosome will be copied (Kramara et al., 2018). BIR in the context of replication has the advantage of limiting this mutagenicity by re-installing semi-conservative replication that replaces the migrating D-loop and thus the conservative mode of replication (Munoz-Galvan et al., 2012, Roseaulin et al., 2008, Mayle et al., 2015). The conversion of the D-loop into a normal replication fork can thereby happen in two ways both requiring Mus81-Mms4 function. On the one hand, the D-loop can merge with a converging replication fork resulting in a single HJ which ultimately requires resolution by an SSE (note that single HJs cannot be dissolved by the STR complex) (Munoz-Galvan et al., 2012, Roseaulin et al., 2008). On the other hand, the D-loop has been suggested to be directly converted into a replication fork by the cleavage of Mus81-Mms4 as assessed in a FLP-nick assay introducing single-ended DSBs in the context of replication (Mayle et al., 2015). Interestingly, using the same experimental setup as (Mayle et al., 2015) we could show that Mus81-Mms4 is unable to fulfil this suggested function during S-phase but instead requires the function of Mus81-Mms4 during M-phase (Fig. 3E,F, (Bittmann et al., 2020)). Such late timing of Mus81-Mms4 function during BIR would thereby be similar to what has been observed in human cells where MUS81-EME1 has been implicated in the initiation of BIR at difficult to replicate regions specifically in M-phase (Minocherhomji et al., 2015). In addition, a study from the Pasero lab published at the same time as my paper equally places the function of Mus81-Mms4 during the repair of CPT-induced (and thus replication-induced) lesions by a BIR-like mechanism into M-phase (Pardo et al., 2020). Thus, although the process of BIR is intuitively associated with S-phase our data provide an alternative view whereby distinct steps – like the endonucleolytic processing by Mus81-Mms4 – could take place at later cell cycle phases.

Despite the evidence that Mus81-Mms4 acts mainly post-replicatively in the response to replication fork stalling in budding yeast – as resolvase or during BIR – we cannot formerly exclude that Mus81-Mms4 might have additional functions during S-phase in other model organisms. In fact, our data cannot provide sufficient explanation for the observed involvement of mammalian MUS81 in replication restart. In mouse and human cell lines, reduced DSB formation in *MUS81* knock-out cell lines in response to replication fork stalling indicated an involvement of MUS81 in replication fork restart by cleaving stalled replication forks (Hanada et al., 2007,

Regairaz et al., 2011, Franchitto et al., 2008, Shimura et al., 2008). While in principal the reduced formation of DSBs in *MUS81* deficient cells might also be the consequence of an indirect effect and thus would not constitute an S-phase function of MUS81, it still raises the possibility of mammalian MUS81 having additional functions outside of M-phase. A critical point to consider when comparing Mus81 function in the yeast and mammalian system are differences in the regulatory mechanisms. While the overall cell cycle regulation and specific upregulation of the catalytic activity are conserved, the control of mammalian MUS81 involves additional features such as the presence of two regulatory subunits, EME1 and EME2, compared to the single Mms4 subunit in yeast (Ciccia et al., 2003). This leaves room for the speculation that the additional EME2 subunit might provide mammalian cells with an additional layer of control that would allow MUS81 to fulfil specific functions in S-phase and would offer an explanation for not detecting such a function in our experimental setup. In fact, so far it is not completely clear which of the two subunits could be responsible for the putative S-phase-specific MUS81 functions and in principal both MUS81-EME1 and MUS81-EME2 are able to cleave Y-shaped structures *in vitro* (Pepe and West, 2014b). While one study provides evidence for an exclusive function of MUS81-EME2 in the restart of replication forks after HU treatment (Pepe and West, 2014a), another study shows that also MUS81-EME1 is required for optimal fork progression (Xing et al., 2015). The relative contributions of MUS81-EME1 and MUS81-EME2 function thus require a more detailed analysis in order to establish a clear model of MUS81 function during S-phase. Interestingly, in contrast to the studies mentioned before which implicate MUS81 function in S-phase it was recently reported that MUS81 function during S-phase is counteracted by the WEE1 kinase and that loss of this control leads to chromosome breakage (Dominguez-Kelly et al., 2011, Beck et al., 2012, Duda et al., 2016). Together with the conserved cell cycle regulation during the upregulation of the MUS81 catalytic activity a principal post-replicative function of MUS81 can therefore also be envisioned in the mammalian system and makes our findings in principal transferable.

Taken together, our cell cycle tag study establishes a post-replicative function of Mus81-Mms4 during the response to replication fork stalling. We reason that, due to the overall conservation of Mus81-Mms4 regulation in the mammalian system, a post-replicative function of mammalian MUS81 is also likely. However, the implications of MUS81 in DSB formation and proper replication progression (Hanada et al., 2007, Regairaz et al., 2011, Franchitto et al., 2008, Shimura et al., 2008, Xing et al., 2015, Fu et al., 2015) – although possibly being the result of indirect effects after MUS81 depletion – emphasize the requirement of an in depth analysis of possible S- and M-phase functions in mammalian cells similar to our study in budding yeast.

2.2 A switch-like upregulation of Mus81-Mms4 activity at the onset of M-phase

Thinking about the timely uncoupled action of Mus81-Mms4 during the response to replication fork stalling consequently raises the question of how such a clear restriction of the function to M-phase is achieved. Interestingly, our new insights into the cell cycle-dependent regulation of Mus81-Mms4 activity (Princz et al., 2017) provide the basis for a model whereby the restriction of Mus81-Mms4 function is assured by a sharp, switch-like upregulation of its catalytic activity at the onset of M-phase.

From previous studies we know that the catalytic activity of Mus81-Mms4 becomes upregulated specifically during M-phase (Matos et al., 2011, Matos et al., 2013, Gallo-Fernandez et al., 2012, Schwartz et al., 2012, Gritenaite et al., 2014) and thus principally matches the temporal profile of the observed *in vivo* function (Bittmann et al., 2020). This upregulation of the catalytic activity depends on phosphorylation of Mms4 by the two cell cycle kinases Cdc5 and CDK (Matos et al., 2011, Matos et al., 2013, Gallo-Fernandez et al., 2012, Schwartz et al., 2012) as well as the incorporation of Mus81-Mms4 into a complex comprising the scaffold proteins Dpb11, Rtt107 and Slx4-Slx1 (Gritenaite et al., 2014). In (Princz et al., 2017) we were thereby able to add an additional kinase – DDK – to this already intricate regulatory network and shed light on the interplay of the different kinases and scaffold proteins. As a result, we could attribute several features to the regulation of Mus81-Mms4 that are typically associated with switch-like transitions.

First, we observed cooperativity of the kinases during the phosphorylation of Mms4 at multiple sites. Cdc5 and DDK were thereby found to target Mms4 in conjunction as binding of either of the two kinases to the substrate is reduced in the absence of the other (Fig. 2C-E, Princz et al., 2017) or when Cdc5 and DDK were unable to physically interact (Fig. 2F, Princz et al., 2017). For the DDK-dependent phosphorylation, peptide based phosphorylation assays furthermore revealed a possible stimulatory effect of priming phosphorylation by CDK (Fig. 1C, Princz et al., 2017) which would connect the action of all three kinases. Together, the three kinases phosphorylate Mms4 at multiple sites (Fig. 3, Princz et al., 2017; (Matos et al., 2011)) and seem to do so in a cooperative manner.

Second, we observed a positive-feedback loop during the concerted multi-site phosphorylation of Mms4 integrated by the Rtt107 scaffold. The binding of Rtt107 to Mms4 is thereby indispensable for the binding of Cdc5 and DDK (Fig. 6A, Princz et al., 2017). In turn, Rtt107 binding depends on prior phosphorylation by the two kinases (Fig. 2E, S2A, EV3, Princz et al., 2017) thus implying an interdependency between Rtt107 binding and Cdc5/DDK-dependent phosphorylation which could be part of a signal amplification mechanism (Princz et al., 2017).

Together, concerted multi-site phosphorylation and signal amplification are required for an efficient upregulation of the catalytic activity of Mus81-Mms4 during M-phase (Fig. 4, 7A,B, Princz et al., 2017). Since such features are commonly associated with switch-like transitions (Nash et al., 2001, Salazar and Hofer, 2009, Ferrell and Ha, 2014) we envision the activation of Mus81-Mms4 during M-phase beeing installed by a sharp and precise timer. Consequently, this switch-like activation of Mus81-Mms4 at the onset of M-phase would provide a model for the restricted *in vivo* function of the resolvase we observed in our cell cycle tag study (Bittmann et al., 2020). Mus81-Mms4 function would thereby be coupled to the window of high catalytic activity during M-phase and thus exclude a premature action during other cell cycle phases.

2.3 Consequences of premature SSE activation

An explanation for the importance of such a limitation of the resolvase function to M-phase could thereby be provided by a potentially harmful interference with replication structures (Matos et al., 2013, Blanco et al., 2014, Szakal and Branzei, 2013). Both Mus81-Mms4 and Yen1 are able to cleave Y-shaped structures (Boddy et al., 2001, Kaliraman et al., 2001, Doe et al., 2002, Bastin-Shanower et al., 2003, Ciccia et al., 2003, Gaillard et al., 2003, Ehmsen and Heyer, 2008, Ip et al., 2008, Rass et al., 2010) and their unrestricted action could thus influence replication progression.

The basis of this hypothesis is provided by experiments analysing the influence of deregulated SSE activity. Indeed, these studies revealed that premature SSE activity has the potential to lead to unscheduled chromosome breakage as well as loss of viability in response to replication fork stalling (Matos et al., 2013, Blanco et al., 2014, Szakal and Branzei, 2013, Duda et al., 2016). However, the use of constitutively active versions of the SSEs complicated the interpretations with regards to when they would induce the observed phenotypes. We realized that our cell cycle tag approach would constitute a unique opportunity to address at which cell cycle stage an active SSE would fulfil its toxic functions. Therefore, we restricted the expression of a constitutively active version of the SSE Yen1 – Yen1-ON – to the different cell cycle phases using our S-, M- and G1-cell cycle tags (Fig. 5A, (Bittmann et al., 2020)). In line with the initial hypothesis, we observed that premature Yen1 activity leads to reduced viability after replication fork stalling (Fig. 5B,C, (Bittmann et al., 2020)). Interestingly, in the case of Yen1 we were unable to specifically attribute the toxicity of an unscheduled activation to S-phase only but also observed a loss in the viability after restriction of Yen1-ON to early M-phase (Fig. 5B,C, (Bittmann et al., 2020)). The toxicity of Yen1 function during S- and early M-phase thus not only highlights the importance of restraining SSE function during replication but also implies a hierarchical use of enzymatic activities during M-phase whereby Mus81-Mms4 functions first followed by Yen1 in late M-phase (see chapter 3 for a more detailed discussion on the hierarchy of JM resolution).

Besides the toxicity of deregulated resolvase function during S-phase (Matos et al., 2013, Blanco et al., 2014, Szakal and Branzei, 2013, Duda et al., 2016, Bittmann et al., 2020), another

indication that the function of SSEs needs to be restrained during S-phase comes from the interplay of the Mus81-Mms4 regulation with the DNA damage checkpoint. The DNA damage checkpoint has been shown to counteract Mus81-Mms4 activity during S-phase which might help to avoid Mus81-Mms4-dependent cleavage of stalled replication forks. This is achieved by an antagonizing role of the DNA damage checkpoint during the phosphorylation of Mms4 by Cdc5 (Szakal and Branzei, 2013) and the formation of the scaffold complex (Slx4-Dpb11-Mus81-Mms4) (Gritenaite et al., 2014). The premature activation of Mus81-Mms4 observed in checkpoint deficient mutants consequently results in resolution of JM structures during S-phase and enhanced CO rates (Szakal and Branzei, 2013). Interestingly, the involvement of DDK in Mms4 phosphorylation introduced in (Princz et al., 2017) yet implies another mechanism by which the DNA damage checkpoint might counteract Mus81-Mms4 function during S-phase. The DDK kinase is principally present and active during S-phase as long as its function is not counteracted by the DNA damage checkpoint (Weinreich and Stillman, 1999, Lopez-Mosqueda et al., 2010, Zegerman and Diffley, 2010). It could be speculated that certain cellular conditions like the presence of stalled replication forks and an active DNA damage checkpoint might limit Mms4 phosphorylation by DDK and consequently Mus81-Mms4 activation during S-phase. A finetuned regulation by the DNA damage checkpoint therefore seems to complement the cell cycle-dependent regulation of Mus81-Mms4 and helps to restrict Mus81-Mms4 function to M-phase.

Overall, a picture emerges whereby the restriction of SSE function to M-phase seems to serve the purpose of avoiding interference with replication progression and limit the amount of CO products during resolution of repair intermediates. The interplay between the cell cycle and the DNA damage checkpoint during the activation of SSEs thereby creates an intricate regulatory network that restrains SSE function and activity to M-phase.

3 Hierarchy during the processing of JM structures

Together with previous findings, our studies on the cell cycle regulation of SSEs can be integrated into a general model whereby the processing of recombination intermediates follows a well-ordered hierarchy (**Figure 9**).

A first level of hierarchy is thereby achieved by the temporal separation of dissolution and resolution activities. While resolution by the SSEs Mus81-Mms4 and Yen1 is controlled by a precise regulatory network which sharply activates and restricts resolvase function to M-phase (Kosugi et al., 2009, Matos et al., 2011, Gallo-Fernandez et al., 2012, Matos et al., 2013, Szakal and Branzei, 2013, Blanco et al., 2014, Eissler et al., 2014, Garcia-Luis et al., 2014, Gritenaite et al., 2014, Bittmann et al., 2020), dissolution by the STR complex has been viewed as active throughout the cell cycle (Bizard and Hickson, 2014, Matos and West, 2014, Pfander and Matos, 2017) suggesting an initial dissolution of JM structures in S-phase followed by a wave of resolution during M-phase. Notably, a recent study by the Matos lab provides first evidence that also the

dissolution activity of the STR complex seems to be cell cycle regulated (Grigaitis et al., 2020). Thereby, Sgs1 activity was found to be specifically upregulated by CDK phosphorylation during S-phase while subsequent phosphorylation by Cdc5 appears to reduce Sgs1 activity during M-phase (Grigaitis et al., 2020). In contrast, using the initial form of the cell cycle tag system, Sgs1 has been shown to sufficiently act in M-phase in response to replication perturbation arguing against an S-phase exclusive function of Sgs1 (Karras and Jentsch, 2010). Nonetheless, dissolution of JMs by the STR complex has been shown to happen early in the cell cycle (Ira et al., 2003, Dayani et al., 2011). Together with our findings highlighting an M-phase-specific function of the two resolvases Mus81-Mms4 and Yen1 (Bittmann et al., 2020) the early function of dissolution strengthens the view of dissolution being the preferred pathway during S-phase and resolution constituting a back-up pathway during M-phase (**Figure 9**). As such, this hierarchy would ensure the continuous removal of JM structures but at the same time allows a finetuned use of the involved enzymatic activities. Since the dissolution pathway produces exclusively NCO outcomes (Ira et al., 2003, Wu and Hickson, 2003) and does not involve nucleolytic digestion of the DNA substrate the initial use of dissolution followed by a restricted wave of resolution suggests to serve a dual purpose: (1) limitation of the number of COs produced during mitosis and (2) avoidance of resolution activities, hence SSEs, interfering with replication.

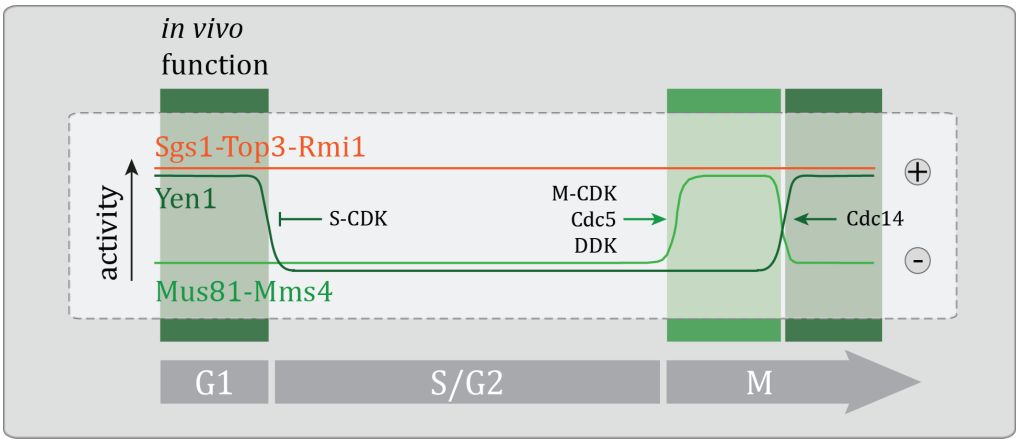

Figure 9: A model for the hierarchical use of dissolution and resolution activities. While dissolution by the STR complex seems to be active throughout the cell cycle, activity and *in vivo* function of the resolvases Mus81-Mms4 and Yen1 are restricted to M-phase. The restriction of resolvase function to M-phase is achieved by sequential phosphorylation and dephosphorylation processes resulting in an initial wave of Mus81-Mms4 activity during early M-phase followed by a second wave of Yen1 activity during late M-phase.

In addition to the sequential use of dissolution and resolution activities, a second layer of hierarchy is provided within the resolution pathways. Thereby, a first wave of resolution is performed by Mus81-Mms4 during early M-phase (Matos et al., 2011, Matos et al., 2013, Gallo-Fernandez et al., 2012, Schwartz et al., 2012, Gritenaite et al., 2014) followed by a second wave by Yen1 during late M-phase (Kosugi et al., 2009, Matos et al., 2011, Matos et al., 2013, Blanco et al., 2014, Eissler et al., 2014, Garcia-Luis et al., 2014). Interestingly, premature expression of active

Yen1 (Yen1-ON) during early M-phase can partially rescue the MMS sensitivity observed for *mus81Δ* cells (Fig. 5B, (Bittmann et al., 2020)) indicating at least some degree of functional overlap between the resolvases. However, in the background of functional *MUS81-MMS4* premature expression of Yen1-ON in early M-phase leads to reduced viability after replication fork stalling (Fig. 5C,D, (Bittmann et al., 2020)) pointing out possible differences between the two resolution pathways and underlining the need for restricting Yen1 function to late M-phase. The molecular mechanism underlying this restriction of Yen1 to late M-phase yet needs to be determined but could imply a different structure selectivity of Yen1 *in vivo* compared to Mus81-Mms4 which might interfere with recombination structures during early M-phase. *In vitro* Mus81-Mms4 and Yen1 are able to cleave different sets of DNA substrates (Boddy et al., 2001, Kaliraman et al., 2001, Doe et al., 2002, Bastin-Shanower et al., 2003, Ciccia et al., 2003, Fricke and Brill, 2003, Gaillard et al., 2003, Ehmsen and Heyer, 2008, Ip et al., 2008, Jessop and Lichten, 2008, Oh et al., 2008, Munoz et al., 2009, Rass et al., 2010, Wechsler et al., 2011, Saugar et al., 2013, Wyatt et al., 2013, Saugar et al., 2017) but the exact *in vivo* targets are still unknown.

To summarize, we would like to propose a working model whereby the removal of JM structures follows a three-tiered hierarchy: JM structures arising during the repair by homologous recombination are preferentially dissolved by the STR complex during S-phase followed by sequential resolution by the SSEs Mus81-Mms4 and Yen1 (**Figure 9**). This hierarchy provides a mechanism to ensure the removal of JM structures before sister chromatids get separated during mitosis but at the same time protects cells from a potentially harmful action of SSEs during S-phase (and early M-phase) and keeps the overall number of COs during mitosis low.

References

AGUILERA, A. & GAILLARD, H. 2014. Transcription and recombination: when RNA meets DNA. *Cold Spring Harb Perspect Biol,* 6.

ANAND, R., RANJHA, L., CANNAVO, E. & CEJKA, P. 2016. Phosphorylated CtIP Functions as a Co-factor of the MRE11-RAD50-NBS1 Endonuclease in DNA End Resection. *Mol Cell,* 64**,** 940-950.

ASHTON, T. M., MANKOURI, H. W., HEIDENBLUT, A., MCHUGH, P. J. & HICKSON, I. D. 2011. Pathways for Holliday junction processing during homologous recombination in Saccharomyces cerevisiae. *Mol Cell Biol,* 31**,** 1921-33.

BACHRATI, C. Z., BORTS, R. H. & HICKSON, I. D. 2006. Mobile D-loops are a preferred substrate for the Bloom's syndrome helicase. *Nucleic Acids Res,* 34**,** 2269-79.

BANTELE, S. C., FERREIRA, P., GRITENAITE, D., BOOS, D. & PFANDER, B. 2017. Targeting of the Fun30 nucleosome remodeller by the Dpb11 scaffold facilitates cell cycle-regulated DNA end resection. *Elife,* 6.

BASTIN-SHANOWER, S. A., FRICKE, W. M., MULLEN, J. R. & BRILL, S. J. 2003. The mechanism of Mus81-Mms4 cleavage site selection distinguishes it from the homologous endonuclease Rad1-Rad10. *Mol Cell Biol,* 23**,** 3487-96.

BECK, H., NAHSE-KUMPF, V., LARSEN, M. S., O'HANLON, K. A., PATZKE, S., HOLMBERG, C., MEJLVANG, J., GROTH, A., NIELSEN, O., SYLJUASEN, R. G. & SORENSEN, C. S. 2012. Cyclin-dependent kinase suppression by WEE1 kinase protects the genome through control of replication initiation and nucleotide consumption. *Mol Cell Biol,* 32**,** 4226-36.

BELLAOUI, M., CHANG, M., OU, J., XU, H., BOONE, C. & BROWN, G. W. 2003. Elg1 forms an alternative RFC complex important for DNA replication and genome integrity. *EMBO J,* 22**,** 4304-13.

BENNETT, C. B., LEWIS, A. L., BALDWIN, K. K. & RESNICK, M. A. 1993. Lethality induced by a single site-specific double-strand break in a dispensable yeast plasmid. *Proc Natl Acad Sci U S A,* 90**,** 5613-7.

BERTI, M. & VINDIGNI, A. 2016. Replication stress: getting back on track. *Nat Struct Mol Biol,* 23**,** 103-9.

BETERMIER, M., BORDE, V. & VILLARTAY, J. P. 2019. Coupling DNA Damage and Repair: an Essential Safeguard during Programmed DNA Double-Strand Breaks? *Trends Cell Biol*.

BHOWMICK, R., MINOCHERHOMJI, S. & HICKSON, I. D. 2016. RAD52 Facilitates Mitotic DNA Synthesis Following Replication Stress. *Mol Cell,* 64**,** 1117-1126.

BITTMANN, J., GRIGAITIS, R., GALANTI, L., AMARELL, S., WILFLING, F., MATOS, J. & PFANDER, B. 2020. An advanced cell cycle tag toolbox reveals principles underlying temporal control of structure-selective nucleases. *Elife,* 9.

BIZARD, A. H. & HICKSON, I. D. 2014. The dissolution of double Holliday junctions. *Cold Spring Harb Perspect Biol,* 6**,** a016477.

BLANCO, M. G. & MATOS, J. 2015. Hold your horSSEs: controlling structure-selective endonucleases MUS81 and Yen1/GEN1. *Front Genet,* 6**,** 253.

BLANCO, M. G., MATOS, J. & WEST, S. C. 2014. Dual control of Yen1 nuclease activity and cellular localization by Cdk and Cdc14 prevents genome instability. *Mol Cell,* 54**,** 94-106.

BOCH, J., SCHOLZE, H., SCHORNACK, S., LANDGRAF, A., HAHN, S., KAY, S., LAHAYE, T., NICKSTADT, A. & BONAS, U. 2009. Breaking the code of DNA binding specificity of TAL-type III effectors. *Science,* 326**,** 1509-12.

BODDY, M. N., GAILLARD, P. H., MCDONALD, W. H., SHANAHAN, P., YATES, J. R., 3RD & RUSSELL, P. 2001. Mus81-Eme1 are essential components of a Holliday junction resolvase. *Cell,* 107**,** 537-48.

BODDY, M. N., SHANAHAN, P., MCDONALD, W. H., LOPEZ-GIRONA, A., NOGUCHI, E., YATES, I. J. & RUSSELL, P. 2003. Replication checkpoint kinase Cds1 regulates recombinational repair protein Rad60. *Mol Cell Biol,* 23**,** 5939-46.

BRANZEI, D. & FOIANI, M. 2010. Maintaining genome stability at the replication fork. *Nat Rev Mol Cell Biol,* 11**,** 208-19.

BRANZEI, D., SEKI, M. & ENOMOTO, T. 2004. Rad18/Rad5/Mms2-mediated polyubiquitination of PCNA is implicated in replication completion during replication stress. *Genes Cells,* 9**,** 1031-42.

BRANZEI, D. & SZAKAL, B. 2016. DNA damage tolerance by recombination: Molecular pathways and DNA structures. *DNA Repair (Amst),* 44**,** 68-75.

BRANZEI, D., VANOLI, F. & FOIANI, M. 2008. SUMOylation regulates Rad18-mediated template switch. *Nature,* 456**,** 915-20.

BRUSH, G. S., MORROW, D. M., HIETER, P. & KELLY, T. J. 1996. The ATM homologue MEC1 is required for phosphorylation of replication protein A in yeast. *Proc Natl Acad Sci U S A,* 93**,** 15075-80.

BUISSON, R., BOISVERT, J. L., BENES, C. H. & ZOU, L. 2015. Distinct but Concerted Roles of ATR, DNA-PK, and Chk1 in Countering Replication Stress during S Phase. *Mol Cell,* 59**,** 1011-24.

BZYMEK, M., THAYER, N. H., OH, S. D., KLECKNER, N. & HUNTER, N. 2010. Double Holliday junctions are intermediates of DNA break repair. *Nature,* 464**,** 937-41.

CANNAN, W. J. & PEDERSON, D. S. 2016. Mechanisms and Consequences of Double-Strand DNA Break Formation in Chromatin. *J Cell Physiol,* 231**,** 3-14.

CANNAVO, E. & CEJKA, P. 2014. Sae2 promotes dsDNA endonuclease activity within Mre11-Rad50-Xrs2 to resect DNA breaks. *Nature,* 514**,** 122-5.

CEJKA, P., CANNAVO, E., POLACZEK, P., MASUDA-SASA, T., POKHAREL, S., CAMPBELL, J. L. & KOWALCZYKOWSKI, S. C. 2010a. DNA end resection by Dna2-Sgs1-RPA and its stimulation by Top3-Rmi1 and Mre11-Rad50-Xrs2. *Nature,* 467**,** 112-6.

CEJKA, P., PLANK, J. L., BACHRATI, C. Z., HICKSON, I. D. & KOWALCZYKOWSKI, S. C. 2010b. Rmi1 stimulates decatenation of double Holliday junctions during dissolution by Sgs1-Top3. *Nat Struct Mol Biol,* 17**,** 1377-82.

CHAGANTI, R. S., SCHONBERG, S. & GERMAN, J. 1974. A manyfold increase in sister chromatid exchanges in Bloom's syndrome lymphocytes. *Proc Natl Acad Sci U S A,* 71**,** 4508-12.

CHAN, K. L., NORTH, P. S. & HICKSON, I. D. 2007. BLM is required for faithful chromosome segregation and its localization defines a class of ultrafine anaphase bridges. *EMBO J,* 26**,** 3397-409.

CHEN, S. H., PLANK, J. L., WILLCOX, S., GRIFFITH, J. D. & HSIEH, T. S. 2014. Top3alpha is required during the convergent migration step of double Holliday junction dissolution. *PLoS One,* 9**,** e83582.

CHEN, X., NIU, H., CHUNG, W. H., ZHU, Z., PAPUSHA, A., SHIM, E. Y., LEE, S. E., SUNG, P. & IRA, G. 2011. Cell cycle regulation of DNA double-strand break end resection by Cdk1-dependent Dna2 phosphorylation. *Nat Struct Mol Biol,* 18**,** 1015-9.

CHEN, X., NIU, H., YU, Y., WANG, J., ZHU, S., ZHOU, J., PAPUSHA, A., CUI, D., PAN, X., KWON, Y., SUNG, P. & IRA, G. 2016. Enrichment of Cdk1-cyclins at DNA double-strand breaks stimulates Fun30 phosphorylation and DNA end resection. *Nucleic Acids Res,* 44**,** 2742-53.

CHOULIKA, A., PERRIN, A., DUJON, B. & NICOLAS, J. F. 1995. Induction of homologous recombination in mammalian chromosomes by using the I-SceI system of Saccharomyces cerevisiae. *Mol Cell Biol,* 15**,** 1968-73.

CHRISTIAN, M., CERMAK, T., DOYLE, E. L., SCHMIDT, C., ZHANG, F., HUMMEL, A., BOGDANOVE, A. J. & VOYTAS, D. F. 2010. Targeting DNA double-strand breaks with TAL effector nucleases. *Genetics,* 186**,** 757-61.

CICCIA, A., CONSTANTINOU, A. & WEST, S. C. 2003. Identification and characterization of the human mus81-eme1 endonuclease. *J Biol Chem,* 278**,** 25172-8.

CICCIA, A. & ELLEDGE, S. J. 2010. The DNA damage response: making it safe to play with knives. *Mol Cell,* 40**,** 179-204.

CONG, L., RAN, F. A., COX, D., LIN, S., BARRETTO, R., HABIB, N., HSU, P. D., WU, X., JIANG, W., MARRAFFINI, L. A. & ZHANG, F. 2013. Multiplex genome engineering using CRISPR/Cas systems. *Science,* 339**,** 819-23.

CONNOLLY, B., WHITE, C. I. & HABER, J. E. 1988. Physical monitoring of mating type switching in Saccharomyces cerevisiae. *Mol Cell Biol,* 8**,** 2342-9.

DAIGAKU, Y., DAVIES, A. A. & ULRICH, H. D. 2010. Ubiquitin-dependent DNA damage bypass is separable from genome replication. *Nature,* 465**,** 951-5.

DALEY, J. M., PALMBOS, P. L., WU, D. & WILSON, T. E. 2005. Nonhomologous end joining in yeast. *Annu Rev Genet,* 39**,** 431-51.

DAYANI, Y., SIMCHEN, G. & LICHTEN, M. 2011. Meiotic recombination intermediates are resolved with minimal crossover formation during return-to-growth, an analogue of the mitotic cell cycle. *PLoS Genet,* 7**,** e1002083.

DEEM, A., BARKER, K., VANHULLE, K., DOWNING, B., VAYL, A. & MALKOVA, A. 2008. Defective break-induced replication leads to half-crossovers in Saccharomyces cerevisiae. *Genetics,* 179**,** 1845-60.

DEEM, A., KESZTHELYI, A., BLACKGROVE, T., VAYL, A., COFFEY, B., MATHUR, R., CHABES, A. & MALKOVA, A. 2011. Break-induced replication is highly inaccurate. *PLoS Biol,* 9**,** e1000594.

DENG, D., YAN, C., PAN, X., MAHFOUZ, M., WANG, J., ZHU, J. K., SHI, Y. & YAN, N. 2012. Structural basis for sequence-specific recognition of DNA by TAL effectors. *Science,* 335**,** 720-3.

DESHPANDE, I., SEEBER, A., SHIMADA, K., KEUSCH, J. J., GUT, H. & GASSER, S. M. 2017. Structural Basis of Mec1-Ddc2-RPA Assembly and Activation on Single-Stranded DNA at Sites of Damage. *Mol Cell,* 68**,** 431-445 e5.

DESHPANDE, R. A., LEE, J. H., ARORA, S. & PAULL, T. T. 2016. Nbs1 Converts the Human Mre11/Rad50 Nuclease Complex into an Endo/Exonuclease Machine Specific for Protein-DNA Adducts. *Mol Cell,* 64**,** 593-606.

DEVEAU, H., BARRANGOU, R., GARNEAU, J. E., LABONTE, J., FREMAUX, C., BOYAVAL, P., ROMERO, D. A., HORVATH, P. & MOINEAU, S. 2008. Phage response to CRISPR-encoded resistance in Streptococcus thermophilus. *J Bacteriol,* 190**,** 1390-400.

DOE, C. L., AHN, J. S., DIXON, J. & WHITBY, M. C. 2002. Mus81-Eme1 and Rqh1 involvement in processing stalled and collapsed replication forks. *J Biol Chem,* 277**,** 32753-9.

DOMINGUEZ-KELLY, R., MARTIN, Y., KOUNDRIOUKOFF, S., TANENBAUM, M. E., SMITS, V. A., MEDEMA, R. H., DEBATISSE, M. & FREIRE, R. 2011. Wee1 controls genomic stability during replication by regulating the Mus81-Eme1 endonuclease. *J Cell Biol,* 194**,** 567-79.

DONNIANNI, R. A. & SYMINGTON, L. S. 2013. Break-induced replication occurs by conservative DNA synthesis. *Proc Natl Acad Sci U S A,* 110**,** 13475-80.

DONOHO, G., JASIN, M. & BERG, P. 1998. Analysis of gene targeting and intrachromosomal homologous recombination stimulated by genomic double-strand breaks in mouse embryonic stem cells. *Mol Cell Biol,* 18**,** 4070-8.

DUDA, H., ARTER, M., GLOGGNITZER, J., TELONI, F., WILD, P., BLANCO, M. G., ALTMEYER, M. & MATOS, J. 2016. A Mechanism for Controlled Breakage of Under-replicated Chromosomes during Mitosis. *Dev Cell,* 39**,** 740-755.

DURO, E., LUNDIN, C., ASK, K., SANCHEZ-PULIDO, L., MACARTNEY, T. J., TOTH, R., PONTING, C. P., GROTH, A., HELLEDAY, T. & ROUSE, J. 2010. Identification of the MMS22L-TONSL Complex that Promotes Homologous Recombination. *Molecular Cell,* 40**,** 632-644.

EHMSEN, K. T. & HEYER, W. D. 2008. Saccharomyces cerevisiae Mus81-Mms4 is a catalytic, DNA structure-selective endonuclease. *Nucleic Acids Res,* 36**,** 2182-95.

EISSLER, C. L., MAZON, G., POWERS, B. L., SAVINOV, S. N., SYMINGTON, L. S. & HALL, M. C. 2014. The Cdk/cDc14 module controls activation of the Yen1 holliday junction resolvase to promote genome stability. *Mol Cell,* 54**,** 80-93.

FABRE, F., CHAN, A., HEYER, W. D. & GANGLOFF, S. 2002. Alternate pathways involving Sgs1/Top3, Mus81/ Mms4, and Srs2 prevent formation of toxic recombination intermediates from single-stranded gaps created by DNA replication. *Proc Natl Acad Sci U S A,* 99**,** 16887-92.

FALCK, J., FORMENT, J. V., COATES, J., MISTRIK, M., LUKAS, J., BARTEK, J. & JACKSON, S. P. 2012. CDK targeting of NBS1 promotes DNA-end resection, replication restart and homologous recombination. *EMBO Rep,* 13**,** 561-8.

FERRELL, J. E., JR. & HA, S. H. 2014. Ultrasensitivity part II: multisite phosphorylation, stoichiometric inhibitors, and positive feedback. *Trends Biochem Sci,* 39**,** 556-69.

FERRETTI, L. P., LAFRANCHI, L. & SARTORI, A. A. 2013. Controlling DNA-end resection: a new task for CDKs. *Front Genet,* 4**,** 99.

FRANCHITTO, A., PIRZIO, L. M., PROSPERI, E., SAPORA, O., BIGNAMI, M. & PICHIERRI, P. 2008. Replication fork stalling in WRN-deficient cells is overcome by prompt activation of a MUS81-dependent pathway. *J Cell Biol,* 183**,** 241-52.

FRICKE, W. M. & BRILL, S. J. 2003. Slx1-Slx4 is a second structure-specific endonuclease functionally redundant with Sgs1-Top3. *Genes Dev,* 17**,** 1768-78.

FROGET, B., BLAISONNEAU, J., LAMBERT, S. & BALDACCI, G. 2008. Cleavage of stalled forks by fission yeast Mus81/Eme1 in absence of DNA replication checkpoint. *Mol Biol Cell,* 19**,** 445-56.

FU, H., MARTIN, M. M., REGAIRAZ, M., HUANG, L., YOU, Y., LIN, C. M., RYAN, M., KIM, R., SHIMURA, T., POMMIER, Y. & ALADJEM, M. I. 2015. The DNA repair endonuclease Mus81 facilitates fast DNA replication in the absence of exogenous damage. *Nat Commun,* 6**,** 6746.

GAILLARD, P. H., NOGUCHI, E., SHANAHAN, P. & RUSSELL, P. 2003. The endogenous Mus81-Eme1 complex resolves Holliday junctions by a nick and counternick mechanism. *Mol Cell,* 12**,** 747-59.

GALLO-FERNANDEZ, M., SAUGAR, I., ORTIZ-BAZAN, M. A., VAZQUEZ, M. V. & TERCERO, J. A. 2012. Cell cycle-dependent regulation of the nuclease activity of Mus81-Eme1/Mms4. *Nucleic Acids Res,* 40**,** 8325-35.

GANGLOFF, S., MCDONALD, J. P., BENDIXEN, C., ARTHUR, L. & ROTHSTEIN, R. 1994. The yeast type I topoisomerase Top3 interacts with Sgs1, a DNA helicase homolog: a potential eukaryotic reverse gyrase. *Mol Cell Biol,* 14**,** 8391-8.

GARCIA-LUIS, J., CLEMENTE-BLANCO, A., ARAGON, L. & MACHIN, F. 2014. Cdc14 targets the Holliday junction resolvase Yen1 to the nucleus in early anaphase. *Cell Cycle,* 13**,** 1392-9.

GASIUNAS, G., BARRANGOU, R., HORVATH, P. & SIKSNYS, V. 2012. Cas9-crRNA ribonucleoprotein complex mediates specific DNA cleavage for adaptive immunity in bacteria. *Proc Natl Acad Sci U S A,* 109**,** E2579-86.

GERMAN, J., CRIPPA, L. P. & BLOOM, D. 1974. Bloom's syndrome. III. Analysis of the chromosome aberration characteristic of this disorder. *Chromosoma,* 48**,** 361-6.

GERMANN, S. M., OESTERGAARD, V. H., HAAS, C., SALIS, P., MOTEGI, A. & LISBY, M. 2011. Dpb11/TopBP1 plays distinct roles in DNA replication, checkpoint response and homologous recombination. *DNA Repair (Amst),* 10**,** 210-24.

GERMANN, S. M., SCHRAMKE, V., PEDERSEN, R. T., GALLINA, I., ECKERT-BOULET, N., OESTERGAARD, V. H. & LISBY, M. 2014. TopBP1/Dpb11 binds DNA anaphase bridges to prevent genome instability. *J Cell Biol,* 204**,** 45-59.

GIANNATTASIO, M., ZWICKY, K., FOLLONIER, C., FOIANI, M., LOPES, M. & BRANZEI, D. 2014. Visualization of recombination-mediated damage bypass by template switching. *Nat Struct Mol Biol,* 21**,** 884-92.

GONZALEZ-PRIETO, R., MUNOZ-CABELLO, A. M., CABELLO-LOBATO, M. J. & PRADO, F. 2013. Rad51 replication fork recruitment is required for DNA damage tolerance. *EMBO J,* 32**,** 1307-21.

GRAVEL, S., CHAPMAN, J. R., MAGILL, C. & JACKSON, S. P. 2008. DNA helicases Sgs1 and BLM promote DNA double-strand break resection. *Genes Dev,* 22**,** 2767-72.

GRIGAITIS, R., RANJHA, L., WILD, P., KASACIUNAITE, K., CEPPI, I., KISSLING, V., HENGGELER, A., SUSPERREGUI, A., PETER, M., SEIDEL, R., CEJKA, P. & MATOS, J. 2020. Phosphorylation of the RecQ

Helicase Sgs1/BLM Controls Its DNA Unwinding Activity during Meiosis and Mitosis. *Dev Cell,* 53**,** 706-723 e5.

GRITENAITE, D., PRINCZ, L. N., SZAKAL, B., BANTELE, S. C., WENDELER, L., SCHILBACH, S., HABERMANN, B. H., MATOS, J., LISBY, M., BRANZEI, D. & PFANDER, B. 2014. A cell cycle-regulated Slx4-Dpb11 complex promotes the resolution of DNA repair intermediates linked to stalled replication. *Genes Dev,* 28**,** 1604-19.

GUERVILLY, J. H. & GAILLARD, P. H. 2018. SLX4: multitasking to maintain genome stability. *Crit Rev Biochem Mol Biol,* 53**,** 475-514.

HABER, J. E. & HEYER, W. D. 2001. The fuss about Mus81. *Cell,* 107**,** 551-4.

HAMPERL, S. & CIMPRICH, K. A. 2016. Conflict Resolution in the Genome: How Transcription and Replication Make It Work. *Cell,* 167**,** 1455-1467.

HANADA, K., BUDZOWSKA, M., DAVIES, S. L., VAN DRUNEN, E., ONIZAWA, H., BEVERLOO, H. B., MAAS, A., ESSERS, J., HICKSON, I. D. & KANAAR, R. 2007. The structure-specific endonuclease Mus81 contributes to replication restart by generating double-strand DNA breaks. *Nat Struct Mol Biol,* 14**,** 1096-104.

HARACSKA, L., TORRES-RAMOS, C. A., JOHNSON, R. E., PRAKASH, S. & PRAKASH, L. 2004. Opposing effects of ubiquitin conjugation and SUMO modification of PCNA on replicational bypass of DNA lesions in Saccharomyces cerevisiae. *Mol Cell Biol,* 24**,** 4267-74.

HELLEDAY, T., PETERMANN, E., LUNDIN, C., HODGSON, B. & SHARMA, R. A. 2008. DNA repair pathways as targets for cancer therapy. *Nat Rev Cancer,* 8**,** 193-204.

HEYER, W. D., EHMSEN, K. T. & LIU, J. 2010. Regulation of homologous recombination in eukaryotes. *Annu Rev Genet,* 44**,** 113-39.

HICKS, W. M., YAMAGUCHI, M. & HABER, J. E. 2011. Real-time analysis of double-strand DNA break repair by homologous recombination. *Proc Natl Acad Sci U S A,* 108**,** 3108-15.

HO, C. K., MAZON, G., LAM, A. F. & SYMINGTON, L. S. 2010. Mus81 and Yen1 promote reciprocal exchange during mitotic recombination to maintain genome integrity in budding yeast. *Mol Cell,* 40**,** 988-1000.

HOEGE, C., PFANDER, B., MOLDOVAN, G. L., PYROWOLAKIS, G. & JENTSCH, S. 2002. RAD6-dependent DNA repair is linked to modification of PCNA by ubiquitin and SUMO. *Nature,* 419**,** 135-41.

HOLLIDAY, R. 1964. A mechanism for gene conversion in fungi. *Genet Res,* 89**,** 285-307.

HOMBAUER, H., SRIVATSAN, A., PUTNAM, C. D. & KOLODNER, R. D. 2011. Mismatch repair, but not heteroduplex rejection, is temporally coupled to DNA replication. *Science,* 334**,** 1713-6.

HUANG, L. C., CLARKIN, K. C. & WAHL, G. M. 1996. Sensitivity and selectivity of the DNA damage sensor responsible for activating p53-dependent G1 arrest. *Proc Natl Acad Sci U S A,* 93**,** 4827-32.

HUERTAS, P. & JACKSON, S. P. 2009. Human CtIP mediates cell cycle control of DNA end resection and double strand break repair. *J Biol Chem,* 284**,** 9558-65.

HUNG, S. H., WONG, R. P., ULRICH, H. D. & KAO, C. F. 2017. Monoubiquitylation of histone H2B contributes to the bypass of DNA damage during and after DNA replication. *Proc Natl Acad Sci U S A,* 114**,** E2205-E2214.

HUSTEDT, N. & DUROCHER, D. 2016. The control of DNA repair by the cell cycle. *Nat Cell Biol,* 19**,** 1-9.

INTERTHAL, H. & HEYER, W. D. 2000. MUS81 encodes a novel helix-hairpin-helix protein involved in the response to UV- and methylation-induced DNA damage in Saccharomyces cerevisiae. *Mol Gen Genet,* 263**,** 812-27.

IP, S. C., RASS, U., BLANCO, M. G., FLYNN, H. R., SKEHEL, J. M. & WEST, S. C. 2008. Identification of Holliday junction resolvases from humans and yeast. *Nature,* 456**,** 357-61.

IRA, G., MALKOVA, A., LIBERI, G., FOIANI, M. & HABER, J. E. 2003. Srs2 and Sgs1-Top3 suppress crossovers during double-strand break repair in yeast. *Cell,* 115**,** 401-11.

IRMISCH, A., AMPATZIDOU, E., MIZUNO, K., O'CONNELL, M. J. & MURRAY, J. M. 2009. Smc5/6 maintains stalled replication forks in a recombination-competent conformation. *EMBO J,* 28**,** 144-55.

JAIN, S., SUGAWARA, N., LYDEARD, J., VAZE, M., TANGUY LE GAC, N. & HABER, J. E. 2009. A recombination execution checkpoint regulates the choice of homologous recombination pathway during DNA double-strand break repair. *Genes Dev,* 23**,** 291-303.

JASIN, M. 1996. Genetic manipulation of genomes with rare-cutting endonucleases. *Trends Genet,* 12**,** 224-8.

JASIN, M. & HABER, J. E. 2016. The democratization of gene editing: Insights from site-specific cleavage and double-strand break repair. *DNA Repair (Amst),* 44**,** 6-16.

JENSEN, R., SPRAGUE, G. F., JR. & HERSKOWITZ, I. 1983. Regulation of yeast mating-type interconversion: feedback control of HO gene expression by the mating-type locus. *Proc Natl Acad Sci U S A,* 80**,** 3035-9.

JENSEN, R. B., CARREIRA, A. & KOWALCZYKOWSKI, S. C. 2010. Purified human BRCA2 stimulates RAD51-mediated recombination. *Nature,* 467**,** 678-83.

JESSOP, L. & LICHTEN, M. 2008. Mus81/Mms4 endonuclease and Sgs1 helicase collaborate to ensure proper recombination intermediate metabolism during meiosis. *Mol Cell,* 31**,** 313-23.

JINEK, M., CHYLINSKI, K., FONFARA, I., HAUER, M., DOUDNA, J. A. & CHARPENTIER, E. 2012. A programmable dual-RNA-guided DNA endonuclease in adaptive bacterial immunity. *Science,* 337**,** 816-21.

JOHNSON, C., GALI, V. K., TAKAHASHI, T. S. & KUBOTA, T. 2016. PCNA Retention on DNA into G2/M Phase Causes Genome Instability in Cells Lacking Elg1. *Cell Rep,* 16**,** 684-95.

JOHNSON, R. D. & JASIN, M. 2000. Sister chromatid gene conversion is a prominent double-strand break repair pathway in mammalian cells. *EMBO J,* 19**,** 3398-407.

KADYK, L. C. & HARTWELL, L. H. 1992. Sister chromatids are preferred over homologs as substrates for recombinational repair in Saccharomyces cerevisiae. *Genetics,* 132**,** 387-402.

KAHLI, M., OSMUNDSON, J. S., YEUNG, R. & SMITH, D. J. 2019. Processing of eukaryotic Okazaki fragments by redundant nucleases can be uncoupled from ongoing DNA replication in vivo. *Nucleic Acids Res,* 47**,** 1814-1822.

KAI, M., BODDY, M. N., RUSSELL, P. & WANG, T. S. 2005. Replication checkpoint kinase Cds1 regulates Mus81 to preserve genome integrity during replication stress. *Genes Dev,* 19**,** 919-32.

KALIRAMAN, V., MULLEN, J. R., FRICKE, W. M., BASTIN-SHANOWER, S. A. & BRILL, S. J. 2001. Functional overlap between Sgs1-Top3 and the Mms4-Mus81 endonuclease. *Genes Dev,* 15**,** 2730-40.

KANNOUCHE, P. L., WING, J. & LEHMANN, A. R. 2004. Interaction of human DNA polymerase eta with monoubiquitinated PCNA: a possible mechanism for the polymerase switch in response to DNA damage. *Mol Cell,* 14**,** 491-500.

KARRAS, G. I., FUMASONI, M., SIENSKI, G., VANOLI, F., BRANZEI, D. & JENTSCH, S. 2013. Noncanonical role of the 9-1-1 clamp in the error-free DNA damage tolerance pathway. *Mol Cell,* 49**,** 536-46.

KARRAS, G. I. & JENTSCH, S. 2010. The RAD6 DNA damage tolerance pathway operates uncoupled from the replication fork and is functional beyond S phase. *Cell,* 141**,** 255-67.

KIM, Y. G., CHA, J. & CHANDRASEGARAN, S. 1996. Hybrid restriction enzymes: zinc finger fusions to Fok I cleavage domain. *Proc Natl Acad Sci U S A,* 93**,** 1156-60.

KOSUGI, S., HASEBE, M., TOMITA, M. & YANAGAWA, H. 2009. Systematic identification of cell cycle-dependent yeast nucleocytoplasmic shuttling proteins by prediction of composite motifs. *Proc Natl Acad Sci U S A,* 106**,** 10171-6.

KRAMARA, J., OSIA, B. & MALKOVA, A. 2018. Break-Induced Replication: The Where, The Why, and The How. *Trends Genet,* 34**,** 518-531.

LAFUENTE-BARQUERO, J., LUKE-GLASER, S., GRAF, M., SILVA, S., GOMEZ-GONZALEZ, B., LOCKHART, A., LISBY, M., AGUILERA, A. & LUKE, B. 2017. The Smc5/6 complex regulates the yeast Mph1 helicase at RNA-DNA hybrid-mediated DNA damage. *PLoS Genet,* 13**,** e1007136.

LEHMANN, A. R. & FUCHS, R. P. 2006. Gaps and forks in DNA replication: Rediscovering old models. *DNA Repair (Amst),* 5**,** 1495-8.

LEMACON, D., JACKSON, J., QUINET, A., BRICKNER, J. R., LI, S., YAZINSKI, S., YOU, Z., IRA, G., ZOU, L., MOSAMMAPARAST, N. & VINDIGNI, A. 2017. MRE11 and EXO1 nucleases degrade reversed forks and elicit MUS81-dependent fork rescue in BRCA2-deficient cells. *Nat Commun,* 8**,** 860.

LI, X., STITH, C. M., BURGERS, P. M. & HEYER, W. D. 2009. PCNA is required for initiation of recombination-associated DNA synthesis by DNA polymerase delta. *Mol Cell,* 36**,** 704-13.

LIANG, F., HAN, M., ROMANIENKO, P. J. & JASIN, M. 1998. Homology-directed repair is a major double-strand break repair pathway in mammalian cells. *Proc Natl Acad Sci U S A,* 95**,** 5172-7.

LIBERI, G., MAFFIOLETTI, G., LUCCA, C., CHIOLO, I., BARYSHNIKOVA, A., COTTA-RAMUSINO, C., LOPES, M., PELLICIOLI, A., HABER, J. E. & FOIANI, M. 2005. Rad51-dependent DNA structures accumulate at damaged replication forks in sgs1 mutants defective in the yeast ortholog of BLM RecQ helicase. *Genes Dev,* 19**,** 339-50.

LISBY, M., BARLOW, J. H., BURGESS, R. C. & ROTHSTEIN, R. 2004. Choreography of the DNA damage response: spatiotemporal relationships among checkpoint and repair proteins. *Cell,* 118**,** 699-713.

LIU, J., DOTY, T., GIBSON, B. & HEYER, W. D. 2010. Human BRCA2 protein promotes RAD51 filament formation on RPA-covered single-stranded DNA. *Nat Struct Mol Biol,* 17**,** 1260-2.

LOPES, M., COTTA-RAMUSINO, C., PELLICIOLI, A., LIBERI, G., PLEVANI, P., MUZI-FALCONI, M., NEWLON, C. S. & FOIANI, M. 2001. The DNA replication checkpoint response stabilizes stalled replication forks. *Nature,* 412**,** 557-61.

LOPEZ-MOSQUEDA, J., MAAS, N. L., JONSSON, Z. O., DEFAZIO-ELI, L. G., WOHLSCHLEGEL, J. & TOCZYSKI, D. P. 2010. Damage-induced phosphorylation of Sld3 is important to block late origin firing. *Nature,* 467**,** 479-83.

LYDEARD, J. R., JAIN, S., YAMAGUCHI, M. & HABER, J. E. 2007. Break-induced replication and telomerase-independent telomere maintenance require Pol32. *Nature,* 448**,** 820-3.

MALI, P., YANG, L., ESVELT, K. M., AACH, J., GUELL, M., DICARLO, J. E., NORVILLE, J. E. & CHURCH, G. M. 2013. RNA-guided human genome engineering via Cas9. *Science,* 339**,** 823-6.

MALKOVA, A., NAYLOR, M. L., YAMAGUCHI, M., IRA, G. & HABER, J. E. 2005. RAD51-dependent break-induced replication differs in kinetics and checkpoint responses from RAD51-mediated gene conversion. *Mol Cell Biol,* 25**,** 933-44.

MANKOURI, H. W., ASHTON, T. M. & HICKSON, I. D. 2011. Holliday junction-containing DNA structures persist in cells lacking Sgs1 or Top3 following exposure to DNA damage. *Proc Natl Acad Sci U S A,* 108**,** 4944-9.

MANKOURI, H. W., HUTTNER, D. & HICKSON, I. D. 2013. How unfinished business from S-phase affects mitosis and beyond. *EMBO J,* 32**,** 2661-71.

MASUDA-SASA, T., IMAMURA, O. & CAMPBELL, J. L. 2006. Biochemical analysis of human Dna2. *Nucleic Acids Res,* 34**,** 1865-75.

MATHIASEN, D. P. & LISBY, M. 2014. Cell cycle regulation of homologous recombination in Saccharomyces cerevisiae. *FEMS Microbiol Rev,* 38**,** 172-84.

MATOS, J., BLANCO, M. G., MASLEN, S., SKEHEL, J. M. & WEST, S. C. 2011. Regulatory control of the resolution of DNA recombination intermediates during meiosis and mitosis. *Cell,* 147**,** 158-72.

MATOS, J., BLANCO, M. G. & WEST, S. C. 2013. Cell-cycle kinases coordinate the resolution of recombination intermediates with chromosome segregation. *Cell Rep,* 4**,** 76-86.

MATOS, J. & WEST, S. C. 2014. Holliday junction resolution: regulation in space and time. *DNA Repair (Amst),* 19**,** 176-81.

MAYLE, R., CAMPBELL, I. M., BECK, C. R., YU, Y., WILSON, M., SHAW, C. A., BJERGBAEK, L., LUPSKI, J. R. & IRA, G. 2015. DNA REPAIR. Mus81 and converging forks limit the mutagenicity of replication fork breakage. *Science,* 349**,** 742-7.

MEHTA, A., BEACH, A. & HABER, J. E. 2017. Homology Requirements and Competition between Gene Conversion and Break-Induced Replication during Double-Strand Break Repair. *Mol Cell,* 65**,** 515-526 e3.

MEHTA, A. & HABER, J. E. 2014. Sources of DNA double-strand breaks and models of recombinational DNA repair. *Cold Spring Harb Perspect Biol,* 6**,** a016428.

MILLER, J., MCLACHLAN, A. D. & KLUG, A. 1985. Repetitive zinc-binding domains in the protein transcription factor IIIA from Xenopus oocytes. *EMBO J,* 4**,** 1609-14.

MIMITOU, E. P. & SYMINGTON, L. S. 2008. Sae2, Exo1 and Sgs1 collaborate in DNA double-strand break processing. *Nature,* 455**,** 770-4.

MINOCHERHOMJI, S., YING, S., BJERREGAARD, V. A., BURSOMANNO, S., ALELIUNAITE, A., WU, W., MANKOURI, H. W., SHEN, H., LIU, Y. & HICKSON, I. D. 2015. Replication stress activates DNA repair synthesis in mitosis. *Nature,* 528**,** 286-90.

MOSCOU, M. J. & BOGDANOVE, A. J. 2009. A simple cipher governs DNA recognition by TAL effectors. *Science,* 326**,** 1501.

MULLEN, J. R., KALIRAMAN, V., IBRAHIM, S. S. & BRILL, S. J. 2001. Requirement for three novel protein complexes in the absence of the Sgs1 DNA helicase in Saccharomyces cerevisiae. *Genetics,* 157**,** 103-18.

MUNOZ, I. M., HAIN, K., DECLAIS, A. C., GARDINER, M., TOH, G. W., SANCHEZ-PULIDO, L., HEUCKMANN, J. M., TOTH, R., MACARTNEY, T., EPPINK, B., KANAAR, R., PONTING, C. P., LILLEY, D. M. & ROUSE, J. 2009. Coordination of structure-specific nucleases by human SLX4/BTBD12 is required for DNA repair. *Mol Cell,* 35**,** 116-27.

MUNOZ-GALVAN, S., TOUS, C., BLANCO, M. G., SCHWARTZ, E. K., EHMSEN, K. T., WEST, S. C., HEYER, W. D. & AGUILERA, A. 2012. Distinct roles of Mus81, Yen1, Slx1-Slx4, and Rad1 nucleases in the repair of replication-born double-strand breaks by sister chromatid exchange. *Mol Cell Biol,* 32**,** 1592-603.

NAKAMURA, K., SAREDI, G., BECKER, J. R., FOSTER, B. M., NGUYEN, N. V., BEYER, T. E., CESA, L. C., FAULL, P. A., LUKAUSKAS, S., FRIMURER, T., CHAPMAN, J. R., BARTKE, T. & GROTH, A. 2019. H4K20meO recognition by BRCA1-BARD1 directs homologous recombination to sister chromatids. *Nature Cell Biology,* 21**,** 311-+.

NARDELLI, J., GIBSON, T. J., VESQUE, C. & CHARNAY, P. 1991. Base sequence discrimination by zinc-finger DNA-binding domains. *Nature,* 349**,** 175-8.

NASH, P., TANG, X., ORLICKY, S., CHEN, Q., GERTLER, F. B., MENDENHALL, M. D., SICHERI, F., PAWSON, T. & TYERS, M. 2001. Multisite phosphorylation of a CDK inhibitor sets a threshold for the onset of DNA replication. *Nature,* 414**,** 514-21.

NEELSEN, K. J. & LOPES, M. 2015. Replication fork reversal in eukaryotes: from dead end to dynamic response. *Nat Rev Mol Cell Biol,* 16**,** 207-20.

NELMS, B. E., MASER, R. S., MACKAY, J. F., LAGALLY, M. G. & PETRINI, J. H. 1998. In situ visualization of DNA double-strand break repair in human fibroblasts. *Science,* 280**,** 590-2.

NEW, J. H., SUGIYAMA, T., ZAITSEVA, E. & KOWALCZYKOWSKI, S. C. 1998. Rad52 protein stimulates DNA strand exchange by Rad51 and replication protein A. *Nature,* 391**,** 407-10.

NGUYEN, B., SOKOLOSKI, J., GALLETTO, R., ELSON, E. L., WOLD, M. S. & LOHMAN, T. M. 2014. Diffusion of human replication protein A along single-stranded DNA. *J Mol Biol,* 426**,** 3246-3261.

NIU, H., CHUNG, W. H., ZHU, Z., KWON, Y., ZHAO, W., CHI, P., PRAKASH, R., SEONG, C., LIU, D., LU, L., IRA, G. & SUNG, P. 2010. Mechanism of the ATP-dependent DNA end-resection machinery from Saccharomyces cerevisiae. *Nature,* 467**,** 108-11.

NOGUCHI, E., NOGUCHI, C., DU, L. L. & RUSSELL, P. 2003. Swi1 prevents replication fork collapse and controls checkpoint kinase Cds1. *Mol Cell Biol,* 23**,** 7861-74.

NOGUCHI, E., NOGUCHI, C., MCDONALD, W. H., YATES, J. R., 3RD & RUSSELL, P. 2004. Swi1 and Swi3 are components of a replication fork protection complex in fission yeast. *Mol Cell Biol,* 24**,** 8342-55.

O'DONNELL, L., PANIER, S., WILDENHAIN, J., TKACH, J. M., AL-HAKIM, A., LANDRY, M. C., ESCRIBANO-DIAZ, C., SZILARD, R. K., YOUNG, J. T. F., MUNRO, M., CANNY, M. D., KOLAS, N. K., ZHANG, W., HARDING, S. M., YLANKO, J., MENDEZ, M., MULLIN, M., SUN, T., HABERMANN, B., DATTI, A., BRISTOW, R. G., GINGRAS, A. C., TYERS, M. D., BROWN, G. W. & DUROCHER, D. 2010. The MMS22L-TONSL Complex Mediates Recovery from Replication Stress and Homologous Recombination. *Molecular Cell,* 40**,** 619-631.

OGAWA, T., YU, X., SHINOHARA, A. & EGELMAN, E. H. 1993. Similarity of the yeast RAD51 filament to the bacterial RecA filament. *Science,* 259**,** 1896-9.

OH, S. D., LAO, J. P., TAYLOR, A. F., SMITH, G. R. & HUNTER, N. 2008. RecQ helicase, Sgs1, and XPF family endonuclease, Mus81-Mms4, resolve aberrant joint molecules during meiotic recombination. *Mol Cell,* 31**,** 324-36.

PAPOULI, E., CHEN, S., DAVIES, A. A., HUTTNER, D., KREJCI, L., SUNG, P. & ULRICH, H. D. 2005. Crosstalk between SUMO and ubiquitin on PCNA is mediated by recruitment of the helicase Srs2p. *Mol Cell,* 19**,** 123-33.

PARDO, B. & AGUILERA, A. 2012. Complex chromosomal rearrangements mediated by break-induced replication involve structure-selective endonucleases. *PLoS Genet,* 8**,** e1002979.

PARDO, B., MORIEL-CARRETERO, M., VICAT, T., AGUILERA, A. & PASERO, P. 2020. Homologous recombination and Mus81 promote replication completion in response to replication fork blockage. *EMBO Rep***,** e49367.

PAVLETICH, N. P. & PABO, C. O. 1991. Zinc finger-DNA recognition: crystal structure of a Zif268-DNA complex at 2.1 A. *Science,* 252**,** 809-17.

PEBERNARD, S., MCDONALD, W. H., PAVLOVA, Y., YATES, J. R., 3RD & BODDY, M. N. 2004. Nse1, Nse2, and a novel subunit of the Smc5-Smc6 complex, Nse3, play a crucial role in meiosis. *Mol Biol Cell,* 15**,** 4866-76.

PEPE, A. & WEST, S. C. 2014a. MUS81-EME2 promotes replication fork restart. *Cell Rep,* 7**,** 1048-55.

PEPE, A. & WEST, S. C. 2014b. Substrate specificity of the MUS81-EME2 structure selective endonuclease. *Nucleic Acids Res,* 42**,** 3833-45.

PFANDER, B. & MATOS, J. 2017. Control of Mus81 nuclease during the cell cycle. *FEBS Lett*.

PFANDER, B., MOLDOVAN, G. L., SACHER, M., HOEGE, C. & JENTSCH, S. 2005. SUMO-modified PCNA recruits Srs2 to prevent recombination during S phase. *Nature,* 436**,** 428-33.

PLESSIS, A., PERRIN, A., HABER, J. E. & DUJON, B. 1992. Site-specific recombination determined by I-SceI, a mitochondrial group I intron-encoded endonuclease expressed in the yeast nucleus. *Genetics,* 130**,** 451-60.

PRAKASH, R., SATORY, D., DRAY, E., PAPUSHA, A., SCHELLER, J., KRAMER, W., KREJCI, L., KLEIN, H., HABER, J. E., SUNG, P. & IRA, G. 2009. Yeast Mph1 helicase dissociates Rad51-made D-loops: implications for crossover control in mitotic recombination. *Genes Dev,* 23**,** 67-79.

PRINCZ, L. N., GRITENAITE, D. & PFANDER, B. 2015. The Slx4-Dpb11 scaffold complex: coordinating the response to replication fork stalling in S-phase and the subsequent mitosis. *Cell Cycle,* 14**,** 488-94.

PRINCZ, L. N., WILD, P., BITTMANN, J., AGUADO, F. J., BLANCO, M. G., MATOS, J. & PFANDER, B. 2017. Dbf4-dependent kinase and the Rtt107 scaffold promote Mus81-Mms4 resolvase activation during mitosis. *EMBO J*.

RASS, U., COMPTON, S. A., MATOS, J., SINGLETON, M. R., IP, S. C., BLANCO, M. G., GRIFFITH, J. D. & WEST, S. C. 2010. Mechanism of Holliday junction resolution by the human GEN1 protein. *Genes Dev,* 24**,** 1559-69.

RAY CHAUDHURI, A., HASHIMOTO, Y., HERRADOR, R., NEELSEN, K. J., FACHINETTI, D., BERMEJO, R., COCITO, A., COSTANZO, V. & LOPES, M. 2012. Topoisomerase I poisoning results in PARP-mediated replication fork reversal. *Nat Struct Mol Biol,* 19**,** 417-23.

REGAIRAZ, M., ZHANG, Y. W., FU, H., AGAMA, K. K., TATA, N., AGRAWAL, S., ALADJEM, M. I. & POMMIER, Y. 2011. Mus81-mediated DNA cleavage resolves replication forks stalled by topoisomerase I-DNA complexes. *J Cell Biol,* 195**,** 739-49.

REGINATO, G., CANNAVO, E. & CEJKA, P. 2017. Physiological protein blocks direct the Mre11-Rad50-Xrs2 and Sae2 nuclease complex to initiate DNA end resection. *Genes Dev,* 31**,** 2325-2330.

RENAUD-YOUNG, M., LLOYD, D. C., CHATFIELD-REED, K., GEORGE, I., CHUA, G. & COBB, J. 2015. The NuA4 complex promotes translesion synthesis (TLS)-mediated DNA damage tolerance. *Genetics,* 199**,** 1065-76.

ROSEAULIN, L., YAMADA, Y., TSUTSUI, Y., RUSSELL, P., IWASAKI, H. & ARCANGIOLI, B. 2008. Mus81 is essential for sister chromatid recombination at broken replication forks. *EMBO J,* 27**,** 1378-87.

ROUET, P., SMIH, F. & JASIN, M. 1994. Introduction of double-strand breaks into the genome of mouse cells by expression of a rare-cutting endonuclease. *Mol Cell Biol,* 14**,** 8096-106.

SAINI, N., RAMAKRISHNAN, S., ELANGO, R., AYYAR, S., ZHANG, Y., DEEM, A., IRA, G., HABER, J. E., LOBACHEV, K. S. & MALKOVA, A. 2013. Migrating bubble during break-induced replication drives conservative DNA synthesis. *Nature,* 502**,** 389-92.

SAKOFSKY, C. J., AYYAR, S., DEEM, A. K., CHUNG, W. H., IRA, G. & MALKOVA, A. 2015. Translesion Polymerases Drive Microhomology-Mediated Break-Induced Replication Leading to Complex Chromosomal Rearrangements. *Mol Cell,* 60**,** 860-72.

SAKOFSKY, C. J., ROBERTS, S. A., MALC, E., MIECZKOWSKI, P. A., RESNICK, M. A., GORDENIN, D. A. & MALKOVA, A. 2014. Break-induced replication is a source of mutation clusters underlying kataegis. *Cell Rep,* 7**,** 1640-1648.

SALAZAR, C. & HOFER, T. 2009. Multisite protein phosphorylation--from molecular mechanisms to kinetic models. *FEBS J,* 276**,** 3177-98.

SAN FILIPPO, J., SUNG, P. & KLEIN, H. 2008. Mechanism of eukaryotic homologous recombination. *Annu Rev Biochem,* 77**,** 229-57.

SANDELL, L. L. & ZAKIAN, V. A. 1993. Loss of a yeast telomere: arrest, recovery, and chromosome loss. *Cell,* 75**,** 729-39.

SAREDI, G., HUANG, H., HAMMOND, C. M., ALABERT, C., BEKKER-JENSEN, S., FORNE, I., REVERON-GOMEZ, N., FOSTER, B. M., MLEJNKOVA, L., BARTKE, T., CEJKA, P., MAILAND, N., IMHOF, A., PATEL, D. J. & GROTH, A. 2016. H4K20me0 marks post-replicative chromatin and recruits the TONSL-MMS22L DNA repair complex. *Nature,* 534**,** 714-718.

SAUGAR, I., JIMENEZ-MARTIN, A. & TERCERO, J. A. 2017. Subnuclear Relocalization of Structure-Specific Endonucleases in Response to DNA Damage. *Cell Rep,* 20**,** 1553-1562.

SAUGAR, I., ORTIZ-BAZAN, M. A. & TERCERO, J. A. 2014. Tolerating DNA damage during eukaryotic chromosome replication. *Exp Cell Res,* 329**,** 170-7.

SAUGAR, I., VAZQUEZ, M. V., GALLO-FERNANDEZ, M., ORTIZ-BAZAN, M. A., SEGURADO, M., CALZADA, A. & TERCERO, J. A. 2013. Temporal regulation of the Mus81-Mms4 endonuclease ensures cell survival under conditions of DNA damage. *Nucleic Acids Res,* 41**,** 8943-58.

SCHWARTZ, E. K. & HEYER, W. D. 2011. Processing of joint molecule intermediates by structure-selective endonucleases during homologous recombination in eukaryotes. *Chromosoma,* 120**,** 109-27.

SCHWARTZ, E. K., WRIGHT, W. D., EHMSEN, K. T., EVANS, J. E., STAHLBERG, H. & HEYER, W. D. 2012. Mus81-Mms4 functions as a single heterodimer to cleave nicked intermediates in recombinational DNA repair. *Mol Cell Biol,* 32**,** 3065-80.

SEBESTA, M., BURKOVICS, P., HARACSKA, L. & KREJCI, L. 2011. Reconstitution of DNA repair synthesis in vitro and the role of polymerase and helicase activities. *DNA Repair (Amst),* 10**,** 567-76.

SHIMURA, T., TORRES, M. J., MARTIN, M. M., RAO, V. A., POMMIER, Y., KATSURA, M., MIYAGAWA, K. & ALADJEM, M. I. 2008. Bloom's syndrome helicase and Mus81 are required to induce transient double-strand DNA breaks in response to DNA replication stress. *J Mol Biol,* 375**,** 1152-64.

SHINOHARA, A. & OGAWA, T. 1998. Stimulation by Rad52 of yeast Rad51-mediated recombination. *Nature,* 391**,** 404-7.

SMIH, F., ROUET, P., ROMANIENKO, P. J. & JASIN, M. 1995. Double-strand breaks at the target locus stimulate gene targeting in embryonic stem cells. *Nucleic Acids Res,* 23**,** 5012-9.

SMITH, C. E., LLORENTE, B. & SYMINGTON, L. S. 2007. Template switching during break-induced replication. *Nature,* 447**,** 102-5.

SOGO, J. M., LOPES, M. & FOIANI, M. 2002. Fork reversal and ssDNA accumulation at stalled replication forks owing to checkpoint defects. *Science,* 297**,** 599-602.

STELTER, P. & ULRICH, H. D. 2003. Control of spontaneous and damage-induced mutagenesis by SUMO and ubiquitin conjugation. *Nature,* 425**,** 188-91.

SUGAWARA, N., WANG, X. & HABER, J. E. 2003. In vivo roles of Rad52, Rad54, and Rad55 proteins in Rad51-mediated recombination. *Mol Cell,* 12**,** 209-19.

SUGIYAMA, T. & KOWALCZYKOWSKI, S. C. 2002. Rad52 protein associates with replication protein A (RPA)-single-stranded DNA to accelerate Rad51-mediated displacement of RPA and presynaptic complex formation. *J Biol Chem,* 277**,** 31663-72.

SUNG, P. 1997. Function of yeast Rad52 protein as a mediator between replication protein A and the Rad51 recombinase. *J Biol Chem,* 272**,** 28194-7.

SUNG, P. & ROBBERSON, D. L. 1995. DNA strand exchange mediated by a RAD51-ssDNA nucleoprotein filament with polarity opposite to that of RecA. *Cell,* 82**,** 453-61.

SYMINGTON, L. S. 2016. Mechanism and regulation of DNA end resection in eukaryotes. *Crit Rev Biochem Mol Biol,* 51**,** 195-212.

SZAKAL, B. & BRANZEI, D. 2013. Premature Cdk1/Cdc5/Mus81 pathway activation induces aberrant replication and deleterious crossover. *EMBO J,* 32**,** 1155-67.

SZOSTAK, J. W., ORR-WEAVER, T. L., ROTHSTEIN, R. J. & STAHL, F. W. 1983. The double-strand-break repair model for recombination. *Cell,* 33**,** 25-35.

TALHAOUI, I., BERNAL, M., MULLEN, J. R., DORISON, H., PALANCADE, B., BRILL, S. J. & MAZON, G. 2018. Slx5-Slx8 ubiquitin ligase targets active pools of the Yen1 nuclease to limit crossover formation. *Nat Commun,* 9**,** 5016.

THORSLUND, T., MCILWRAITH, M. J., COMPTON, S. A., LEKOMTSEV, S., PETRONCZKI, M., GRIFFITH, J. D. & WEST, S. C. 2010. The breast cancer tumor suppressor BRCA2 promotes the specific targeting of RAD51 to single-stranded DNA. *Nat Struct Mol Biol,* 17**,** 1263-5.

TOMIMATSU, N., MUKHERJEE, B., CATHERINE HARDEBECK, M., ILCHEVA, M., VANESSA CAMACHO, C., LOUISE HARRIS, J., PORTEUS, M., LLORENTE, B., KHANNA, K. K. & BURMA, S. 2014. Phosphorylation of EXO1 by CDKs 1 and 2 regulates DNA end resection and repair pathway choice. *Nat Commun,* 5**,** 3561.

TORRES-ROSELL, J., MACHIN, F., FARMER, S., JARMUZ, A., EYDMANN, T., DALGAARD, J. Z. & ARAGON, L. 2005. SMC5 and SMC6 genes are required for the segregation of repetitive chromosome regions. *Nat Cell Biol,* 7**,** 412-9.

TRUJILLO, K. M., YUAN, S. S., LEE, E. Y. & SUNG, P. 1998. Nuclease activities in a complex of human recombination and DNA repair factors Rad50, Mre11, and p95. *J Biol Chem,* 273**,** 21447-50.

URNOV, F. D., MILLER, J. C., LEE, Y. L., BEAUSEJOUR, C. M., ROCK, J. M., AUGUSTUS, S., JAMIESON, A. C., PORTEUS, M. H., GREGORY, P. D. & HOLMES, M. C. 2005. Highly efficient endogenous human gene correction using designed zinc-finger nucleases. *Nature,* 435**,** 646-51.

URNOV, F. D., REBAR, E. J., HOLMES, M. C., ZHANG, H. S. & GREGORY, P. D. 2010. Genome editing with engineered zinc finger nucleases. *Nat Rev Genet,* 11**,** 636-46.

VAN BRABANT, A. J., YE, T., SANZ, M., GERMAN, I. J., ELLIS, N. A. & HOLLOMAN, W. K. 2000. Binding and melting of D-loops by the Bloom syndrome helicase. *Biochemistry,* 39**,** 14617-25.

VASAN, S., DEEM, A., RAMAKRISHNAN, S., ARGUESO, J. L. & MALKOVA, A. 2014. Cascades of genetic instability resulting from compromised break-induced replication. *PLoS Genet,* 10**,** e1004119.

VILENCHIK, M. M. & KNUDSON, A. G. 2003. Endogenous DNA double-strand breaks: production, fidelity of repair, and induction of cancer. *Proc Natl Acad Sci U S A,* 100**,** 12871-6.

WANG, X., IRA, G., TERCERO, J. A., HOLMES, A. M., DIFFLEY, J. F. & HABER, J. E. 2004. Role of DNA replication proteins in double-strand break-induced recombination in Saccharomyces cerevisiae. *Mol Cell Biol,* 24**,** 6891-9.

WARD, J. F. 1988. DNA damage produced by ionizing radiation in mammalian cells: identities, mechanisms of formation, and reparability. *Prog Nucleic Acid Res Mol Biol,* 35**,** 95-125.

WECHSLER, T., NEWMAN, S. & WEST, S. C. 2011. Aberrant chromosome morphology in human cells defective for Holliday junction resolution. *Nature,* 471**,** 642-6.

WEINREICH, M. & STILLMAN, B. 1999. Cdc7p-Dbf4p kinase binds to chromatin during S phase and is regulated by both the APC and the RAD53 checkpoint pathway. *EMBO J,* 18**,** 5334-46.

WILSON, T. E., GRAWUNDER, U. & LIEBER, M. R. 1997. Yeast DNA ligase IV mediates non-homologous DNA end joining. *Nature,* 388**,** 495-8.

WOHLBOLD, L., MERRICK, K. A., DE, S., AMAT, R., KIM, J. H., LAROCHELLE, S., ALLEN, J. J., ZHANG, C., SHOKAT, K. M., PETRINI, J. H. & FISHER, R. P. 2012. Chemical genetics reveals a specific requirement for Cdk2 activity in the DNA damage response and identifies Nbs1 as a Cdk2 substrate in human cells. *PLoS Genet,* 8**,** e1002935.

WRIGHT, W. D., SHAH, S. S. & HEYER, W. D. 2018. Homologous recombination and the repair of DNA double-strand breaks. *J Biol Chem,* 293**,** 10524-10535.

WU, L. & HICKSON, I. D. 2003. The Bloom's syndrome helicase suppresses crossing over during homologous recombination. *Nature,* 426**,** 870-4.

WYATT, H. D., SARBAJNA, S., MATOS, J. & WEST, S. C. 2013. Coordinated actions of SLX1-SLX4 and MUS81-EME1 for Holliday junction resolution in human cells. *Mol Cell,* 52**,** 234-47.

XIAO, W., CHOW, B. L. & MILO, C. N. 1998. Mms4, a putative transcriptional (co)activator, protects Saccharomyces cerevisiae cells from endogenous and environmental DNA damage. *Mol Gen Genet,* 257**,** 614-23.

XING, M., WANG, X., PALMAI-PALLAG, T., SHEN, H., HELLEDAY, T., HICKSON, I. D. & YING, S. 2015. Acute MUS81 depletion leads to replication fork slowing and a constitutive DNA damage response. *Oncotarget,* 6**,** 37638-46.

YU, X., JACOBS, S. A., WEST, S. C., OGAWA, T. & EGELMAN, E. H. 2001. Domain structure and dynamics in the helical filaments formed by RecA and Rad51 on DNA. *Proc Natl Acad Sci U S A,* 98**,** 8419-24.

ZEGERMAN, P. & DIFFLEY, J. F. 2010. Checkpoint-dependent inhibition of DNA replication initiation by Sld3 and Dbf4 phosphorylation. *Nature,* 467**,** 474-8.

ZELENSKY, A., KANAAR, R. & WYMAN, C. 2014. Mediators of homologous DNA pairing. *Cold Spring Harb Perspect Biol,* 6**,** a016451.

ZELLWEGER, R., DALCHER, D., MUTREJA, K., BERTI, M., SCHMID, J. A., HERRADOR, R., VINDIGNI, A. & LOPES, M. 2015. Rad51-mediated replication fork reversal is a global response to genotoxic treatments in human cells. *J Cell Biol,* 208**,** 563-79.

ZHANG, H. & LAWRENCE, C. W. 2005. The error-free component of the RAD6/RAD18 DNA damage tolerance pathway of budding yeast employs sister-strand recombination. *Proc Natl Acad Sci U S A,* 102**,** 15954-9.

ZHU, Z., CHUNG, W. H., SHIM, E. Y., LEE, S. E. & IRA, G. 2008. Sgs1 helicase and two nucleases Dna2 and Exo1 resect DNA double-strand break ends. *Cell,* 134**,** 981-94.

ZOU, L. & ELLEDGE, S. J. 2003. Sensing DNA damage through ATRIP recognition of RPA-ssDNA complexes. *Science,* 300**,** 1542-8.

Acknowledgements

First of all, I want to thank my supervisor and mentor Boris Pfander. I really could not have wished for a better guidance into the world of science and I am really thankful for the freedom you provided me with, your always open ear and support. Thank you also for collecting a crew of people and creating a lab atmosphere that will be truly hard to leave behind.

Furthermore, I would like to thank my PhD examination board Prof. Heinrich Leonhardt, Prof. Peter Becker, Prof. Michael Boshart, Dr. Esther Zanin, Prof. Kirsten Jung and Prof. Robert Schneider for reviewing this thesis and participating in my PhD examination. I also thank the members of my TAC committee Prof. Karl-Peter Hopfner, Dr. Sigurd Braun and Prof. Joao Matos for fruitful discussions and helpful input throughout my PhD thesis. A special thanks goes to Prof. Joao Matos and Rokas Grigaitis for invaluable contributions to our projects on Mus81-Mms4 regulation.

I am thankful to Stefan Jentsch and all the former members of the Jentsch department. Although I just had the short pleasure of experiencing the atmosphere in his department, this time left me deeply impressed by the truly inspiring way Stefan conducted science and guided his people. Thanks also to all members of the junior group wing who made it very easy to settle in after our move from Stefans department. Here, I especially want to mention and thank Bianca for simply making things possible; no matter what, where or when! Massimo, Beate, Klara: thank you for the constant supply of media and the administrative help which really made my life so much easier.

A big thank you also goes to the IMPRS coordination team, Hans-Jörg Schäffer, Ingrid Wolf and Maxi Reif, who did a great job in providing a framework of workshops, lectures and overall advice to the time in the lab.

This time in the lab would not have been the same without the people sharing it with me. Thanks to every single shark in the Pfander lab for working so well together, for always taking the time to discuss and simply creating a unique atmosphere! Uschi, thank you a thousand times for your invaluable help with my project and standing by my side at early lab hours. Dalia, Lissa, Giulia, thanks for welcoming me in the lab and introducing me to general lab practices. Susi, thanks for countless coffee hours during which you passed on your small and large lab granny wisdoms. Thank you for your positivity and crazy stories that never failed to keep the mood high. Kalle, thank you so much for being a solid and reliant rock (and this is really just meant as a metaphor) in the chaos of every day lab life. Thanks for always being interested and available for quick or extensive discussions in and outside of the lab. Lorenzo, thank you for your kind words (and the rude ones), insights into your opinion of dinosaurs (and other important matters of life), your

creative ideas, your willingness to discuss scientific problems at any time of the day and of course for lending me (the cutest) socks when I needed them most. Martina, thanks for taking on the job as my coffee companion and your always open ear. Thanks for sweetening our days with delicious cakes and Italian food. Leo, thanks for providing the lab with some more maturity and sharing many funny moments in and outside of the lab. Thanks also to all the students and helpers who joined me during my project: Silas Amarell, Tobias Freimann, Michael Chan and Jennifer Willmann.

Nina, Domi, Mama! Thank you for always being there for me. Knowing I can rely on you means a lot and I´m looking forward to all the small and big moments still waiting to be celebrated together. Papa, I´m sure you would have gone through this in a quite minute (directly after my bachelor thesis… ☺). I miss you every day, your pride still keeps me going! Oma, this thesis is meant for your collection of course. Have fun reading ;)

Ulrich, this definitely has been a special time and I am grateful for having you by my side. I´m really looking forward to all the chapters ahead of us.